University of Illinois at Urbana-Champaign

ACRC

Air Conditioning and Refrigeration Center A National Science Foundation/University Cooperative Research Center

Steady-State Performance of a Domestic Refrigerator/Freezer Using R12 and R134a

D. M. Staley, C. W. Bullard, and R. R. Crawford

ACRC TR-22 June 1992

For additional information:

Air Conditioning and Refrigeration Center
University of Illinois
Mechanical & Industrial Engineering Dept.
1206 West Green Street
Urbana, IL 61801

(217) 333-3115

Prepared as part of ACRC Project 12
Analysis of Refrigerator-Freezer Systems
C. W. Bullard, Principal Investigator

The Air Conditioning and Refrigeration Center was founded in 1988 with a grant from the estate of Richard W. Kritzer, the founder of Peerless of America Inc. A State of Illinois Technology Challenge Grant helped build the laboratory facilities. The ACRC receives continuing support from the Richard W. Kritzer Endowment and the National Science Foundation. The following organizations have also become sponsors of the Center.

Acustar Division of Chrysler
Allied-Signal, Inc.
Amana Refrigeration, Inc.
Bergstrom Manufacturing Co.
Caterpillar, Inc.
E. I. du Pont de Nemours & Co.
Electric Power Research Institute
Ford Motor Company
General Electric Company
Harrison Division of GM
ICI Americas, Inc.
Johnson Controls, Inc.
Modine Manufacturing Co.
Peerless of America, Inc.
Environmental Protection Agency
U. S. Army CERL
Whirlpool Corporation

For additional information:

Air Conditioning & Refrigeration Center
Mechanical & Industrial Engineering Dept.
University of Illinois
1206 West Green Street
Urbana, IL 61801

217 333 3115

Abstract

This paper develops a steady-state system design model for a standard 18 ft^3 refrigerator/freezer. Models for the compressor, condenser, evaporator, and suction line interchanger are considered. Experimental data for both R12 and R134a are used as a basis to calibrate the models and as a basis of comparison of model validity for different refrigerants. For each model, a set of independent model parameters are determined from the experimental data using optimization methods. For the heat exchangers both constant conductance and variable conductance models are considered. Lastly, a preliminary overview is made of the applicability of a quasi-steady refrigerator model for use in describing normal cycling operation of a refrigerator/freezer.

Table of Contents

List of Figures

Page

List of Tables

Chapter 1: Introduction

Since the original discovery that chlorofluorocarbons destroy ozone [1], the European community and 24 nations have signed the Montreal Protocol [2] which contains the framework for the reduction and elimination of CFC's. Concurrently in the U.S., Congress enacted legislation [3] that sets minimum energy efficiency standards for household appliances. Further, recent measurements [4] indicate that the depletion of ozone may be worse than originally thought. This has increased the pressure to accelerate the phase out time tables for R12. As a result, the refrigeration industry and the appliance industry in particular must bear the double burden of eliminating the use of R12, a CFC, and at the same time increase the efficiency of their appliances.

The need to evaluate and test alternative refrigerants in domestic refrigerators is immediate. The original hope for a drop-in replacement has disappeared. At the present time it appears that R134a will most likely be the chosen replacement for R12. However, this is by no means the final solution. As a result, the evaluation of alternatives continues.

As part of this effort, a good refrigerator simulation model can be used to make relative comparisons among different replacement candidates. Many more possible alternatives can be evaluated than either time or money would allow for testing. The best candidates can then be chosen for testing. Further for the model to be useful, it should be able to handle different refrigerants without complication.

The primary purpose of the work presented here is to develop a steady-state system design model, as well as component models, for a standard 18 ft^3 top-mount domestic refrigerator/freezer and evaluate how the models must be adapted to accurately predict refrigerator performance with alternative refrigerants. In the process experimental data will be collected for both R12 and R134a to provide a data base for analysis. Further, methods for obtaining system parameters such as volumetric flow rates etc. will also be presented. Once the models are validated for different refrigerants, they then can be used as building blocks for the development of a system simulation model for alternative refrigerants. A simulation model consists of the same component models as a design model, plus models of the capillary tube and the charge inventory.

Chapter 2 reviews some of the recent work on refrigerator modeling and alternative refrigerants. Chapters 3 and 4 describe the experimental instrumentation and procedures used in creating the R12 and R134a data bases. Chapter 5 introduces some of the topics common to all the component chapters. Chapters 6 through 9 present the results for the components studied and Chapter 10 discusses conclusions and recommendations for future research. Appendix A summarizes some initial analysis of normal cycling operation of a domestic refrigerator. The applicability of a quasi-steady state model is investigated.

References

[1] Molina, M.J. and F.S. Rowland. 1974. "Stratospheric Sink for Chlorofluoromethanes: Chlorine Atom Catalyzed Destruction of Ozone," Nature 249: pp. 810 to 812.

[2] United Nations Environmental Programme. 1987. Montreal protocol on substances that deplete the ozone layer. Final act., New York: United Nations.

[3] NAECA. 1987. Public law 100-12, March 17.

[4] Science. v. 254, no. 5032, 1991.

Chapter 2: Literature Review

2.1 Purpose

The intent of this literature review is to examine some of the recent work on the modeling of refrigerator/freezers. It builds on the review conducted by Reeves [1] which contains additional references. This review also covers some of the work on alternative refrigerants for use in domestic refrigerators.

2.2 Steady-State Simulation Models

Rogers and Tree [2] present an algebraic model for each component in a refrigerator/freezer and combine them to form a steady-state system simulation model. Their model for the compressor considers both heat transfer within the compressor and from the compressor shell. For the heat transfer from the compressor shell, a three zone model consisting of the top, side, and bottom of the compressor is developed. An overall heat transfer coefficient is calculated from internal and external film coefficients for each section. No mention is made of how these heat transfer coefficients were determined.

Given the shell heat transfer, the heat transfer from the motor windings and the inlet suction gas temperature, the inlet temperature to the compressor cylinder is determined. The compression process is treated as a polytropic compression. From this expression the discharge temperature from the compressor cylinder is determined.

With the exit temperature from the compressor cylinder known, the heat transfer from the discharge gas tube to the surrounding suction gas is determined. This heat transfer process was modeled as a simple counterflow heat exchanger. After considering the heat transfer to the suction gas, the discharge temperature from the compressor is now known.

For the mass flow rate, a volumetric efficiency equation is used. Their expression is exactly the same as Equation 6.4 in Chapter 6. No mention is made of how the volumetric efficiency or polytropic exponent etc. were determined. However, comparison with experimental results showed the measured mass flow rate to agree within ±3%.

The relationship between the pressure difference across the capillary tube and the mass flow rate is developed from the homogeneous model for two phase flow [3]. Comparisons with experimental data for a real capillary tube/suction line interchanger showed good agreement for cases where subcooled liquid entered the cap tube. The model did not do a very good job when the inlet was two phase.

The models for the heat exchangers are based on effectiveness-NTU relations for each zone similar to those in Chapters 7 and 9. Equations were written for each zone in each heat exchanger, i.e. desuperheating, two phase, subcooled and superheated. However, only overall heat transfer coefficients or UA's were considered. No attempt was made to separate the areas from the conductances.

The above component models were combined into a system model. The capacity of the evaporator as well as the evaporating temperature are inputs to the model. Further, the power input to the compressor must be given. No mention is made of the existence of a condenser or evaporator fan. The outputs from the model are the mass flow rate, the condensing pressure, the UA's for each section of the the heat exchangers, and the evaporator outlet temperature.

The need to input important parameters such as evaporator heat transfer limits the usefulness of this model. It is not a design model where the evaporator capacity and the evaporator temperature would be outputs and parameters such as the ambient temperature would be inputs.

2.3 Quasi-Steady Models

Hara et. al. [4] applied a quasi-steady model to simulate the transient response of the cooling capacity of a refrigerator/freezer from startup to a steady-state condition. No attempt was made to develop component models. Rather, the standard vapor compression cycle diagram with no pressure drops in the heat exchangers was used as a starting point. Their diagram was based on the assumptions that the compressor suction temperature was equal to the ambient temperature and the evaporator exit temperature was 10°C lower. The exit quality from the condenser and the condensing temperature were also fixed.

A simple first order lumped capacitance model was written for each compartment of the refrigerator. The difference between the specified evaporator load and the sum of the cabinet load plus evaporator fan power determined the response of the system. The cabinet load was calculated from a finite element model of all the exterior walls.

The refrigerator studied by Hara et. al. had a convectively cooled condenser. The condenser tubing was run along the inside of the sheet metal of the exterior walls. Essentially the same configuration is used in many domestic refrigerators to prevent moisture condensation. As for the cabinet walls a finite element program was written to determine the amount of heat from the condenser tubing that flows back into the cabinet. This heat transfer was also measured experimentally by placing small heaters inside the condenser tubing. When the surface temperature of the exterior wall adjacent to a heater tube was equal to ambient conditions, the power input to the heater is equal the heat transfer into the refrigerator cabinet. It was found that this heat transfer was of the order of 10 to 15 W.

Sugalski, Jung, and Radermacher [5] developed a quasi-transient model that simulates the normal cycling operation of a refrigerator/freezer. They assume that the temperatures, pressures, etc. in the system change slowly enough that thermal equilibrium exists in the system. This model is a combination of a purely steady-state model like Rogers and Tree's and a fully transient model like Xiuling's. However, the model does not have the capability of simulating start up transients.

As a starting point, a steady-state model was produced. The model did not include a mass flow/pressure drop equation for the cap tube or consider refrigerant inventory. As a result the amount of subcooling at the condenser outlet and the amount of superheat at the evaporator outlet must be specified by the user. Effectiveness-NTU relations were used to model the heat exchangers. No mention is made of whether multiple zones are considered. It appears that they were not considered because the user only specifies one overall heat transfer coefficient for each heat exchanger. The user must also specify the volumetric flow rates across the coils.

The compressor model follows the same general approach as Rogers and Tree. It requires the user to input a long list of parameters including a polytropic coefficient, isentropic efficiency, motor efficiency, displacement volume etc, to specify the performance of the compressor. The model for the suction line heat exchanger is exactly the same as the constant UA model given in Chapter 8 of this report. The outputs from this model include the compressor power, the mass flow rate, and the evaporator load.

This refrigerant system model is combined with a cabinet model to produce the final quasi-steady state model. The cabinet model is based on a steady-state UAΔT approach where the overall heat transfer coefficient was determined from theoretical inside and outside film coefficients and the wall resistance. The cabinet model also considers cabinet heat storage. A finite element program was written to investigate the shape the temperature profile in the cabinet wall as the temperature inside the refrigerator varied. It was found that the temperature profile remained essentially linear even when the internal compartment temperatures started at ambient conditions. As a result, the cabinet heat storage term could be easily calculated.

The model was run with both R12 and R22/R142b mixture. The results showed that a R22/R142b mixture required about 4.5% less energy a day than R12. Experimental measurements confirmed that the energy consumption was less but only by 2 to 3%. It is not stated if in running the models any consideration was given of the effect of the different fluids on the UA's of the heat exchangers or if any corrections were made.

2.4 Transient Models

Xiuling et. al. [6] developed a first order fully transient model for a refrigerator/freezer. Basic continuity and energy equations containing refrigerant mass storage and energy storage terms were written for both the evaporator and the condenser. A linear quality model was assumed for the two phase sections and the desuperheating section in the condenser was neglected. Both convective heat transfer and radiative heat transfer is accounted for on the air side of the coils.

The mass flow rate through the compressor cylinder was determined from a volumetric efficiency equation. The compressor power was calculated assuming a polytropic compression process. Equations were also written containing refrigerant mass storage and energy storage terms to account for the thermal mass of the compressor. No mention is made of how the capacitance for the compressor was determined.

The model for the capillary tube was restricted to the adiabatic case and only considers the condition where the inlet refrigerant is subcooled. Mass flow and pressure drop equations were developed for both the subcooled and two phase sections. The equation for the two phase section assumed that the two phase flow is compressible Fanno Flow.

The system of differential equations was solved using Euler's method with interval-halving to simulate the startup of a refrigerator. Comparison of the simulation results with the refrigerator studied showed good agreement for pressures and temperatures and only fair agreement for power input. The mass flow rate did not agree very well during the initial startup of the refrigerator; only after approximately a minute did the predicted and measured flow rates agree.

2.5 Alternate Refrigerants

Vineyard [7] screened many different possible replacements for R12 in domestic refrigerators based on ozone depletion potential, global warming potential, predicted cycle efficiency and safety concerns such as flammability. A set of three pure refrigerants, R134a, R134, R152a, one binary blend R134a/R152a, and two ternary blends, R22/R152a/R124 and R134a/R152a/R124 were chosen for testing based on these criteria. For each refrigerant the compressor was replaced to adjust for different required volumetric capacities. One of three capillary tubes were available for use. The final selection of a capillary tube was based on which one gave the best performance.

The results for all the pure components showed a higher daily energy consumption compared to R12. R152a was the best performer with an increase in daily energy consumption of of 3% after being corrected for compressor efficiency. However, it has the major drawback of being flammable. R134a and R-134 had the same energy consumption increase of 5.5%. It was found that lower viscosity oil improved the efficiency of R134a. This is effect could not be solely accounted for by a decrease in compressor losses. It was speculated that higher refrigerant/oil miscibility may improve evaporator heat transfer and account for the difference.

Camporese et. al. [8] compared the performance of R134a and the flammable refrigerants R152a, RC270, DME, R290-R134a and R290-RC270 to R12. Their tests were strictly drop-in replacement tests. No modifications were made to the compressor or the capillary tube. However, the results are consistent with Vineyard's. R152a showed a 2% increase in daily energy consumption and R134a showed a 4.3% increase over R12. The refrigerants DME and RC270 did worse than R134a. As a result of their flammability, the authors considered that these refrigerants were not worth further investigation. The refrigerant mixture R290-RC270 had an equivalent performance to R12 but has a low flammability limit. The remaining mixture R290-R134a with 20% propane showed better performance than R12 but still contains a flammable component.

Pereira, Neto, and Thiessen [9] tested both R12 and R134a in a 420 dm^3 top-mount refrigerator. The R12 compressor was replaced with a compressor that had nearly the same refrigerating capacity and exactly the same power requirement as the R12 compressor at the same rating conditions. The capillary tube was also replaced and optimized to give equivalent performance to the R12 refrigerator. With these changes it was found that the R134a system consumed about 2.4% more energy than the R12 system. However, there is a good deal of uncertainty in the measurements and the comparison is more qualitative than quantitative. The authors suggest that it may be possible to increase the efficiency of the R134a refrigerator by reoptimizing the heat exchangers. Note that the same evaporator and condenser were used for both tests.

He, Spindler, Jung, and Radermacher [10], tested mixtures of R22/R142b as a possible replacement for R12. They started with a standard 18 ft^3 top-mount refrigerator. Extensive modifications were made to the heat exchangers to make them counterflow. This was done to take advantage of the temperature glide inherent in NARMs. The capillary tube was also reoptimized for each refrigerant mixture tested to give the same subcooling at the condenser exit and superheat at the evaporator outlet as for the R12 case.

For the initial tests, the compressor was the same as that used in the R12 tests. A 0.55/0.45 mixture of R22/R142b was chosen for this test because theoretical calculations revealed the mixture had the same volumetric capacity as R12. In this way the compressor run times would be nearly equal making the comparison between the mixture and R12 more fair. Even though simulation results showed a 3% increase in COP, the real system with various mixture concentrations was always 3 to 4% worse. However, the replacement of the mineral oil in the compressor with the same viscosity alkybenzene showed a dramatic increase in performance for the R22/R142b mixtures.

Further tests revealed the best mixture to have an R22 mass fraction of 0.52. The daily energy consumption for this mixture was 1.9 to 3.5% lower than that for R12. The authors speculate that the better performance is the result of a larger latent heat of evaporation for the mixture. However, the drawback of this mixture is the fact that

R142b is flammable. Since R22 is the more volatile component, the potential for leaks causing an increase in R142b concentration is a concern.

2.6 Implications for Current Study

The work considered here is an extension of the work by Rogers and Tree and the steady-state part of the work by Sugalski, Jung, and Radermacher. Emphasis will be placed on the heat exchangers. Rather than consider overall heat transfer coefficients for each zone in the heat exchangers, an attempt will be made to separate the conductances from the areas. Further, the variation in the conductances due to variations in mass flow rate and refrigerant properties will also be investigated. If these variations can be accounted for by calibrating appropriate heat transfer correlations with one refrigerant, it should then be possible to predict performance with another refrigerant by simply using the thermodynamic properties of the new refrigerant in the model. This result would allow the investigation of many different alternate refrigerants without the cost of testing each one. In this way such a model would be very valuable.

References

[1] Reeves, R.N., Modeling and Experimental Parameter Estimation of a Refrigerator/Freezer System, Air Conditioning and Refrigeration Center, Dept. of Mechanical and Industrial Engineering, University of Illinois at Urbana-Champaign, 1992, Chapter 2, pp. 4 to 12.

[2] Rogers, S. and D.R. Tree. 1991. "Algebraic Modelling of Components and Computer Simulation of Refrigerator Steady-State Operation.", Proceedings of the XVIII International Congress of Refrigeration, Vol. III, pp. 1225 to 1229.

[3] Collier, J. G., Convective Boiling and Condensation, Second Edition, McGraw-Hill, New York, 1980, pp. 30 to 35.

[4] Hara, T., and M. Shibayama, H. Kogure, and A. Ishiyama. 1991. "Computer Simulation of Cooling Capacity for a Domestic Refrigerator-Freezer.", Proceedings of the XVIII International Congress of Refrigeration, Vol. III, pp. 1193 to 1197.

[5] Sugalski, A., D. Jung, and R. Radermacher. 1991. "Quasi-Transient Simulation of Domestic Refrigerators.", Proceedings of the XVIII International Congress of Refrigeration, Vol. III, pp. 1244 to 1249.

[6] Xiuling, C., C. Youhong, X. Deling, G. Yain, and L. Xing. 1991. "A Computer Simulation and Experimental Investigation of the Working Process of a Domestic Refrigerator.", Proceedings of the XVIII International Congress of Refrigeration, Vol. III, pp. 1198 to 1202.

[7] Vineyard, E.A. 1991. "The Alternative Refrigerant Dilemma for Refrigerator-Freezers: Truth of Consequences.", ASHRAE Transactions, Vol. 97, Part 2, pp. 955 to 960.

[8] Camporese, R., G. Bogolaro, G. Cortella, and M. Scattolini. 1991. "Flammable Refrigerants in Domestic Refrigeration.", Proceedings of the XVIII International Congress of Refrigeration, Vol. III, pp. 1175 to 1179.

[9] Pereira, R.H., L.M. Neto, and M.R. Thiessen. 1991. "An Experimental Approach to Upgrade the Performance of a Domestic Refrigeration System Considering the HFC-134a.", Proceedings of the XVIII International Congress of Refrigeration, Vol. III, pp. 1180 to 1184.

[10] He, X., U.C. Spindler, D.S. Jung, and R. Radermacher. 1992. "Investigation of R-22/R-142b Mixture as a Substitute for R-12 in Single-Evaporator Domestic Refrigerators.", ASHRAE Transactions, Vol. 98, Part 2, 1992.

Chapter 3: Instrumentation

3.1 Refrigerator Instrumentation

The GE refrigerator was equipped with four basic instrumentation systems. First, thermocouples and pressure gages were installed to measure the thermodynamic properties in the system. A set of power transducers were used to measure system and selected component power consumption. A heater system was designed to allow the refrigerator to be run under steady-state conditions. Finally, a turbine flow meter was used to measure refrigerant mass flow rates.

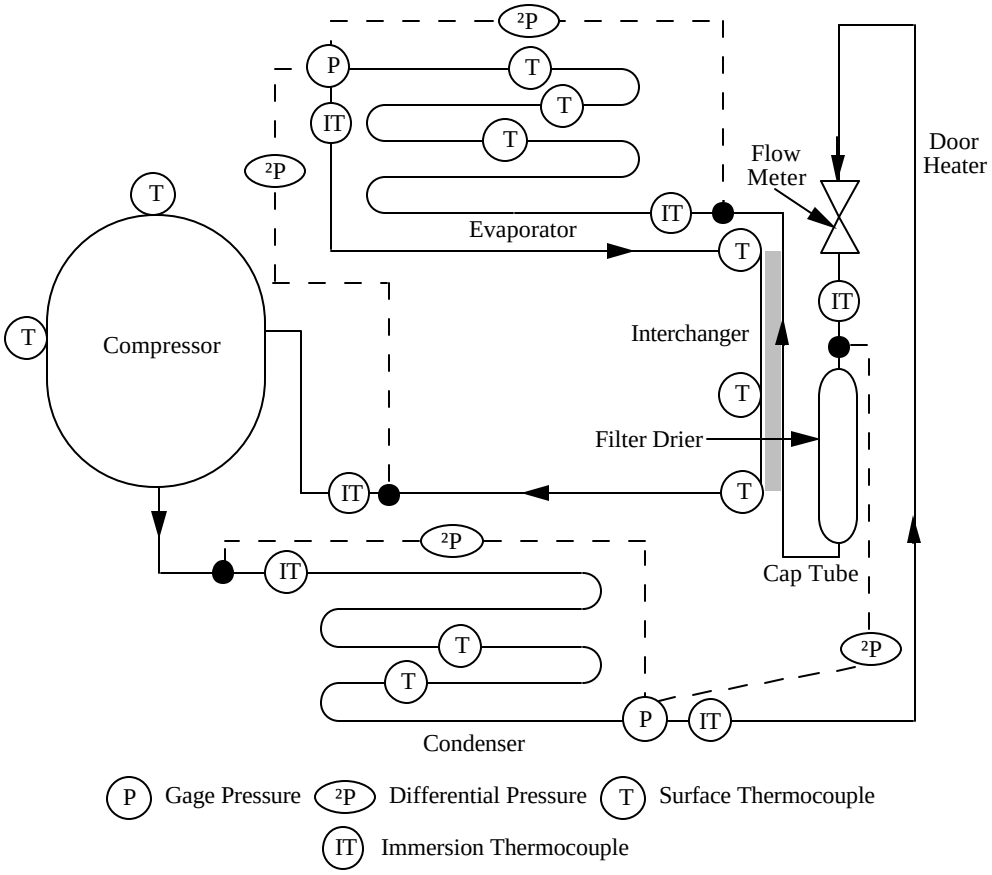

Figure 3-1. Refrigerant Side Pressure and Temperature Measurement Locations

The location of the refrigerant side thermocouples and pressure taps are shown in Figure 3-1. Type T thermocouples were used for both surface mounted and immersion applications. The surface thermo couples were made by welding the two thermocouple wires in a commercial welder. It is recommended that the thermocouples be welded rather than soldered. The presence of solder in the junction can alter the thermal characteristics of the thermocouple. The immersion thermocouples were obtained commercially.

The mounting technique used for the surface thermocouples is as follows. First, the tubing surface was roughened. The thermocouples were held tightly in place with thread. A two part epoxy was used to permanently bond the thermocouples to the tube walls. Great care was exercised to ensure that no epoxy got between the

thermocouple and the tube wall. After the epoxy set, the surface thermocouples were insulated with foam insulation to minimize heat transfer to or from the surrounding air. However, it was found that the surface thermocouples would not yield consistent results. For example it would be expected that as a result of pressure drop in the evaporator the temperatures along the evaporator tubing would decrease from the inlet up to the dry-out point. However, some of the surface thermocouples showed the opposite trend. In fact some of the temperatures measured were off by several degrees. These inconsistencies were probably a result of the failure to get good thermal contact between the thermocouple and the evaporator tubing. Because of these uncertainties the surface temperature measurements were not used in any of the data analysis.

The mounting technique for the immersion thermocouples and pressure taps are shown in Figure 3-2. In all cases the pressure taps were mounted upstream of the temperature taps to prevent any induced turbulence affecting the pressure measurements if the arrangement were reversed. In most cases, the Gyrolok fittings were mounted where a 90° bend occurred in the refrigerant line to minimize the additional pressure losses in the fitting. The pressure taps were constructed from standard piping tees. The actual pressure line was made from capillary tubing silver soldered into a short piece of copper tubing the end of which was filed to remove any roughness. This piece was then soft soldered into the tee mounted in the refrigerant line.

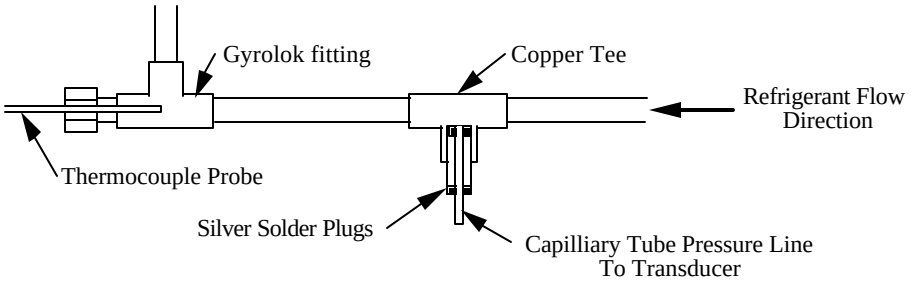

Figure 3-2. Immersion Thermocouple and Pressure Tap Mounting Technique

This arrangement worked fairly well except for small persistent leaks around the Gyrolok fittings. To alleviate this problem it is suggested that the thermocouple probe and the Gyrolok fitting be silver soldered together into one piece. This hopefully will stop the leaks. Note that to be able to do this the sheathing on the thermocouple must be compatible with the solder and be able to withstand temporary high temperatures when soldering. It is also suggested that smaller immersion thermocouples be used. The sheathing diameter for the immersion thermocouples used in this refrigerator were 1/16" in diameter. In a 1/4" tube, this doesn't leave much space for the refrigerant to get past. As a result, the thermocouples induce additional pressure drops in the system (see also Appendix C).

The air side temperature measurement locations are shown in Figure 3-3. Note that some of the measured temperatures come from thermocouple arrays such as at the condenser inlet. In this way an average temperature is measured directly.

The pressure transducers used are compatible with both two phase and vapor refrigerant. Early tests with incompatible pressure transducers resulted in erroneous pressure readings. The gage pressure transducer at the evaporator outlet must be able to read a vacuum. This is needed because when the system is operating with R134a, the evaporator is below atmospheric pressure. Further, the range of the differential pressure transducers can be

reduced, from the 0 to 25 psig range used in this refrigerator, to improve the accuracy of the readings. The typical range of pressure drops across both the evaporator and the condenser is roughly 0 to 5 psig.

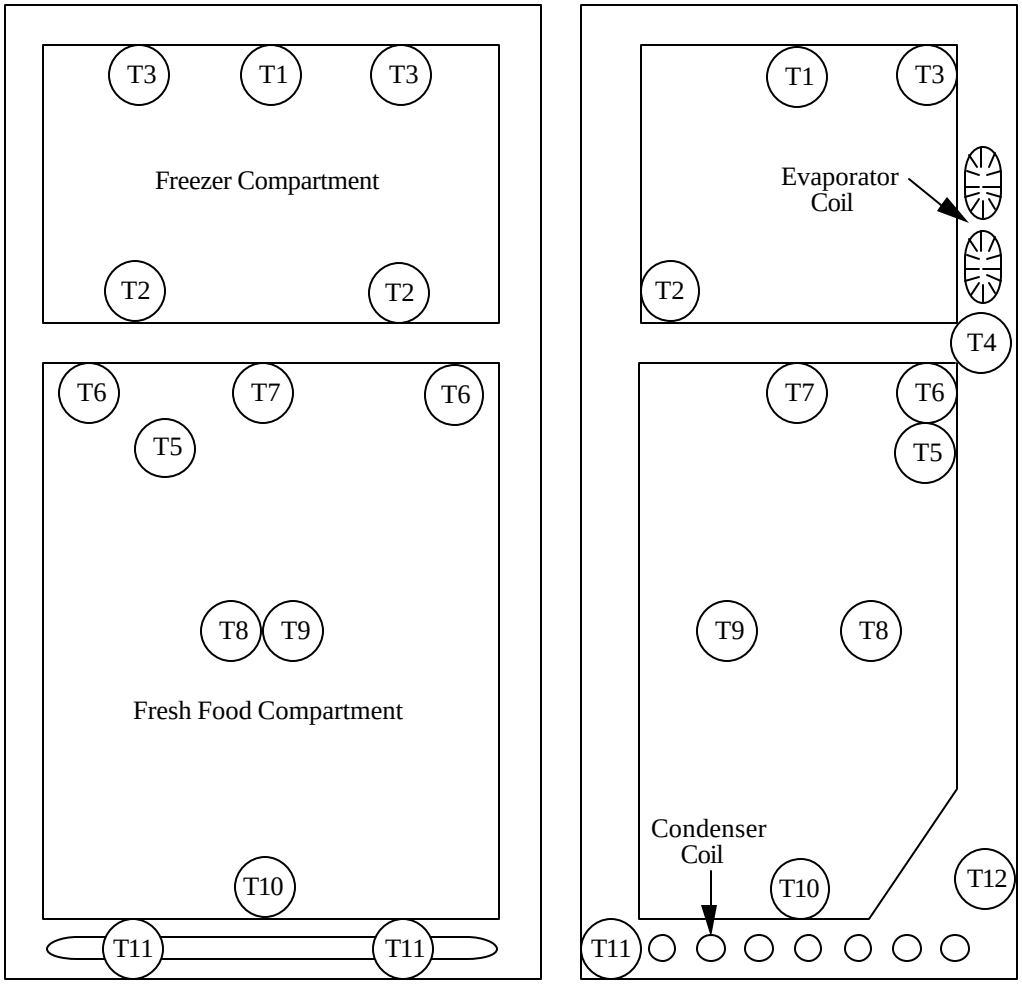

Legend

T1 = Top Freezer Air Temperature
T2 = Return Freezer Air Temperature
T3 = Freezer Supply Air Temperature
T4 = Evaporator Inlet Air Temperature
T5 = Fresh Food Supply Air Temperature
T6 = Fresh Food Return Air Temperature
T7 = Top Fresh Food Air Temperature
T8 = Back Center Fresh Food Air Temperature
T9 = Front Center Fresh Food Air Temperature
T10 = Bottom Fresh Food Air Temperature
T11 = Condenser Inlet Air Temperature
T12 = Condenser Outlet Air Temperature

Figure 3-3. Air Side Thermocouple Layout

The turbine flow meter was only installed for the R134a tests. A description of the system and calibration technique is given by Reeves [1]. The same procedure was followed for this refrigerator. The calibration equation for the flow meter relating the the voltage output to the refrigerant mass flow rate in lbm/hr is given by Equation 3.1. The total uncertainty in the predicted refrigerant mass flow rates from Equation 3.1 is ±2.9%.

$$\text{Mass Flow} = -1.83109 + 3.78474V - 4.59636e^{-3}VT - 4.69389e^{-3}T \ \text{lbm/hr} \qquad (3.1)$$

where V = transducer output voltage (V)

T = subcooled refrigerant temperature (°F)

The power transducers are the same ones used by Reeves [1]. However, they were connected differently. Rather than measure the power input to the condenser fan, the power input to the evaporator fan was measured separately for this refrigerator. Further, the compressor power input was measured independently. The condenser fan power was determined by subtracting the compressor power and the evaporator fan power from the total system power.

The above instrumentation has worked reasonably well although several problems did arise worth noting. The first involves the connections made between the thermocouples and the data acquisition system. Because some of the thermocouples touch metal surfaces, a ground loop was inadvertently set up through the ground connection on the data acquisition input boards (see Reeves [1]). As a result, the thermocouples did not accurately measure temperatures inside the refrigerator. At first the grounding leads were removed but this resulted in electrical noise problems. The solution involved connecting the ground leads through a 1MΩ resistor. The resistor isolated the thermocouples from each other but still allowed voltage spikes to be shorted to ground. The other problem is the effect the above instrumentation has on the performance of the refrigerator. This discussion is taken up in Appendix C.

3.2 Heater System

Steady-state operation of the refrigerator was achieved by using a heater system to maintain constant internal compartment temperatures. The heater system has the capability to maintain both compartment temperatures independent of each other and ambient conditions. A diagram of the heater system is shown in Figure 3-4. The system consists of a PID temperature controller, a hairdryer, a control box for the hairdryer and a watt transducer. Note that two identical systems were built, one for the fresh food compartment and one for the freezer.

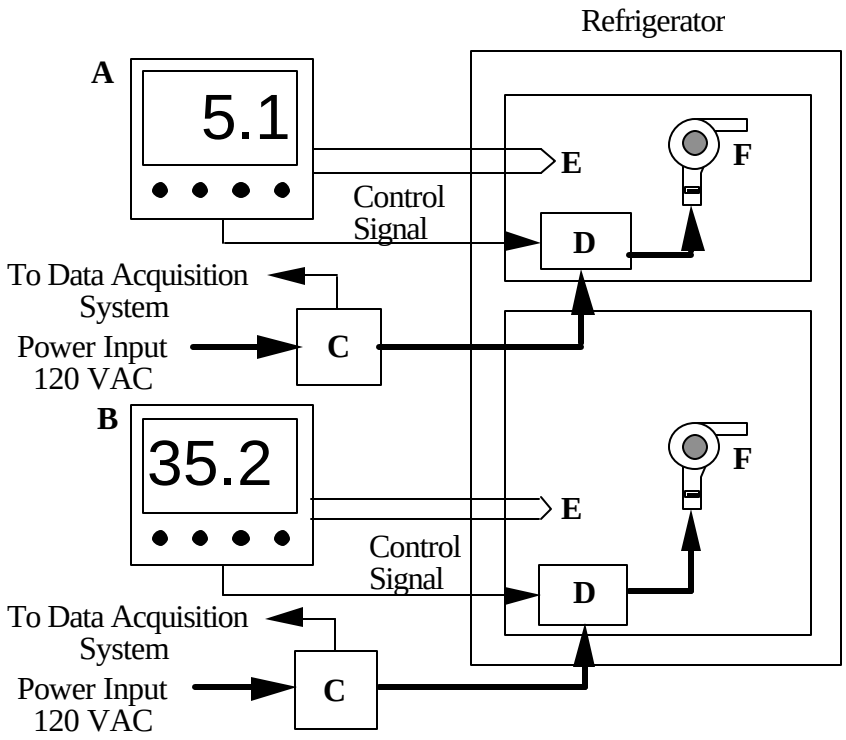

A Freezer Temperature Controller
B Fresh Food Temperature Controller
C Watt Transducer + Signal Conditioner
E Type T Thermocouple
F Hairdryer Assembly
D Control Box

Figure 3-4. Heater System

The operation of the system is relatively simple. Based on the temperature setpoint inputed by the user and the cabinet temperature measured with the thermocouple, the PID controller outputs a pulse width modulated signal to the control box. The control box contains the appropriate electronics to switch power on and off to the hairdryer heater element. The watt transducer and associated circuitry outputs the average power dissipated by the hairdryer. Both the power input to the hairdryer and the compartment temperatures are recorded by the data acquisition system.

The electrical circuit for the heater system is shown in Figure 3-5. The control box contains the transformer to drive the fan motor in the hairdryer and a solid state relay. It is the solid state relay that does the actual power switching in response to the input signal from the PID controller. Since these components dissipate part of the energy measured by the watt transducer, the control box is located inside the refrigerator as shown in Figure 3-4 to eliminate a source of error in determining the load on the refrigerator.

The hairdryer is a standard commercially available model. The heater elements were wired in series to reduce the maximum power output of the hairdryer. The high/low selector switch controls the power input to the heater element, nominally either 300W or 150W respectively. Note that the fan is wired so that it runs continuously.

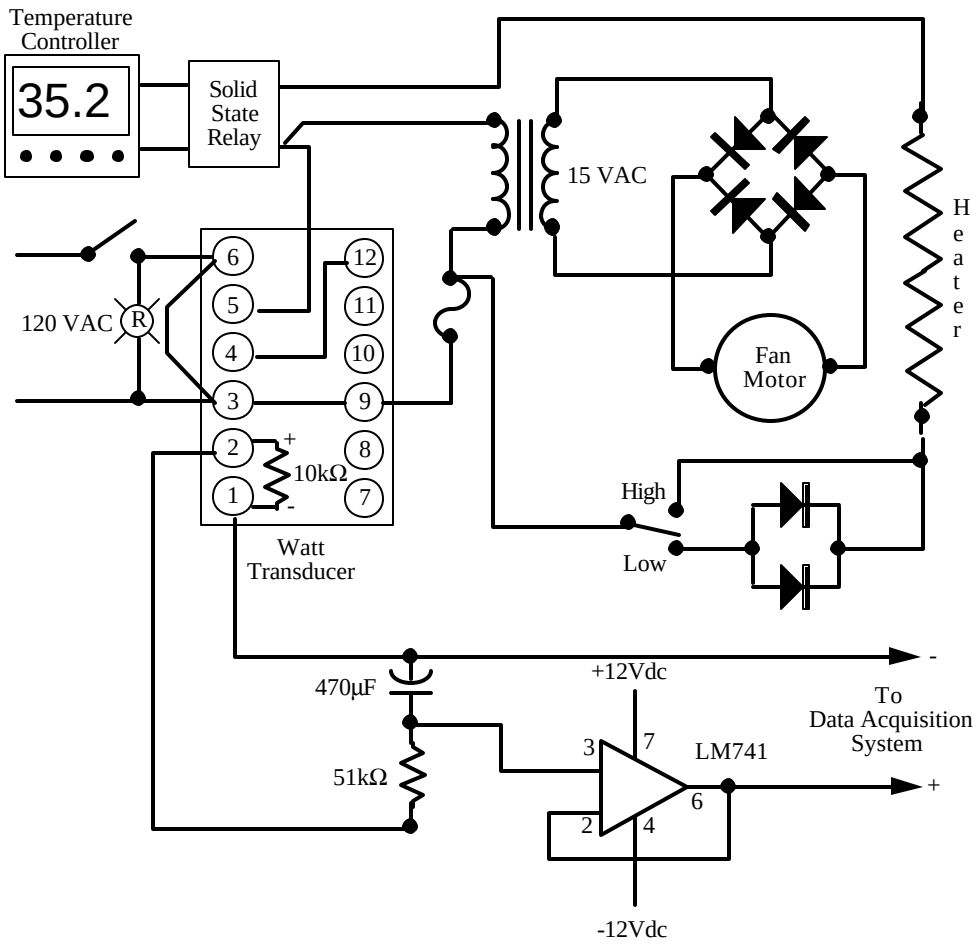

Figure 3-5. Heater System Circuit

Handling the output from the watt transducer is complicated by the fact that power to the hairdryer is not steady but fluctuating. To better understand this it is instructive to look at how the controller works. Figure 3-6 below shows what this controller output looks like. The output is essentially a square wave. When the controller output is at 5V, the solid state relay is activated sending power to the hairdryer heater element. When the output drops to 0V, only the fan in the hairdryer is drawing power. Note that the square wave output has a period of 1 sec. By varying the width of the pulse from zero to one second, the power to the hairdryer can be varied from just the fan running to full power to the heater element. The controller can maintain the temperature in a given compartment by adjusting the power input to the hairdryer heater element.

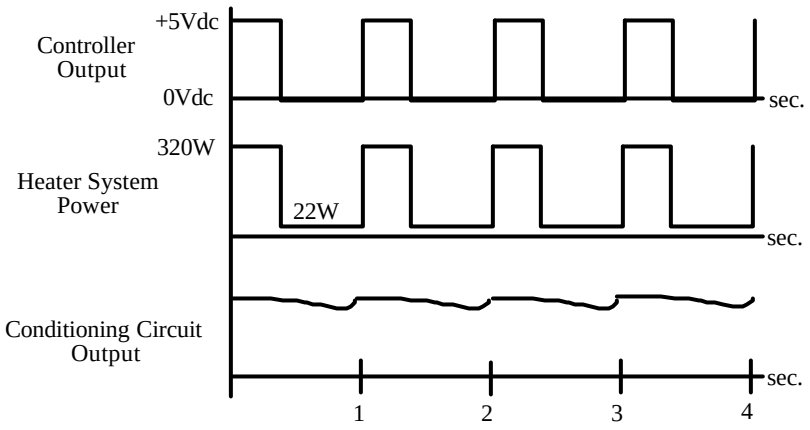

Figure 3-6. Heater System Control Signals

The heater system power in Figure 3-6 shows the theoretical response of the watt transducer to the fluctuation in the power input to the hairdryer. It basically follows the square wave output of the controller. However, the average power dissipated by the heater system is the quantity of interest not the instantaneous power. To obtain the average power, a simple filter circuit containing a resistor and a capacitor was added to the output circuitry of the watt transducer as shown in Figure 3-5. A time constant of 24 sec. was chosen for the RC network to reduce the voltage ripple in the output to a minimum. The conditioning circuit output in Figure 3-6 shows a facsimile of the result. This filtered signal is feed to the data acquisition system and converted into an average power measurement.

Finally the purpose of the operational amplifier should be noted. Measurements of the conditioned watt transducer output with a voltmeter and the data acquisition system revealed a discrepancy. The data acquisition system always measured a lower voltage. It was found that the input impedance of the data acquisition system is only 200kΩ. Because the filter circuit contains resistances of the same order of magnitude as the input impedance of the data acquisition system, the voltage signal is attenuated. To alleviate the problem, the operational amplifier was added and wired to function as a voltage follower with essentially infinite input impedance and zero output impedance. With the op-amp installed, no difference could be observed between the voltmeter and the data acquisition system.

Because the complication of fluctuating power necessitated the need for filtering circuits, it is important to verify that the actual power being utilized is correctly measured by the data acquisition system. It is also important to determine if the watt transducer can respond to the fluctuating power signal without attenuation of the output. To this end, Figure 3-7 shows a temporary modification to the heater system for the purpose of testing the accuracy of the power measurements.

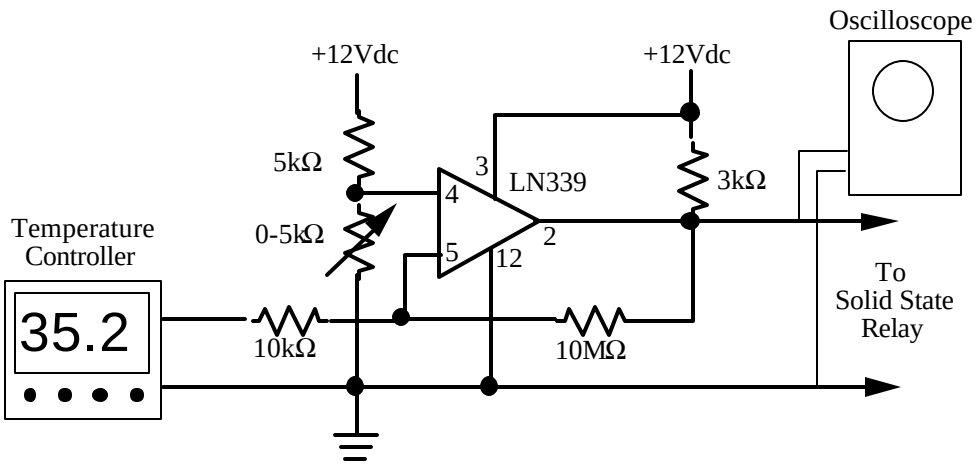

Figure 3-7. Power Verification Circuit

The circuit is the same as before except for the addition of a voltage comparator. Since the output of the temperature controller is not a true square wave, it was difficult to determine exactly when the state, either on or off, of the solid state relay changes. To remove this uncertainty, the voltage comparator shown was inserted between the temperature controller and the solid state relay to clean up the output of the temperature controller. The comparator was set with the potentiometer to trigger at 4.5 Vdc.

With a storage oscilloscope connected across the output of the comparator circuit, a direct measurement of the amount of time the hairdryer heater element is drawing power during the one second cycle period can be made. Further, the power utilized by the hairdryer when current is supplied continuously was measured with a voltmeter. Two measurements of this kind were made, one with just the fan running and one with full power to the heater element. These two power levels are constant. Given this fact, it is possible to calculate the average power dissipated from

$$\text{Average Power} = (\%\ \text{heater on time})(\text{full power}) + (1-\%\ \text{heater on time})(\text{fan power}) \qquad (3.2)$$

where full power = 267W

fan power = 20W

Equation 3.2. The time percentages are calculated from the oscilloscope data. Note that this equation is only valid for the one second cycle rate of the controller. Further note that the maximum and minimum power are dependent on line voltage, which is not constant.

A comparison of the result from the calculation above can be made with a voltmeter measurement of the output from the RC network of the watt transducer. If the watt transducer is correctly following the fluctuation in power and the filter circuit is working properly, the two numbers should be the same. Table 3.1 shows the results of the comparison. A maximum percent difference of -10.1% is reasonable. The watt transducers therefore are correctly measuring the actual power being dissipated by the hairdryers.

Table 3.1. Watt Transducer Verification Data

Transducer Output (Vdc)	Watt Transducer Power (W)	% Time at Full Power	Calculated Power (W)	Error (%D)
1.67	84	23	77	-8.3
1.62	81	25	81	0.0
1.68	84	28	89	6.0
2.75	138	42	124	-10.1
2.61	131	43	126	-3.8
2.56	128	43	126	-1.6
3.44	172	60	168	-2.3
3.3	165	60	168	1.8
3.29	165	60	168	1.8

Although the heater system works reasonably well some comments should be made about difficulties with the system. The first difficulty concerns tuning the controllers. For reference, the settings for the controllers are listed in Table 3.2. It was originally intended that both integral and proportional control would be used. However, it was discovered that only the proportional function could be utilized. Using integral control resulted in oscillations in the refrigerator compartment temperatures.

The cause is subtle. Even though the control signal may change state, a solid state relay has the characteristic that it will not turn off or on until the line voltage passes through zero. It is not possible to turn the relay off or on in the middle of a cycle. With a line frequency of 60Hz, power can only be delivered to the heaters in discrete quantities of 1/120 of the total output from the heater i.e. one half cycle of power. As a result the output from the heater does not vary continuously but changes in discrete steps. For the total heater output of 300W the power changes in steps of 2W. Normally this small change would not be a problem. Unfortunately for a refrigerator though, a few watts represents a measurable temperature change. Temperature oscillations occur because the controller temperature resolution is smaller than the temperature change caused by 2W. To prevent the oscillations, the solution is to turn off the integral control and only use proportional control. However, proportional control inherently results in a temperature offset from the set point. Although this is not fatal it is a source of irritation because the actual desired set point can not be inputed directly into the controller; the offset must be accounted for.

There are two improvements to the system that would be desirable. The first is replacing the pulse width modulated output of the current controller with a proportional voltage output. This signal could be used to drive a variac or the electronic equivalent of it. The variac would change the voltage level to vary the heater power instead of the length of time full power is applied. A continuous current would eliminate the need for the RC circuit and make performance verification easier. Further the elimination of the RC circuit would possibly allow some transient data to be taken for which the current system is unsuitable. The second improvement would be to install a power conditioning unit because the line voltage is not very stable. As a result, the maximum power output of the hairdryer fluctuates making it harder on the controller system to maintain a constant temperature.

Table 3.2. Heater System Controller Settings

Freezer Controller				Fresh Food Controller			
Function #	Setting		Setting	Function #	Setting		Setting
1	0.0	13	0	1	0.0	13	0
2	0.0	14	0	2	0.0	14	0
3	00	15	0	3	00	15	0
4	1	16	6	4	1	16	6
5	5	17	1	5	7	17	1
6	1	18	1	6	1	18	1
7	2	19	0	7	2	19	0
8	1	20	0	8	1	20	0
9	-1.8	21	0	9	-7.8	21	0
10	0	22	1	10	0	22	1
11	0	23	2	11	0	23	2
12	0			12	0		

References

[1] Reeves, R.N., Modeling and Experimental Parameter Estimation of a Refrigerator/Freezer System, Air Conditioning and Refrigeration Center, Dept. of Mechanical and Industrial Engineering, University of Illinois at Urbana-Champaign, 1992, Chapter 5, pp. 30 to 41.

Chapter 4: Experimental Procedure

4.1 Refrigerator Testing

For the purpose of parameter estimation, it is desirable to operate the refrigerator over the widest range of test conditions as possible. To accomplish this both the evaporator inlet air temperature and the condenser inlet air temperature must be varied. These two temperatures are the controlling parameters affecting the performance of the vapor-compression system.

The condenser inlet air temperature was controlled by changing the operating temperature of the environmental chamber. The refrigerator was run at four ambient temperatures: 55°F, 70°F, 90°F, and 100°F. At each one of these ambient conditions the evaporator inlet air temperature was varied by changing the temperature settings of the auxiliary heaters. The typical range of inlet temperatures was from 0°F to 70°F. For some test conditions it was not possible to reach the upper temperature limit. This resulted from the fresh food compartment temperature approaching the room ambient temperature with the heater in this compartment set at its' lowest power setting or even off. At no time were either the fresh food compartment or the freezer compartment operated above ambient conditions for the steady state tests. If this were to occur for a compartment, the cabinet heat load for that compartment would be reversed.

For all tests the anti-sweat heater and the defrost controller were disabled. The defrost controller had to be disconnected to prevent the refrigerator from going into a defrost cycle in the middle of a test. Further, the freezer temperature control damper located in the fresh food compartment was set to the middle position. Lastly, the refrigerator was positioned with the back of the refrigerator as close to the wall as possible without going below the specified minimum clearance of one inch.

The refrigerant charge was optimized for steady-state operation by running a series of charge optimizing tests. An explanation of the tests and the results can be found in Appendix C. The optimum charge was different for the R12 and R134a tests. However, for each refrigerant tested the charge was kept constant for that refrigerant. The system pressure when the refrigerator was turned off and the system temperatures equalized to 70°F was monitored. If the pressure decreased by more than a few pounds, the system was recharged. Note that the pressure measured in the system is below the saturation pressure at the ambient temperature of the system. It can't be directly concluded that the refrigerant in the system is superheated. The presence of a large amount of oil, about 8 ounces, alters the vapor pressure of the refrigerant. This effect must be considered when determining whether saturated or superheated refrigerant exists in the system.

A typical test run involved inputting the desired temperatures for the fresh food comp artment and the freezer compartment into the auxiliary heater system controllers. Usually it would take one to two hours for the system to reach steady state. Some care should be exercised in deciding if the refrigerator has reached steady state. For these tests, steady state conditions were assumed if after 50 minutes the average fresh food and freezer compartment temperatures did not vary by more than 0.5°F during that time period. It was found that if shorter time periods were taken such as 10 minutes it would appear that steady state conditions had been reached when in fact the temperatures were still changing. Once steady state conditions had been reached data was collected every two minutes for a minimum of at least one hour. This provided at least 30 measurements on which to base averages.

The refrigerator was operated as long as possible without having to allow the system to defrost. To facilitate checking for frost, a small Plexiglass window was installed over a hole in the sheet metal divider between the evaporator coil and the freezer compartment. Periodic checks were made to see how much frost had formed. When noticeable frost formed on the coil, the system was shut down to allow the coil to warm up to melt the frost. The time period between defrosts was usually two to three days.

Some comments should also be made about the heater system. As discussed in the instrumentation chapter, the heat controllers had to be set up as proportional only controllers. A fundamental characteristic of proportional control is the fact that there will always be an offset between the temperature entered into the controller and the actual temperature in the system. This is somewhat inconvenient but the system will still provide the desired temperature. The only complication is adding an offset to the temperature entered into the controller. Typically this offset is of the order of 5°F to 10°F. Note that once steady state conditions have been reached a 2°F set point change, for example, will result in a 2°F change in the measured temperature. Therefore the measured temperature can be adjusted to the within the sensitivity limit of the controller or ±0.1°F.

The heater elements that are controlled are contained inside domestic hairdryers. The hairdryers were placed in the bottom of each refrigerator compartment. Further, the hairdryers were positioned such that the warm air discharge was directed toward the top of the compartment and away from the front of the refrigerator. In this way the dynamic air pressure on the gaskets was minimized. It was found that the temperature gradient in the compartments with the hairdryers operating was on the order of a few degrees. This is equivalent to the temperature gradients in the compartments when the refrigerator is running in normal cycling operation. Lastly some care should be taken not to run the hairdryers much above 105°F. At these elevated temperatures, the insulation on the motor windings break down leading to the motor shorting out.

Some care should also taken to ensure that the operating pressures and temperatures don't exceed the range over which the compressor is designed to operate. It is important that the discharge pressure does not go too far above the highest recommended pressure. If the pressure is too high the discharge temperature will be high enough to cause valve damage and accelerate the breakdown of the compressor oil. This will lead to compressor failure. The suction side of the compressor should also be monitored. It is possible to have liquid refrigerant drawn into the compressor even after going through the interchanger. This operating condition should be avoided because of the potential of damage to the compressor.

Finally, the pressure transducers and the thermocouples were periodically checked for drift in calibration. When the vapor compression system was open to the atmosphere for repairs or modifications, the gage pressure transducers were zeroed. Further, the differential pressure transducers were zeroed when the system was turned off and in equilibrium with the environment. The thermocouples that were accessible were immersed in an ice bath to check their calibration. These procedures should be carried out particularly after modifications to the system or instrumentation.

4.2 R134a Refrigerator Conversion

The conversion of the refrigerator for use with R134a required four basic modifications to the vapor compression system. The capillary tube/suction line interchanger had to be replaced. Further, the compressor was

replaced and the turbine flow meter was added. Lastly, the filter dryer had to be replaced with one that is compatible with R134a.

After the old compressor and interchanger were removed, the system was flushed to eliminate as much of the remaining mineral oil from the system as possible. Clean R11 was run from a refrigerant tank through the system to another tank in ice water for a 24 hour period. The difference in vapor pressures forced the liquid R11 through the system. The system was then evacuated for another day to remove any residual R11. The refrigerator was now ready for the new components.

The capillary tube/suction line interchanger was replaced with the same size suction line and initially a 0.026" I.D. capillary tube as suggested [1]. The filter drier and the turbine flow meter were installed next. The new compressor was installed last. The new compressor was charged with an ester oil. Since esters are hygroscopic, great care was taken to make sure the compressor was exposed to the atmosphere for the shortest period of time as possible.

Initial tests with the 0.026" capillary tube resulted in little cooling effect in the evaporator. As a result, the capillary tube was replaced with the same size tube, 0.028" I.D., as was used in the original R12 system. For both cap tube sizes, the length of the cap tube was progressively shortened and the effect on system performance determined. The objective was to make the cap tube as short as possible thus increasing system capacity and still maintain subcooling in the condenser. Subcooling in the condenser is an absolute necessity if the turbine flow meter is to function properly. The final length of the cap tube for the R134a system was 10ft. It was noted that changes in cap tube length have a small effect on system performance while changes in internal diameter have a large impact. Note that after the R134a data set was taken the cap tube was shortened another two feet to see if lower superheat data could be obtained. This modification did not change system performance at all.

Table 4.1 summarizes these modifications to the system. All other components were left unchanged from the original R12 system.

Table 4.1. Summary of R134a System Modifications

Refrigerant	Cap Tube Size (I.D.)	Cap Tube Length (in.)	Compressor Model	Compressor Oil	Displacement Rate (ft^3/hr)
R12	0.028"	80.7	MEI D123	Mineral Oil	53.2
R134a	0.028"	120	MEI D128	Ester - Kyoto Oil # MR-5-22	67.2

References

[1] Personal communication., Mr. Tom Benton., General Electric Company, Appliance Park, Louisville, Kentucky, 40225.

Chapter 5: Overview of Parameter Estimation

5.1 Refrigerator State Points

Before looking at the models for the components in the refrigerator/freezer, it is helpful to touch on some of the aspects of parameter estimation that is common to all the components. The first important topic is the nomenclature for the state points used in the parameter estimation equations. Figure 5-1 shows the refrigeration system in the refrigerator/freezer with the state points for each component labeled. The diagram also shows the control volumes as dashed lines that were used for each component. The reader should refer to this diagram as needed when reading Chapters 6 through 9.

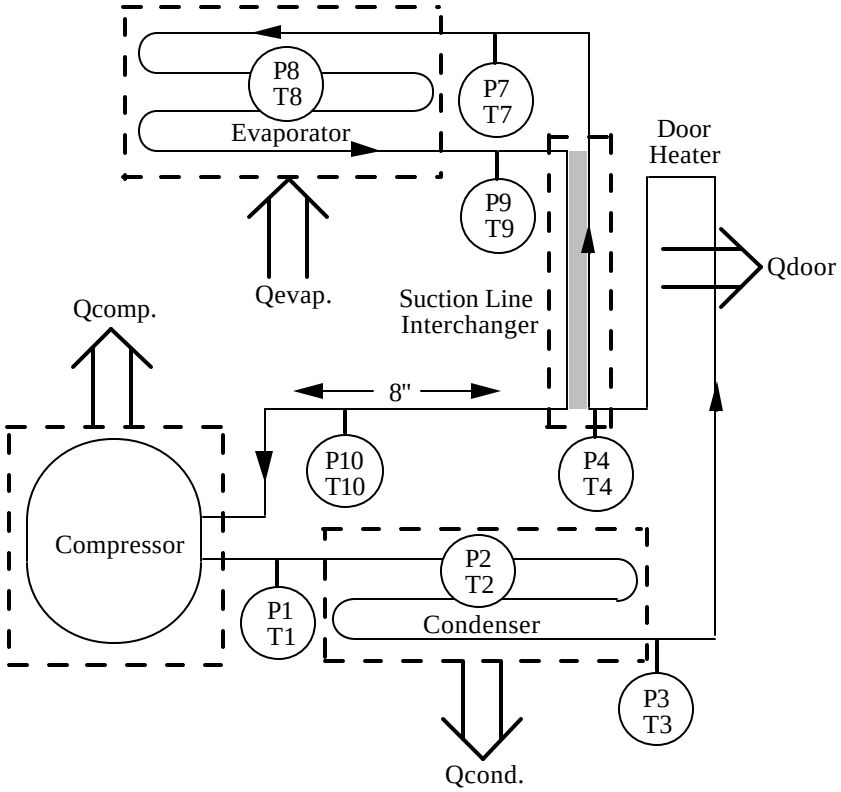

Figure 5-1. Refrigerator/Freezer State Point Diagram

5.2 Optimization Techniques

Two basic techniques were used to determine the best estimates of the parameters in the models. The first method of non-linear least squares [1] was used for the interchanger and the compressor shell heat transfer parameters. The method is relatively straight forward. Suppose for example that two quantities y and x are measured in the lab. Further it is desired to find a functional relationship between y and x such that given an x value y can be predicted. For the parameter estimation work considered here x is usually a temperature or pressure etc. and y is a heat transfer rate. The functional relationship between the two variables must be assumed and usually comes from such things as energy balances based on the first law of thermodynamics etc. For this discussion it is assumed that this quantity y is related to the quantity x by Equation 5.1. Because of data scatter and the assumption that Equation

5.1 describes the physical process fully which may not be entirely true, the values of y predicted by Equation 5.1 for a given x will not exactly equal the experimental y.

$$y = mx^2 + b \tag{5.1}$$

However, if the assumed functional relationship is good, the difference between the predicted y from Equation 5.1 and the measured y will be small. It is natural to ask if it is possible to find values for the constants m and b which will minimize this difference. Indeed, this minimum difference occurs when the derivative of Equation 5.1 with respect to the constants m and b for all the data points is zero. This statement is translated into mathematical form by Equation 5.2 and 5.3 where n is the number of data points.

$$\frac{\delta}{\delta m}\sum_{i=1}^{n}\left[y_{measuredi} - y_{predictedi}\right]^2 = \frac{\delta}{\delta m}\sum_{i=1}^{n}\left[y_{measuredi} - (mx_i^2 + b)\right]^2 = 0.0 \tag{5.2}$$

$$\frac{\delta}{\delta b}\sum_{i=1}^{n}\left[y_{measuredi} - y_{predictedi}\right]^2 = \frac{\delta}{\delta b}\sum_{i=1}^{n}\left[y_{measuredi} - (mx_i^2 + b)\right]^2 = 0.0 \tag{5.3}$$

Equation 5.2 and 5.3 form a system of two equations in two unknowns, m and b. They can be solved for example by a Newton-Raphson routine. Note that the differences are squared so that only positive errors are added. For the parameter estimation work for the interchanger and the compressor, similar systems of non-linear equations were solved by a commercial package called Engineering Equation Solver or E.E.S.[2].

This software has the great advantage of having refrigerant property routines are already built into the program. This eliminates the need to develop separate property routines. The program also allows parametric studies to be easily carried out. However, the program has an upper limit on the number of equations it can solve. As the complexity of Equation 5.1, for example, increases the number of equations also increases. For the evaporator and the condenser parameter estimation work, the number of equations exceeded the capability of the program. As a result a different approach had to be taken.

This problem was solved by writing a computer program to find the best estimates of the parameters being sought. The program was written in True Basic [3] and is listed in Appendix E. The general process of finding the best estimates of the parameters involves calculating the sum of the squared differences between the measured and predicted variables and deciding how to change the parameters to minimize these differences. The first major task performed by the program is to calculate the sum of these differences for all data points or equivalently to evaluate the objective function. A typical objective function for the condenser is given by Equation 5.4.

$$\text{Objective Function} = \sum_{i=1}^{n}\left[\dot{Q}c_i - \dot{Q}crate_i\left(U_{desup}, U_{2ph}, U_{sub}\right)\right]^2 \tag{5.4}$$

where $\dot{Q}c$ = measured condenser heat transfer rate (Btu/hr)

$\dot{Q}crate$ = predicted condenser heat transfer rate (Btu/hr)

n = number of data points

U_{desup} = conductance of desuperheating section (Btu/hr-ft^2°F)

U_{2ph} = conductance of two-phase section (Btu/hr-ft^2°F)

U_{sub} = conductance of the subcooled section (Btu/hr-ft^2°F)

$\dot{Q}\,crate_i$ is determined from a system of effectivenes-NTU equations which contain the U parameters. These equations will be discussed in Chapter 7. To solve this system of nonlinear equations, a set of Newton-Raphson routines were used. The routines required are subroutine nr, subroutine calcfp, subroutine calcr, subroutine nzero and subroutine xgauss (see Appendix E). The subroutine calcr contains the effectiveness-NTU relations in residual form.

The subroutine object for objective function evaluates Equation 5.4 by calling the Newton-Raphson routines for each data point and summing the squared error. Note that during the evaluation of Equation 5.4, the parameters that are being sought; U_{desup},$U_{2ph,}$ and U_{sub}; are constants. Both the R12 and R134a data sets contain approximately 30 points. One evaluation of the objective function requires the solution of approximately 30 sets of 12 simultaneous equations. This involves a fair amount of number crunching so an efficient optimization routine is a necessity.

The next task is to vary the parameters U_{desup},U_{2ph}, and U_{sub} such that the objective function is minimized. To carry this out, the method of steepest-descent was used [4]. The basic process is to first calculate the gradient at the current estimate of the parameters. The gradient indicates the direction of greatest change in the objective function. The subroutine grad does the needed calculations. The next step is to search in the direction of the gradient to find a new minimum in that direction. When this point is found the parameters are updated and the process is repeated. The process continues until the components of the gradient vector approach zero which occurs at the true minimum of the objective function.

The subroutine fibonacci (See Appendix E) performs the actual search procedure in the direction of the gradient. The routine is based on a Fibonacci search method [4]. This method is more efficient than an exhaustive search or dichotomous search because it requires the fewest number of function calls. As noted above each objective function call is time consuming so it is very desirable to minimize the number of calls required. The routine was written so that it could be used either to search for a minimum in a specified direction or perform a univariate search in a direction parallel to a given parameter axis.

Unfortunately no one optimization method will work in all cases. Many types of problems can be encountered. One problem that arises in this particular case is the existence of long, narrow, curved valleys in the objective function. Contour plots for the actual surfaces will be shown in the appropriate chapters. Figure 5-2 shows a contour plot of some hypothetical objective function. The method of steepest-descent will find a minimum for example at a point formed by the intersection of lines aa and bb. However, once in the valley the method searches back and forth across the valley, only very slowly progressing toward the true minimum.

To speed convergence it is necessary to search in a different direction. The direction to search in is found by determining a new estimated minimum, i, near the old estimate. A linear curve fit of these two points forms a line, indicated as the dotted line cc, directed along the valley floor. Searching along this line moves the estimated minimum closer to the true minimum much more quickly. By repeating both the gradient search and this search routine, the true

minimum can be found. As a final check to see if the true minimum has been found, a lattice search in directions parallel to the parameter axis and on diagonals is performed.

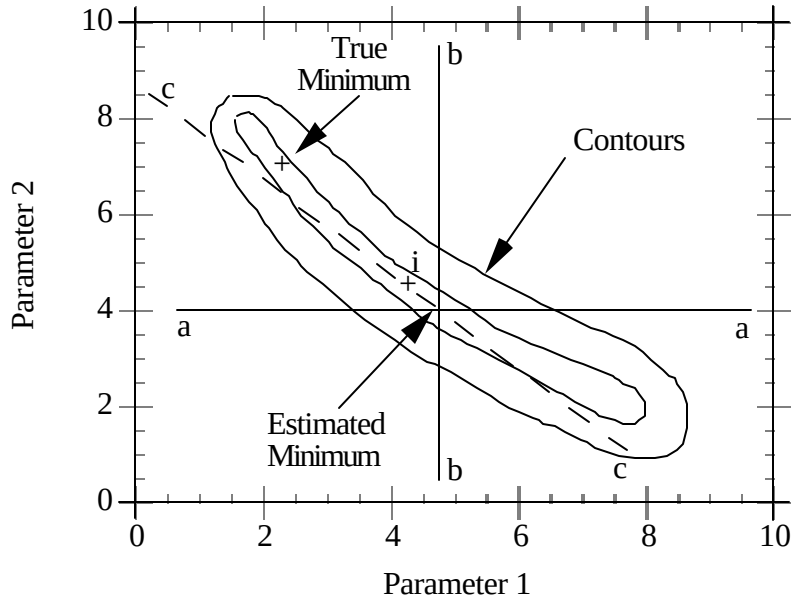

Figure 5-2. Contour Plot of a Hypothetical Objective Function

Figure 5-2 also illustrates a problem in using either a simple lattice search or a multivariate search [4] only. Once at the estimated minimum, searching along line aa or bb will indicate that the objective function increases along both lines. It could then be erroneously concluded that the true minimum had been found. This problem can be partially avoided by searching along diagonals. However, the number of function calls increases rapidly and therefore slows convergence.

Although the program did a fairly good job, it was slow. A typical computer run would take many hours before convergence was obtained even with the efficient search routines. As a possible alternative, a Gauss-Seidel iteration technique could be used to solve the system of equations resulting from a non-linear least squares approach.

5.3 Experimental Uncertainty Analysis

As part of the experimental effort, estimates of the uncertainties in the experimental measurements such as pressure and temperature were determined. Further, these uncertainties were then used to estimate the uncertainty in the calculated quantities such as heat transfer rates. It is absolutely imperative that such calculations be made. The uncertainties, even though estimates, give a feel for how well a quantity is known. This is particularly important when trying to make comparisons.

For example, suppose two different data sets show the effectiveness of the interchanger to be 0.7 for the first set and 0.8 for the second set. Many hours would be wasted in trying to explain the increase if the uncertainty in these numbers is ±0.2. It does little good to try to explain trends when the trends are smaller than the uncertainty in

the measurements. To calculate these uncertainties, the method recommended in ASHRAE Guideline 2-1986 is followed [5]. The book by Coleman and Steele also provides an excellent discussion of these topics [6].

The uncertainties in experimental measurements include at least the transducer accuracy and measurement scatter. Other uncertainties can also be introduced as the result of temperature stability or transient response etc. As an example, Figure 5-3 shows a real distribution of steady-state chamber temperature measurements. Because of electrical noise and/or temperature fluctuations, the measured temperature will vary about some mean value. If it is assumed that the distribution in measurements is Gaussian then there is a 95% probability that all of the data points will fall within two standard deviations of the mean. Note this is only true for an infinite number of data points. However, it is very nearly true if the number of data points is at least 30 points or more. Therefore, the uncertainty in the temperature measurement is plus or minus two standard deviations for a 95% confidence level.

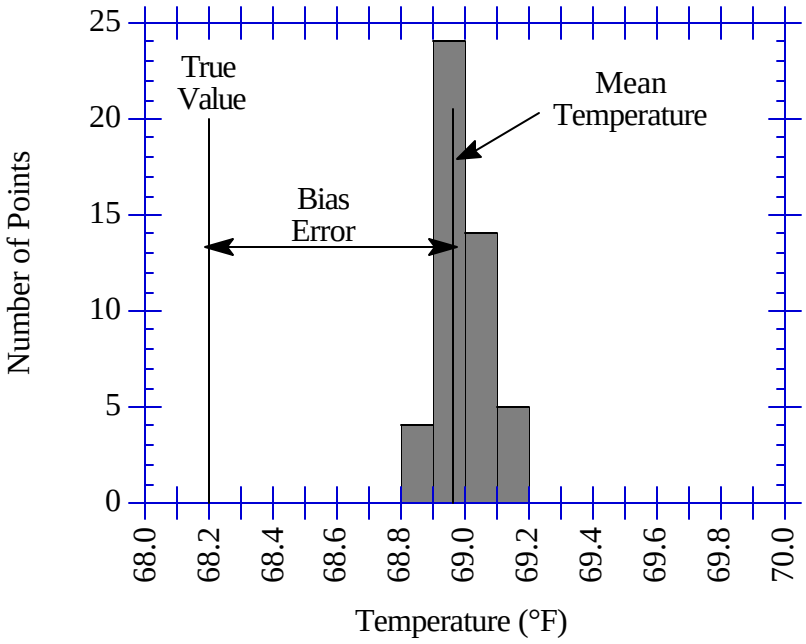

Figure 5-3. Temperature Measurement Uncertainty

However this is only the uncertainty in the temperature measurement due to data scatter. The transducer accuracy must also be accounted for. This number comes from the manufacturer usually in the form of some percentage of the transducer's full scale output. The true temperature falls somewhere between the measured temperature plus or minus this transducer accuracy. The total uncertainty in the temperature measurement is determined from Equation 5.5. Note that the transducer accuracy is also termed the bias error and the data scatter the precision error.

$$\text{Total Measurement Uncertainty} = \sqrt{(\text{BiasError})^2 + (2\sigma)^2} \qquad (5.5)$$

Once the total uncertainties in the measured quantities are known, the uncertainties in calculated quantities can be determined. For example, the uncertainty in the heat transfer rate $\dot{Q}$ in Equation 5.6 results from the uncertainties in the mass flow rate $\dot{m}$ and the enthalpies h2 and h1. The calculation of the uncertainty in $\dot{Q}$ is carried out by evaluating Equations 5.7 and 5.8 for both enthalpies where w() is understood to mean the uncertainty of the quantity within the brackets.

$$\dot{Q} = \dot{m}(h2 - h1) \tag{5.6}$$

$$w(\dot{Q}) = \sqrt{\left(\frac{\delta \dot{Q}}{\delta \dot{m}} w(\dot{m})\right)^2 + \left(\frac{\delta \dot{Q}}{\delta h1} w(h1)\right)^2 + \left(\frac{\delta \dot{Q}}{\delta h2} w(h2)\right)^2} \tag{5.7}$$

where

$$w(h) = \sqrt{\left(\frac{\delta h}{\delta T} w(T)\right)^2 + \left(\frac{\delta h}{\delta P} w(P)\right)^2} \tag{5.8}$$

Each term in brackets is the uncertainty of a given independent variable multiplied by the sensitivity of Equation 5.6 to that independent variable. The derivatives can be evaluated mathematically or numerically. In either case, nominal values of the independent variables must be substituted into the derivative expressions to determine the sensitivities. It is possible that the uncertainty of an independent variable is high while the sensitivity is very small making the uncertainty of the dependent variable with respect to this independent variable small. The converse can also occur.

The terms in brackets in Equations 5.7 and 5.8 also have another useful purpose. Instead of asking how uncertain is the heat transfer rate given the data reduction equation and instrumentation, the reverse question can be asked. How certain do the experimental measurements have to be so that the heat transfer rate is known to within a specified accuracy? This question can be answered by looking at the magnitude of each term inside the brackets of Equation 5.7. For example, it is desired to know the heat transfer rate to within ±50 Btu/hr. The first term in brackets in Equation 5.7 might equal 80 Btu/hr. It could then be concluded that either the accuracy of the mass flow measurement must be increased or some alternate equation that is not as sensitive to mass flow rate must be found. The same analysis can be carried out for each term. However, since each uncertainty is squared, the terms inside the brackets that are larger in magnitude will tend to dominate the uncertainty in the heat transfer rate. Therefore, improvements should be concentrated on these terms first.

This analysis should be carried out before ever going into the lab and taking measurements. It is a total waste of time to spend months setting up instrumentation and taking data only to find out later that the accuracy of a given transducer did not allow determining a quantity to within the desired accuracy. The instrumentation and the equations that are going to be used must be investigated first. Changes in instrumentation or experimental methods up front will help to ensure that the desired results are obtained later.

Equation 5.7 only determines the uncertainty in the heat transfer rate as a result of the experimental uncertainties. For some of the parameter estimation work, a parameter is estimated which is theoretically a constant

such as volumetric flow rate. As a result of scatter in the data, the estimated parameter will be a mean value. A total uncertainty calculated from Equation 5.5 is needed to reflect both the experimental uncertainty and the scatter in the estimates. The standard deviation is based on the differences between the average estimated flow rate and that calculated for each data point.

The calculation of the experimental uncertainties of the measured quantities and calculated parameters are listed in Appendix D. Unless otherwise noted, a given uncertainty is the experimental uncertainty in a parameter, not the total uncertainty. The total uncertainty, where given, will be labeled explicitly. The reader should refer to the calculations in Appendix D as needed to see where the uncertainties originate.

References

[1] Stoecker, W.F., Design of Thermal Systems, Third Edition, McGraw-Hill, New York, 1989, pp. 67 to 70.

[2] E.E.S., F-Chart Software, 4406 Fox Bluff Road, Middleton, WI, 53562.

[3] True Basic., True Basic, Inc., 39 South Main St., Hanover, N.H., 03755.

[4] Stoecker, W.F., Chapter 9.

[5] Engineering Analysis of Experimental Data - ASHRAE Guideline 2-1986., (Available from American Society of Heating, Refrigerating and Air-Conditioning Engineers, Inc., 1791 Tullie Circle, N.E., Atlanta, GA 30329.

[6] Coleman, H.W. and W.G. Steele., Experimentation and Uncertainty Analysis for Engineers, John Wiley & Sons, New York, 1989.

Chapter 6: Compressor Parameter Estimation

6.1 Overview

The development of the compressor model is based on the viewpoint of a system engineer who selects a compressor from commercially available types and sizes. It is assumed that the mass flow rate, the power requirement, and the capacity for this compressor are known functions of the saturated evaporating and condensing temperatures. This information is either found from compressor maps or equivalently from isentropic and volumetric efficiencies. The latter approach will be investigated more fully later as it has some advantages over compressor maps.

6.2 R12 Compressor Maps

Curve fits for the R12 compressor are based on compressor calorimeter data that is summarized in Table 6.1 [1]. The form of the curve fit equations is a blind quadratic given by Equation 6.1. For both the curve fit for mass flow rate and power, the evaporating temperature T_7 and the condensing temperature T_2 are in degrees Fahrenheit.

$$f(T_2,T_7) = (A + BT_7 + C(T_7)^2) + (D + ET_7 + F(T_7)^2)T_2 + (G + HT_7 + I(T_7)^2)(T_2)^2 \quad (6.1)$$

Equation 6.2 lists the curve fit for mass flow rate. Equation 6.3 lists the curve fit for power. Note that these curve fits are valid for an evaporating temperature range from -20 to 10°F and a condensing temperature range from 107 to 130°F.

$$\begin{aligned}\dot{m} &= \left\{ 26.5986 + 0.67125T_7 + 7.22222e\text{-}3(T_7)^2 \right\} \\ &+ \left\{ -3.52355e\text{-}2 - 1.83152e\text{-}3T_7 - 5.36232e\text{-}5(T_7)^2 \right\} T_2 \\ &+ \left\{ -1.50966e\text{-}4 + 5.43478e\text{-}6T_7 + 2.41546e\text{-}7(T_7)^2 \right\} (T_2)^2 \ \{\text{lbm/hr}\}\end{aligned} \quad (6.2)$$

$$\begin{aligned}\dot{P}\,\text{comp} &= \left\{ 347.178 - 6.85444T_7 - 0.991666(T_7)^2 \right\} \\ &+ \left\{ 4.00409 + 0.195135T_7 + 1.69784e\text{-}2(T_7)^2 \right\} T_2 \\ &+ \left\{ -9.06836e\text{-}3 - 4.94638e\text{-}4T_7 - 7.00737e\text{-}5(T_7)^2 \right\} (T_2)^2 \ \{\text{Btu/hr}\}\end{aligned} \quad (6.3)$$

Table 6.1. R12 Compressor Calorimeter Data

T2 °F	T7 °F	Capacity Btu/hr	Power W	Discharge Temperature °F	Suction Temperature °F	Flow Rate lbm/hr
-20	107	746	149	199	92	12
-20	107	752	152	200	94	12.1
-10	107	997	172	203	91	16.1
-10	107	1006	174	204	94	16.2
10	107	1659	221	206	91	26.9
10	107	1654	223	207	92	26.9
-20	115	718	152	201	92	11.6
-20	115	724	153	202	95	11.6
-10	115	965	175	206	91	15.6
-10	115	971	177	207	94	15.7
10	115	1618	228	210	90	26.3
10	115	1620	230	211	92	26.3
-20	130	666	153	207	93	10.7
-20	130	667	154	206	95	10.7
-10	130	908	180	212	92	14.6
-10	130	909	181	212	94	14.7
10	130	1543	240	222	92	25.1
10	130	1549	240	221	93	25.2

Figure 6-1 compares the predicted mass flow rate from Equation 6.2 to the calorimeter data from Table 6.1. As can be seen the biquadratic curve fit does a good job at matching the calorimeter data. The error bounds are ±0.4% with a standard deviation of 0.17%. The total uncertainty in the mass flow rate prediction is unknown because the experimental error in the measurements in Table 6.1 are unknown. However, typical total uncertainties in compressor maps are of the order of ±5% [2,3]. Figure 6-2 compares the predicted compressor power input from Equation 6.3 to the calorimeter data. As for the mass flow rate, the curve fit does a nice job at matching the calorimeter data. The maximum curve fit error is ±1.0% with a standard deviation of 0.26%.

Although compressor maps do a fairly good job at predicting compressor performance, there are several problems associated with their use. The first problem relates to the calorimeter data. As can be seen from Table 6.1, the suction gas temperature at the compressor inlet is kept nearly constant at 90°F. For the refrigerator tested at the standard rating condition of 90°F the suction temperature is indeed close to 90°F. However, the experimental data for the refrigerator using R12 showed the suction temperature to vary from 47°F to 102°F. The variation in suction temperature causes the suction specific volume to change which affects compressor performance. To account for the variation in suction temperatures, it is necessary to apply a correction factor to the map data. For a discussion of the effect of superheat on compressor performance and possible correction factors see Dabiri and Rice [4].

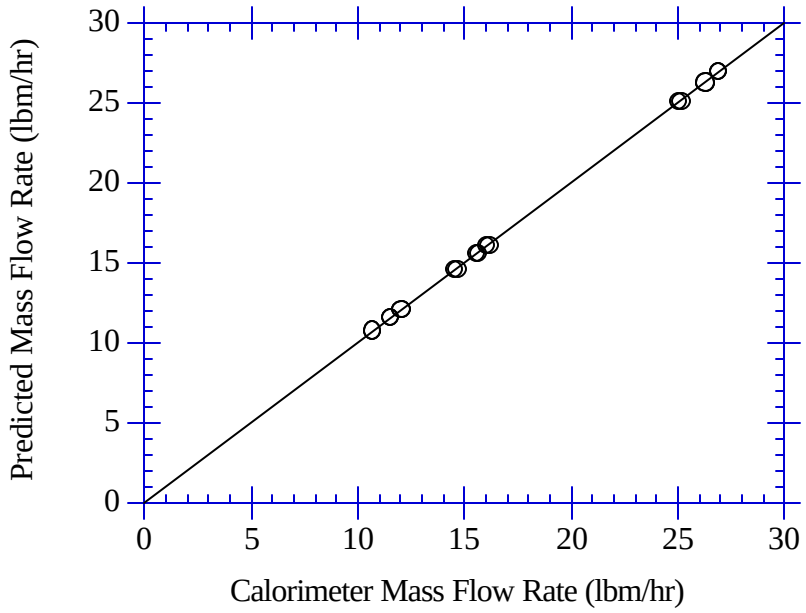

Figure 6-1. Biquadratic Curve Fit of Compressor Calorimeter Mass Flow Data

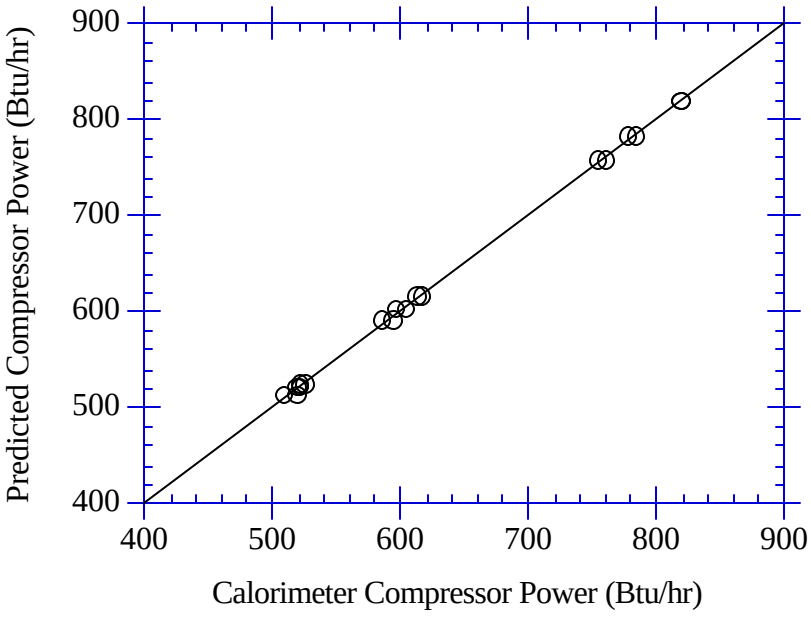

Figure 6-2. Biquadratic Curve Fit of Compressor Calorimeter Power Data

The maps are also based on the assumption that the pressure drops through the heat exchangers and interconnecting piping are zero. Obviously in a real system this is not true. This problem, however, can be overcome by determining fictitious saturated evaporating and condensing temperatures corresponding to the inlet and outlet

pressures to the compressor. Using these temperatures in Equations 6.2 and 6.3 results in a better estimate of the mass flow rate and power consumption in the actual system.

A more difficult problem from an experimental perspective is the limited range of the maps. Figure 6-3 shows all the R12 data points plotted as a function of evaporating and condensing temperatures. The box indicates the range in which the compressor maps are applicable. As can be seen from the graph, only half of the data fall within the range for which the maps can be utilized.

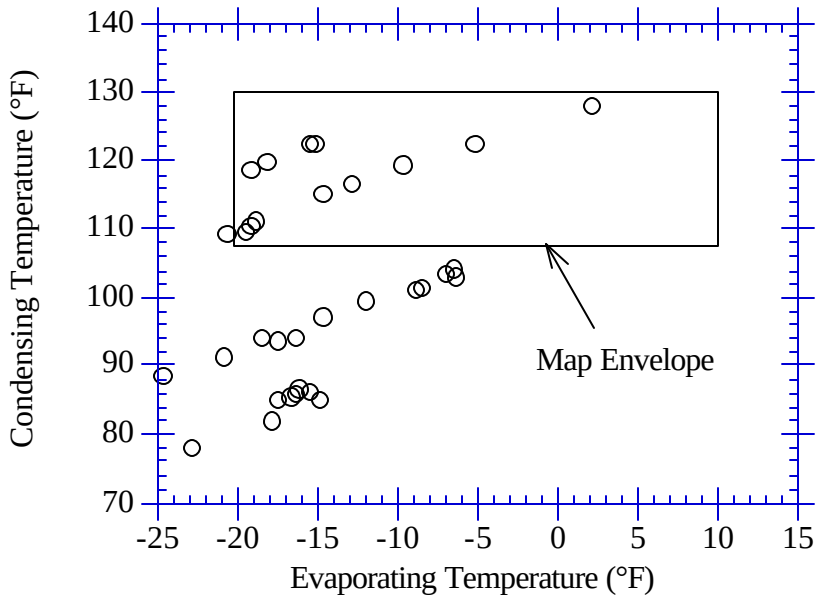

Figure 6-3. Comparison of R12 Data Set to Compressor Map Range

6.3 Volumetric Efficiency Approach for the R12 Compressor

For the purpose of parameter estimation is would be very desirable to use the entire data set. To make this possible, an alternative to the compressor maps must be found. The method finally used takes advantage of the performance characteristics of a reciprocating compressor. For a reciprocating compressor, the mass flow rate through the compressor is given by Equation 6.4 [5].

$$\dot{m} = \eta_v \frac{V_{disp}}{\upsilon_{suc}} \qquad (6.4)$$

where $\dot{m}$ = mass flow rate (lbm/hr)

η_v = volumetric efficiency

V_{disp} = displacement rate (ft^3/hr)

υ_{suc} = suction specific volume (ft^3/lbm)

Further, the power consumed by the compressor can be described by Equation 6.5.

$$\dot{P} = \frac{\dot{P}_s}{\eta_s} \tag{6.5}$$

where $\dot{P}$ = compressor power consumption (W or Btu/hr)

$\dot{P}_s$ = isentropic power consumption (W or Btu/hr)

η_s = isentropic efficiency

By utilizing the calorimeter data in Table 6.1, both the volumetric efficiency and is entropic efficiency can be determined. The volumetric efficiency can be calculated from the mass flow rate, inlet conditions, and the displacement rate. The displacement rate of a reciprocating compressor is a physical characteristic of the compressor and is assumed to be a constant. For the compressor used in the R12 experiments, the displacement rate is 53.188 ft^3/hr [6]. Fortunately, the volumetric efficiency is very nearly a linear function of the absolute pressure ratio of the condensing pressure to the evaporating pressure only [7]. The volumetric efficiency for this compressor as a function of pressure ratio is shown in Figure 6-4.

The value of this approach over using compressor maps lies in the fact that the pressure ratios for all the R12 data points are within the upper and lower bounds of Figure 6-4. Stated differently: for the R12 data points having condensing or evaporating pressures outside the map bounds, it turns out that the ratio of those pressures are within the bounds of the range of ratios in Figure 6-4. The range of the compressor maps can, therefore, be effectively extended by using a volumetric efficiency approach.

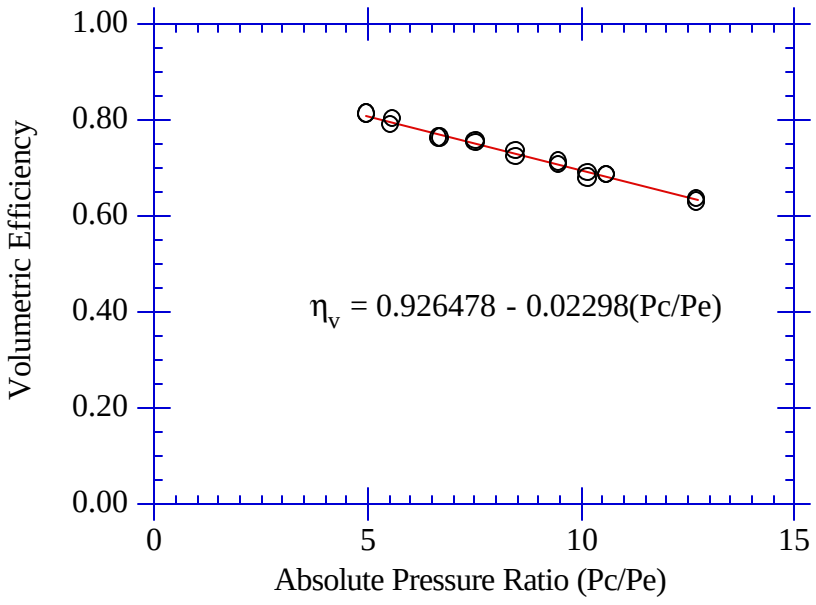

Figure 6-4. Volumetric Efficiency Curve for the R12 Compressor

The use of volumetric efficiency instead of maps also eliminates the problem with varying suction temperatures. Because Equation 6.4 is a function of the suction specific volume, any changes in suction temperature will be reflected in this parameter. The suction specific volume, therefore, automatically accounts for variations in suction temperature. The problem of pressure loss in the heat exchangers is also avoided because Equation 6.4 only depends on inlet and outlet conditions to the compressor.

A similar approach can be used for the compressor power. Like the volumetric efficiency, the isentropic efficiency was determined from the compressor calorimeter data. Further, the isentropic efficiency is also very nearly a linear function of the absolute pressure ratio only. The isentropic power is easily calculated from the compressor inlet pressure and temperature, and outlet pressure. Figure 6-5 shows the relationship between isentropic efficiency and the absolute pressure ratio across the compressor. As with the volumetric efficiency, using an isentropic efficiency effectively extends the range of applicability of the compressor maps.

To check the accuracy of the above approach, it is instructive to compare the mass flow rates and powers determined from Equations 6.4 and 6.5 against the measured values in Table 6.1. Figure 6-6 compares the calculated flow rates against the calorimeter data. As can be seen, the agreement between the calculated mass flow rates and the calorimeter values is very good. The maximum deviation of the predicated flow rates from the calorimeter mass flow rates is ±1.5% with a standard deviation of 0.38%. The same comparison can be made for the compressor power.

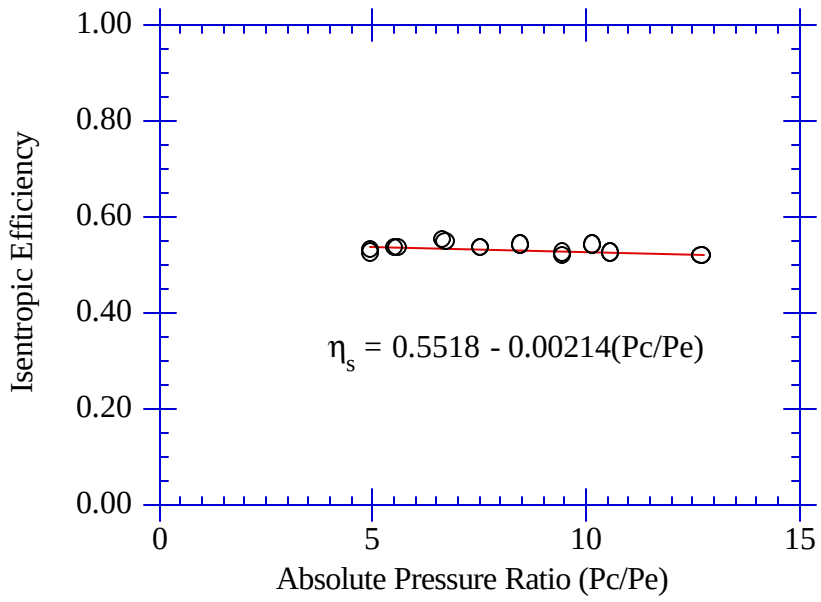

Figure 6-5. Isentropic Compressor Efficiency Curve for the R12 Compressor

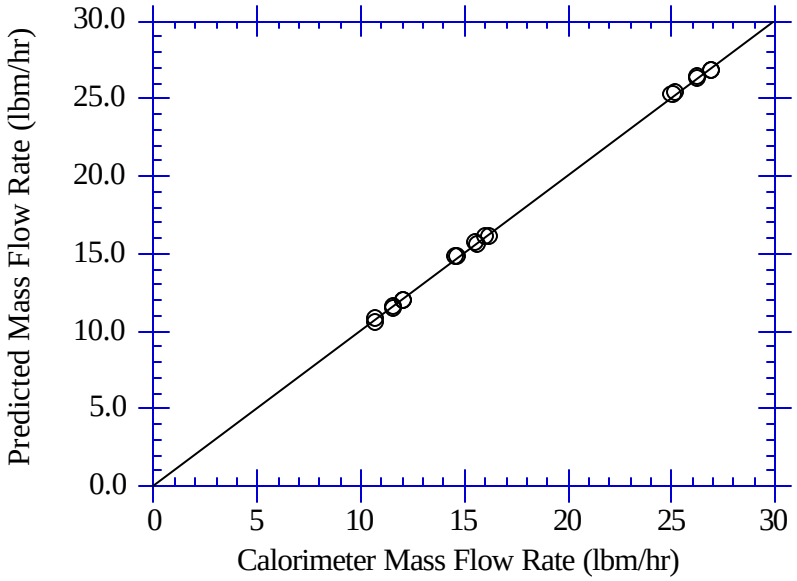

Figure 6-6. R12 Mass Flow Rate Curve Fit Using Volumetric Efficiency

Figure 6-7 shows this comparison. The maximum deviation between the predicted powers and the calorimeter data is ±2.6% with a standard deviation of 0.83%. Although these curve fits are not quite as good as the biquadratic fits, the slight increase in error is more than offset by the wider range of applicability.

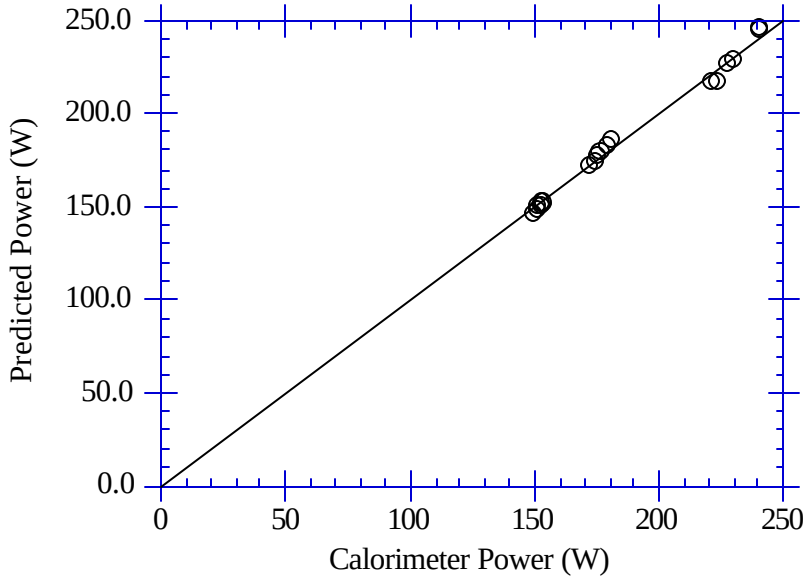

Figure 6-7. R12 Compressor Power Curve Fit Using Isentropic Efficiency

6.4 Volumetric Efficiency Curve Fits for the R134a Compressor

Converting the refrigerator for use with R134a required replacing the R12 compressor with a compressor having a larger volumetric displacement. Compressor maps were not available for the new compressor using R134a. To take their place, the mass flow rate through the system was measured with a turbine flow meter. Further, the power input was also measured directly. These measurements provided all the necessary information for parameter estimation. However, for the purpose of modeling the new compressor, the volumetric efficiency and isentropic efficiency are needed.

The volumetric efficiency from Equation 6.4 was calculated for all points in the R134a data set and plotted against the absolute pressure ratio in Figure 6-8. The experimental uncertainty in the volumetric efficiency is ±0.056 with a standard deviation in the linear curve fit of 0.03. The total uncertainty in the equation for volumetric efficiency is ±0.082. The volumetric efficiencies are based on the compressor having a displacement rate of 67.2 ft^3/hr [8]. Note that the large uncertainty in the absolute pressure ratio is caused by the uncertainty in the suction pressure (see Appendix D).

The y-intercept for the volumetric efficiency equation is 1.27 which is physically not possible. This suggests that the volumetric efficiency is not a linear function of absolute pressure ratio from a pressure ratio of 0 to 16. The equation should, therefore, only be used within the upper and lower bounds of the pressure ratios shown.

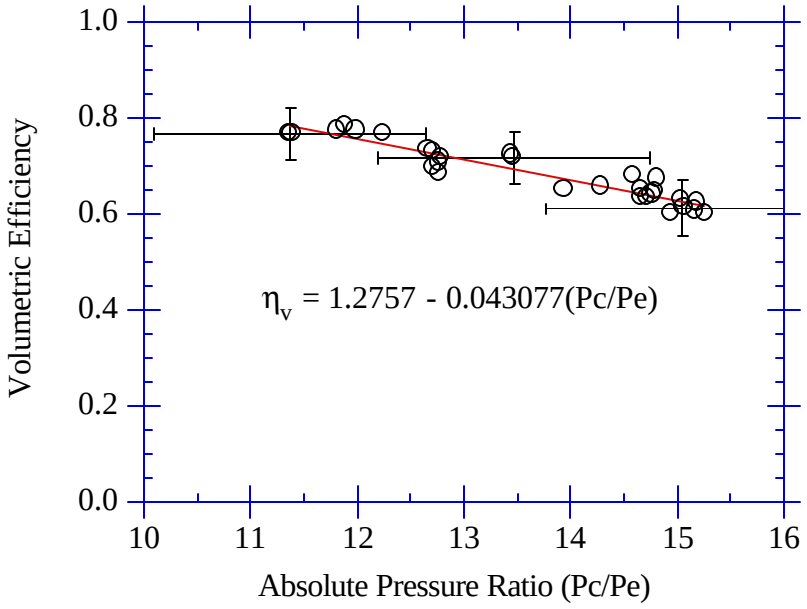

Figure 6-8. Volumetric Efficiency for R134a Compressor

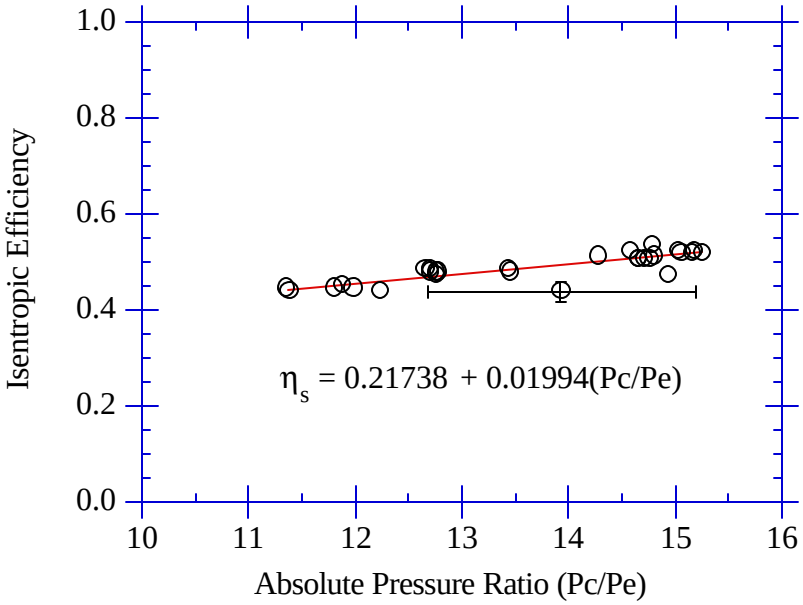

Figure 6-9. Isentropic Efficiency for R134a Compressor

The isentropic efficiency from Equation 6.5 for the R134a data is plotted against the absolute pressure ratios in Figure 6-9. The experimental uncertainty in the isentropic efficiency is ±0.024 with the standard deviation of the data scatter equal to 0.013. The total uncertainty in the equation for isentropic efficiency is ±0.035. As with the volumetric equation, the use of the isentropic equation should be limited to within the range of data used for the curve fit.

To see how well these curve fits do in predicting compressor performance, it is useful to compare predicted and measured performance. Figure 6-10 compares the experimentally measured mass flow rates with those predicted from the volumetric equation in Figure 6-8. The error bounds are ±5.0% with a standard deviation of 1.5%. Figure 6-11 compares the measured compressor power to that predicted using the isentropic efficiency equation from Figure 6-9. The power with error bounds of ±7.0% and a standard deviation of 2.4%. is not predicted as accurately as the mass flow rate. However, these accuracies are nearly the same as for the compressor maps for the R12 compressor. The use of volumetric and isentropic efficiencies will, therefore, work reasonably well for the R134a compressor.

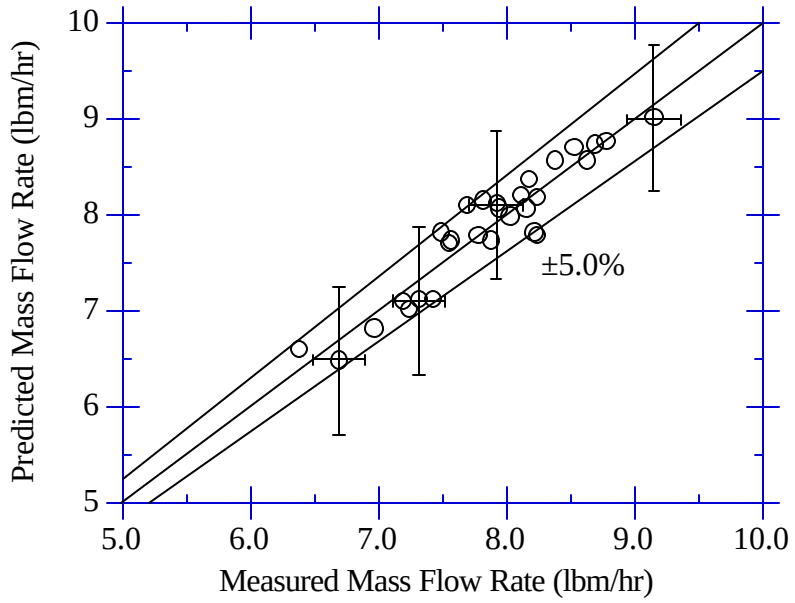

Figure 6-10. R134a Mass Flow Rate Curve Fit Using Volumetric Efficiency

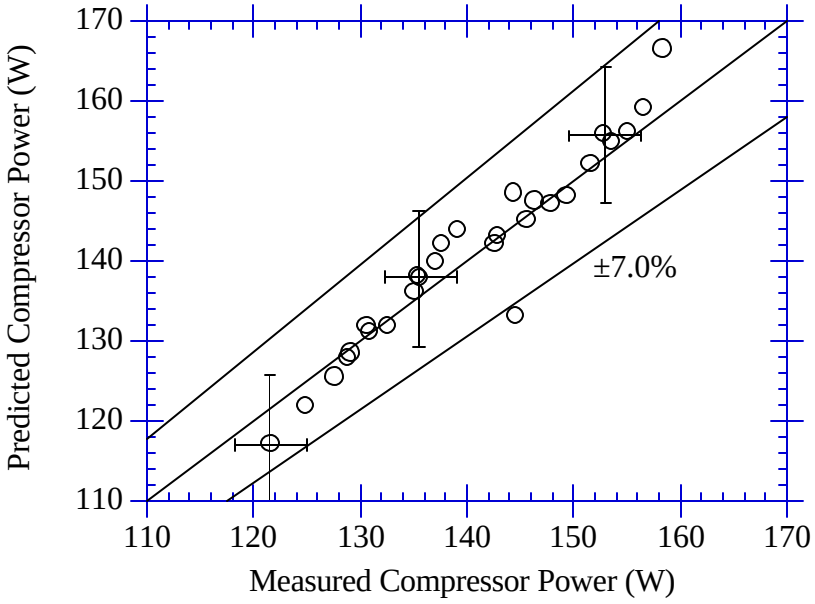

Figure 6-11. R134a Compressor Power Curve Fit Using Isentropic Efficiency

6.5 Compressor Shell Heat Transfer

Compressor maps or equivalently volumetric and isentropic efficiencies don't entirely characterize the performance of a compressor. It is also necessary to know the amount of heat transfer from the compressor shell. For the compressors studied this heat transfer is not negligible.

The simplest model to correlate heat transfer from the compressor shell with compressor operating conditions is to assume a constant convective film coefficient over the entire compressor shell. With this film coefficient known, the heat transfer rate from the compressor shell can be calculated from Equation 6.6. The temperature difference chosen to base the film coefficient on is

$$\dot{Q}_{comp} = \bar{h}\ \Delta T \tag{6.6}$$

somewhat arbitrary. Since the compressor shells for the units tested were on the discharge side of the compressor, the discharge temperature minus the ambient temperature was taken as the most appropriate temperature difference.

To determine the best film coefficients for both the R12 and R134a compressors, a non-linear least squares worksheet in E.E.S. was formulated (See Appendix E for listing). The equations to be solved are given in Equations 6.7 through 6.10. Equation 6.7 determines the compressor heat transfer from the measured power requirement, refrigerant mass flow rate and inlet and outlet conditions to the compressor. Equation 6.8 calculates the condenser fan power requirement. This quantity is not measured directly. Equation 6.9 determines the temperature of the air surrounding the compressor shell, $Tcompair_i$, from an air-side energy balance across the condenser fan. Once these quantities are calculated for all the data points, Equation 6.10 can be evaluated to determine the best estimate of $\bar{h}$.

$$\dot{Q}_{comp_i} = (3.413\,\dot{P}_{comp_i}) - \dot{m}_i (h1_i - h10_i) \quad i = 1,n \tag{6.7}$$

$$\dot{P}_{confan_i} = \dot{P}_{system_i} - \dot{P}_{comp_i} - \dot{P}_{evapfan_i} \quad i = 1,n \tag{6.8}$$

$$3.413\,\dot{P}_{confan_i} = 60\rho C_p \dot{V} (Tconfanout_i - Tcompair_i) \quad i = 1,n \tag{6.9}$$

$$\frac{\delta}{\delta \bar{h}} \sum_{i=1}^{n} \left[\dot{Q}_{comp_i} - \bar{h}(T1_i - Tcompair_i) \right]^2 = 0.0 \tag{6.10}$$

where $\dot{Q}_{comp}$ = compressor shell heat transfer (Btu/hr)

$\dot{P}_{comp}$ = compressor power input (W)

$\dot{m}$ = refrigerant mass flow rate (lbm/hr)

h1 = enthalpy at the compressor discharge (Btu/lbm)

h10 = enthalpy at the compressor inlet (Btu/lbm)

$\dot{P}_{confan}$ = condenser fan power (W)

$\dot{P}_{system}$ = total refrigerator power (W)

$\dot{P}$ evapfan = evaporator fan power (W)

Tconfanout = condenser fan outlet air temperature (°F)

Tcompair = air temperature surrounding compressor (°F)

T1 = compressor discharge temperature (°F)

Solving Equation 6.10 for the R12 data set results in a convective film coefficient of 5.92 Btu/hr°F ±0.2 Btu/hr°F. The slope of the line in Figure 6-12 is equal to the film coefficient. Note also that the experimental uncertainty is the same order of magnitude as the scatter in the data. This suggests that some of the model assumptions are incorrect. One very likely source of error is assuming that the surface temperature of the compressor shell is uniform. However, even with this assumption, the heat transfer from the R12 compressor shell as shown in Figure 6-13 can be predicted to within ±8.0% with a standard deviation of 1.9%. It is doubtful that this model can be improved without making it a great deal more complicated.

Repeating the same calculations for the R134a data set results in a convective film coefficient of 5.83 Btu/hr°F ±0.2 Btu/hr°F. Within the experimental uncertainty this is the same as the film coefficient for the R12 compressor. This is a logical result because both compressors have very similar shell geometries and the same airflow rates over the shell. However, it is unlikely that this film coefficient will work for other geometries. The slope of the line in Figure 6-14 is the film coefficient for the R134a compressor. As for the R12 case, the scatter in the data is the same order of magnitude as the experimental uncertainty. Figure 6-15 shows that the constant film coefficient model does a somewhat worse job for the R134a data with error bounds of ±10% and a standard deviation of 2.1%. However, this is still a reasonable amount of error.

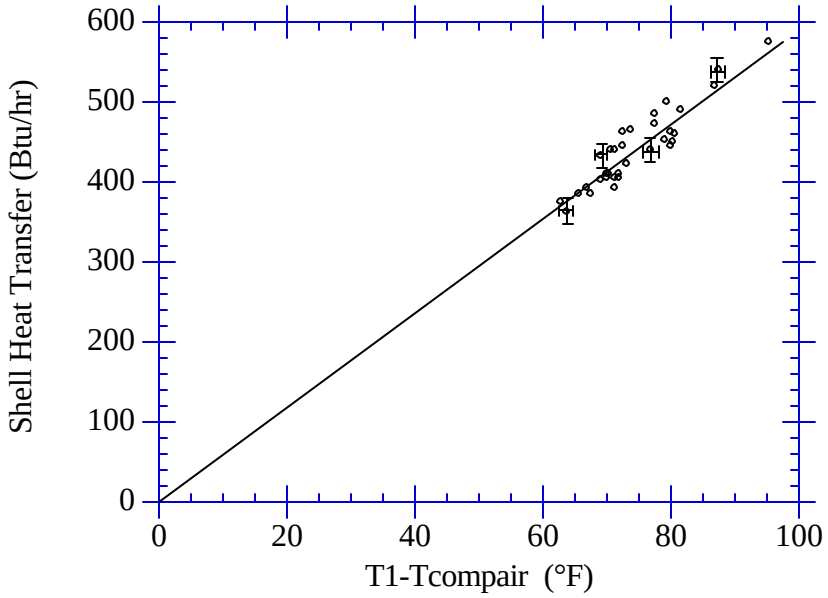

Figure 6-12. Convective Film Coefficient for the R12 Compressor

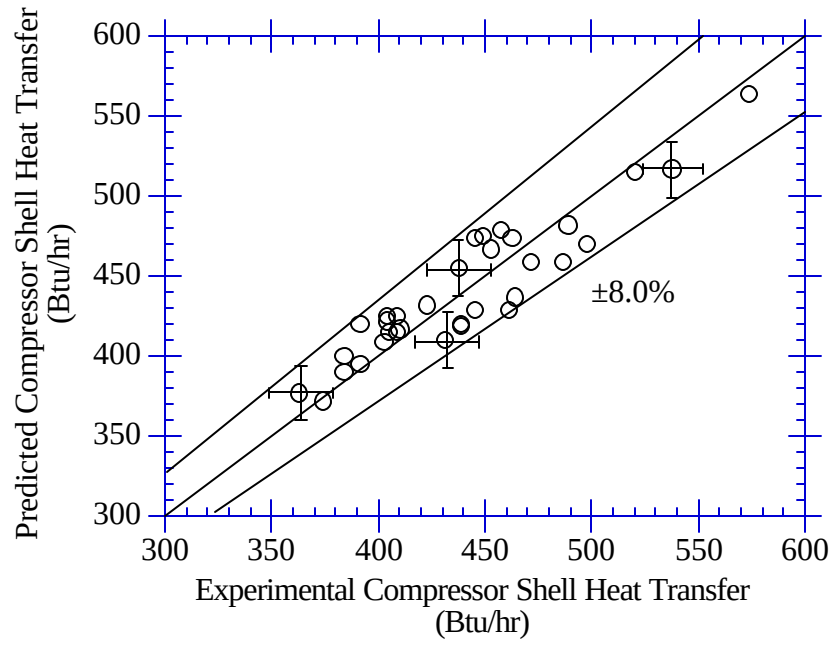

Figure 6-13. R12 Compressor Shell Heat Transfer

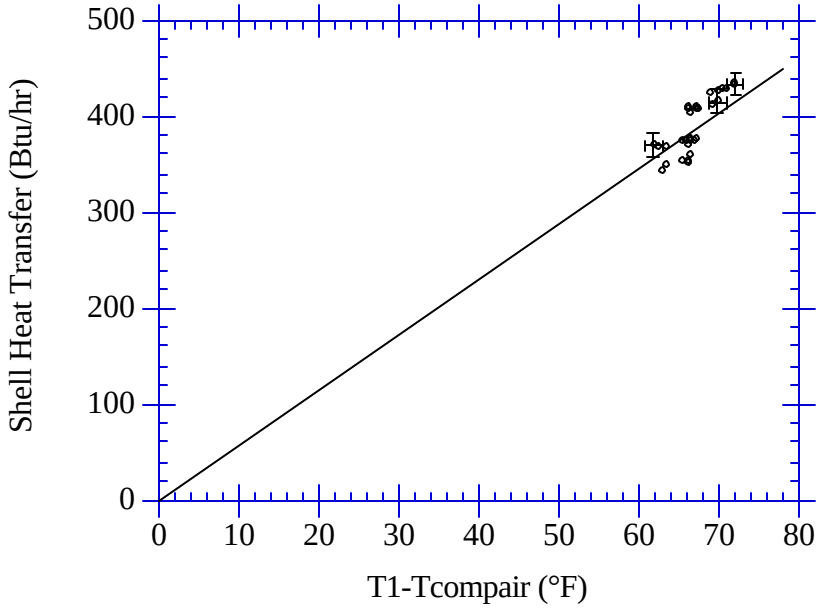

Figure 6-14. Convective Film Coefficient for R134a Compressor

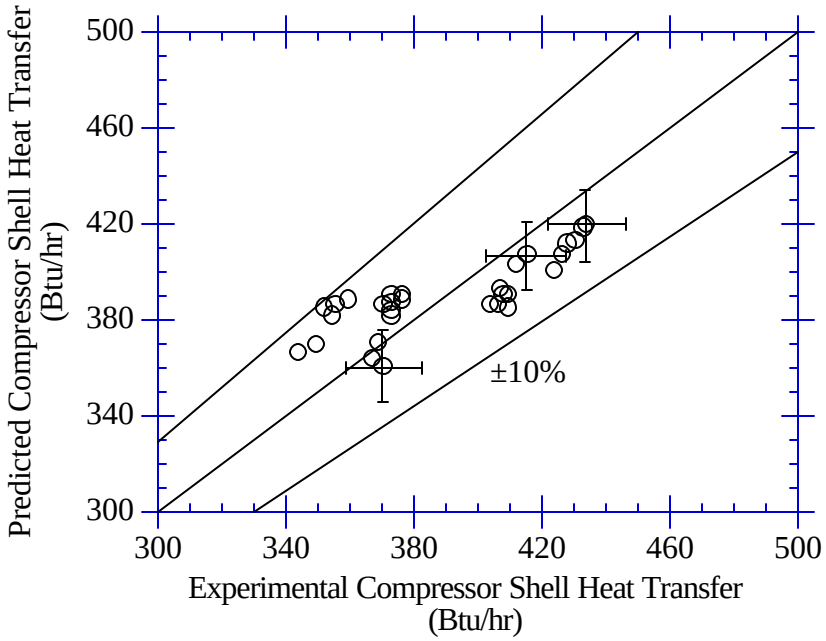

Figure 6-15. R134a Compressor Shell Heat Transfer

6.6 Conclusions

The constant convective film coefficient model does a reasonably good job. The model was able to predict heat transfer from the compressor shell to with ±8.0% for the R12 compressor and ±10.0% for the R134a compressor. Improvements in the model will probably require a large increase in complexity such as making the compressor shell surface temperature a function of location on the compressor. It is questionable whether the added complexity is justified.

These results are restricted to small reciprocating compressors that have the compressor shell on the discharge side of the compressor. Other compressor types such as rotary compressors should be investigated. Further, compressors where the compressor shell is on the low side of the compressor should also be looked at.

For the purpose of modeling the other compressor performance parameters such as mass flow rate etc., the use of either compressor maps or volumetric efficiencies work equally well. However, the volumetric efficiency approach has the advantage of not requiring any correction factors for superheat. The volumetric efficiency approach also has the advantage of being applicable to a wider range of conditions. This can be an advantage in analyzing experimental data.

References

[1] Personal communication., Mr. Spike Kline., General Electric Company, Appliance Park, Louisville, Kentucky, 40225.

[2] Reeves, R.N., Modeling and Experimental Parameter Estimation of a Refrigerator/Freezer System, Air Conditioning and Refrigeration Center, Dept. of Mechanical and Industrial Engineering, University of Illinois at Urbana-Champaign, 1992, p. 66.

[3] Copeland Copeleweld Data Book, Copeland Corporation, Sidney, Ohio (1990).

[4] Dabiri, A.E. and C.K. Rice. 1981. "A Compressor Simulation Model with Corrections for the Level of Suction Gas Superheat.", ASHRAE Transactions,Vol. 87, Part 2, pp. 77 to 782.

[5] Stoecker, W.F. and J.W. Jones, Refrigeration and Air Conditioning, McGraw-Hill, New York, 1986, Chapter 11.

[6] Personal communication , Mr. John Driver, General Electric Company, Appliance Park, Louisville, Kentucky, 40225.

[7] Stoecker, p. 217.

[8] Personal communication., Mr. Spike Kline., General Electric Company, Appliance Park, Louisville, Kentucky, 40225.

Chapter 7: Condenser Parameter Estimation

7.1 Overview

The condenser model is based in part on the work by Reeves [1] and Kempiak and Crawford [2]. Kempiak and Crawford modeled a condenser in a mobile air-conditioning system. Their model considers the condenser to be a long tube within which there are three zones that have different heat transfer characteristics. The zones are: a desuperheating section in which refrigerant vapor transfers heat with air, a two-phase section in which saturated refrigerant transfers heat with air, and a subcooled section in which heat exchange is between liquid refrigerant and air. For each section an overall heat transfer coefficient or UA value and fraction of that section's length to the total was determined. The UA value was considered a function of condenser air flow rate and refrigerant mass flow rate. The model was able to predict the total heat transfer from the condenser to within ±1.8%.

Reeves adapted this approach to domestic refrigerator/freezer condensers. The model was somewhat simplified because variations in condenser air flow rate were not considered. Further, rather than determine a fraction of a given section length to the total, equivalently an appropriate surface area proportional to the section length was determined. With this area known, the UA for a given section (x) can be split into a conductance U based on surface area A. To accomplish this, it is necessary to make some assumptions. Equation 7.1 relates the overall heat transfer coefficient for a given section to the thermal resistances inside and outside of the tube and of the tube itself [3].

$$\frac{1}{UxAx} = \frac{1}{h_o A_o} + \frac{\ln(r_o / r_i)}{2\pi L k} + \frac{1}{h_i A_i} \qquad (7.1)$$

where U_x = overall conductance based on A_x

A_x = arbitrary surface area

h_o = air side convective film coefficient

A_o = effective air side surface area

r_o = outside radius of condenser tube

r_i = inside radius of condenser tube

L = length of a given condenser section

k = thermal conductivity of tube

h_i = refrigerant side convective film coefficient

Ai = effective refrigerant side surface area

Since the air flow rate across the condenser is not varied, the convective film coefficient on the outside can be assumed to be constant if variations in thermodynamic properties are considered negligible. Likewise, the resistance of the wall is also constant. The refrigerant film coefficient is a function of mass flow rate. If the mass flow rate does not vary significantly, then the internal coefficient can also be assumed constant. With these assumptions Equation 7.1 can be rewritten as Equation 7.2. Solving Equation 7.2 for U_x yields Equation 7.3. The result is if the film coefficients are assumed to be constants then the conductance for that section is also constant. This is the basis for assuming that the conductances for each section of the condenser are constant.

$$\frac{1}{U_x C_1 \pi D_x L} = \left(\frac{1}{h_o C_2 \pi D_o} + \frac{\ln(r_o / r_i)}{2\pi k} + \frac{1}{h_i C_3 \pi D_i} \right) \frac{1}{L} = \frac{K_1}{L} \qquad (7.2)$$

where C_1, C_2, C_3 and K_1 = constants

D_x = diameter associated with surface area A_x

D_o = outside diameter of condenser tube

D_i = inside diameter of condenser tube

$$U_x = \frac{1}{K_1 C_1 \pi D_x} = \text{constant} \qquad (7.3)$$

The same constant U model can also be derived from the assumption that the air side resistance dominates the heat transfer process in the condenser. If this is true then the tube wall and refrigerant side resistances can be neglected. Further, since the air side volumetric flow rate is constant, the resistance or conversely the conductance will be constant if changes in thermodynamic properties are small. A necessary consequence of the air side resistance dominating the heat transfer process is the fact that the U values for all sections will be the same; the effect of the refrigerant side being negligible. Indeed, Reeves found that the desuperheating and the two-phase sections had nearly the same conductance. However, in the subcooled section the U value was half that of the desuperheating and two-phase sections. This indicates that the internal resistance of the liquid refrigerant does have an impact on the overall heat transfer coefficient. This suggests that the U for this section is a function of refrigerant mass flow rate and therefore not constant.

A possible improvement to a constant U assumption is to make the U's for each section of the condenser a function of refrigerant mass flow rate. Equation 7.1 could then be written in the form of Equation 7.4. The constant B_1 includes the constant air side resistance and wall resistance The constant B_2 is a ratio of areas.

$$\frac{1}{U_x} = B_1 + \frac{B2}{hi} \qquad (7.4)$$

where B_1, B_2 = constants

The constant U approach and a refrigerant mass flow dependent U method will be considered for both the R12 and R134a cases. Like Reeves, effectiveness - NTU relations in conjunction with estimated conductances will be used to predict condenser performance. However, before the U parameters can be estimated from the experimental data, it is necessary to determine the condenser volumetric air flow rate. This quantity must be known in order to evaluate the effectiveness-NTU relations.

7.2 Condenser Volumetric Flow Rate

The volumetric air flow rate was determined by equating a refrigerant side and air side energy balance. The most obvious choice is to set the condenser heat rejection equal to the air temperature rise across the coil. However, the air temperature at the exit of the condenser was too difficult to accurately measure. A much more suitable location to measure an air temperature is downstream of the condenser fan. The temperature difference between this point and the condenser inlet is the result of heat transfer from not only the condenser but also from the compressor and the condenser fan.

Figure 7-1 shows the layout of the underside of the refrigerator as viewed from above. The condenser air inlet is at the front of the refrigerator. The condenser is a simple serpentine coil with small wire fins on the outside of the tubes. There is no internal surface enhancement. The condenser coil is fundamentally a counter-flow heat exchanger.

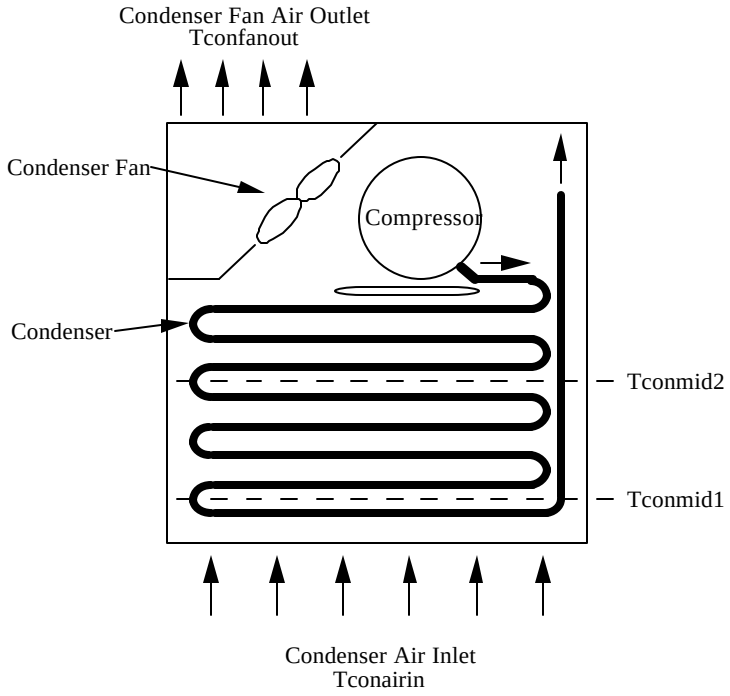

Figure 7-1. Refrigerator Condenser/Compressor Geometry

Equation 7.5 relates the air temperature rise to the appropriate heat transfer rates. Equations 7.6, 7.7, and 7.8 equate measured quantities to these heat transfer rates. Substituting these equations into Equation 7.5 and canceling terms results in Equation 7.9, the final form. Equation 7.9 can be solved for the volumetric flow rate for one data point.

$$\rho C_p 60 \dot{V}_c \Delta T = \dot{Q}_{comp} + \dot{Q}_{cfan} + \dot{Q}_c \qquad (7.5)$$

where $\dot{Q}_{comp}$ = compressor shell heat transfer rate (Btu/hr)

$\dot{Q}_{c\,fan}$ = condenser fan heat transfer rate (Btu/hr)

$\dot{Q}_c$ = condenser heat transfer rate (Btu/hr)

$\dot{V}_c$ = volumetric flow rate (ft^3/min)

ρ = density of air (lbm/ft^3)

C_p = specific heat of air (Btu/lbm°F)

ΔT = temperature difference (°F)

$$\dot{Q}_{cfan} = 3.413 (\dot{P}_{system} - \dot{P}_{comp} - \dot{P}_{efan}) \qquad (7.6)$$

$$\dot{Q}_{comp} = 3.413\dot{P}_{comp} - \dot{m}\ (h1 - h10) \qquad (7.7)$$

$$\dot{Q}_c = \dot{m}\ (h1 - h3) \qquad (7.8)$$

where $\dot{P}_{system}$ = power input to the refrigerator (W)

$\dot{P}_{comp}$ = power input to the compressor (W)

$\dot{P}_{efan}$ = power input to the evaporator fan (W)

$\dot{m}$ = refrigerant mass flow rate (lbm/hr)

h1 = refrigerant enthalpy at the compressor discharge/condenser inlet (Btu/lbm)

h3 = refrigerant enthalpy at the exit to the condenser (Btu/lbm)

h10 = refrigerant enthalpy at the compressor suction port (Btu/lbm)

$$\rho C_p 60\dot{V}_c \Delta T = 3.413\,(\dot{P}_{system} - \dot{P}_{efan}) + \dot{m}\ (h10 - h3) \qquad (7.9)$$

To find the optimum value for all the data points, a nonlinear least squares approach was applied. An E.E.S. worksheet was used to solve Equation 7.10 which is satisfied only at the optimum flow rate (see Appendix E for a copy of the worksheet). The condenser volumetric air flow rate is estimated to be 116 ft^3/min ±11.0 %. This agrees with the manufacturer's estimate of between 115 and 120 ft^3/min [4]. The slope of the line in Figure 7-2 is the condenser volumetric flow rate. Note that these calculations are based on the R134a data set. Unfortunately, since the outlet state from the condenser was not subcooled for the R12 tests, h3 in Equation 7.10 is unknown. Therefore the volumetric air flow rate could not be estimated from the R12 data set.

$$\frac{\delta}{\delta\dot{V}_c}\sum_{i=1}^{n}\left[\rho_i C_{pi} 60\dot{V}_c \Delta T_i - 3.413(\dot{P}system_i - \dot{P}efan_i) - \dot{m}_i(h10_i - h3_i)\right]^2 = 0.0 \qquad (7.10)$$

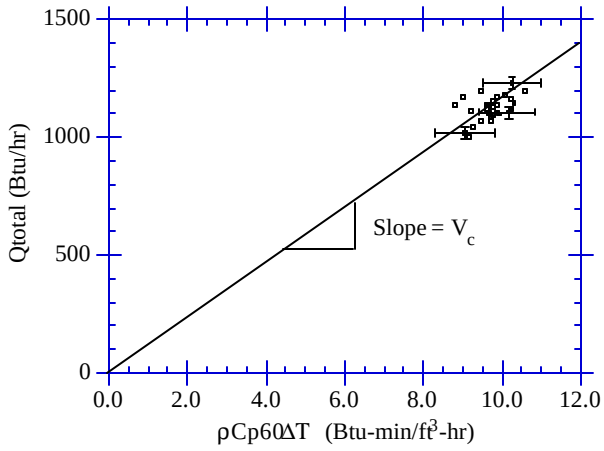

Figure 7-2. Condenser Volumetric Flow Rate

7.3 Constant Conductance Model

The equations that were evaluated to correlate the R134a data set for the constant conductance model are listed in Equations 7.11 through 7.28. The unknowns are: $\dot{Q}$crate, $\dot{Q}$cdesuprate, $\dot{Q}$c2phrate, $\dot{Q}$csubrate, edesup, Ntudesup, adesup, a2ph, asub, esub, Ntusub and $\dot{Q}$c. All the other quantities are either measured experimentally or calculated from the experimental data and thermodynamic properties. The effectiveness equations for the desuperheating and subcooled sections are for a counterflow heat exchanger. The approximate location of the intermediate condenser air temperatures Tconmid1 and Tconmid2 are shown in Figure 7-1.

$$\dot{Q}\,crate_i = \dot{Q}\,cdesuprate_i + \dot{Q}\,c2phrate_i + \dot{Q}\,csubrate_i \quad i = 1,n \tag{7.11}$$

$$\dot{Q}\,cdesuprate_i = edesup_i\, cmin_i\, (T1_i - Tconmid2_i) \quad i = 1,n \tag{7.12}$$

$$edesup_i = \frac{1 - e^{-Ntudesup_i\,(1-cmin_i/cacond_i)}}{1 - (cmin_i/cacond_i)\, e^{-Ntudesup_i\,(1-cmin_i/cacond_i)}} \quad i = 1,n \tag{7.13}$$

$$Ntudesup_i = \frac{U_{desup}\, adesup_i}{cmin_i} \quad i = 1,n \tag{7.14}$$

$$\dot{Q}\,c2phrate_i = \left(1 - e^{(-U_{2ph}\, a2ph_i/cacond_i)}\right) cacond_i\, (T2_i - Tconmid1_i) \quad i = 1,n \tag{7.15}$$

$$\dot{Q}\,csubrate_i = esub_i\, cminsub_i\, (T2_i - Tconairin_i) \quad i = 1,n \tag{7.16}$$

$$esub_i = \frac{1 - e^{-Ntusub_i\,(1-cminsub_i/cacond_i)}}{1 - (cminsub_i/cacond_i)\, e^{-Ntusub_i\,(1-cminsub_i/cacond_i)}} \quad i = 1,n \tag{7.17}$$

$$Ntusub_i = \frac{U_{sub}\, asub_i}{cminsub_i} \quad i = 1,n \tag{7.18}$$

$$\frac{\dot{Q}c2ph_i}{\dot{Q}c_i} = \frac{\dot{Q}c2phrate_i}{\dot{Q}crate_i} \quad i = 1,n \tag{7.19}$$

$$\frac{\dot{Q}cdesup_i}{\dot{Q}c_i} = \frac{\dot{Q}cdesuprate_i}{\dot{Q}crate_i} \quad i = 1,n \tag{7.20}$$

$$acond = adesup_i + a2ph_i + asub_i \quad i = 1,n \tag{7.21}$$

$$\dot{Q}\,c_i = \dot{w}_i\, (h1_i - h3_i) \quad i = 1,n \tag{7.22}$$

$$\dot{Q}\,cdesup_i = \dot{w}_i\, (h1_i - h1satvap_i) \quad i = 1,n \tag{7.23}$$

$$\dot{Q}\,c2ph_i = \dot{w}_i\,(h1satvap_i - h2_i) \quad i = 1,n \tag{7.24}$$

$$\dot{Q}\,sub_i = \dot{w}_i\,(h2_i - h3_i) \quad i = 1,n \tag{7.25}$$

$$Tconmid1_i = \frac{\dot{Q}sub_i}{cacond_i} + Tconairin_i \quad i = 1,n \tag{7.26}$$

$$Tconmid2_i = \frac{\dot{Q}c2ph_i}{cacond_i} + Tconmid1_i \quad i = 1,n \tag{7.27}$$

$$\text{Objective Function} = \sum_{i=1}^{n} \left[\dot{Q}c_i - \dot{Q}crate_i\,(U_{desup}, U_{2ph}, U_{sub})\right]^2 \tag{7.28}$$

where $\dot{Q}\,cdesuprate$ = predicted heat transfer rate from desuperheating section (Btu/hr)

$\dot{Q}\,c2phrate$ = predicted heat transfer rate from two-phase section (Btu/hr)

$\dot{Q}\,csubrate$ = predicted heat transfer rate from subcooled section (Btu/hr)

edesup = effectiveness of desuperheating section

cmin = $\dot{w}\ C_p$ for refrigerant in desuperheating section (Btu/hr °F)

T1 = condenser inlet refrigerant temperature (°F)

Tconmid2 = condenser air temperature after two-phase section (°F)

Ntudesup = number of heat transfer units in desuperheating section

cacond = $\dot{m}\ C_p$ on the air-side of the condenser (Btu/hr °F)

U_{desup} = U value for the desuperheating section (Btu/hr*ft^2 °F)

adesup = area of the desuperheating section (ft^2)

U_{2ph} = U value for the two-phase section (Btu/hr*ft^2 °F)

a2ph = area of two-phase section (ft^2)

T2 = saturated condensing temperature (°F)

Tconmid1 = condenser air temperature after subcooled section (°F)

esub = effectiveness of subcooled section

cminsub = $\dot{w}\ C_p$ for the refrigerant in the subcooled section (Btu/hr °F)

Tconairin = condenser air inlet temperature (°F)

Ntusub = number of heat transfer units in the subcooled section

U_{sub} = U value for the subcooled section (Btu/hr °F)

asub = area of the subcooled section (ft^2)

acond = total surface area of the condenser (ft^2)

$\dot{Q}\,c$ = measured heat transfer from the condenser (Btu/hr)

$\dot{Q}_{c2ph}$ = measured heat transfer from the two-phase section (Btu/hr)

$\dot{Q}_{cdesup}$ = measured heat transfer from the desuperheating section (Btu/hr)

$\dot{w}$ = refrigerant mass flow rate (lbm/hr)

h1 = refrigerant enthalpy at the inlet to the condenser (Btu/lbm)

h1satvap = saturated vapor enthalpy in condenser (Btu/lbm)

h2 = saturated liquid enthalpy in condenser (Btu/lbm)

h3 = refrigerant enthalpy at the outlet to the condenser (Btu/lbm)

The R12 equations are essentially the same except for how the heat transfer rates are determined from measured quantities. Because no subcooling at the condenser exit was detected in the R12 data, the heat transfer rate from the condenser could not be calculated from Equation 7.22. Instead the heat transfer rate had to be determined from an air side energy balance using Equation 7.5 rewritten in the form of Equation 7.29. The volumetric flow rate is now a known quantity determined from the R134a data. With $\dot{Q}_c$ known, the air temperature rise across the condenser can be calculated from Equation 7.30. The heat transfer rate from the desuperheating section is determined from Equation 7.31. Equation 7.32 can then be solved for the air temperature after the two-phase section, Tconmid, and this temperature substituted into Equation 7.33 to determine the two-phase heat transfer rate. With these variables known, Equations 7.34 through 7.40 can be solved. Equation 7.41 lists the objective function that was minimized for the R12 data.

$$\dot{Q}_c = \rho C_p 60 \dot{V}_c \Delta T - 3.413 (\dot{P}_{system} - \dot{P}_{efan}) + \dot{m} (h1 - h10) \quad (7.29)$$

$$\dot{Q}_c = \rho C_p 60 \dot{V}_c (Tconairout - Tconairin) \quad (7.30)$$

$$\dot{Q}_{desup} = \dot{m} (h1 - h2) \quad (7.31)$$

$$\dot{Q}_{desup} = \rho C_p 60 \dot{V}_c (Tconairout - Tconmid) \quad (7.32)$$

$$\dot{Q}_{2ph} = \rho C_p 60 \dot{V}_c (Tconmid - Tconairin) \quad (7.33)$$

$$\dot{Q}_{crate_i} = \dot{Q}_{cdesuprate_i} + \dot{Q}_{c2phrate_i} \quad i = 1,n \quad (7.34)$$

$$\dot{Q}_{cdesuprate_i} = edesup_i \, cmin_i \, (T1_i - Tconmid_i) \quad i = 1,n \quad (7.35)$$

$$edesup_i = \frac{1 - e^{-Ntudesup_i (1-cmin_i/cacond_i)}}{1 - (cmin_i/cacond_i) \, e^{-Ntudesup_i (1-cmin_i/cacond_i)}} \quad i = 1,n \quad (7.36)$$

$$Ntudesup_i = \frac{U_{desup} \, adesup_i}{cmin_i} \quad i = 1,n \quad (7.37)$$

$$\dot{Q}_{c2phrate_i} = \left(1 - e^{(-U_{2ph} \, a2ph_i/cacond_i)}\right) cacond_i \, (T2_i - Tconairin_i) \quad i = 1,n \quad (7.38)$$

$$\frac{\dot{Q}c2ph_i}{\dot{Q}c_i} = \frac{\dot{Q}c2phrate_i}{\dot{Q}crate_i} \quad i = 1,n \tag{7.39}$$

$$acond = adesup_i + a2ph_i \quad i = 1,n \tag{7.40}$$

$$\text{Objective Function} = \sum_{i=1}^{n} \left[\dot{Q}c_i - \dot{Q}crate_i\,(U_{desup}, U_{2ph})\right]^2 \tag{7.41}$$

where Tconmid = air temperature after the two-phase section (°F)

The results from the optimization program for both the R12 and R134a cases are summarized in Table 7.1. The U values are based on variable section areas that sum to 2.09 ft^2. Note that this area is totally arbitrary. However to add some physical significance, it was set equal to the approximate surface area of the outside of the condenser tubing. Typical areas for each section are also listed. It should be understood that these areas are not constants but vary with condenser operating conditions. The last column in Table 7.1 lists the standard deviation of the error in the objective function for 33 data points for R12 and 30 data points for R134a.

Table 7.1. Constant Conductance Model Parameters

Case	U_{desup} (Btu/hr-ft^2°F)	U_{2ph} (Btu/hr-ft^2°F)	U_{sub} (Btu/hr-ft^2°F)	Standard Deviation
R12	3.7 ±0.55	38.3 ±14.9	-	47.4 Btu/hr
R134a	4.8 ±0.52	29.6 ±2.2	11.1 ±2.0	14.8 Btu/hr
Based on total condenser outside tube surface area = 2.09 ft^2				

Typical Section Areas			
Case	adesup (ft^2)	a2ph (ft^2)	asub (ft^2)
R12	1.174	0.916	-
R134a	0.658	1.185	0.247

The most important result shown in Table 7.1. is the fact that the conductance for a given section is significantly different from the other sections. The differences between the sections must be the result of the effect of the refrigerant side on the overall heat transfer coefficients. It would be expected from theoretical calculations for straight tubes (see Appendix G) that the overall conductance for the R134a desuperheating section would be roughly equal to the R12 value. However, as Table 7.1 shows the conductance in the desuperheating section is larger than the R12 value by 30%. Therefore, the difference can not be accounted for by the use of a simple straight tube correlation. The difference may be the result of variations in the conductances not accounted for in the constant conductance model. In fact the theoretical calculations also predict the desuperheating conductance for the R134a data set to vary over the range of mass flow rates by 31% and by 23% for the R12 desuperheating conductance. These variances are significant.

However, the difference is most likely the result of how accurately the conductances can be estimated. Contour plots (see Section 7.5) show that the minima are contained in long shallow valleys. As a result, the uncertainty in the estimates is fairly large. The reason for the uncertainty relates to the independence of the equation

set, in particular Equations 7.19 and 7.20, used to estimate the minima. A detailed discussion of this topic can be found in Chapter 9, Section 9.3.

For the two phase section, the straight tube correlations indicate that the R12 and R134a two phase conductances should be nearly equal and twice the desuperheating conductances. From Table 7.1 the two phase conductances are much higher than the desuperheating conductances but the large experimental uncertainty in the R12 two phase conductance does not allow the prediction that they are equal to be verified. This large uncertainty is the result of the need to use air side measurements to determine the two phase heat transfer. The propagation of error through Equations 7.29 and 7.33 take a toll on the final accuracy (see Appendix D for the uncertainty analysis). However, within the range of the uncertainty the conductances are equal. For the subcooled section, no comparison can be made to an equivalent R12 subcooled conductance.

Another important observation shown in Table 7.1 is the amount of area that is taken up by the different sections. In the R12 case, the results imply that the desuperheating section takes up 56% of the total available surface area. It cannot be determined at this point whether this is an accurate estimate due to the uncertainty in the parameters. If the desuperheating conductance is actually higher than estimated, the area taken up would be smaller. However the results do imply that the area taken up by the desuperheating section can not be neglected. Further, since the two-phase section has a much higher conductance and therefore heat transfer rate compared to the desuperheating section, it is desirable to have as small a desuperheating section as possible. In this case the desuperheating section may significantly reduce the potential heat transfer rate from the condenser because it takes such a large part of the total condenser area. Likewise for the R134a case, the desuperheating and subcooled sections take up 43% of the available area in the condenser.

From a modeling viewpoint these results underscore the importance of considering all three zones in the condenser. Although the desuperheating and subcooled sections provide a small percentage of the total heat transfer, they can not be neglected because of the amount of heat transfer surface area they take away from the two-phase section. A reduction in the two-phase section area has a big impact on the total heat transfer from the condenser.

Figures 7-3 and 7-4 compare the predicted heat transfer rate for the R12 and R134a cases to the actual measured heat transfer rates. The constant conductance model does a pretty good job of predicting the condenser heat transfer rate to within 10% for the R12 case and 5% for the R134a case.

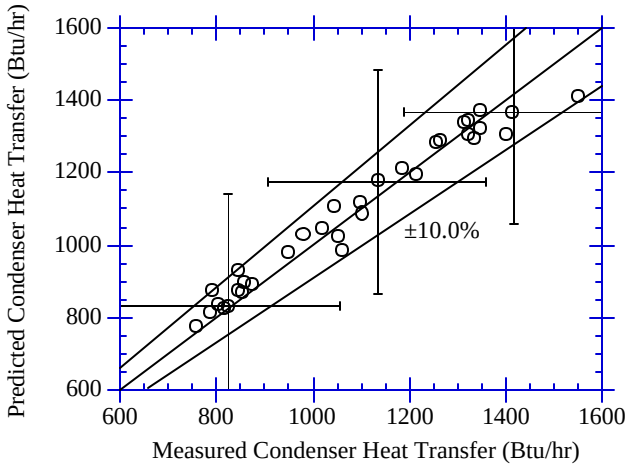

Figure 7-3. Condenser Heat Transfer - R12 Constant Conductance Model

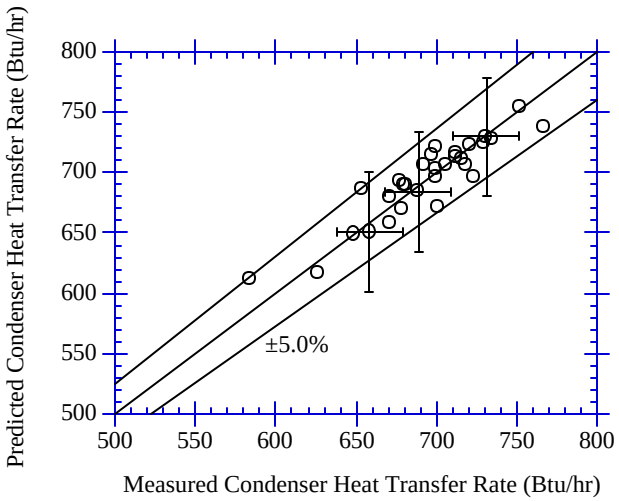

Figure 7-4. Condenser Heat Transfer - R134a Constant Conductance Model

7.4 Variable Conductance Model

Although the constant conductance model works fairly well, the fact that the conductances in Table 7.1 vary suggest that a variable conductance model may improve the model accuracy. Theoretical calculations (see Appendix G) predict that for the two phase and subcooled sections the conductances vary with refrigerant mass flow by less than 11%. This may not be enough variation to allow the conductances for these sections to be separated into a refrigerant and air side component. However, in the desuperheating section the conductances vary with refrigerant mass flow by as much as 31% as noted previously. Therefore, it may be possible to separate the desuperheating conductances into a refrigerant side and air side component. Further, the theoretical calculations are

only approximations to what is happening in the real condenser. It may be that the two phase and subcooled conductances are varying more than predicted. It is therefore worth the attempt to try to separate the conductances.

Taking Equation 7.4 and writing it for each section in the condenser yields Equations 7.42 through 7.44. For each section, the conductance is now a function of the internal convective film coefficient. These equations are substituted for the constant U parameters in Equations 7.14, 7.15, and 7.18 for the R134a case and Equations 7.37 and 7.38 for the R12 case. The film coefficients are the same ones used in theoretical calculations previously (see also Appendix G). Any discrepancies between these values and the actual film coefficients in the real condenser should be absorbed by the constants.

$$\frac{1}{U_{desup}} = B_1 + \frac{B_2}{h_{desup}} \tag{7.42}$$

$$\frac{1}{U_{2ph}} = B_1 + \frac{B_3}{h_{2ph}} \tag{7.43}$$

$$\frac{1}{U_{sub}} = B_1 + \frac{B_4}{h_{sub}} \tag{7.44}$$

The results for the R134a data set for this model are given by Equations 7.45 to 7.47. In these equations the constants found from the parameter estimation routine are substituted for the B's. Clearly the order of magnitude of the predicted conductances with these constants in incorrect. The reason relates to the small variation in the two phase conductance. If the two phase conductance is constant then there is no way to estimate the constants B_1 and B_3. The attempt to separate a constant into two other constants is a futile exercise.The same line of reasoning also applies to the subcooled section where the theoretical variation in the subcooled conductance is small. The same conclusions also hold for the R12 condenser.

$$\frac{1}{U_{desup}} = 5.1e\text{-}6 + \frac{16.6}{h_{desup}} \qquad U_{desup} \sim 196{,}000 \tag{7.45}$$

$$\frac{1}{U_{2ph}} = 5.1e\text{-}6 + \frac{0.12}{h_{2ph}} \qquad U_{2ph} \sim 196{,}000 \tag{7.46}$$

$$\frac{1}{U_{sub}} = 5.1e\text{-}6 + \frac{0.65}{h_{sub}} \qquad U_{sub} \sim 196{,}000 \tag{7.47}$$

These results suggest that Equations 7.42 through 7.44 should be revised to the forms given by Equations 7.48 through 7.50. Unfortunately, the objective function did not show a minimum for finite values of B_2 and U_{2ph} for either the R12 or the R134a data sets using these equations. It again appears that the air side and refrigerant side resistances for even the desuperheating section can not be separated.

$$\frac{1}{U_{desup}} = B_1 + \frac{B_2}{h_{desup}} \tag{7.48}$$

$$\frac{1}{U_{2ph}} = \text{constant} \tag{7.49}$$

$$\frac{1}{U_{sub}} = \text{constant} \tag{7.50}$$

This fact is reinforced by the sensitivity of the objective function to these parameters. Table 7.2 shows the sensitivities of the objective function to a 1% change in a given parameter while the others remain constant. The objective function is not very sensitive to changes in the air side resistance; it can more or less have any value. This in itself suggests that there is something wrong with the assumed form of the model used to correlate the data. Further, if the air side resistance is not well defined then the conductance for the desuperheating section is also uncertain. Because the desuperheating section effects the area available for two phase heat transfer, the two phase conductance becomes uncertain. Therefore, uncertainties in the air side resistance propagate through the other conductances.

Table 7.2. Objective Function Sensitivities - Variable Conductance Model

Case	Change in Objective Function for 1% Increase in B_1	Change in Objective Function for 1% Increase in B_2	Change in Objective Function for 1% Increase in U2ph	Change in Objective Function for 1% Increase in Usub
R12	+0.08%	+0.82%	+0.34%	-
R134a	+0.29%	+1.13%	+1.04%	-0.09%

As one last try at separating the air side resis tance from the refrigerant side resistance for the desuperheating section, the objective function defined by Equation 7.51 was used. In this case, the measured subcooled refrigerant temperature is compared to the calculated value given by Equation 7.52. As with the previous attempt, the objective function did not converge for finite values of the two phase conductances or the B_2 constants.

$$\text{Objective Function} = \sum_{i=1}^{n} [T3calc_i - T3_i]^2 \tag{7.51}$$

$$T3calc_i = T2_i - \frac{\dot{Q}csubrate_i}{cminsub_i} \quad i = 1,n \tag{7.52}$$

7.5 Contour Plots

To add some reality to the process of estimating the parameters for the condenser, Figure 7-5 and 7-6 show three dimensional plots of the objective function for the R134a data set. For each plot the parameter not listed on one of the axes is held constant. The best estimate of the parameters occurs at the minimum value of the objective function. As the plots show the objective function is not a very nice surface. In fact the long curved valleys really play havoc with optimization routines as mentioned in Chapter 5. The presence of valleys is what causes slow convergence.

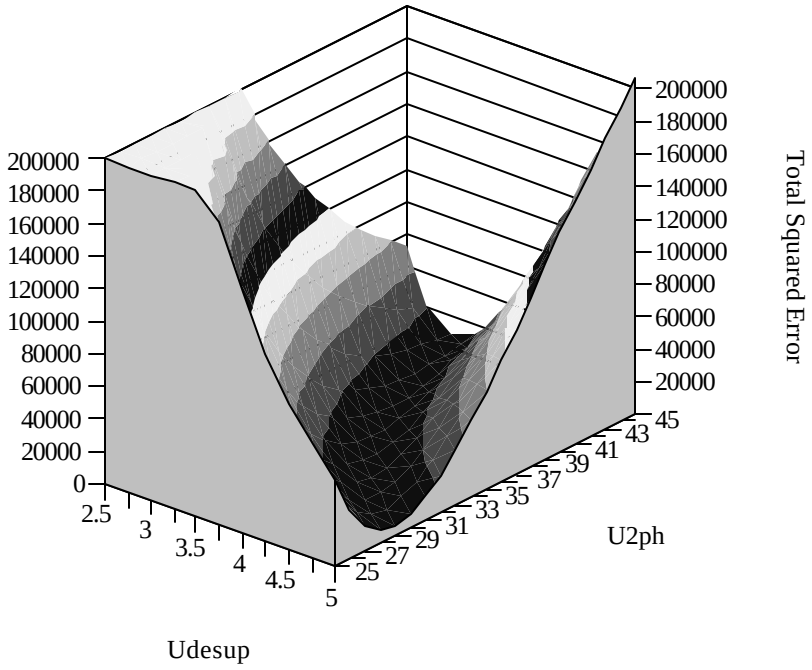

Figure 7-5. R134a Squared Errors Plotted as a Function of U_{desup} and U_{2ph}

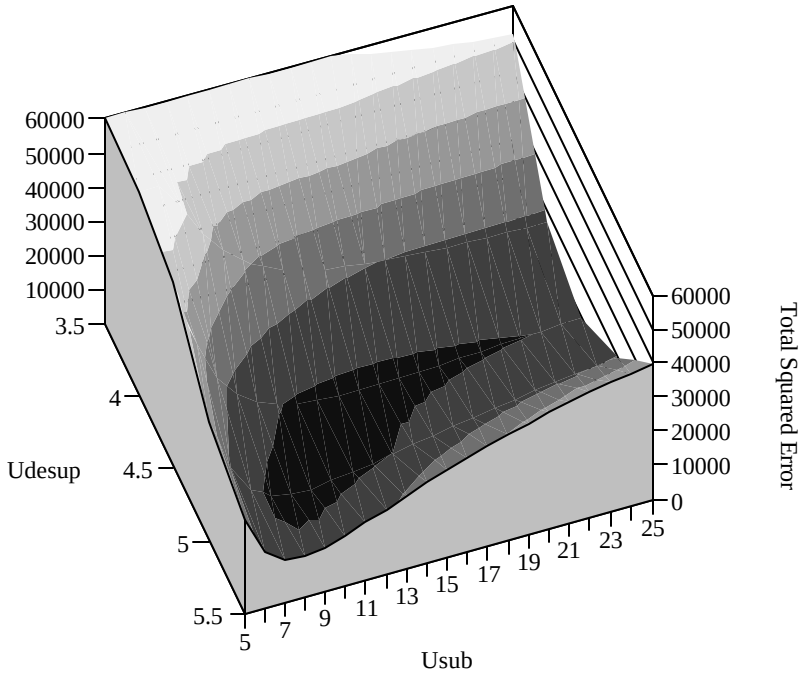

Figure 7-6. R134a Squared Errors Plotted as a Function of U_{desup} and U_{sub}

7.6 Conclusions

The constant conductance model does a pretty good job at predicting condenser heat transfer performance. The model is able to predict the heat transfer rate for the R12 condenser to within ±10% and ±5.0% for the R134a condenser. In all likelihood the R12 model can be improved if the uncertain air side measurements could be replaced

with more accurate refrigerant side measurements. This fact underscores the need for having subcooling in the condenser. In fact, for the purpose of estimating parameters, it is very desirable to adjust the capillary tube if needed to yield subcooled conditions at the condenser outlet.

Theoretical calculations showed that the air side resistance is roughly 80% of the total in the two phase section of the condenser. As a result, the theoretical two phase conductances only varied by 9% for the R12 data and 4.4% for the R134a data due to variations on the refrigerant side. For the desuperheating section, the air side and refrigerant side resistances are the same order of magnitude. The refrigerant side should have an effect on the overall conductance for this section. For the desuperheating section, the variation in the refrigerant side resistance resulted in the overall conductance varying by 31% for the R12 data and 23% for the R134a data. Lastly, because the subcooled section had laminar flow, the film coefficient is only affected by property variations. The theoretical variation in the subcooled conductance for the R134a data is only 13%.

The apparently small variations in the conductances thwarted efforts to separate the conductances into a refrigerant side and air side component. This is true even for the desuperheating section where the variation in the conductances appears to be the largest. As a result of the inability to separate the conductances, the effect of switching refrigerants could not be experimentally determined. To accomplish this task, it will be necessary to vary the condenser air flow rate. In this way the air side resistance will be varied which will result in variations in the conductances.

References

[1] Reeves, R.N., Modeling and Experimental Parameter Estimation of a Refrigerator/Freezer System, Air Conditioning and Refrigeration Center, Dept. of Mechanical and Industrial Engineering, University of Illinois at Urbana-Champaign, 1992, Chapter 5, pp. 30 to 41.

[2] Kempiak, M.J. and R.R. Crawford., Three-Zone Modeling of a Mobile Air Conditioning Condenser, Air Conditioning and Refrigeration Center, Dept. of Mechanical and Industrial Engineering, University of Illinois at Urbana-Champaign, 1992.

[3] Incropera, F.P. and D.P. DeWitt., Fundamentals of Heat and Mass Transfer, Second Edition, John Wiley & Sons, Inc., New York, 1985, p. 505.

[4] Personal communication., Mr Mark Wattley, General Electric Company, Appliance Park, Louisville, Kentucky, 40255.

Chapter 8: Suction Line Heat Exchanger Parameter Estimation

8.1 Overview

The suction line heat exchanger, or interchanger, consists of the capillary tube soldered to the compressor suction line. It not only improves system efficiency but also helps to prevent liquid refrigerant from the evaporator entering the compressor. The interchanger is essentially a counterflow heat exchanger on a macroscopic level. On a microscopic level the interaction between the capillary tube and the suction line is quite complex. The presence of two phase flow with large pressure gradients in the capillary tube coupled with heat transfer to the refrigerant in suction line makes modeling difficult.

To simplify the model, only the thermal characteristics of the interchanger will be considered here (see Purvis for an in depth look at the thermal and hydraulic characteristics of capillary tubes [1]). Further, the heat exchange and expansion processes are considered to occur in two separate steps. First the liquid refrigerant in the capillary tube exchanges heat with the suction line gas. Second, the cooled refrigerant in the capillary tube undergoes an isenthalpic expansion. Figure 8-1 shows the idealized interchanger based on these two processes.

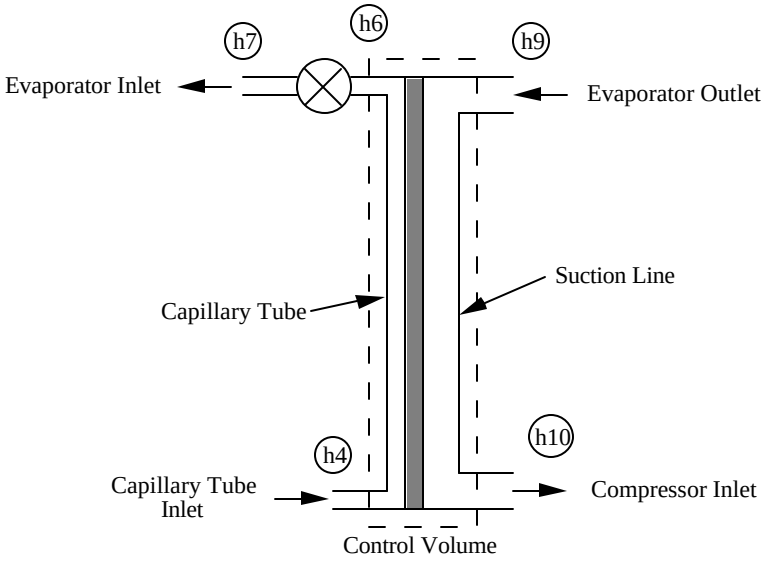

Figure 8-1. Idealized Suction Line Heat Exchanger

8.2 Constant Effectiveness Model

The first model to be considered is a constant effectiveness model. Equation 8.1 determines the heat transfer rate in the interchanger given the effectiveness for the interchanger. By comparing the rate equation with the measured heat transfer rate defined by Equation 8.2, the effectiveness for a given point can be determined. To estimate the best effectiveness, a non-linear least squares worksheet in E.E.S. was formulated to solve Equation 8.3.

$$\dot{Q}\,rate_i = \varepsilon_{int} cmin_i (T4_i - T9_i) \quad i = 1,n \tag{8.1}$$

$$\dot{Q}\,int_i = \dot{m}\,(h10_i - h9_i) \quad i = 1,n \tag{8.2}$$

$$\frac{d}{d\varepsilon}\sum_{i=1}^{n}\left[\dot{Q}\,int_i - \dot{Q}rate_i\right]^2 = 0.0 \qquad (8.3)$$

where $\dot{Q}$ rate = predicted heat transfer rate (Btu/hr)

ε_{int} = interchanger effectiveness

cmin = minimum $\dot{m}$ C_p (Btu/lbm°F)

T4 = capillary tube inlet refrigerant temperature (°F)

T9 = evaporator outlet refrigerant temperature (°F)

$\dot{Q}$ int = measured interchanger heat transfer rate (Btu/hr)

$\dot{m}$ = refrigerant mass flow rate (lbm/hr)

h9 = refrigerant enthalpy at evaporator outlet (Btu/lbm)

h10 = refrigerant enthalpy at compressor inlet (Btu/lbm)

Table 8.1. Constant Effectiveness Model Results

Case	Effectiveness	Experimental Uncertainty	Standard Deviation	Total Uncertainty
R12	0.80	±0.06	0.014	±0.066
R134a	0.88	±0.04	0.008	±0.043

The results of this approach are summarized in Table 8.1. The small standard deviation for both cases indicates the effectiveness is relatively constant as assumed. This can also be seen in Figures 8-2 and 8-3 where the slope of the line is the effectiveness. Note the very small scatter in the data!

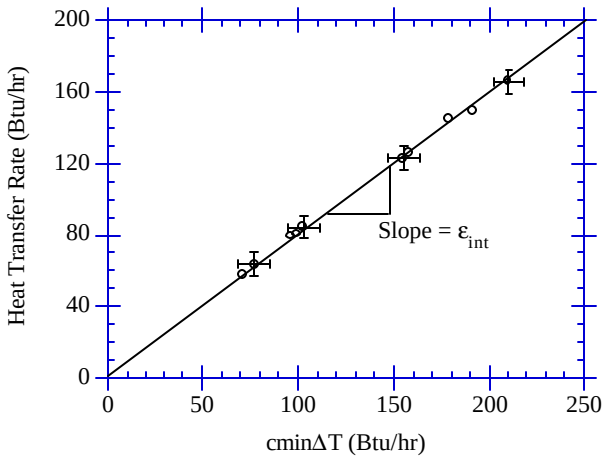

Figure 8-2. Interchanger Effectiveness - R12 data

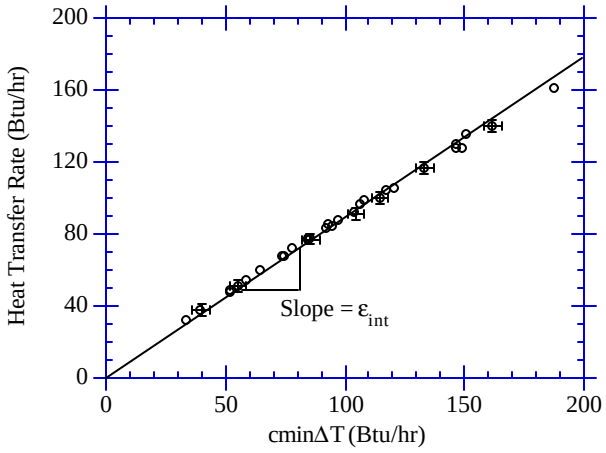

Figure 8-3. Interchanger Effectiveness - R134a

Since the effectiveness is nearly constant, it would be expected that the constant effectiveness model would do a good job at predicting interchanger heat transfer. Figures 8-4 and 8-5 compare the predicted interchanger heat transfer rates to the measured rates. The model is able to predict the heat transfer rates to within ±3.0% for the R12 data and ±5.0% for the R134a data.

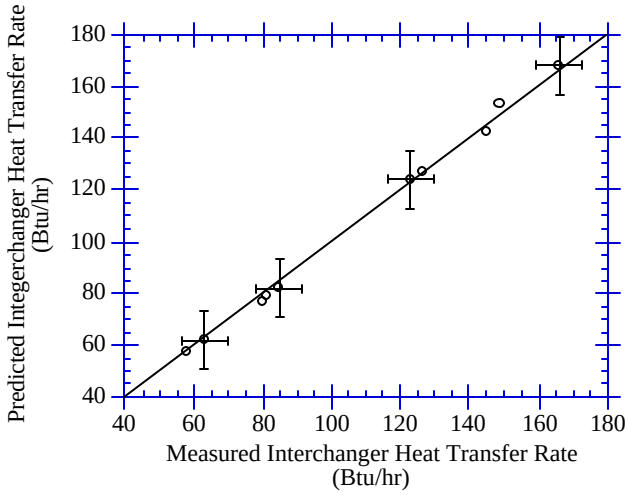

Figure 8-4. R12 Interchanger Heat Transfer - Constant Effectiveness Model

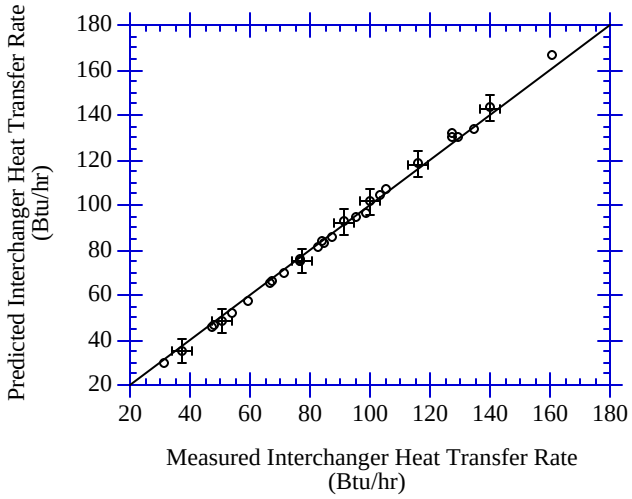

Figure 8-5. R134a Interchanger Heat Transfer - Constant Effectiveness Model

8.3 Constant UA Model

Although the constant effectiveness model does a very good job at predicting interchanger heat transfer, it can not explain why the effectiveness of the interchanger using R134a is 10% higher than for R12. To explore this question, it is necessary to look at the overall heat transfer coefficient for the interchanger. This quantity is dependent on fluid properties which may account for the difference.

It is assumed that the overall heat transfer coefficient for the interchanger is constant. The UA for the interchanger can be determined from an effectiveness-NTU relation for a simple counterflow heat exchanger [2] given by Equation 8.4. By substituting this expression into Equation 8.1, the rate equation based on UA can be compared to the measured heat transfer rate. Equation 8.5 was solved to determine the best UA value for all the data points.

$$\varepsilon_i = \frac{1 - e^{(-UA_{int}/cmin_i)(1-R_i)}}{1 - R_i\, e^{(-UA_{int}/cmin_i)(1-R_i)}} \qquad i = 1,n \tag{8.4}$$

where $R_i = cmin_i/cmax_i$

$cmax = \text{maximum } \dot{m}\ C_p$ (Btu/lbm°F)

$$\frac{\delta}{\delta UA_{int}} \sum_{i=1}^{n} \left[\dot{Q}\,int_i - \varepsilon_i c\,min_i\,(T4_i - T9_i)\right]^2 = 0.0 \tag{8.5}$$

The results for this model are summarized in Table 8.2. The overall heat transfer coefficient for the R12 data is 10% higher than for the R134a data. This result at first does not seem consistent with the results in Table 8.1. A higher overall heat transfer coefficient should relate to a higher effectiveness. However, the heat capacity rates are significantly different. If the UA's in Table 8.2 are substituted into Equation 8.4 along with nominal heat capacity rates for both data sets, the effectiveness is predicted to be 0.82 for the R12 data and 0.89 for the R134a data. This is consistent with the results in Table 8.1.

Table 8.2. Constant Overall Heat Transfer Coefficient Model Results

Case	UA_{int} (Btu/hr°F)	Uncertainty (Btu/hr°F)	Standard Deviation (Btu/hr°F)	Total Uncertainty (Btu/hr°F)
R12	6.14	±1.4	0.12	±1.42
R134a	5.59	±1.1	0.30	±1.25

To see if the difference in the overall heat transfer coefficients can be attributed to fluid properties, it is necessary to separate the overall heat transfer coefficient into its constituent parts. Equation 8.6 relates the overall heat transfer coefficient for the interchanger to from left to right: the capillary tube convective resistance, the wall resistance, and the suction line convective resistance. This expression can be simplified by first assuming the wall resistance is negligible. Second, two phase flow exists inside most of the capillary tube. Since two phase flow convective coefficients are at least an order of magnitude higher than forced convective coefficients, the first term in Equation 8.6 is assumed small and can be neglected. Making these assumptions reduces Equation 8.6 to Equation 8.7.

$$\frac{1}{UA_{int}} = \frac{1}{h_{cap}A_{cap}} + R_w + \frac{1}{h_{suc}A_{suc}} \tag{8.6}$$

where h_{cap} = capillary tube side convective film coefficient

A_{cap} = heat transfer surface area on capillary tube side

R_w = wall resistance

h_{suc} = suction side film coefficient

A_{suc} = heat transfer surface area on suction side

$$UA_{int} \sim h_{suc}A_{suc} \tag{8.7}$$

The suction side film coefficient can be estimated from the Dittus-Boelter equation given by Equation 8.8 [3]. Table 8.3 lists the film coefficients along with the ranges of the Reynolds number and Prandtl number for both refrigerants. The ratio of the film coefficients should be equal to the ratio of the overall heat transfer coefficients because the surface area is constant. The ratio of the R12 film coefficient to the R134a film coefficient is 1.23 while the ratio of the overall heat transfer coefficients is 1.1. Therefore, the same trend is predicted by the theoretical equations. However, the discrepancy between the two is probably the result of neglecting the other resistances in Equation 8.6.

$$h_{suc} = 0.023 Re^{0.8} Pr^{0.4} \left(\frac{k_{suc}}{D}\right) \tag{8.8}$$

where Re = Reynolds number of gas

Pr = Prandtl number of gas

k_{suc} = thermal conductivity of gas

Table 8.3. Internal Suction Line Convective Film Coefficients

Case	Reynolds Number	Prandtl Number	Average Film Coefficient (Btu/hr-ft^2°F)
R12	36257 to 44409	0.817 to 0.829	28.3
R134a	18775 to 22557	0.719 to 0.736	23.0

If Equation 8.6 is rewritten in the form of Equation 8.9, it is possible to estimate the constant A which contains both the assumed constant wall resistance and capillary tube resistance. Using the film coefficient for R12 from Table 8.3 and an estimated suction line length of 62 in. which corresponds to a surface area of 0.296 ft^2, the value of A is 0.0435 hr-ft^2°F/Btu. Using this value for A, Equation 8.9 predicts the R134a overall heat transfer coefficient to be 5.3 Btu/hr-ft^2°F which is within 5.5% of the value given in Table 8.2.

$$\frac{1}{UA_{int}} = A + \frac{1}{h_{suc}A_{suc}} \tag{8.9}$$

Therefore Equation 8.9 can be used to predict at least relative changes in the overall heat transfer coefficient for the interchanger. However, note that there is a good deal of uncertainty in the values in Table 8.2. As a result Equation 8.9 should be used with caution.

Figures 8-6 and 8-7 compare the predicted interchanger heat transfer using the constant UA model to the measured values. The constant UA model is able to predict the interchanger heat transfer to within ±5% for the R12 data and ±4% for the R134a data. These are essentially the same errors as for the constant effectiveness model. Therefore for these data sets it appears that both models work equally well.

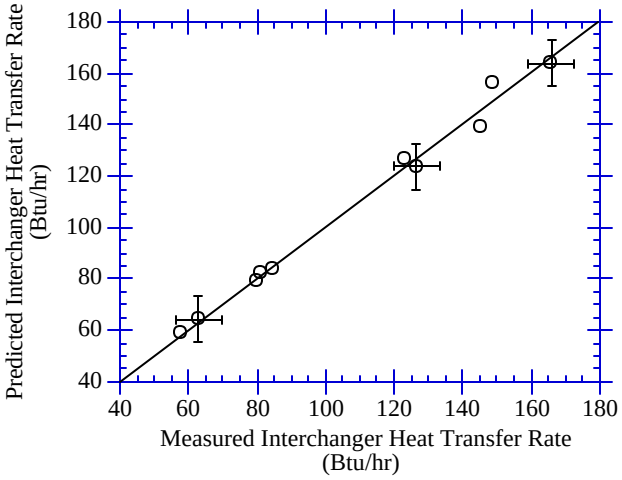

Figure 8-6. R12 Interchanger Heat Transfer - Constant UA Model

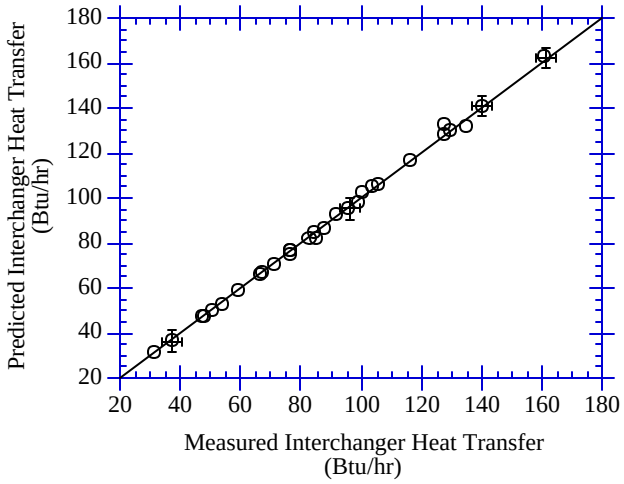

Figure 8-7. R134a Interchanger Heat Transfer - Constant UA Model

This is an interesting result. Reeves [4] found that the constant conductance model did a much poorer job than the constant effectiveness model. The explanation for the discrepancy may be the different sizes of the cap tubes. The capillary tube for the refrigerator studied here is 0.004 in. smaller than the one used in Reeves' experiments. It could be that the smaller capillary tube significantly reduces the distance to the flash point. As a result, almost the entire length of the capillary tube is two phase. For the mass flow rates studied, the heat transfer characteristics may be relatively constant in this two phase zone. In Reeves' experiments the flash point may be further down the capillary tube. As a result there are two zones: a subcooled region and a two phase region. Heat transfer with the suction gas with two regions could result in more scatter in the data as refrigerant mass flow rates changes.

8.4 Conclusions

Both the constant effectiveness and the constant UA models for the interchanger are able to predict heat transfer in the interchanger to within ±5%. For the data analyzed, both models do equally well with no clearly better choice between the models.

A theoretical expression for the overall heat transfer coefficient was able to predict the trends in the data. It was found that the capillary tube side heat transfer resistance and the wall resistance account for approximately 25% of the total resistance. It is most likely that the wall resistance is still negligible. Therefore, future work on the interchanger will need to include the effects of the film coefficient in the capillary tube on the overall heat transfer coefficient as it is probably not constant as assumed here.

References

[1] Purvis, B.D., A Computer Model for Refrigerant Flow in Small Bore Tubes, Forthcoming, Air Conditioning and Refrigeration Center, University of Illinois at Urbana-Champaign, 1992.

[2] Kays, W.M. and A.L. London., Compact Heat Exchangers, Third Edition, McGraw-Hill, New York, 1984, pp. 11 to 49.

[3] Incropera, F.P. and D.P. DeWitt., Fundamentals of Heat and Mass Transfer, Second Edition, John Wiley & Sons, Inc., New York, 1985, p. 394.

[4] Reeves, R.N., Modeling and Experimental Parameter Estimation of a Refrigerator/Freezer System, Air Conditioning and Refrigeration Center, University of Illinois at Urbana-Champaign, 1992, pp. 30 to 41.

Chapter 9: Evaporator Parameter Estimation

9.1 Overview

The model for the evaporator is based in part on the work by Reeves [1]. Reeves evaluated the approach used by DOE and ADL [2,3] and found that modeling the evaporator as containing all two phase liquid from inlet to outlet did not do a very good job at predicting evaporator heat transfer. This was particularly true for cases where the evaporator had a significant amount of superheat at the exit. This simple model was markedly improved by splitting the evaporator into a two phase section and a superheated section.

Reeves used effectiveness-NTU relations [4] with the assumption that the overall conductances contained in these relations were constants. Once the heat exchanger effectiveness was determined for each section, the appropriate rate equations were then solved to predict heat transfer from the two phase and superheated sections. Reeves found that the conductance for the two phase section was 14 times larger than in the superheated section for his R12 data.

These constant conductances given by Equation 9.1 and 9.2 are a combination of internal and external resistances to heat transfer. The total resistance to heat transfer, which is the inverse of the overall conductance, is given by Equation 9.3 [5] where the x refers to either the two phase or superheated section. The terms on the right side of Equation 9.3 are from left to right: the resistance to heat transfer on the air side, the resistance of the evaporator tube wall, and the resistance to heat transfer on the refrigerant side. The assumption of constant conductances is good if the air side and refrigerant side convective film coefficients in Equation 9.3 are constant. The model should also work if the air side resistance is held constant by keeping the air side volumetric flow rate constant and the magnitude of the air side resistance is much larger than the other resistances. Under these conditions, variations in the refrigerant side resistance have little impact on the overall conductance. As a result the overall conductance is again constant. Note that the area ratios in Equation 9.3 are also constants.

$$\frac{1}{U_{sup}} = \text{constant} \tag{9.1}$$

$$\frac{1}{U_{2ph}} = \text{constant} \tag{9.2}$$

where U_{sup} = conductance for the superheated evaporator section

U_{2ph} = conductance for the two phase evaporator section

$$\frac{1}{U_x} = \frac{A_x/A_o}{h_o} + \frac{A_x \ln(r_o/r_i)}{2\pi L k} + \frac{A_x / A_i}{h_i} \tag{9.3}$$

where U_x = overall conductance based on A_x

A_x = arbitrary surface area

h_o = air side convective film coefficient

A_o = effective air side surface area

r_o = outside radius of evaporator tube

r_i = inside radius of evaporator tube

L = length of a given evaporator section

k = thermal conductivity of tube

h_i = refrigerant side convective film coefficient

Ai = effective refrigerant side surface area

Further, if the air side resistance had dominated the heat transfer process in both sections of Reeve's evaporator, it would be expected that the conductances for each section would have been nearly equal. However, the large difference between the two conductances suggests the refrigerant side must be having an impact on the overall conductance. Rather than assume constant conductances, Reeve's model may be improved by making the overall conductances functions of the internal film coefficients which vary as functions of mass flow rate and refrigerant properties.

For the data sets considered here, the evaporator air flow rate was held constant. The air side convective film coefficient can then be assumed to be constant if property variations in the Reynolds number and Prandtl number are neglected. This assumption is good for the 0°F to 60°F range of evaporator air temperatures considered. With these assumptions Equation 9.3 can be written in the form of Equations 9.4 and 9.5. The constant B_1, which is the same for both sections, represents the constant air side resistance plus the assumed constant wall resistance . The constant B_2 is the ratio of the surface area A_x to the refrigerant side surface area A_i in Equation 9.3. The conductances are now functions of the internal film coefficients.

$$\frac{1}{U_{sup}} = B_1 + \frac{B_2}{h_{sup}} \tag{9.4}$$

$$\frac{1}{U_{2ph}} = B_1 + \frac{B_3}{h_{2ph}} \tag{9.5}$$

where hsup = superheated section refrigerant film coefficient

h2ph = two phase section refrigerant film coefficient

Both the constant conductance model and the variable conductance model will be considered for the R12 and R134a data sets. However, before these conductances can be found, the volumetric air flow rate must be determined. This quantity is required to evaluate the effectiveness- NTU relations.

9.2 Evaporator Volumetric Flow Rate

The volumetric air flow rate across the evaporator was estimated by setting air side and refrigerant side heat transfers across the evaporator equal to each other. Equation 9.6 lists the relation used. The refrigerant side enthalpy difference shown is not across the evaporator but rather across the interchanger. It is assumed that the interchanger is adiabatic relative to the environment. Under this condition the enthalpy difference (h10 - h4) is equal to that across the evaporator, (h9-h7).

$$\rho C_p 60 \dot{V}_e \Delta T = \dot{m}(h10 - h4) = \dot{Q}_e \tag{9.6}$$

$\dot{V}_e$ = volumetric flow rate (ft^3/min)

ρ = density of air (lbm/ft^3)

C_p = specific heat of air (Btu/lbm°F)

ΔT = temperature difference across evaporator (°F)

$\dot{m}$ = refrigerant mass flow rate (lbm/hr)

h10 = refrigerant enthalpy at compressor inlet (Btu/lbm)

h4 = refrigerant enthalpy at capillary tube inlet (Btu/lbm)

$\dot{Q}_e$ = evaporator heat transfer rate (Btu/hr)

The air temperatures at the inlet and outlet of the evaporator unfortunately are not directly measurable. The return air from the freezer compartment and the fresh food compartment mix right at the bottom of the evaporator coil as shown in Figure 9-1. Air temperature measurements with a thermocouple couple array mounted to the sheet metal defrost heater shroud, which is just below the coil, revealed large temperature fluctuations. The same fluctuations would be expected to occur at the outlet to the evaporator. These air temperatures were too uncertain to use so other points had to be chosen.

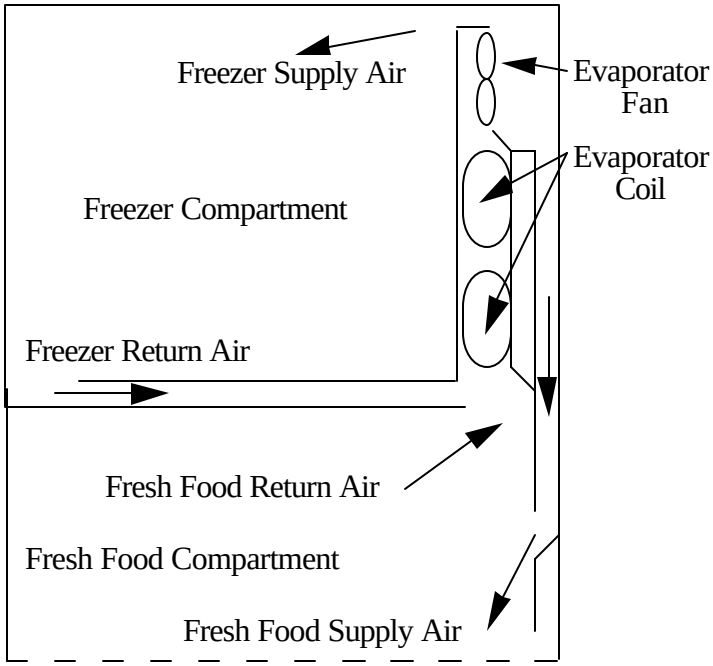

Figure 9-1. Refrigerator Evaporator Air Flow Patterns

The inlet air temperature to the evaporator was determined from Equation 9.7. This is simply a mixing equation for the two evaporator return air streams. In this equation the freezer return air temperature, Tfz, and the fresh food return air temperature, Tff, are both steady temperatures compared to the evaporator inlet. As a result a much better estimate of the average mixed air temperature at the inlet to the evaporator can be made. Note that in this equation the air mass flow rates are as yet unknown.

$$\dot{m}_{fz}\, h(Tfz) + \dot{m}_{ff}\, h(Tff) = \dot{m}_a\, h(Tma) \qquad (9.7)$$

where $\dot{m}_{fz}$ = mass flow rate of air returning from freezer (lbm/hr)

h(Tfz) = freezer return air enthalpy (Btu/lbm)

Tfz = freezer return air temperature (°F)

$\dot{m}_{ff}$ = mass flow rate of air from the fresh food compartment (lbm/hr)

h(Tff) = fresh food compartment return air enthalpy (lbm/hr)

Tff = fresh food compartment return air temperature (°F)

$\dot{m}_a$ = mass flow of mixed air across evaporator (lbm/hr)

h(Tma) = mixed air enthalpy (Btu/lbm)

Tma = mixed air temperature (°F)

The evaporator outlet air temperature was determined by considering an energy balance across the evaporator fan given by Equation 9.8. In this equation both the fan outlet air temperature and the fan power are measured. However, as in Equation 9.7, the mass flow rate of air is still not known.

$$3.413\dot{P}_{fan} = \dot{m}_a C_p (Tfanout - Taevapout) \tag{9.8}$$

where $\dot{P}_{fan}$ = evaporator fan power (W)

$\dot{m}_a$ = mass flow rate of air across evaporator (lbm/hr)

C_p = specific heat of air (Btu/lbm°F)

Tfanout = air temperature downstream of evaporator fan (°F)

Taevapout = evaporator outlet air temperature (°F)

Equations 9.6, 9.7 and 9.8 form a system of three equations in six unknowns. To solve the system, three more equations are required. Two more equations come from applying conservation of mass to the return air streams and relating the mass flow rate of air across the evaporator to the volumetric flow rate. Equation 9.9 and 9.10 show these relations. The last equation needed comes from the application of non-linear least squares to find the best estimate of the volumetric flow rate. Equation 9.11 compares the calculated evaporator heat transfer based on the air side to the measured heat transfer from the refrigerant side. The best estimate of the volumetric flow rate occurs when the derivative of this function with respect to $\dot{V}_e$ is zero.

$$\dot{m}_a = \dot{m}_{fz} + \dot{m}_{ff} \tag{9.9}$$

$$\dot{m}_a = \rho 60 \dot{V}_e \tag{9.10}$$

$$\frac{\delta}{\delta \dot{V}_e} \sum_{i=1}^{n} \left[\rho_i C_{pi} 60 \dot{V}_e (Tma_i - Taevapout_i) - \dot{m}_i (h10_i - h4_i) \right]^2 = 0.0 \tag{9.11}$$

Equation 9.12 defines the ratio of the freezer air mass flow rate to the total across the evaporator. This should be constant and is required for the refrigerator system model [6]. Solving Equation 9.13 yields the best

estimate of the parameter a. Note that for taking the partial derivative, $\dot{V}e$ is a function of $\dot{m}a$ from Equation 9.10 and $\dot{m}a$ is a function of (a) by Equation 9.12.

$$a = \frac{\dot{m}fz}{\dot{m}a} \tag{9.12}$$

$$\frac{\delta}{\delta a}\sum_{i=1}^{n}\left[\rho_i C_{pi}\, 60\,\dot{V}_e\,(Tma_i - Taevapout_i) - \dot{m}_i\,(h10_i - h4_i)\right]^2 = 0.0 \tag{9.13}$$

The results of solving Equations 9.6 through 9.13 simultaneously are summarized in Table 9.1 for both the R12 and R134a data sets. Within the experimental uncertainty both data sets predict the same volumetric air flow rate. These numbers are fairly close to the manufacture's estimate of 54.3 ft^3/min with an air split ratio of 0.93 [7]. The slope of the line in Figure 9-2 is equal to the evaporator volumetric flow rate for the R134a data. Note that for the conductance parameter estimation work, the volumetric flow rate from the R134a data was used. This flow rate was chosen because it is based on 30 data points compared to 10 for the R12 data even though the uncertainty is slightly higher.

Table 9.1. Evaporator Volumetric Flow Rate Results

Case	Volumetric Flow Rate ft^3/min	Standard Deviation ft^3/min	Total Uncertainty ft^3/min	a (Air Split)	Standard Deviation	Total Uncertainty
R12	62.6 ±5.3	1.7	±6.3	0.871 ±0.062	~ 0.0	±0.062
R134a	60.2 ±7.1	2.6	±8.8	0.899 ±0.045	~ 0.0	±0.045

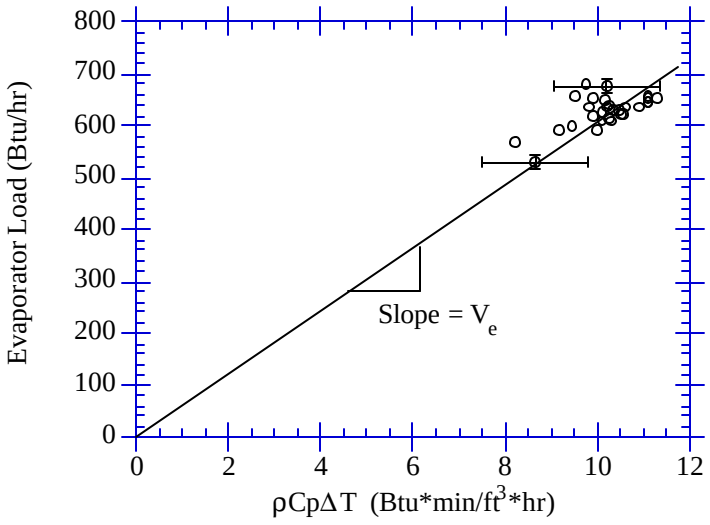

Figure 9-2. Evaporator Volumetric Flow Rate

9.3 Constant Conductance Model

To determine the conductances based on Equations 9.1 and 9.2 for both the two phase and superheated sections of the evaporator, the system of Equations 9.14 through 9.28 were solved. These equations were solved by the optimization program described in Chapter 5. One of the objective functions that was minimized is given by Equation 9.14, which is the difference between the measured heat transfer on the refrigerant side and that calculated from the rate equation.

$$\text{Minimizee} \sum_{i=1}^{n} \left[\dot{Q}e_i - \dot{Q}erate_i\,(U_{sup}, U_{2ph})\right]^2 \tag{9.14}$$

Subject to:

$$\dot{Q}\,erate_i = \dot{Q}e\,suprate_i + \dot{Q}\,e2phrate_i \quad i = 1,n \tag{9.15}$$

$$\dot{Q}\,esuprate_i = esup_i\,cmin_i\,(Tsup_i - T7_i) \quad i = 1,n \tag{9.16}$$

$$esup_i = \frac{1 - e^{\left(\frac{-U_{sup}\,asup_i}{cmin_i}\right)(1+cmin_i/casup_i)}}{1 + (cmin_i/casup_i)} \quad i = 1,n \tag{9.17}$$

$$\dot{Q}\,e2phrate_i = \left(1 - e^{(-U_{2ph}\,a2ph_i/ca2ph_i)}\right) ca2ph_i\,(Tma_i - T7_i) \quad i = 1,n \tag{9.18}$$

$$\frac{\dot{Q}e2ph_i}{\dot{Q}e_i} = \frac{\dot{Q}e2phrate_i}{\dot{Q}erate_i} \quad i = 1,n \tag{9.19}$$

$$aevap = asup_i + a2ph_i \quad i = 1,n \tag{9.20}$$

$$\dot{Q}\,e_i = \dot{w}_i\,(h10_i - h4_i) \quad i = 1,n \tag{9.21}$$

$$\dot{Q}\,esup_i = \dot{w}_i\,(h9_i - h8satvap_i) \quad i = 1,n \tag{9.22}$$

$$\dot{Q}\,e_i = \dot{Q}\,e2ph_i + \dot{Q}\,esup_i \quad i = 1,n \tag{9.23}$$

$$ca2ph_i = caevap_i \;\text{ if }\; a2ph_i/aevap >= 0.5 \quad i = 1,n \tag{9.24}$$
$$= caevap_i\,(2\,a2ph_i/aevap) \;\text{ if }\; a2ph_i/aevap < 0.5$$

$$casup_i = caevap_i \;\text{ if }\; a2ph_i/aevap <= 0.5 \quad i = 1,n \tag{9.25}$$
$$= caevap_i\,(2\,asup_i/aevap) \;\text{ if }\; a2ph_i/aevap > 0.5$$

$$Tsup_i = Tmid_i \;\text{ if }\; a2ph_i/aevap >= 0.5 \quad i = 1,n \tag{9.26}$$
$$= Tma \;\text{ if }\; a2ph_i/aevap < 0.5$$

$$Tmid_i = Tma - \frac{\dot{Q}2phpartial_i}{caevap_i} \quad i = 1,n \tag{9.27}$$

$$\dot{Q}2phpartial_i = \left(1 - e^{\left(\frac{-0.5\,U_{2ph}\,aevap}{caevap_i}\right)}\right) caevap_i\,(Tma_i - T7_i) \quad i = 1,n \tag{9.28}$$

where $\dot{Q}$erate = predicted heat transfer rate from the evaporator (Btu/hr)

$\dot{Q}$esuprate = predicted heat transfer rate from superheated section (Btu/hr)

$\dot{Q}$e2phrate = predicted heat transfer rate from two phase section (Btu/hr)

esup = effectiveness of superheated section

cmin = heat capacity rate for refrigerant in superheated section (Btu/hr °F)

Tsup = air temperature at inlet to the superheated section (°F)

T7 = saturated refrigerant temperature in evaporator (°F)

U_{sup} = conductance for the superheated section (Btu/hr-ft^2 °F)

asup = area of the superheated section (ft^2)

casup = air-side heat capacity rate for superheated section (Btu/hr °F)

U_{2ph} = conductance for the two-phase section (Btu/hr-ft^2 °F)

a2ph = area of two-phase section (ft^2)

ca2ph = air-side heat capacity rate for two phase section (Btu/hr °F)

caevap = air-side heat capacity rate for the evaporator (Btu/hr °F)

Tma = mixed air temperature at inlet to the evaporator (°F)

aevap = total surface area of the evaporator (ft^2)

$\dot{Q}$e = measured refrigerant heat transfer from the evaporator (Btu/hr)

$\dot{Q}$e2ph = measured refrigerant heat transfer from the two-phase section (Btu/hr)

$\dot{Q}$esup = measured refrigerant heat transfer from the superheated section (Btu/hr)

$\dot{w}$ = refrigerant mass flow rate (lbm/hr)

h4 = refrigerant enthalpy at the inlet to the cap-tube (Btu/lbm)

h8satvap = saturated vapor enthalpy in the evaporator (Btu/lbm)

h9 = refrigerant enthalpy at the exit of the evaporator (Btu/lbm)

h10 = refrigerant enthalpy at the compressor inlet (Btu/lbm)

Tmid = air temperature after first row of the evaporator coil (°F)

$\dot{Q}$2phpartial = heat transfer from first row of coil if all two phase (Btu/hr)

Another objective function given by Equation 9.29 was also used to see if this objective function could provide more accurate estimates than Equation 9.14. Note that T9 is measured in the lab. Further, the heat transfer rate for the superheated section comes from the solution of Equations 9.15 to 9.28.

$$\text{Objective Function} = \sum_{i=1}^{n} \left[T9calc_i - T9 \right]^2 \qquad (9.29)$$

where

$$T9calc_i = T7_i + \frac{\dot{Q}esuprate_i}{cmin_i} \quad i = 1,n \tag{9.30}$$

To help visualize the solution process, Figure 9-3 shows a flow chart for the equations using the objective function given by Equation 9.29. The labeled arrows represent inputs. The quantities inside the boxes are variables that are calculated from the inputs.

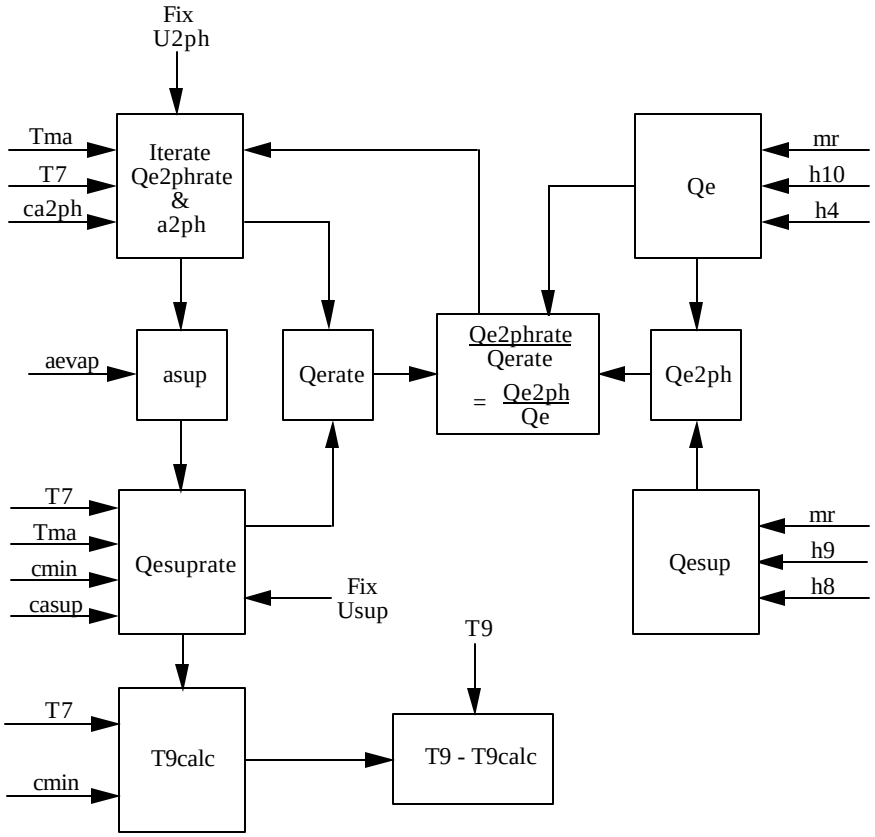

Figure 9-3. Evaporator Equation Flow Diagram

It should be noted that the calculated evaporator exit temperature, T9calc, is not totally independent of the measured temperature, T9. The loss of independence occurs as a result of not knowing the enthalpy of the refrigerant at the evaporator inlet. In its place the enthalpies h10, h4 and h9 must be used. Since h9 is a function of measured T9, the equations are not totally independent. The effect the loss of independence has on the parameter estimation process will be discussed later.

The equations shown in Figure 9-3 are not the only possible set. One variation is to replace Equation 9.19 with an expression that sets the two phase heat transfer rate equal to the measured refrigerant side value. Computer runs were made with this set of equations and it was found that it made little difference in the estimated parameters. This is reasonable since multiplying Equation 9.19 through by the nearly equal total rate and measured evaporator heat transfers yields the same expression. It is also possible to replace the measured heat transfer from the evaporator given by Equation 9.21 with an equivalent expression based on the refrigerator cabinet load (Refer to Appendix B).

However, for this refrigerator the cabinet load was not known because of the uncertainty introduced by the door heater.

Some other details about the equations should also be mentioned. The expression for the effectiveness for the two phase section in Equation 9.18 is independent of geometry. However, the effectiveness equation for the superheated section is not. Figure 9.4 illustrates the geometry of the evaporator coil. The coil is essentially two helical coils with spine fins in the inside of the helices. The first obvious choice is to model the superheated section as a crossflow heat exchanger. However, it was found that this form did not show a minimum in the objective function for finite values of the conductances. Many other forms were tried but the only effectiveness equation that would work was for parallel flow. However, for a typical ratio of cmin/casup equal to 0.038 the various effectiveness equations yield nearly equivalent results [4]. Apparently there must be enough variation in the different expressions to make a difference in the objective function.

An explanation of the temperature Tsup and the terms ca2ph and casup is needed. The air temperature at the inlet to the superheated section, Tsup, can be either the mixed air temperature at the inlet to the evaporator or some lower temperature air off the first row of the coil. In the case shown in Figure 9-4, the superheated section does not see Tma. Instead it sees the temperature after the first row, Tmid, determined by Equation 9.27. Equation 9.28 calculates the heat transfer from the first row of the coil needed in Equation 9.27 using the best estimate of the conductance for the two phase section.

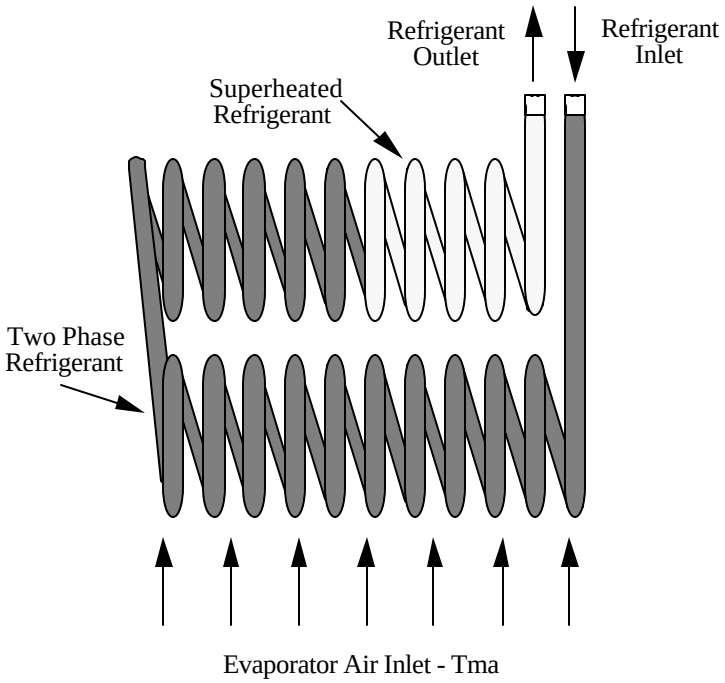

Figure 9-4. Evaporator Coil Geometry

It is also possible, and indeed for most of the R134a data it is the case, that the two phase section occupies less than half of the coil. In this situation, the superheated section sees the inlet air temperature to the evaporator. This is the temperature that should then be used in Equation 9.16. It was found that if these geometric considerations

were not taken into account it was impossible to get the model to produce any results. Note that the solution of these equations is part of the simultaneous solution of the other equations.

A further refinement to the equations involves the terms ca2ph and casup which are the air side capacity rates for the two phase and superheated sections respectively. For the superheated section shown in Figure 9-4, only part of the inlet air flows over this section. To account for this, the total air side capacity rate, caevap, is multiplied by the ratio of the superheated section area to half the total evaporator area as shown in Equation 9.25. If however, the superheated section occupies more than 50% of the coil then the total air side capacity rate is used.

The same situation arises for the two phase section. For the case shown in Figure 9-4 the total air side capacity rate is used in Equation 9.18. If however less than half the coil is two phase then the total air capacity rate, caevap, is multiplied by the ratio of the two phase section area to half the total evaporator area. This relation is given by Equation 9.24.

The result of solving the above equations for both the R12 and R134a data sets using both forms of the objective function are summarized in Table 9.2. Equation 9.14 was used for the R12-Qe case and Equation 9.29 was used for the R12-T9 and R134a cases. The sensitivities listed equal the percentage change in the objective function for a one percent increase in the indicated parameter while all others remained constant. Further, the conductances are based on the total surface area, aevap, equaling 3.8 ft^2. Note that this area is totally arbitrary. However, to give some physical significance it was set equal to an estimate of the outside surface area of the evaporator tubing only.

The last column lists the standard deviation of the respective objective functions evaluated at the optimum conductances.

Table 9.2. Constant Conductance Model Results

Case	U_{sup} (Btu/hr-ft^2°F)	Sensitivity U_{sup}	U_{2ph} (Btu/hr-ft^2°F)	Sensitivity U_{2ph}	Standard Deviation
R12-Qe	1.58 ±0.25	+0.27%	20.5 ± 1.7	+0.18%	59.4 Btu/hr
R12-T9	1.11 ±0.25	-0.7%	36.2 ±1.7	-0.23%	1.4°F
R134a	0.54 ±0.06	-0.38%	~ 36.2	-0.032%	3.2°F
Based on total evaporator outside tube surface area = 3.8 ft^2					

The first result indicated in Table 9.2 is the fact that for the R12 data set the objective function based on temperature gives significantly different results from the objective function based on heat transfer. This difference can not be explained by the experimental uncertainty in the estimates. To see if either set of conductances are better estimates than the other, Figures 9-5 through 9-8 compare the predicted and measured heat transfer rates and the predicted and measured evaporator exit temperatures for each set. The conductances based on the heat transfer objective function predicts the heat transfer from the evaporator to within ±11.0% while the conductances from the temperature objective function do a little worse at ±13.0%. For the evaporator exit temperature, the conductances based on the heat transfer objective function predict the exit temperature from the evaporator to within ±4°F while the conductances from the temperature objective function do better at ±2.5°F. It is not surprising that the objective function based on temperature does better at predicting temperature and the objective function based on heat transfer does a better job at predicting heat transfer. It is surprising, however, that the results are so close, given the

substantial difference between the two sets of conductances. As a result, there is no convincing basis for choosing one set over the other.

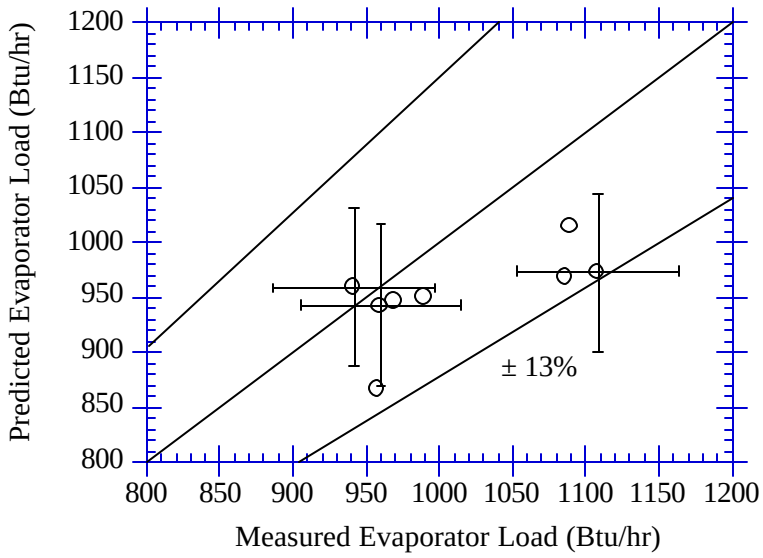

Figure 9-5. R12 Evaporator Heat Transfer Based on Temperature Objective Function

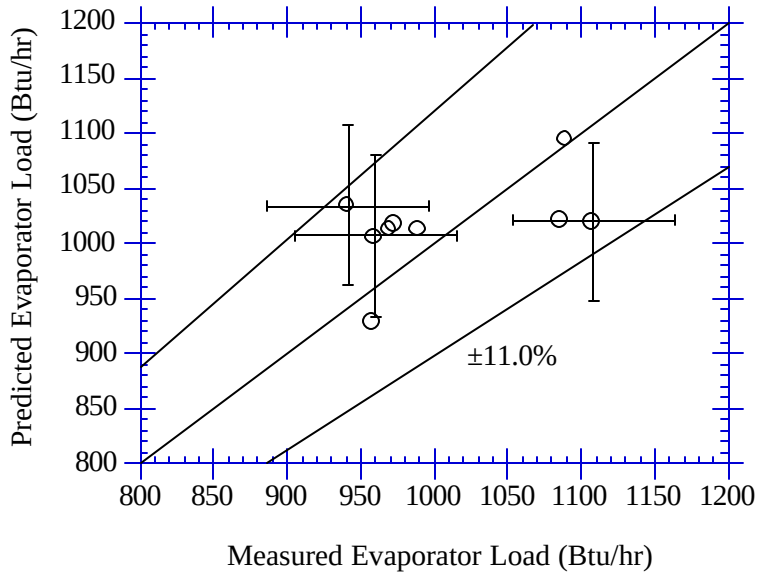

Figure 9-6. R12 Evaporator Heat Transfer Based on Heat Transfer Objective Function

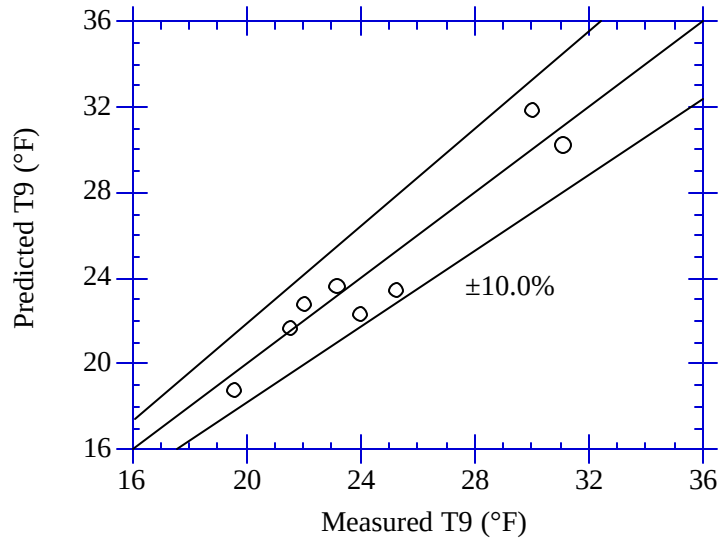

Figure 9-7. R12 Evaporator Exit Temperature Based on Temperature Objective Function

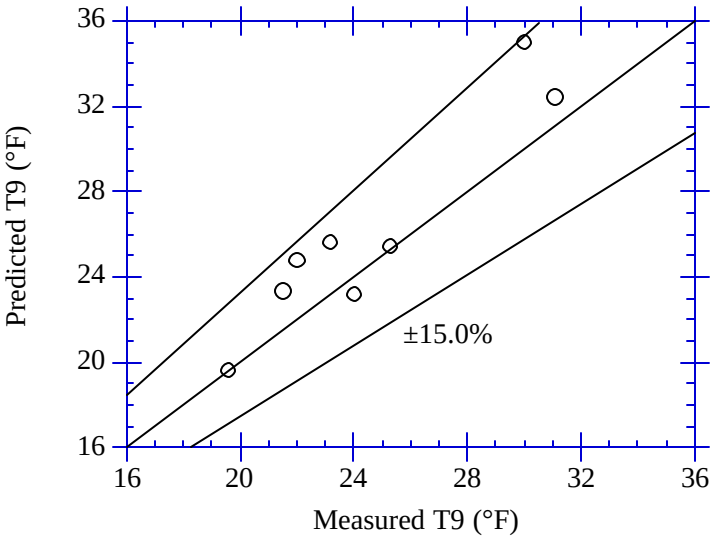

Figure 9-8. R12 Evaporator Exit Temperature Based on Heat Transfer Objective Function

However, there must be an explanation for the lack of sensitivity of the results to the values of the estimated conductances. To begin to understand this difference, it is helpful to make contour plots of both objective functions. Figure 9-9 shows the objective function for the R12 data based on heat transfer. For this plot, all the predicted heat transfer rates should fall within two standard deviations of the optimum value. Two standard deviations for this objective function is equivalent to a squared error of 113,000. From Figure 9-9, the contour line corresponding to this

squared error encompasses a range of two phase and superheated conductances. The two phase conductance ranges from 18 to 40 Btu/hr-ft^2°F and the superheated conductance ranges from 1.2 to 1.9 Btu/hr-ft^2°F.

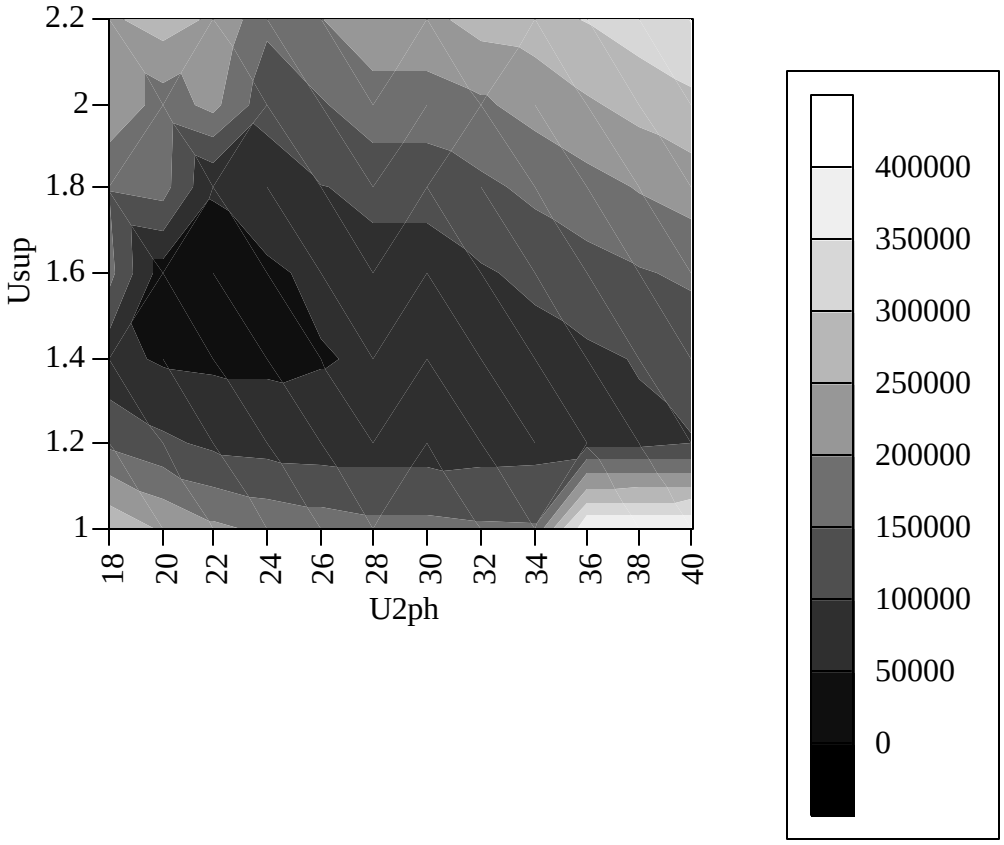

Figure 9-9. Contour Plot of R12 Objective Function Based on Heat Transfer

The contour plot of the objective function based on temperature is shown in Figure 9-10. For this plot, all the predicted evaporator exit temperatures should fall within two standard deviations of the optimum. Two standard deviations for this objective function is equivalent to a squared error of 63. This contour line encompasses a range of conductances. For the range of superheated conductances from 0.9 to 1.4 , the two phase conductance ranges from 24 to 78.

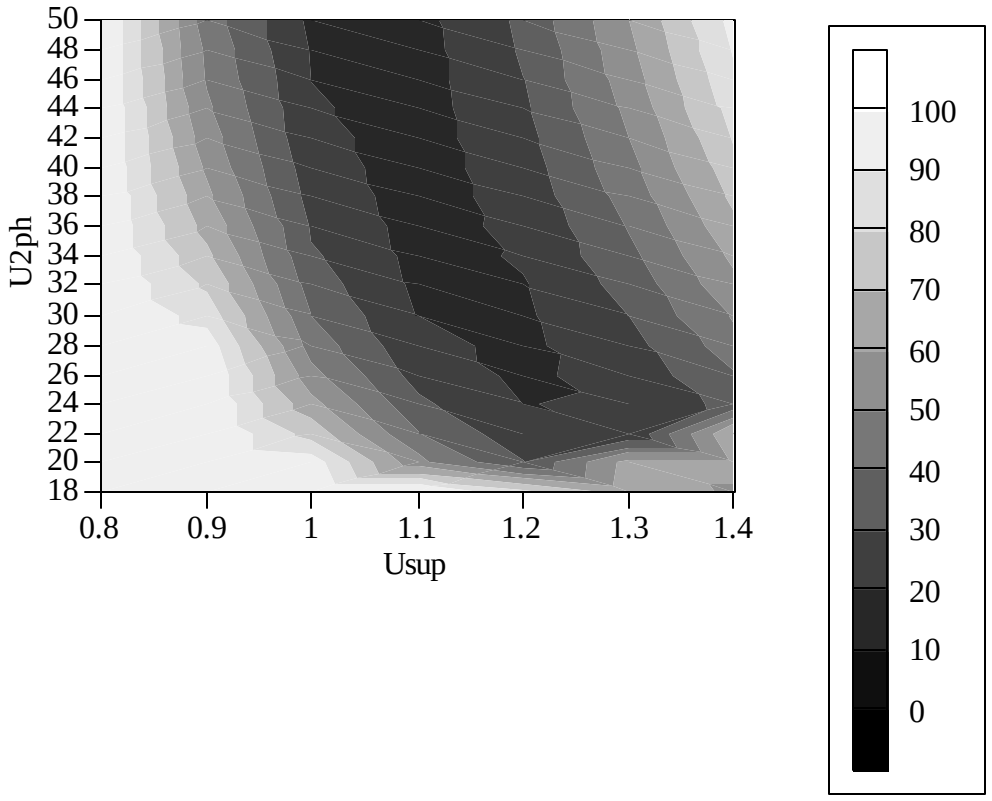

Figure 9-10. Contour Plot of R12 Objective Function Based on Temperature

The fundamental question posed by these contour plots is why can the assumed constant conductances for both objective functions apparently vary over such a large range and still give reasonable results as shown in Figures 9-5 through 9-8? The answer lies in the form of the objective function and the number of independent measurements that are available.

Each rate equation contains a conductance and associated area. A given heat transfer rate can be predicted from the rate equation for a large conductance and small area, or vice versa. The problem with Equations 9.15 through 9.28 is the fact the areas for each zone are not known. Therefore, the conductances and areas need to be fully constrained. If the areas were known then the comparison of the heat transfer rates with the measured heat transfers would pin down the conductances.

Since the zone areas are not known this information must come from some other source. The other source is indirectly Equation 9.19. This ratio helps to constrain the possible range of conductances and areas. However, in the process of using this equation, some measured quantities are used in both terms of the objective function resulting in a loss of independence in the equation set. In the objective function given by Equation 9.14, the measured evaporator heat transfer is used in the rate equations through Equation 9.19. For the objective function given by Equation 9.29, the measured temperature T9 is also used in the process of calculating T9calc through Equation 9.19. The penalty to be paid for even a partial loss of independence in the equation set is an inability to independently estimate the two conductances.

A truly independent set of equations can be obtained from independent measurements of the refrigerator cabinet load. The cabinet load along with the other power inputs into the cabinet can be used to determine the volumetric air flow rate across the evaporator. Using this air side volumetric flow rate, the evaporator load could be determined from temperature measurements of the return air streams from the freezer and fresh food compartments and the evaporator fan outlet. The objective function can then be based on making a comparison between an air side evaporator heat transfer and the rate equations. The refrigerant side measurements can be used to eliminate the areas from Equations 9.17 and 9.18, thus eliminating the need for Equation 9.19.

Unfortunately for the refrigerator studied, the cabinet load was not known because of the uncertainty introduced by the door heater. However, work just recently completed by Boughton [8] on the heat transfer into the refrigerator cabinet around the door flanges and from the door heater etc. may allow determining the cabinet load. The solution process just described may yet allow the determination of the conductances from the measured data sets.

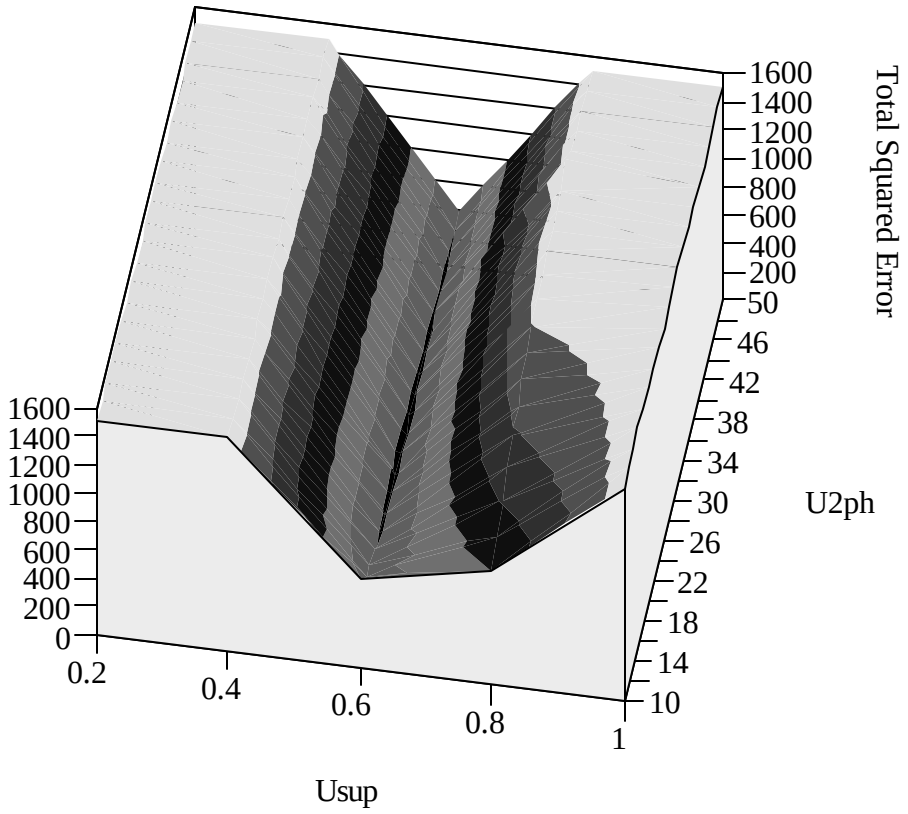

Figure 9.11. Contour Plot of R134a Objective Function Based on Temperature

The discussion up to this point has dealt with the R12 data. For the R134a data, Figure 9-11 shows a three dimensional contour plot for the objective function based on temperature. The same general trends shown in the R12 data also appear here. The conductance in the superheated section is fairly well defined but the two phase conductance is uncertain. As Figure 9-12 shows, there is more scatter in the predicted heat transfer than for the R12 data. This may be a result of the conductances varying more for the R134a data than for the R12 data.

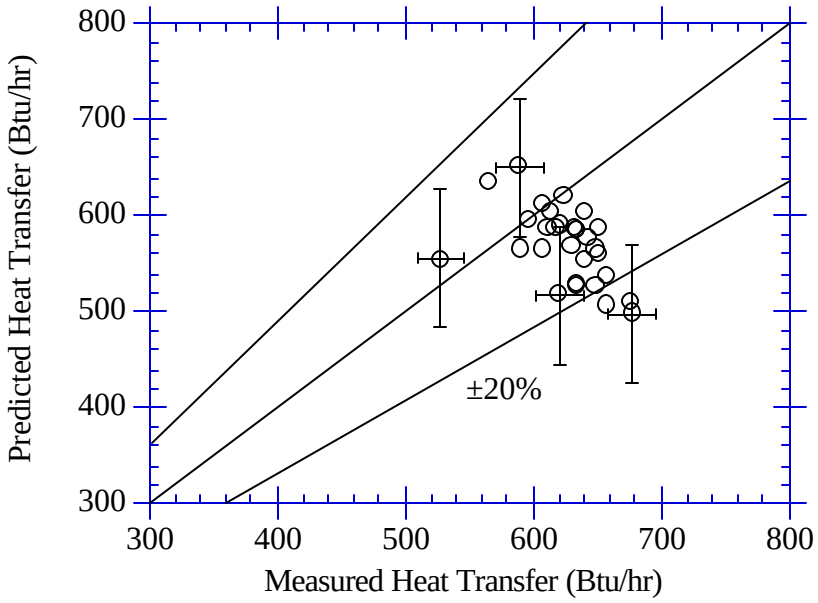

Figure 9-12. Evaporator Heat Transfer - R134a Constant Conductance Model

The lack of total independence in the equation set may not be the only explanation for the differences between the estimated conductances. It may als o be true that the conductances are varying. Theoretical calculations show (see Appendix G) that the conductances for the superheated section may be expected to vary by 11% for the R12 data and 17% for the R134a. In the two phase section, the conductances vary by 2% in the R12 data and 3% in the R134a data. Further, the two phase conductances are predicted to be much higher than the superheated conductances as a result of the much lower resistance on the refrigerant side compared to the refrigerant side resistance in the superheated zone. The same trend is seen in Table 9.2

The differences between the theoretical conductances for R12 and R134a are mainly the result of changes in mass flow rates. Fluid properties appear to have a much smaller impact [9]. It would be expected that this result also holds for the estimated conductances in Table 9.2. Indeed the average mass flow rate for the R134a data is half the average for the R12 data. As a result the conductance should be lower in the R134a case which is the trend shown in Table 9.2. A similar comparison can not be made for the two phase conductances because the R134a objective function did not show in minimum for finite values of the two phase conductance. However, the theoretical calculations show that since the air side resistance dominates in the two phase section, the two phase conductances for R12 and R134a should be nearly equal. On this basis, the value of the two phase conductance for the R12-T9 can be used to approximate the two phase conductance for R134a.

The theoretical variation in the conductances are relatively small. However, the straight tube correlations are only very crude approximations to the helical geometry in the real evaporator. The helical geometry may significantly alter flow regimes causing large variations in the conductances. Further more uncertainty is probably introduced by the uneven distribution in the air inlet temperature and its velocity over the coil.

9.4 Variable Conductance Model

Since the conductances may be varying significantly in the real evaporator, a variable conductance model may yield better results than a constant conductance model. For the variable conductance model, Equations 9.4 and 9.5 are substituted into Equations 9.17 and 9.18. Since the same equations are used as for the constant conductance model, the variable conductance model can not be expected to yield quantitative results because of the large uncertainties introduced by the loss of independence in the equations. However it is worth seeing if this model qualitatively makes any improvement over the constant conductance model. Equations 9.4 and 9.5 are repeated here for reference as Equations 9.31 and 9.32. The refrigerant side film coefficients needed in Equation 9.31 and 9.32 are the same ones used in the theoretical calculations (see Appendix G). Any discrepancies between these values and the actual film coefficients in the real evaporator should be taken up by the constants.

$$\frac{1}{U_{sup}} = B_1 + \frac{B_2}{h\,sup} \tag{9.31}$$

$$\frac{1}{U_{2ph}} = B_1 + \frac{B_3}{h2ph} \tag{9.32}$$

where hsup = superheated section refrigerant film coefficient

h2ph = two phase section refrigerant film coefficient

The first attempt to find a minimum for the R12 data using this model is summarized by Equation 9.33 and 9.34. The standard deviation in the objective function is 1.13°F which is an improvement over the constant conductance case which has a standard deviation of 1.4°F. Note that the air side resistance, which is the first term on the right side of Equations 9.34 and 9.35, is equal to the theoretical value of 0.035 Btu/hr-ft^2°F given in Appendix G.

$$\frac{1}{U_{sup}} = 0.0355 + \frac{28.71}{hsup} \qquad 1.10 < U_{sup} < 1.31 \text{ Btu/hr-ft}^2\text{°F} \tag{9.33}$$

$$\frac{1}{U_{2ph}} = 0.0355 + \frac{0.146}{h2ph} \qquad 27.9 < U_{2ph} < 28.0 \text{ Btu/hr-ft}^2\text{°F} \tag{9.34}$$

Further the variation in the superheated conductance from 1.10 to 1.31 is within the range of conductances where the two objective functions in Figures 9-9 and 9-10 overlap. A comparison can also be made with the theoretically determined conductances. The theoretical superheated conductances vary by 11% which is the slightly more than half the 19% variation in Equation 9.34. Both these results suggest that the conductance in the superheated region is affected by the refrigerant side. For the two phase section, the theoretical conductance varies by 2% which is much larger than the 0.4% variation in Equation 9.35. These results confirm that the overall conductance in the two phase section is dominated by the air side resistance. Note also that the values of the two phase conductance fall close to the middle of the range where the two objective functions in Figures 9-9 and 9-10 overlap. The same model given by Equations 9.31 and 9.32 did not show a minimum for finite values of the constants for the R134a data.

Since theoretical straight tube considerations suggest that the two phase conductances should be nearly constant, a simplified form of Equations 9.31 and 9.32 given by Equations 9.35 and 9.36 was also tried. The results for the R12 data set is given by Equations 9.37 and 9.38. The results for the R134a data is given by Equations 9.39 and 9.40. Note that for the R134a case, the two phase conductance was fixed at the value for the R12-T9 case in Table 9.2. The two phase conductance for the R12 case was determined by the optimization routine.

$$\frac{1}{U_{sup}} = B_1 + \frac{B_2}{h_{sup}} \tag{9.35}$$

$$U_{2ph} = \text{constant} \tag{9.36}$$

The standard deviation for the R12 data is 1.1°F and 2.4°F for the R134a data. This is an improvement over the constant conductance model for both the R12 and R134a data. The inverse of the estimated two phase conductance should be equal to the air side resistance if the air side resistance dominates in the two phase zone as expected. Indeed for the R12 case the inverse of 30.1 is 0.033 which is within 10% of the value given for the constant B_1. However, note that the inverse of the air side resistance for the R134a case is not equal to the two phase conductance. The results don't appear consistent for the R134a data. More than likely the uncertainty in the parameters is having an effect here too.

$$\text{R12} - \frac{1}{U_{sup}} = 0.0302 + \frac{29.4}{h_{sup}} \qquad 1.08 < U_{sup} < 1.29 \text{ Btu/hr-ft}^2\text{°F} \tag{9.37}$$

$$U_{2ph} = 30.1 \text{ Btu/hr-ft}^2\text{°F} \tag{9.38}$$

$$\text{R134a} - \frac{1}{U_{sup}} = 0.0105 + \frac{52.1}{h_{sup}} \qquad 0.49 < U_{sup} < 0.63 \text{ Btu/hr-ft}^2\text{°F} \tag{9.39}$$

$$U_{2ph} = 36.2 \text{ Btu/hr-ft}^2\text{°F} \tag{9.40}$$

9.5 Conclusions

The loss of independence in the equation set used to estimate the conductances for both the constant conductance model and the variable conductance model prevented the conductances from being accurately determined. This underscores the need to keep the measured quantity and the predicted quantity in the objective function independent from each other as much as possible. An independent set of equations can be developed if the refrigerator cabinet load is better defined. If the uncertainties in the cabinet load for the refrigerator studied can be eliminated, these data sets may still yield relatively certain estimates of the conductances.

Despite the uncertainty in the estimated parameters, the areas where the two standard deviation lines overlap for both objective functions suggest the real range in the conductances. Conductances in this region predict both the evaporator heat transfer and exit temperature equally well. The probable range is 1.2 to 1.4 for the superheated conductance and 20 to 40 for the two phase conductance. To determine whether these ranges can be narrowed will require additional independent measurements. If they cannot, it may indicate that the conductances actually vary over a wide range due to changes in refrigerant flow rates or other factors.

The theoretical calculations indicate that in the superheated section the air side and refrigerant side resistances are of the same order of magnitude. As a result the refrigerant side has an impact on the overall conductance. The theoretical variation in the superheated conductances is 11% within the R12 data set and 17%

within the R134a data set. These variations are small and may prevent the separation of the overall conductances into an air side and refrigerant side component even with an independent set of equations. It might therefore be necessary to expand the data set by varying the air side volumetric flow rate. Qualitatively, the variable conductance model in the superheated zone is an improvement over the constant conductance model. However, more research is needed to determine if the improvement is just a result of adding another degree of freedom to the objective function or whether the model is actually accounting for the apparent small variations in the superheated conductance.

In the two phase section the air side resistance dominates the refrigerant side resistance. As a result, variations in the refrigerant side resistance have little impact on the overall conductance. The theoretical variation in the two phase conductances is only 2% for the R12 data and 3% for the R134a data. This suggests that for this section, the constant conductance model ought to be sufficient and the same conductance value can be used for both refrigerants.

However, the possibility remains that the helical geometry of the evaporator actually causes the two phase resistance to vary substantially as a function of refrigerant mass flow rate, and that the refrigerant side resistance and flow regimes are highly sensitive to the refrigerant type. Further exploration of these issues will require the use of two phase flow correlations more complicated than those for straight tubes, and should resolve some of the other issues raised here.

References

[1] Reeves, R.N., Modeling and Experimental Parameter Estimation of a Refrigerator/Freezer System, Air Conditioning and Refrigeration Center, University of Illinois at Urbana-Champaign, 1992, pp. 30 to 41.

[2] Arthur D. Little, Inc., Development of a High Efficiency Automatic Defrosting Refrigerator/Freezer: Phase I Final Report, ORNL/Sub-7255/2, February 1980.

[3] Arthur D. Little, Inc., Refrigerator and Freezer Computer Model User's Guide, U.S. Department of Energy DE-AC01-78CS20420, November 1982.

[4] Kays, W.M. and A.L. London., Compact Heat Exchangers, Third Edition, McGraw-Hill, New York, 1984, pp. 11 to 49.

[5] Stoecker, W.F. and J.W. Jones., Refrigeration and Air Conditioning, McGraw-Hill, New York, 1986, p. 236.

[6] Porter, K.J., Modeling and Sensitivity Analysis of a Refrigerator/Freezer System, ACRC Technical Report, Air Conditioning and Refrigeration Center, University of Illinois at Urbana-Champaign, forthcoming 1992.

[7] Personal communication., Mr. Martin Zenter, General Electric Company, Appliance Park, Louisville, Kentucky, 40255.

[8] Boughton, B.E., An Investigation of Household Refrigerator Cabinet Loads, Air Conditioning and Refrigeration Center, University of Illinois at Urbana-Champaign, 1992.

[9] Personal communication, Mr. John Wattelet, Air Conditioning and Refrigeration Center, University of Illinois at Champaign-Urbana, Champaign-Urbana, Illinois, 61801.

Chapter 10: Conclusions and Recommendations

The purpose of this project was to verify that the component models developed by Reeves [1] are valid for the refrigerator/freezer studied here and that the models could be extended to handle refrigerants other than R12. For the heat exchangers, the constant multi-zone conductance models used by Reeves were extended to variable conductance models to see if they could account for the differences in heat transfer characteristics between R12 and R134a. In the process several important results were obtained.

For the compressor, the constant overall heat transfer coefficient model for shell heat transfer was verified for two more reciprocating compressors. A volumetric and isentropic efficiency approach for predicting compressor performance was investigated as an alternative to the compressor maps used by Reeves. It was found that both the volumetric efficiency approach and the compressor maps predicted compressor performance equally well. Each method was able to predict compressor mass flow rate and power consumption to within ±5.0%. The volumetric efficiency approach has the added advantage of being applicable to a wider range of compressor operating conditions. In fact, the same compressor calorimeter data used to generate compressor maps can be used to develop a volumetric and isentropic efficiency model that applies to test conditions outside the evaporating and condensing temperatures of the original data points. In the future these models should be further validated for other compressor geometries such as a rotary compressor and compressors that have the shell on the low side of the compressor.

For the condenser, the three-zone constant conductance model developed by Reeves was validated for the refrigerator/freezer studied. The model was able to predict condenser heat transfer to within ±10.0% for both R12 and R134a. The attempt to go one step further to a variable conductance model to account for the observed differences between R12 and R134a revealed that within a given data set the conductances were relatively constant over the range of refrigerant side test conditions observed. The variation in the conductances was apparently not enough to allow the air side and refrigerant side components to be separated. It is recommended that the air side volumetric flow rate be varied so that the effects can be separated. This should yield a variable conductance model capable of predicting the effects of changing refrigerants.

The reason the conductances appear to be relatively constant is a result of the magnitude of the air resistance relative to the total resistance to heat transfer. In the two phase section the air side resistance is theoretically 80% of the total and approximately 50% in the desuperheating section. As a result variations in the refrigerant side resistance due to varying mass flow rates and properties have little impact in the two phase section of the condenser and only slight impact on the desuperheating section for the measured refrigerant mass flow rate range of 7 to 20 lbm/hr. In the subcooled section, the Reynolds number is so small that the flow is laminar for the conditions tested. As a result, the resistance in this section is expected to be a function of refrigerant properties alone. For the R134a data set, the refrigerant properties did not vary over a wide enough range to significantly vary the overall conductance.

For the interchanger, it was verified that a constant effectiveness model does an excellent job at predicting heat transfer in the interchanger. Interestingly, it was also found that a constant overall heat transfer coefficient model also does an excellent job. Reeves found that the constant overall heat transfer coefficient model did a much worse job for his refrigerator/freezer. The refrigerator studied here had a 0.028" I.D. capillary while the one studied by

Reeves had a 0.032" capillary tube. Further investigation into the reasons why a change in tube diameter has such a pronounced effect is warranted as it may yield a better understanding of the interaction between the capillary tube and suction line. Part of the variation might also be attributed to differences in the locations of the flash point.

For the evaporator it was found that the constant conductance model used by Reeves did not do a very good job at predicting heat transfer from the evaporator. An investigation into the underlying reasons revealed two possibilities: either 1) the conductances vary substantially with refrigerant mass flow rate due to the helical geometry of the evaporator or 2) a much more subtle reason involving the equation set is the cause. In fact, both effects may be occurring simultaneously. In the process of developing a set of equations on which to base an objective function it is possible that the same measured quantities can be used twice in both the predicted and measured terms. As a result the measured and predicted terms are not totally independent of one another. The effect of this loss of independence is the introduction of more uncertainty into the estimated parameters. However, even with these uncertainties it was found that the variable conductance model showed an improvement over the constant conductance model for both R12 and R134a.

Better estimates of the parameters in both models is needed to determine if the variable conductance model is indeed better. This may still be possible for the R12 and R134a data sets by using an independent set of equations employing measurements of the refrigerator cabinet load. The cabinet load along with the other power inputs into the cabinet can be used to determine the volumetric air flow rate across the evaporator. Using this air side volumetric flow rate, the evaporator load can be determined. Better parameter estimates may be obtained by finding which values minimize the difference between the measured heat transfer and that calculated by the rate equations. In this case, the refrigerant side measurements can be used to eliminate the need to know the areas in each zone. The necessary measurements of cabinet load may be contained in the data sets obtained here to calibrate a recently developed model of door edge losses. This would remove the uncertainty about the contribution of the door heater and provide the independent information needed.

In summary, the goal of accurately predicting the effect of alternative refrigerants in domestic refrigerator/freezers will require better models of the condenser and evaporator than those presented here. On the one hand it will be necessary to vary airflow rates to obtain a better separation between refrigerant and air-side heat transfer phenomena. On the other hand it might be possible to simulate performance of a system with fixed air flow rates by using a constant conductance model of the type presented here for the condenser and suction line heat exchanger. The same might be possible for the evaporator if the resolution of door heater uncertainties yields the independent source of measurements required.

References

[1] Reeves, R.N., Modeling and Experimental Parameter Estimation of a Refrigerator/Freezer System, Air Conditioning and Refrigeration Center, University of Illinois at Urbana-Champaign, 1992, pp. 30 to 41.

List of References

American Society of Heating, Refrigerating and Air-Conditioning Engineers, Inc., Fundamentals Handbook, ASHRAE, Atlanta, 1989, p. 4.2.

Arthur D. Little, Inc., Development of a High Efficiency Automatic Defrosting Refrigerator/Freezer: Phase I Final Report, ORNL/Sub-7255/2, February 1980.

Arthur D. Little, Inc., Refrigerator and Freezer Computer Model User's Guide, U.S. Department of Energy DE-AC01-78CS20420, November 1982.

Boughton, B.E., An Investigation of Household Refrigerator Cabinet Loads, Air Conditioning and Refrigeration Center, University of Illinois at Urbana-Champaign, 1992.

Camporese, R., G. Bogolaro, G. Cortella, and M. Scattolini. 1991. "Flammable Refrigerants in Domestic Refrigeration.", Proceedings of the XVIII International Congress of Refrigeration, Vol. III, pp. 1175 to 1179.

Coleman, H.W. and W.G. Steele., Experimentation and Uncertainty Analysis for Engineers, John Wiley & Sons, New York, 1989.

Collier, J. G., Convective Boiling and Condensation, Second Edition, McGraw-Hill, New York, 1980, pp. 30 to 35.

Copeland Copeleweld Data Book, Copeland Corporation, Sidney, Ohio (1990).

Dabiri, A.E. and C.K. Rice. 1981. "A Compressor Simulation Model with Corrections for the Level of Suction Gas Superheat.", ASHRAE Transactions,Vol. 87, Part 2, pp. 77 to 782.

Department of Energy. 1979. "Test procedures for central air conditioners, including heat pumps." Federal Register, Vol. 44, No. 249, pp. 76700 to 76723.

Department of Energy. 1989. "Uniform test method for measuring the energy consumption of central air-conditioners." Code of Federal Regulations, Part 430, Subpart B, Appendix M, pp. 101 to 126, January 1.

E.E.S., F-Chart Software, 4406 Fox Bluff Road, Middleton, WI, 53562.

Engineering Analysis of Experimental Data - ASHRAE Guideline 2-1986., (Available from American Society of Heating, Refrigerating and Air-Conditioning Engineers, Inc., 1791 Tullie Circle, N.E., Atlanta, GA 30329).

Goldschmidt, V.W., G.H. Hart, and R. C. Reiner. 1980. "A note on the transient performance and degradation coefficient of a field tested heat pump - cooling and heating mode." ASHRAE Transactions, Vol. 86, Part 2, pp. 368 to 375.

Hara, T., and M. Shibayama, H. Kogure, and A. Ishiyama. 1991. "Computer Simulation of Cooling Capacity for a Domestic Refrigerator-Freezer.", Proceedings of the XVIII International Congress of Refrigeration, Vol. III, pp. 1193 to 1197.

He, X., U.C. Spindler, D.S. Jung, and R. Radermacher. 1992. "Investigation of R-22/R-142b Mixture as a Substitute for R-12 in Single-Evaporator Domestic Refrigerators.", ASHRAE Transactions, Vol. 98, Part 2, 1992.

Incropera, F.P. and D.P. DeWitt., Fundamentals of Heat and Mass Transfer, Second Edition, John Wiley & Sons, Inc., New York, 1985.

Katipamula, S. and D.L. O'Neal. 1991. "Performance degradation during on-off cycling of single-speed heat pumps operating in the cooling mode: experimental results." ASHRAE Transactions, Vol. 97, Part 2, In print.

Kays, W.M. and A.L. London., Compact Heat Exchangers, Third Edition, McGraw-Hill, New York, 1984.

Kempiak, M.J. and R.R. Crawford., Three-Zone Modeling of a Mobile Air Conditioning Condenser, Air Conditioning and Refrigeration Center, Dept. of Mechanical and Industrial Engineering, University of Illinois at Urbana-Champaign, 1992.

Molina, M.J. and F.S. Rowland. 1974. "Stratospheric Sink for Chlorofluoromethanes: Chlorine Atom Catalyzed Destruction of Ozone.", Nature 249: pp. 810 to 812.

Mulroy, W.J. and D.A. Didion. 1985. "Refrigerant migration in a split-unit air conditioner." ASHRAE Transactions, Vol. 91, Part 1A, pp. 193 to 206.

Murphy, W.E., and V.W. Goldschmidt. 1979. "The degradation coefficient of a field-tested self-contained 3-ton air conditioner." ASHRAE Transactions, Vol. 85, Part 2, pp. 396 to 405.

Murphy, W.E., and V.W. Goldschmidt. 1984. "Transient response of air conditioners-a qualitative interpretation through a sample case." ASHRAE Transactions, Vol. 90, Part 1B, pp. 997-1008

NAECA. 1987. Public law 100-12, March 17.

Pereira, R.H., L.M. Neto, and M.R. Thiessen. 1991. "An Experimental Approach to Upgrade the Performance of a Domestic Refrigeration System Considering the HFC-134a.",Proceedings of the XVIII International Congress of Refrigeration, Vol. III, pp. 1180 to 1184.

Porter, K.J., Modeling and Sensitivity Analysis of a Refrigerator/Freezer System, ACRC Technical Report, Air Conditioning and Refrigeration Center, University of Illinois at Urbana-Champaign, forthcoming 1992.

Purvis, B.D., A Computer Model for Refrigerant Flow in Small Bore Tubes, Air Conditioning and Refrigeration Center, University of Illinois at Urbana-Champaign, forthcoming 1992.

Reeves, R.N., Modeling and Experimental Parameter Estimation of a Refrigerator/Freezer System, Air Conditioning and Refrigeration Center, Dept. of Mechanical and Industrial Engineering, University of Illinois at Urbana-Champaign, 1992.

Rogers, S. and D.R. Tree. 1991. "Algebraic Modelling of Components and Computer Simulation of Refrigerator Steady-State Operation.", Proceedings of the XVIII International Congress of Refrigeration, Vol. III, pp. 1225 to 1229.

Rohsenow, W.M., "Boiling" in W.M. Rohsenow et al., Eds., Handbook of Heat Transfer Fundamentals , Chapter 12, McGraw-Hill, New York, 1985.

Science. v. 254, no. 5032, 1991.

Stoecker, W.F. and J.W. Jones, Refrigeration and Air Conditioning, McGraw-Hill, New York, 1986.

Stoecker, W.F., Design of Thermal Systems , Third Edition, McGraw-Hill, New York, 1989.

Sugalski, A., D. Jung, and R. Radermacher. 1991. "Quasi-Transient Simulation of Domestic Refrigerators.", Proceedings of the XVIII International Congress of Refrigeration, Vol. III, pp. 1244 to 1249.

True Basic., True Basic, Inc., 39 South Main St., Hanover, N.H., 03755.

United Nations Environmental Programme. 1987. Montreal protocol on substances that deplete the ozone layer. Final act., New York: United Nations.

Vineyard, E.A. 1991. "The Alternative Refrigerant Dilemma for Refrigerator-Freezers: Truth of Consequences.", ASHRAE Transactions, Vol. 97, Part 2, pp. 955 to 960.

Xiuling, C., C. Youhong, X. Deling, G. Yain, and L. Xing. 1991. "A Computer Simulation and Experimental Investigation of the Working Process of a Domestic Refrigerator.", Proceedings of the XVIII International Congress of Refrigeration, Vol. III, pp. 1198 to 1202.

Appendix A: Performance Degradation of Domestic Refrigerators during Cyclic Operation

A.1 Overview

The intent of this discussion is to investigate the differences between steady-state and cycling performance of a domestic refrigerator at one test condition. Experimental data were collected for a standard 18 ft^3 refrigerator in both steady-state and cyclic operation. The refrigerator was operated in a controlled environment in an environmental chamber. Both tests were run at 90°F ambient (chamber temperature) with a refrigerant charge of 7oz. Note that for these tests the mullion heater was deactivated. The freezer and fresh-food compartment temperature controls were set at their midpoint positions for the cycling test. The average freezer and fresh-food compartment temperatures in the cycling test were matched in the steady-state test. Other approaches could be taken to make a comparison such as running the refrigerator with the same evaporator load for each test. However, maintaining equivalent temperatures seems the most logical because the purpose of the refrigerator is to maintain a given set-point temperature.

A.2 Cycling Performance in Heat Pumps and Air-Conditioning Equipment

Before discussing results for refrigerators, it is instructive to briefly review the significant amount of work that has been done in this area on heat pumps and air-conditioning equipment (see for example, Murphy and Goldschmidt [1], Goldschmidt et al. [2], Murphy and Goldschmidt [3], and Katipamula and O'Neal [4]). The methods and trends identified should be useful in analyzing and understanding the cyclic performance of domestic refrigerators.

The approach taken to quantify the efficiency of a heat pump or air conditioner during cyclic operation was first proposed by the Department of Energy [5].The method involves taking a steady-state efficiency and multiplying it by a factor that accounts for transient losses caused by cyclic compressor operation. The resulting quantity is called a Seasonal Energy Efficiency Ratio or SEER. This efficiency should be more representative of the actual efficiency of a heat pump compared to a steady-state value. To evaluate this quantity, several steady-state tests and a cycling test are required. DOE [6] defined SEER by Equation 1 where EER_B is a steady-state energy efficiency rating for the heat pump at 82°F outdoor and 80°F indoor ambient conditions and PLF is the part load factor determined at a cooling load factor or CLF of 50% .

$$SEER = EER_B \times PLF(CLF = 50\%) \qquad (A.1)$$

The part load factor is defined as the average efficiency of the heat pump during the cooling phase of a specified cycle test D divided by the efficiency of steady-state test C as given by Equation 2 where t_o is the cooling-process time or on-cycle time. The part load factor indicates how closely the cycling efficiency of the unit approaches the steady-state value. The cooling load factor or CLF is defined by Equation 3 where $\dot{Q}(t)_D$ is the instantaneous heat transfer rate for cyclic operation in test D and $\dot{Q}_{ss_C}$ is the heat transfer rate for steady-state operation in test C. For this parameter the integration is performed over the complete cycle time t_c. The cooling load factor represents the ratio of the heat transferred in a cycle to that which could be transferred if the unit ran continuously.

$$PLF = \frac{\frac{1}{t_o}\int_{o}^{t_o} EER_D(t)dt}{EER_C} \quad (A.2)$$

$$CLF = \frac{\int_{o}^{t_c} \dot{Q}(t)_D\, dt}{\dot{Q}ss_C t_c} \quad (A.3)$$

An alternative approach that makes use of a degradation coefficient was also given [6] to calculate the part load factor needed in Equation 1. The degradation coefficient is defined by Equation 4. It was assumed that as the cooling load factor increased the part load factor would also increase in such a way that the degradation coefficient would remain constant. Once C_D was known at one test point it could be applied to other conditions. Further, with C_D known and CLF set to 0.5, Equation 4 can be solved for the part load factor needed in Equation 1.

$$C_D = \frac{1 - PLF}{1 - CLF} \quad (A.4)$$

Later work by Murphy and Goldschmidt [1] and Goldschmidt et al. [2] has shown that the degradation coefficient is not constant. Katipamula and O'Neal [4] tested a heat pump in cooling mode with different cycling rates and percent compressor on-times at constant ambient conditions. They found that the part load factor increased with percent compressor on-time and decreased with the cycle rate. The degradation in performance was worse at high cycle rates and low percent compressor on-times. Further, the degradation coefficient varied significantly over the conditions tested.

Unfortunately there doesn't seem to be a simple relationship between the cycle rate, percent compressor on-time and the cooling efficiency of a heat pump. However, the trends outlined by Katipamula and O'Neal [4] should also hold for domestic refrigerators. More work will obviously be needed to fully characterize the relationship between steady-state and cycling performance of heat pumps and air conditioning equipment.

A.3. Comparison of Steady-State Performance and a "Snapshot" of Cycling Performance

Two methods will be used to investigate the differences between cycling and steady-state performance of a domestic refrigerator. The first method is to make the comparison between the steady-state and cyclic cases by looking at a point in time where the instantaneous evaporator inlet air temperatures are the same. For this case an instantaneous coefficient of performance or COP can be compared to the steady-state value where COP is defined as the ratio of the evaporator load to the system power requirement. The second approach is to compare an average COP for the cycling case to the steady-state value. Since the cyclic COP is a function of time, an average can be found by integrating over a complete cycle. Both methods yield valuable insights. The equal evaporator air temperature approach will be investigated first.

Table A.1 lists the temperatures, pressures, and power requirements for the system when the evaporator inlet temperature was the same for the cycling and steady-state tests. The cyclic evaporator load was determined from an air-side energy balance across the evaporator. The same method was applied to the steady-state case.

The cyclic COP is 11% lower than the steady-state value which is a significant decrease in the efficiency of the refrigerator. The cyclic losses appear as a significant loss in evaporator capacity and not in the power requirement which is equal to the steady-state. To begin to understand why it takes the same amount of power to move much less heat in the cyclic case, a closer look at the differences between the two tests must be taken.

There is little difference between the steady-state case and this "snapshot" of the cycling case except for the compressor discharge temperature, refrigerant temperature at the exit of the evaporator, and the evaporator air discharge temperature. The decrease in the compressor discharge temperature can be explained by thermal capacity effects. Since the compressor has a large thermal capacity, it can store a significant amount of energy. During the off-cycle, the compressor shell transfers heat to the cooler environment. When the compressor resumes operation, the metal in the compressor can absorb energy from the refrigerant stream until steady-state conditions are reached between the compressor shell and the environment. This reduces the enthalpy of the refrigerant stream leaving the compressor resulting in a lower discharge temperature. Note that this effect tends to increase, not decrease, system efficiency.

Table A.1. Steady-State and Instantaneous Cyclic Performance

Measured Quantity	Steady-State	Cyclic
Condenser Inlet Pressure (psig)	136	137
Condenser Outlet Pressure (psig)	135	136
Evaporator Inlet Pressure (psig)	3.8	3.8
Evaporator Outlet Pressure (psig)	1.4	1.4
Fresh Food Compartment Temp. (°F)	41.6	39.3
Freezer Compartment Temp. (°F)	3.4	3.4
Evaporator Inlet Air Temp. (°F)	6.7	6.6
Evaporator Outlet Air Temp. (F)	-1.6	-0.8
Evaporator Inlet R12 Temp. (°F)	-11.3	-11.3
Evaporator Outlet R12 Temp. (°F)	-13.8	-8.2
Compressor Suction Inlet Temp. (°F)	86.3	87.9
Compressor Discharge Temp. (°F)	170.1	160.8
Condenser Inlet R12 Temp. (°F)	170.1	160.8
Condenser Outlet R12 Temp. (°F)	112.5	112.7
Capillary Tube Inlet Temp. (°F)	111.7	111.8
Ambient Temperature (°F)	89.8	89.6
Compressor Power (W)	161	163
Evaporator Load - Air Side (W)	170	153
System Power (W)	187	189
COP	0.91	0.81

Evidence for this process can be seen in Figure A-1. An on-cycle and off-cycle are also indicated. For each cycle the compressor shell experiences a temperature fluctuation of 9°F. The mass of the compressor minus the oil charge is 18.5 lbm. If it is assumed that all of this mass is steel (neglecting the higher thermal capacitance of the copper motor windings) and that all of it undergoes the same 9°F temperature fluctuation, 17.3 Btu are stored and dissipated each cycle. Averaging over the 25.1 minute on-cycle yields 41.4 Btu/hr or 12.1 W. It should also be

possible to determine this heat transfer rate from the actual discharge enthalpies for the cycling and steady-state cases and the refrigerant flow rate which is equal for both cases. Using Equation 5 and a mass flow rate of 12.6 lbm/hr results in a heat transfer rate of 6.3 W. Although not exactly equal, this value is the same order of magnitude as the 12.1 W calculated previously given the assumptions made. It is therefore probable that the decrease in the discharge temperature for the cycling case is the result of thermal storage effects in the compressor.

$$\dot{Q}_{stored} = \dot{m}(h_{ss} - h_{cycling}) \qquad \text{(A.5)}$$

where h_{ss} = discharge enthalpy, steady-state

$h_{cycling}$ = discharge enthalpy, cycling

$\dot{m}$ = refrigerant flow rate

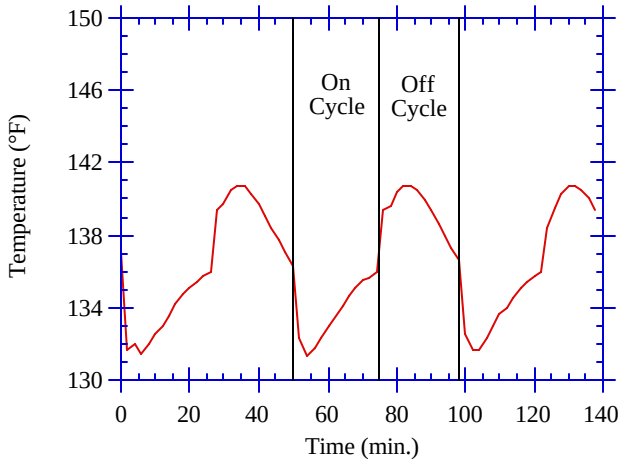

Figure A-1. Compressor Shell Temperature for Cycling Operation

The other main difference between the two cases is in evaporator performance. For the measured temperature and pressure, the steady-state evaporator has 4 °F of superheat at the exit. Likewise the cycling case has 9.5 °F of superheat, a significant difference. In fact the superheat levels for the cycling case are much higher over most of the compressor on-cycle. Figure A-2 shows that the evaporator superheat rises to a maximum of 17°F before slowly decreasing toward the steady-state value. The steady-state superheat level is only reached at the end of the compressor on-cycle.

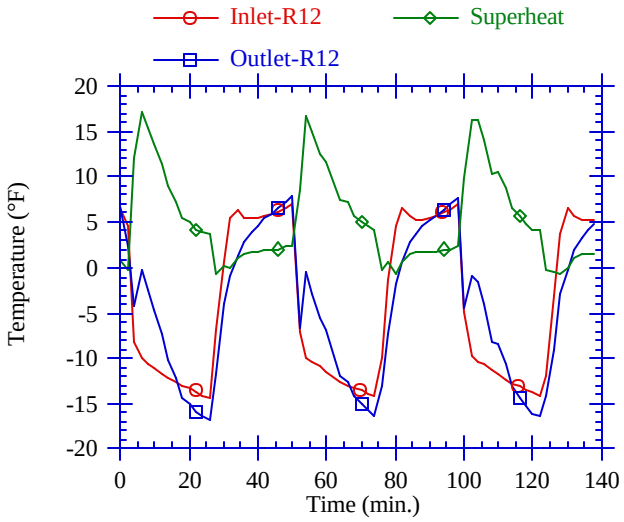

Figure A-2. Superheat in the Cycling Evaporator

High superheat levels greatly reduce the capacity of the evaporator. This explains why the evaporator load is lower and leaving air temperature is higher for the cycling case than for the steady-state case. However there must be a reason why the evaporator superheat is higher for the cycling case and the most logical inference is that the evaporator is starved for refrigerant. It could also be argued that the mass flow rate is lower for the cycling case. However, since the compressor sees the same inlet and outlet pressures and the same suction temperature, the mass flow rate through the compressor for the two cases must be nearly the same. Note that the compressor inlet pressure is the same as the evaporator outlet pressure and the compressor discharge pressure is the same as the condenser inlet pressure; the line losses being negligible.

The low charge in the evaporator can be explained if when the compressor first turns on a significant amount of liquid refrigerant is removed from the evaporator and is stored in the condenser or compressor shell for most of the compressor on-cycle. Murphy and Goldschmidt reported the same type of behavior in an air conditioner [3]. Qualitative evidence for this can be seen in Figure A-1 and A-3. In Figure A-1 the compressor shell temperature drops 5°F after the compressor begins operating instead of increasing indicating that liquid refrigerant is entering the compressor. In Figure A-3 the very sharp drop in suction temperature right after the compressor turns on indicates liquid refrigerant is drawn from the evaporator into the suction line heat exchanger.

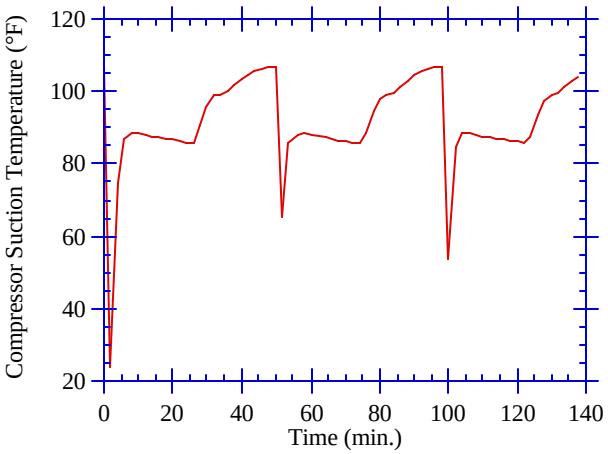

Figure A-3. Compressor Suction Temperature for the Cyclic Case

From the variation in superheat over the entire on-cycle, the refrigerant must migrate back into the evaporator slowly. For this to occur, the mass flow rate through the capillary tube must be slightly higher than the mass flow rate through the compressor. In fact if all the 7oz. charge migrated over the entire 25.1 minute on-cycle, the capillary tube would have to allow approximately 1.0 lbm/hr more mass flow than the compressor or about 8%. However, high superheat levels in the evaporator result in higher exiting refrigerant temperatures from the evaporator. Higher evaporator exit temperatures mean less heat transfer in the suction line heat exchanger. Since the capillary tube is soldered to the suction line, less energy is removed from the liquid refrigerant in the cap-tube. The liquid refrigerant has a lower density at a higher average temperature which results in a lower mass flow rate for a given pressure differential across the capillary tube. From this viewpoint, the suction line heat exchanger retards the redistribution of refrigerant in the system which prevents the system from approaching steady-state efficiency.

A.4 Refrigerant Charge Migration from the Condenser

The removal of charge from the evaporator is not the only migration of refrigerant in the system during a cycle. Refrigerant also migrates from the condenser to the evaporator during the off-cycle. When the compressor shuts down, the pressure in the condenser decreases as refrigerant bleeds through the capillary tube to the much lower pressure evaporator. Depending on how this process occurs, heat can also be transferred as a result. This could be an important additional load on the evaporator in the cycling case. Murphy and Goldschmidt [3] also discuss this phenomenon.

Two hypothetical migration processes are illustrated in Figure A-4. In case one, refrigerant forms a continuous column of liquid from the outlet of the condenser to the inlet of the capillary tube. For this situation, when the compressor stops, the pressure in the condenser forces the liquid refrigerant out of the condenser through the cap-tube. This would result in additional cooling in the evaporator even though the compressor is not running. If this process were to occur in a real refrigerator, the migration would not be considered a loss because some cooling would be accomplished.

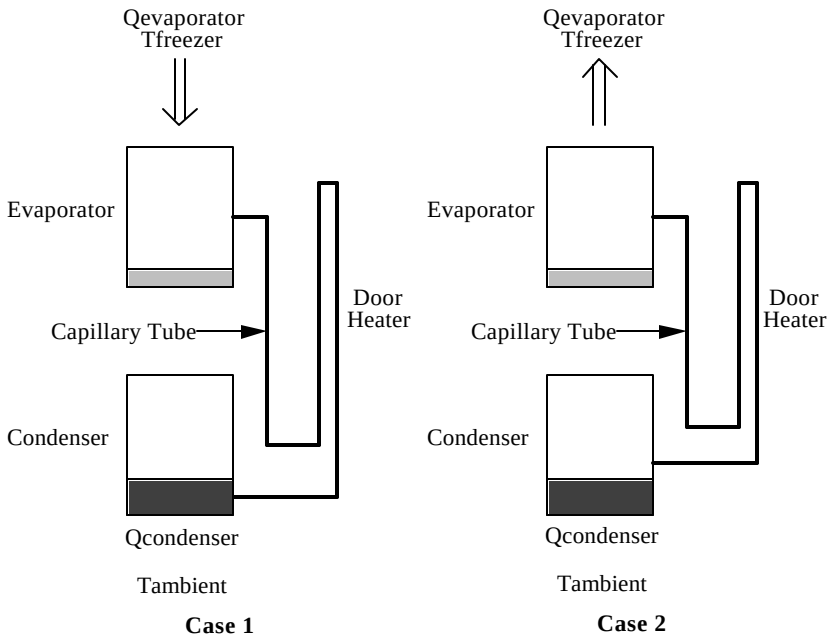

Figure A-4. Hypothetical Refrigerant Migration Processes

In case 2, the column of liquid is not continuous but is broken as the result of drainage back into the condenser due to gravity and the likely formation of vapor. For this scenario, only vapor is transferred to the evaporator. Initially the liquid refrigerant in the condenser is above the ambient temperature. However since saturated conditions exist in the condenser, as the pressure falls so does the refrigerant temperature. Eventually the pressure drops far enough to cause the refrigerant temperature to drop below the ambient temperature. At this point the direction of heat transfer from the refrigerant to the environment is reversed and the refrigerant begins to boil. The heat absorbed in the condenser is transported by refrigerant migration to the evaporator where condensation occurs transferring the heat into the refrigerator cabinet. For this case, the migration of refrigerant during the off-cycle is a loss. Note that for both cases it was assumed that the pressure in the condenser was sufficient to keep the discharge valve on the compressor closed thus preventing flow back through the compressor.

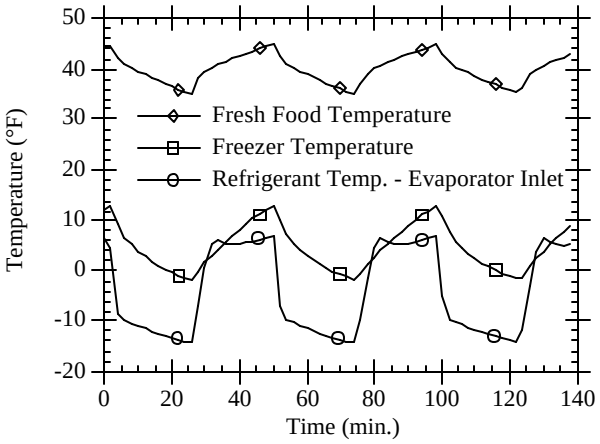

Figure A-5. Effect of Refrigerant Migration on Evaporator Refrigerant Temperature

Although the actual process could not be observed, all the evidence indicates that case 2 closely approximates what is occurring in the real refrigerator. Evidence for this process is shown in Figure A-5. When the compressor shuts down both the fresh food and freezer compartment temperatures begin increasing. Likewise, the refrigerant temperature inside the evaporator also begins to rise. However as shown, the internal temperature of the evaporator is higher than the surrounding freezer air temperature during the initial period of the off-cycle. The only way the evaporator could be warmer is if hot gas from the condenser is migrating into the evaporator. Further, Figure A-6 shows the internal condenser temperature actually falling below the ambient temperature of 90°F. The direction of heat transfer must therefore be into the condenser indicating that refrigerant is boiling off. Apparently the boiling process ends after approximately 6 minutes into the off-cycle as indicated by the increasing temperature in the condenser for example at 32 minutes. Further, near the end of the off-cycle the temperature of the refrigerant in the condenser rises above the ambient temperature. This is the probable result of heat transfer from the stagnant air underneath the refrigerator that has been warmed by the compressor shell.

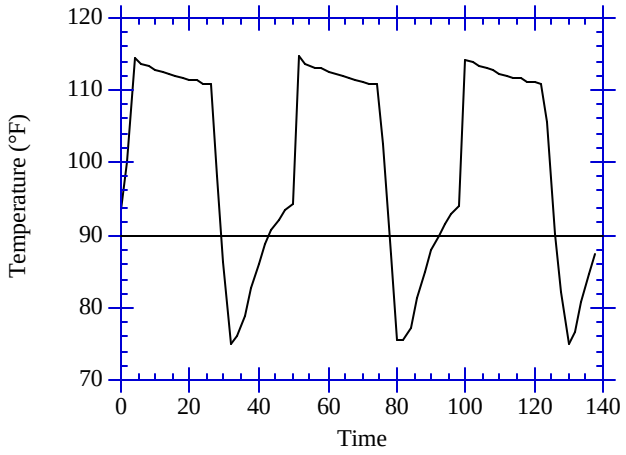

Figure A-6. Condenser Outlet Refrigerant Temperature

It is worth seeing if the heat transfer due to refrigerant migration can be quantified. However, before the amount of heat transfer due to refrigerant migration can be calculated, the amount of charge that actually migrates must be known. As a starting point for this calculation the initial refrigerant charge in the condenser right before the compressor turns off must be known. An estimate of this quantity can be determined if the quality of the two phase vapor is assumed to vary linearly along the condenser tubing. Note that this is the same as assuming that the heat flux along the condenser tubing is constant. Figure A-7 shows a small differential element of the condenser tubing of length dl, volume $d\bar{V}$ and cross-sectional area Ac. The mass of refrigerant in this volume is given by Equation 6. Substitution of $d\bar{V} = Acdl$ leads to Equation 7. It is important to realize that the mass of refrigerant within the tube is independent of the flow rate.

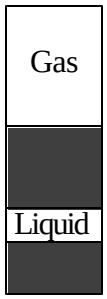

$Ac = \pi D$

$$dm = d\bar{V}_l \rho_l + d\bar{V}_g \rho_g$$

$$\frac{dm}{dl} = A_l \rho_l + A_g \rho_g$$

dm = differential mass

dl = differential length

$d\bar{V}_{l,g}$ = diff. volume of liquid/gas

ρ_l, ρ_g = density liquid/gas

A_l, A_g = cross-sectional area of liquid/gas

Figure A-7. Condenser Tube Element

Equation 8 defines quality in terms of the the slip ratio α which is V_l/V_g and the areas. Substitution of Equation 8 into Equation 7 and using the fact that $A_g = A_c - A_l$ yields Equation 9. Since the slip ratio is unknown, to a first approximation it can be assumed to be 1. This simplifies Equation 9 to 10. Now substitution of the linear quality assumption given by Equation 11 into Equation 10 and integrating over the length of the condenser tube yields the final result given in Equation 12.

$$x = \frac{m_g}{m} = \frac{r_g A_g}{r_g A_g + r_l A_{la}} \tag{A.8}$$

where m_g = mass of gas

m = total mass

$$\frac{dm}{dl} = \frac{\rho_l \rho_g A_c (1-x) + \rho_l \rho_g A_c \alpha x}{\rho_l \alpha x + \rho_g (1-x)} \tag{A.9}$$

$$\frac{dm}{dl} = \frac{\rho_l \rho_g A_c}{\rho_l x + \rho_g (1-x)} \tag{A.10}$$

$$x(l) = x_i - \left(\frac{x_i - x_o}{L} \right) l \tag{A.11}$$

where l = position along tube

L = total tube length

x_i = inlet quality

x_o = outlet quality

$$m = \left(\frac{\rho_l \rho_g \bar{V}}{\rho_{fg} (x_i - x_o)} \right) \ln \left[\frac{\rho_{fg} x_i + \rho_g}{\rho_{fg} x_o + \rho_g} \right] \tag{A.12}$$

where $\bar{V}$ = total volume

$\rho_{fg} = \rho_l - \rho_g$

The condenser consists of approximately 384 inches of 1/4 inch steel tubing. With a wall thickness estimated to be 0.03125 inches, the volume $\bar{V}$ is 10.6 in^3. Substituting this into Equation 12 with the properties of R12 at 100°F and assuming the quality goes from 1 to 0 in the condenser, the mass of refrigerant in the condenser is 0.0658 lbm or 1.05 oz. Note that the subcooled section of the condenser was ignored since no subcooling was detected in the real refrigerator. Added to this charge is the liquid refrigerant in the liquid line. The liquid line consists of 170 inches of 3/16 inch copper tubing. Assuming an internal diameter of 1/8 inch, the liquid line contains 1.4 oz. of refrigerant. The total charge available for migration is estimated to be 2.45 oz.

Figure A-6 indicates that all the liquid refrigerant migrates. To verify this assumption, a simple computer model was developed to find the amount of charge migration and the resulting heat transfer. The model is based on the assumption that the refrigerant boiling process is in the nucleate boiling regime and is the dominant heat transfer process. The other heat transfer processes like that to the environment immediately after compressor shut-down are assumed negligible. The model uses Equation 13 to calculate the heat flux into the condenser at a given time step. This correlation was developed for nucleate boiling by Rohsenow [7].

$$q_s'' = \mu_l h_{fg} \frac{g(\rho_1 - \rho_v)}{\sigma}^{\frac{1}{2}} \left(\frac{C_{pl}\Delta Te}{C_{sf}\, h_{fg}\, Pr_1^{\,n}} \right)^3 \qquad \text{(A.13)}$$

where μ_l = viscosity of the liquid

h_{fg} = enthalpy of vaporization

ρ_l = density of the liquid

ρ_v = density of the vapor

σ = surface tension

C_{pl} = specific heat of the liquid

Pr_l = Prandtl number of the liquid

ΔTe = excess temperature

C_{sf}, n = surface/liquid specific constants

It should be noted that this correlation is for boiling at constant pressure with variable excess temperatures. However, the boiling process in the condenser is driven by the change in saturation pressure. It is assumed that the two processes are equivalent. The constants C_{sf} and n depend on the surface - liquid combination. The closest set of values for C_{sf} and n that could be found were for R11 and steel. They were used to approximate the values for R12 and steel in the actual system [8].

To solve for the flux, it is necessary to know what the excess temperature (Tambient - Tc) is. It would be difficult to model the complex interaction between the condenser and evaporator to determine the saturation pressure and therefore temperature in the condenser. To simplify the simulation, a curve fit of the actual variation in condenser pressure with time as shown in Figure A-8 was used. It was assumed that the gas phase and liquid phase in the condenser were in thermal equilibrium. The saturation temperature of the liquid could then be determined directly. With the liquid temperature known, the excess temperature as a function of time could be calculated by subtracting

the liquid temperature from the constant 90°F ambient temperature. All the other properties are functions of temperature only and were calculated from curve fits of tabular R12 data. The variation in heat flux with time can now be determined.

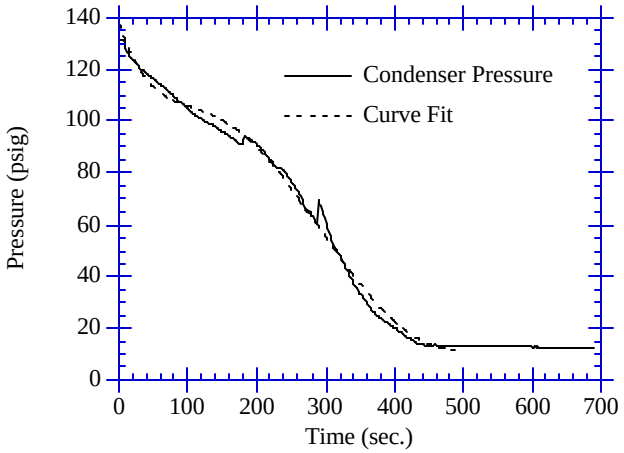

Figure A-8. Condenser Pressure Variation during Off-Cycle

Of more interest than the flux is the actual heat transfer rate which means an appropriate wetted surface area must be determined. Figure A-9 shows a cross-section of the condenser tube with liquid refrigerant in the bottom of the tube. Given the mass of refrigerant in the condenser and the density, the volume of liquid refrigerant can be easily calculated. Once the volume is known the surface contact angle can be determined from Equation 14. The wetted surface area can then be found from Equation 15. The heat transfer rate is determined by multiplying the flux by this area.

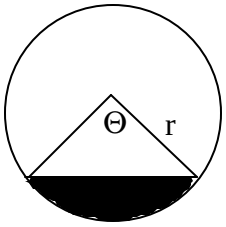

$$\bar{V} = \frac{r^2}{2}(\Theta - \sin\Theta)\ L \qquad \text{(A.14)}$$

$$A_w = r\Theta L \qquad \text{(A.15)}$$

where $\bar{V}$ = total condenser volume

A_w = wetted surface area

r = condenser tube radius

L = condenser tube length

Θ = surface contact angle

Figure A-9. Condenser Tube Cross-Section

Note that as the mass of refrigerant decreases the wetted surface area decreases. The smaller heat transfer area reduces the heat transfer rate.

The only remaining calculation is to determine the decrease in refrigerant in the condenser for a given time step. This is easily calculated from the Equation 16. The value of h_{fg} is the same as that used in the heat flux calculation.

$$Charge_{t+1} = Charge_t - \frac{q_t}{h_{fg}} \Delta t \qquad (A.16)$$

The simulation process involves three steps. At a particular time step, the saturation pressure for that time step is determined from a curve fit of the experimental data. From the saturation pressure, the saturation temperature and excess temperature are calculated. The heat transfer flux is then determined. Given the flux and the wetted surface area, the actual heat transfer rate can be determined. With the heat transfer rate known, the amount of charge left in the condenser is calculated. These steps are repeated for the entire process.

The results of the simulation are shown in Figure A-10 for the 2.45 oz. charge determined above. To find the upper bound on the heat transfer rate, the case were the total charge in the system migrates is also shown. The area under the heat transfer rate curves represents the amount of energy transferred to the inside of the refrigerator cabinet. If these values are then divided by the compressor on time, an estimate of the added load on the evaporator due to migration can be determined. The values are 6.4 W and 18.5 W for the 2.45 oz. and 7 oz. cases respectively. The results also show that all of the refrigerant in the condenser migrates as assumed previously.

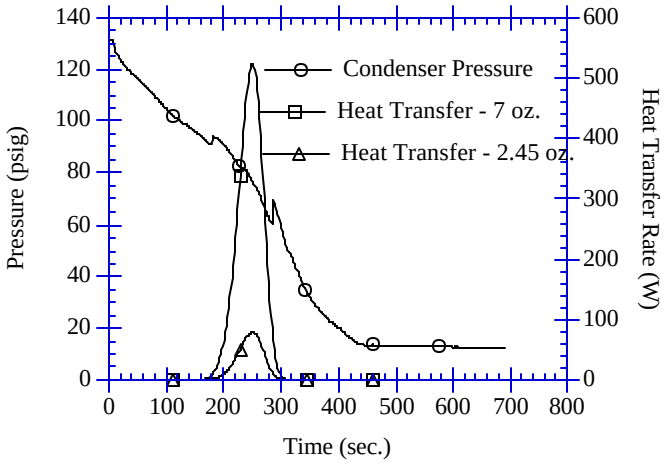

Figure A-10. Refrigerant Migration Simulation Results.

The other interesting result is the shape of the heat transfer rate curves which do make sense. At first the temperature of the boiling refrigerant decreases. This increases the difference between refrigerant and ambient temperatures resulting in higher heat transfer rates. However, as the refrigerant boils away the wetted surface area available for heat transfer rapidly decreases. This drives the heat transfer rate back to zero, at which point all the liquid has boiled off.

Amazingly enough, the inception and cessation of boiling are revealed in the actual pressure data. When boiling starts, the pressure in the condenser rises slightly. This is probably caused by the amount of vapor in the condenser increasing faster than it can be transferred to the evaporator thus increasing the pressure. Likewise when boiling ceases, there is also a slight pressure increase. The cause of this is less clear. It may be the result of instability in the capillary tube due to the transition to a different flow regime.

The final conclusion given the assumptions made is that the migration of refrigerant during the off-cycle does not significantly increase the load on the evaporator for this case. In other situations where the condenser volume and charge are greater, the heat transfer due to refrigerant migration may be an important consideration. However, the fact that all the charge ends up in the evaporator at the end of the off-cycle is important. With all the liquid in the evaporator when the compressor starts, it is easy to visualize the refrigerant being forced out of the helical evaporator in big slugs. This results in a starved evaporator with high superheat as noted above. The loss of refrigerant in the evaporator at start-up and other refrigerant migration effects were also investigated by Mulroy and Didion [9] for a split-unit air conditioner. The conclusions presented here are consistent with their results.

A.5 Comparison of Steady-State and Cyclic Performance Over an Entire Cycle

Although the efficiency of the refrigerator is degraded at one point during the on-cycle, the efficiency over an entire cycle may be higher. To explore this possibility, the second approach mentioned above to compare steady-state and cycling performance will now be investigated. To calculate an average COP both the total evaporator energy input and the total energy input to the system must be determined. Figure A-11 shows a control volume enclosing the air inside the refrigerator cabinet for the cycling case. Applying the first law to this control volume over the entire cycle results in Equation 17.

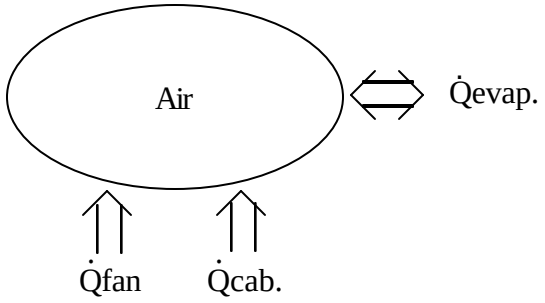

Figure A-11. Refrigerator Cabinet Air Control Volume

$$\int_0^{t_c} \dot{Q}\,dt = \int_0^{t_c} \frac{du_{air}}{dt}\,dt = 0 \qquad \text{(A.17a)}$$

$$\int_0^{t_c} \dot{Q}\,dt = \int_0^{t_c} \dot{Q}_{cab}\,dt + \int_0^{t_o} \dot{Q}_{fan}\,dt - \int_0^{t_c} \dot{Q}_{evap}\,dt \qquad \text{(A.17b)}$$

$$\int_0^{t_o} \dot{Q}_{evap}\,dt + \int_{t_o}^{t_c} \dot{Q}_{evap}\,dt = \int_0^{t_c} \dot{Q}_{cab}\,dt + \int_0^{t_o} \dot{Q}_{fan}\,dt \qquad \text{(A.17c)}$$

where t_c = cycle time

t_o = on-cycle time

Equation 17c states that the energy removed by the evaporator during the on-cycle plus that removed during the off-cycle must equal the energy transferred through the refrigerator cabinet plus the evaporator fan energy input. Note that the evaporator can absorb energy from the cabinet during the off-cycle after all the refrigerant has migrated from the condenser. Further, the evaporator fan only runs during the on-cycle. Unfortunately Equation 17c can not be solved explicitly because the energy input into the evaporator during the off cycle and the cabinet load are unknown. The cabinet load is not known because of the uncertainty introduced by the door heater. The only known terms are the energy input to the evaporator during the on cycle and the energy input to the evaporator fan.

However upper and lower bounds can be placed on the total energy input to the evaporator, which is the left side of Equation 17c, during a cycle. The lower bound occurs for the case where the energy input to the evaporator during the off cycle is zero. The upper bound occurs when all the refrigerant in the evaporator boils off during the off cycle.

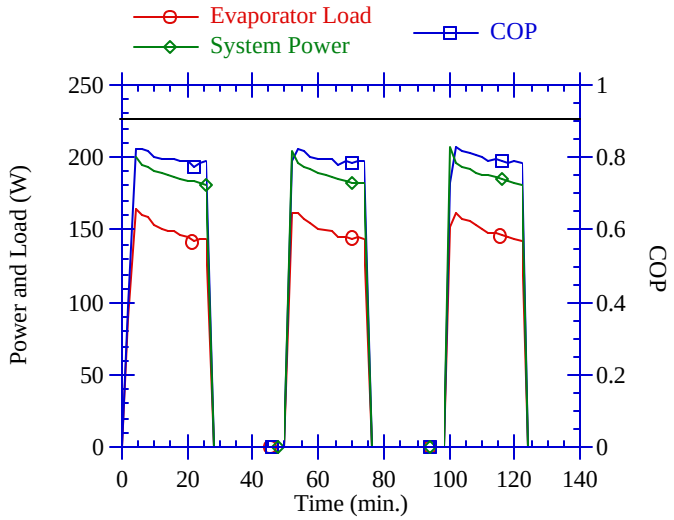

Figure A-12. Cycling & Steady-State Evaporator Load

Figure A-12 shows the evaporator load for the on-cycle based on an air side energy balance. Integrating under this curve yields an average on-cycle evaporator load of 148 W. Multiplying this by the on-cycle time results in the energy removed by the evaporator during the on-cycle or 223.5 kJ. Therefore the lower bound on the energy input to the evaporator is 223.5 kJ. The upper bound is easily calculated by multiplying the mass of refrigerant that boils off by the enthalpy of vaporization of the refrigerant and adding this to the lower bound. If the evaporator is assumed to contain the entire 7 oz. charge and all the charge boils off during the off cycle at 5°F, then the maximum energy input to the evaporator during the off cycle is 28.5 kJ. Therefore, the maximum energy input to the evaporator over an entire cycle is 252 kJ.

The last piece of information needed to calculate an average cycling COP is an average system power requirement. The variation in the refrigerator power requirement is shown in Figure A-13. The refrigerator power includes the compressor, the evaporator fan, the condenser fan and the small amount of power drawn by the controls. The average power for the three on-cycles shown is 188 W. Multiplying this by the on-cycle time of 25.1 minutes yields the energy required over the entire cycle or 283.1 kJ.

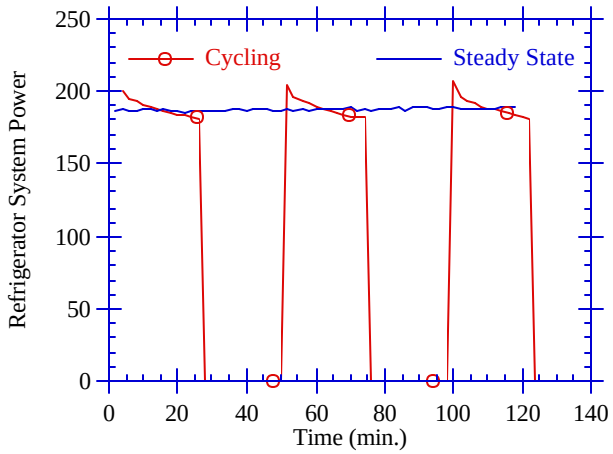

Figure A-13. System Power for Cyclic & Steady-State Operation

By dividing the minimum and maximum energy inputs to the evaporator by the energy input to the system over an entire cycle, a minimum and maximu m COP can be determined. Table A.2 summarizes these results. The average cycling performance is at best 2% lower than the steady state performance and at worst 13%. It again appears that cycling degrades the performance of the system as for the "snapshot" comparison.

Table A.2. Steady-State and Average Cyclic Performance

Case	Steady-State	Cycling
Cycle Time (min.)	48.5	48.5
On-Cycle (min.)	48.5	25.1
Off-Cycle (min.)	0.0	23.4
Ambient Temperature (°F)	89.8	89.6
Average Fresh Food Temperature (°F)	41.6	40.1
Average Freezer Temperature (°F)	3.4	4.6
Refrigerant Charge (oz.)	7.0	7.0
Evaporator Load (kJ)	497.7	223.5 to 252
System Energy Input (kJ)	544.2	283.1
Average COP	0.91	0.79 to 0.89

A.6 Conclusions

The most important result from this analysis is the fact that refrigerant dynamics have an impact on performance. Migration of refrigerant between the components of the system results in significant decreases in efficiency. This means a model to calculate cycling performance must include time dependent charge inventory terms. Further, it appears that the thermal mass of the compressor must also be considered. A quasi-steady approximation for the compressor will work. Lastly, the additional heat input to the cabinet due to refrigerant migration appears to be small for this refrigerator given the assumptions made.

References

[1] Murphy, W.E., and V.W. Goldschmidt. 1979. "The degradation coefficient of a field-tested self-contained 3-ton air conditioner." ASHRAE Transactions, Vol. 85, Part 2, pp. 396 to 405.

[2] Goldschmidt, V.W., G.H. Hart, and R. C. Reiner. 1980. "A note on the transient performance and degradation coefficient of a field tested heat pump - cooling and heating mode." ASHRAE Transactions, Vol. 86, Part 2, pp. 368 to 375.

[3] Murphy, W.E., and V.W. Goldschmidt. 1984. "Transient response of air conditioners-a qualitative interpretation through a sample case." ASHRAE Transactions, Vol. 90, Part 1B, pp. 997-1008

[4] Katipamula, S. and D.L. O'Neal. 1991. "Performance degradation during on-off cycling of single-speed heat pumps operating in the cooling mode: experimental results." ASHRAE Transactions, Vol. 97, Part 2, In print.

[5] Department of Energy. 1979. "Test procedures for central air conditioners, including heat pumps." Federal Register, Vol. 44, No. 249, pp. 76700 to 76723.

[6] Department of Energy. 1989. "Uniform test method for measuring the energy consumption of central air-conditioners." Code of Federal Regulations, Part 430, Subpart B, Appendix M, pp. 101 to 126, January 1.

[7] Rohsenow, W.M., "Boiling" in W.M. Rohsenow et al., Eds., Handbook of Heat Transfer Fundamentals , Chapter 12, McGraw-Hill, New York, 1985.

[8] American Society of Heating, Refrigerating and Air-Conditioning Engineers, Inc., Fundamentals Handbook, p. 4.2, ASHRAE, Atlanta, 1989.

[9] Mulroy, W.J. and D.A. Didion. 1985. "Refrigerant migration in a split-unit air conditioner." ASHRAE Transactions, Vol. 91, Part 1A, pp. 193 to 206.

Appendix B: Reverse Heat Leak Tests

As part of the parameter estimation effort, the energy transferred through the refrigerator cabinet or cabinet load may need to be known. The cabinet load can be calculated from Equation 1.

$$\dot{Q}_{cab} = UA_{freezer}(T_{amb} - T_{frez}) + UA_{food}(T_{amb} - T_{food}) \qquad (B.1)$$

where $UA_{freezer}$ = freezer compartment heat transfer coefficient (W/°F)

UA_{food} = fresh-food compartment heat transfer coefficient (W/°F)

T_{amb} = chamber temperature (°F)

T_{frez} = freezer compartment temperature (°F)

T_{food} = fresh-food comp artment temperature (°F)

The freezer compartment, fresh-food compartment and ambient temperatures can be measured directly. The cabinet over-all heat transfer coefficients or UA values must be determined independently.

These values were found experimentally by performing a reverse heat leak test on the refrigerator cabinet. The test involves heating both the fresh-food and freezer compartments above ambient conditions with auxiliary heaters (see Instrumentation Chapter) while the refrigerator is turned off. The temperatures in both compartments were made equal to prevent heat transfer between compartments. Further, the air passages between the compartments were taped shut. Since the temperature inside the refrigerator is higher than the ambient temperature, heat is transferred to the environment in the reverse direction it would normally have when the refrigerator is operating. Once steady-state conditions have been reached, the heat transfer through the cabinet is equal to the power input to the auxiliary heaters. By dividing the measured powers by the temperature difference between the internal cabinet temperature and ambient, a UA value can be determined for each compartment.

The power input to the heaters was measured over a range of temperature differences. Figure B-1 shows the data points taken. The actual temperatures and powers measured are also summarized in Table B.1. The slope of the lines in Figure B-1 equal the UA values for the freezer and fresh-food compartments. The UA value for the freezer is 0.49 W/°F ± 0.11 W/°F and the UA for the fresh-food compartment is 1.04 W/°F ± 0.11 W/°F.

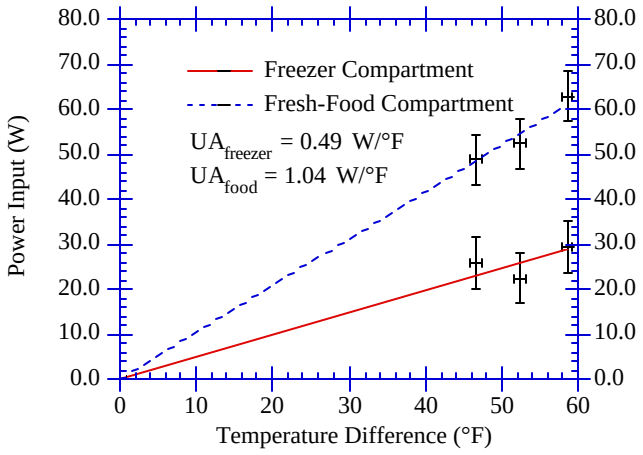

Figure B-1. Reverse Heat Leak Test Results

Table B.1. Reverse Heat Leak Data Summary

Test	Ambient Temperature (°F)	Freezer Temperature (°F)	Fresh-Food Temperature (°F)	Freezer Heater Power (W)	Fresh-Food Heater Power (W)
1	50.4	102.9	102.8	22.4	52.3
2	56.1	102.8	102.6	25.9	48.7
3	51.2	109.8	109.9	29.4	62.9

Implicit in the use of Equation 1 are several assumptions. The most important is assuming that the UA values are constant over the temperature range that they will be applied to. From Figure B-1, the linear relationship between heater power and temperature difference confirms that the UA values are relatively constant. However this is a small data set. This conclusion can be substantiated by looking at the relative resistances to heat transfer in a hypothetical refrigerator cabinet.

Figure B-2 shows a cross-section of a hypothetical refrigerator cabinet with a temperature profile drawn in. The thermal resistances for each section of the wall are given in Table B.2. Typical values were used for the thicknesses of each section and for the film coefficients as provided by Clausing [1]. An arbitrary cross-sectional area of 3 m^2 was used in calculating the heat transfer resistances.

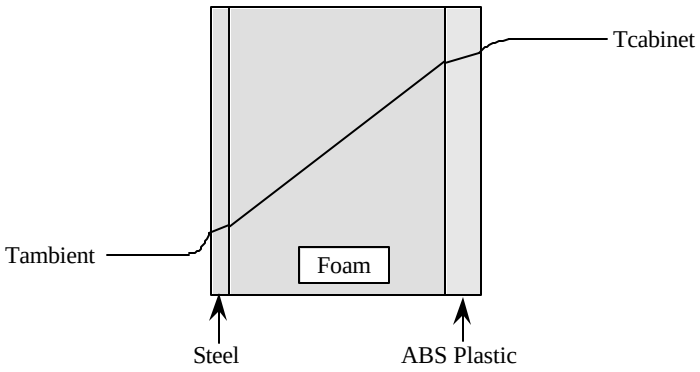

Figure B-2. Hypothetical Temperature Distribution in a Refrigerator Cabinet Wall

Table B.2. Thermal Resistances in Refrigerator Cabinet

Section	Thickness (mm)	Film Coefficient or Thermal Conductivity	Resistance (K/W)
Ambient Air	-	7 W/m^2K	0.0476
Steel	0.6	60 W/m-K	$3.33e^{-6}$
Urethane Foam	36	0.0245 W/m-K	0.490
ABS Plastic	2.5	0.17 W/m-K	0.0049
Cabinet Air	-	6 W/m^2K	0.0556

Adding the last column of Table B.2 yields the total resistance to heat transfer or 0.598 K/W. The resistance of the foam, at 82 % of the total, dominates the heat transfer process. Therefore variations in the film coefficients resulting from changes in temperature dependent properties have little impact on over-all heat transfer. Further, since the thermal conductivity of the foam varies less than 11% from -100°F to 100°F [2], the heat transfer through the wall

will depend only on the temperature difference across the wall and not on the temperature of the wall. From this it would be expected that the conductance through the wall or UA value would be relatively constant as concluded from the experimental results. Another related conclusion can also be drawn. Since the UA values are independent of temperature, the direction of heat transfer through the cabinet wall is irrelevant. Therefore the UA values determined by a reverse heat leak test are valid for use in Equation 1 when the refrigerator is operating in a steady-state manner with internal temperatures lower than ambient conditions.

The use of Equation 1 also assumes that the effect of the evaporator fan, the compressor, and the door heater on cabinet load are negligible when the refrigerator is operating. Results from the parameter estimation work indicate that at least the door heater does transfer a significant amount of heat into the freezer compartment. Figure B-3 shows the door heater heat transfer plotted as a function of the temperature difference between the refrigerant and the freezer air. Although the correlation is not great there does appear to be a trend. When the same door heater heat transfers are plotted as a function of the difference between the refrigerant temperature and the ambient temperature, no correlation exists at all. This suggests that a fair percentage of the heat rejection from the door heater ends up back inside the refrigerator cabinet. Further investigation into the door heater heat transfer may help to explain the large discrepancies between the evaporator load based on cabinet heat transfer and based on a refrigerant side energy balance.

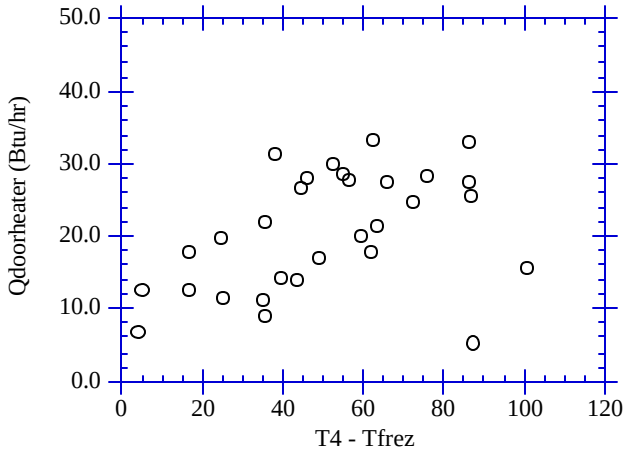

Figure B-3. Door Heater Heat Transfer

Further, the evaporator fan in the refrigerator studied discharges air directly toward the gaskets surrounding the freezer door. This may increase the air exchange rate from the inside of the refrigerator to the outside. An increase in the air exchange rate should increase the cabinet load. Further, operation of the compressor results in elevated temperatures underneath the refrigerator cabinet. This increases the temperature difference across this part of the refrigerator cabinet and should also slightly increase the cabinet load.

More accurate measurements of the cabinet load is desirable. To this end it will probably be necessary to improve the instrumentation used for the reverse heat leak tests. The auxiliary heaters used for the tests have a lower power limit of 23 W. Even this small amount of power is enough to cause a 50 °F temperature difference between the

freezer compartment and ambient conditions as shown in Figure B-1. A heater system that can deliver less than 23 W would be desirable. This change will also require watt transducers that can accurately read the small power inputs required.

One possibility for improving the accuracy of the measurements is to switch to a direct current system. The voltage and current input to the heater elements could be measured accurately even at these lower power levels. The system should still include some sort of fan to distribute the air in both compartments to help prevent temperature gradients within the cabinet. Note that the presence of a fan restricts the maximum internal cabinet temperature that can be tested. The temperature rating of the insulation of the motor windings should be considered when performing tests. Typically the insulation on the windings can tolerate temperatures up to 105°F.

References

[1] Personal communication., Dr. A. E. Clausing., Associate Head, Department of Mechanical Engineering, University of Illinois, 1206 West Green Street, Urbana, IL. 61801.

[2] American Society of Heating, Refrigerating and Air-Conditioning Engineers, Inc., Fundamentals Handbook, pg 22.17, ASHRAE, Atlanta, 1989.

Appendix C: Refrigerator Charge Tests

As part of the experimental program a series of charge tests was performed on the refrigerator as received from the manufacturer and after the pressure transducers and the immersion thermocouples were installed (See Instrumentation Chapter). The purpose of these tests is twofold. First the optimum charge for steady-state operation based on efficiency for the refrigerator can be determined. Further by ensuring that the refrigerator always runs with the optimum charge, errors resulting from changes in the amount of charge can be eliminated from a given data set. Second the effect of the instrumentation on refrigerator performance can be determined.

The procedure for the charge tests is relatively simple. The charge in the refrigerator is varied in roughly one ounce increments. At each charge level, the internal cabinet temperatures are set as close to 41.4°F in the fresh-food compartment and 3.3°F in the freezer compartment as possible. For some cases the capacity of the system was sufficiently reduced such that these compartment temperatures could not be reached. This does not, however, affect the results. The ambient temperature is also kept constant. Once steady-state conditions are reached, system data is collected for at least an hour. After each test point, the refrigerant charge in the system is removed.

The charge in the system is removed through the process tube on the compressor with a vacuum pump. The pump should be allowed to run for a minimum of 2 hours. Shorter evacuation times do not remove all the refrigerant dissolved in the compressor oil. After evacuation, the system is charged from a refrigerant tank that is placed on top of a digital scale. The scale allows the mass of charge metered into the system to be controlled to within ±0.035 ounce. After being recharged with a different amount of refrigerant, the test is repeated using the same procedure outlined above.

In all, 4 sets of charge tests were performed. Two tests were run on the refrigerator as received from the manufacturer: one at 70°F and one at 90°F ambient. For these two tests, only power inputs, air temperatures and surface temperatures on the heat exchangers were measured. The instrumentation for the first two tests did not penetrate the refrigerant piping and should not affect the performance of refrigerator. After the pressure transducers and immersion thermocouples were installed, two more tests were run at the same ambient conditions as for the first two tests. The experimental results are summarized in Table C.1. The evaporator load is the sum of the power inputs to the auxiliary heaters (see Instrumentation Chapter), the evaporator fan and the cabinet load. The cabinet load was determined from Equation 1 given in Appendix B. COP or coefficient of performance is the ratio of the evaporator load to the system power requirement.

Table C.1. Refrigerant Charge Tests Data Summary

Refrigerant Charge (oz.)	Ambient Temperature (°F)	Fresh-Food Temperature (°F)	Freezer Temperature (°F)	Evaporator Load (W)	System Power (W)	COP
Uncertainty	±0.73°F	± 0.73°F	±0.73°F	±5.9 W	±8.1 W	±0.05
Steady-State Performance As Received from Factory						
4.5	69.2	41.3	3.3	187	170	1.1
5 ?	70	41.6	3.1	207	179	1.16
6.0	69.7	41.5	3.3	198	187	1.06
7.0	69.4	41.4	3.4	159	210	0.76
4.5	89.4	41.6	3.4	186	183	1.02
5 ?	89.9	41.2	3.1	196	186	1.05
6.0	89.3	41.5	3.2	194	190	1.02
7.0	89.9	41.5	5.9	152	215	0.71
Performance After Pressure Transducers & Immersion Thermocouples were Installed						
5 ?	70.9	41.4	3.7	173	167	1.04
6	70.6	41.3	3.2	183	171	1.07
7	70.5	41.1	3.4	196	182	1.08
8	70.2	41.4	3.2	164	198	.83
5 ?	89.5	41.5	4.2	160	184	.87
6	90	41.5	3.2	174	188	.93
7	89.8	41.6	3.4	175	187	.94
8	90.4	46.6	7.4	152	208	.73

Figure C-1 shows the COP of the refrigerator plotted as functions of charge and ambient conditions. Three important conclusions can be drawn from Figure C-1. The first is the fact that the data indicates that there is indeed an optimum charge at which to run the system. A least-squares curve fit using a second order polynomial was performed on the 4 data sets. The coefficients for the curve fits are summarized in Table C.2. The optimum charge for each data set was calculated by taking the derivative of the curve fit equations and setting them equal to zero. Once the optimum charge is known, the best system COP can be calculated and is given in Table C.2. also. For both the before and after cases, the optimum charge is essentially independent of ambient temperature.

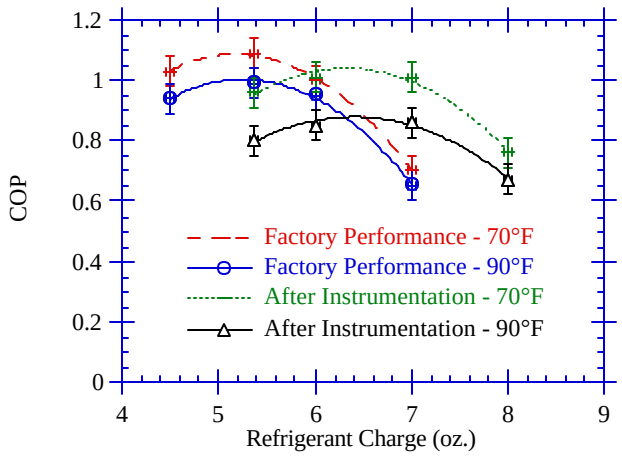

Figure C-1. Effect of Charge on Refrigerator Performance - R12

Table C.2. Coefficients for Curve Fits of Charge Data

Test Case	A	B	C	Optimum Charge (oz.)	Optimum COP
Before - 70°F	-0.11721	1.21431	-2.05876	5.2	1.09
Before - 90°F	-0.11532	1.21244	-2.18375	5.3	1.0
After - 70°F	-0.09819	1.24228	-2.8896	6.3	1.04
After - 90°F	-0.07986	1.02248	-2.39549	6.4	0.88
Curve Fits of the Form $COP = A(charge)^2 + B(charge) + C$					

The second important trend shown in Figure C-1 is the shift in the average optimum operating charge from 5.25 oz. to 6.35 oz. The most logical cause for the shift is the extra volume added to the system by the pressure transducers and the immersion thermocouples. The added volume has no effect on system performance other than increasing the amount of charge required to bring the refrigerator up to optimum performance.

The third and most important trend shown in Figure C-1 is the decrease in the optimum efficiency of the system for equivalent ambient conditions. This indicates that the pressure transducers and immersion thermocouples have an effect on refrigerator performance. One possible explanation for the reduction is an increase in the pressure drop in the system caused by the instrumentation tees (See Instrumentation Chapter). Increased pressure drop in the system would increase the pressure difference across the compressor which would reduce the mass flow rate. A lower mass flow rate results in a lower capacity and a lower efficiency for equivalent operating conditions.

Table C.3. System Pressure Losses Before and After Additional Instrumentation Installation

	Factory Performance	After Pressure Transducer Installation
Evaporator Inlet Air Temperature °F	6.6 ±0.5	6.5 ±0.5
Evaporator Inlet Temperature-R12 °F	- 6.8 ±0.5 (s)*	- 11.5 ±0.5 (i)*
Evaporator Outlet Temperature-R12 °F	- 9.4 ±0.5 (s)	- 8.5 ±0.5 (s)
Evaporator Pressure Drop (psig)	1.2 ±0.30	2.34 ± 0.02
Condenser Inlet Air Temperature °F	88.9 ±0.5	90.0 ±0.5
Condenser 1/2 Way-R12 °F	110.4 ±0.5 (s)	109.5 ±0.5 (s)
Condenser Outlet-R12 °F	109.9 ±0.5 (s)	112.6 ±0.5 (i)
Condenser Pressure Drop (psig)	1.0 ±1.4	1.23 ±0.06
Door Heater Pressure Drop (psig)	-	0.5 ±0.06
Suction Line Pressure Drop (psig)	-	0.0 ±0.06
* s = surface thermocouple i = immersion thermocouple		

Evidence for increased pressure drop in the refrigerator evaporator and condenser before and after the pressure transducers etc. were installed is shown in Table C.3. Both cases are for the 90°F tests. Pressure losses in the refrigerator with factory performance were inferred from the surface temperature measurements. It was assumed that the refrigerant at these points was two-phase. This is supported by the fact that the refrigerant temperature in the evaporator falls from inlet to outlet which could only occur if the evaporator was entirely two-phase. Further since no subcooling was detected in the condenser, the condenser could also be assumed to be entirely two-phase if the desuperheating section is ignored. The pressure drop across the door heater and suction line could not be determined because the outlet of each of these components was not saturated. The pressure drops for the after case are from the actual pressure transducer measurements.

From Table C.3. the pressure drop across the evaporator increased by roughly a factor of two after the immersion thermocouples etc. were installed. The change in the pressure drop in the condenser is inconclusive because of the measurement uncertainty in the factory performance case. It is likely, however, that the pressure drop across the condenser does increase. Although by no means conclusive at least qualitatively the pressure drop in the refrigerator system has increased.

The effect of the increased pressure drop on performance can be investigated qualitatively by running a refrigerator system model with and without pressure losses. For this purpose, the ACRC1 [1] model was run for the 90°F test condition. The pressure losses in the system after the immersion thermocouples were installed are used for the non-zero pressure drop case. The results are summarized in Table C.4.

Table C.4. Predicted Effect of System Pressure Losses on Performance

Case	Zero System Pressure Drop	System with Pressure Drop
Evaporator Load (Btu/hr)	753	718
Compressor Power (Btu/hr)	573	553
Mass Flow Rate (lbm/hr)	13.5	12.8
COP	1.08	1.06

The model predicts pressure losses in the system will cause a 2% decrease in system efficiency. The actual data shows a much larger decrease of 12%. The discrepancy is in part a result of simplifying assumptions made in the model that are not realistic such as a flooded evaporator for all operating conditions [2]. The experimental data indicates the evaporator has a superheated section after the immersion thermocouples were installed. The evaporator for the factory performance case is flooded. Superheat in the evaporator significantly reduces the capacity and efficiency of the system. More sophisticated models that account for superheat will probably predict a larger decrease in system efficiency due to pressure losses. Although the quantitative differences can not be accounted for it can be at least concluded that pressure losses will have to be considered in a good system model.

Lastly, a set of charge tests at 90°F was also performed on the refrigerator after it was modified to work with R134a. For reference the results are shown in Figure C-2. The performance of the system with R134a appears to be independent of the amount of refrigerant charge within the range of the data available. More accurate measurements will need to be made to verify this result.

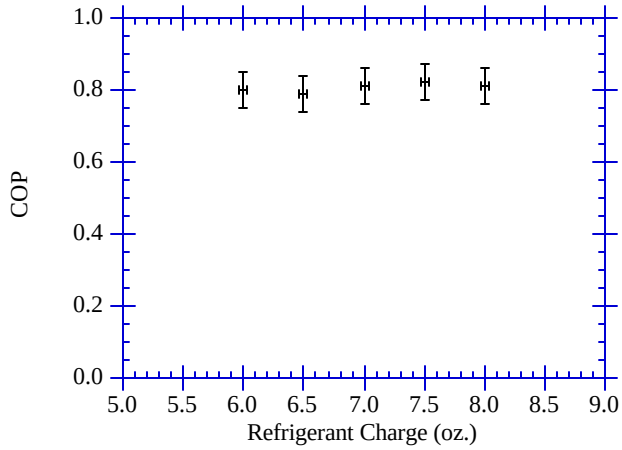

Figure C-2. Effect of Charge on Refrigerator Performance - R134a

References

[1] Porter, K.J., Modeling and Sensitivity Analysis of a Refrigerator/Freezer System, Forthcoming, Air Conditioning and Refrigeration Center, University of Illinois at Urbana-Champaign, 1992.

[2] Reeves, R.N., Modeling and Experimental Parameter Estimation of a Refrigerator/Freezer System, Air Conditioning and Refrigeration Center, University of Illinois at Urbana-Champaign, 1992.

Appendix D: Experimental Uncertainty Analysis

Temperature Measurement Uncertainty

Data Acquisition Supplier Estimate	±1.3 °F
Lab Estimate	±0.73 °F

$$\text{Uncertainty} = \sqrt{(\text{Bias})^2 + (\text{Precision error})^2}$$

Precision error = $2S_x = 2(0.266\ °F) = \pm 0.532\ °F$

$$\text{Uncertainty} = \sqrt{(0.5\ °F)^2 + (0.532\ °F)^2} = \pm 0.73\ °F$$

Pressure Transducer Uncertainties

Pressure Transducer Type	Transducer Accuracy	Load Resistor	Atmospheric Pressure Variation	Precision Error	Total Uncertainty
0-100 psi gage	±0.13 psi	-	±0.4 psi	±0.38 psi	±0.57 psi
0-250 psi gage	±0.325 psi	-	±0.4 psi	±0.66 psi	±0.84 psi
0-10 psi differential	±0.015 psi	±0.015 psi	-	±0.14 psi	±0.14 psi
0-25 psi differential	±0.05 psi	±0.038 psi	-	±0.09 psi	±0.11 psi

Sample calculation 0-10 psi differential pressure transducer:

(Transducer output = 4 to 20 mA through 25 Ω resistor to get 0.1 V to 0.5 V output)

Transducer accuracy = (instrument accuracy)(full scale)

= (0.15 %)(10 psi) = ±0.015 psi

$$\text{Load resistor error} = \frac{10\ \text{psi}}{0.4\ \text{V}}\ [(\text{variation in voltage output due to temperature})]$$

$$= \frac{10\ \text{psi}}{0.4\ \text{V}}\ [(30\ \text{ppm/°F})(40\ °F)(25\ \Omega)(20\ \text{mA})(1/1000)] = \pm 0.015\ \text{psi}$$

Precision error = 2(0.07 psi) = ±0.14 psi

$$\text{Uncertainty} = \sqrt{(0.015\ \text{psi})^2 + (0.015\ \text{psi})^2 + (0.14\ \text{psi})^2} = \pm 0.14\ \text{psi}$$

Sample calculation 0-100 psig pressure transducer

Transducer output = 0.1 V to 5.1 V

Transducer accuracy = (instrument accuracy)(full)(scale)

= (0.13 %)(100 psig) = ±0.13 psig

Atmospheric pressure variation from lab data = ±0.4 psi

Precision error = 2(0.19 psi) = ±0.38 psi

$$\text{Uncertainty} = \sqrt{(0.13\ \text{psi})^2 + (0.4\ \text{psi})^2 + (0.38\ \text{psi})^2} = \pm 0.57\ \text{psi}$$

Uncertainty in Measured Pressures

Pressure (psi)	Uncertainty
Evaporator Inlet	±0.59 psi
Evaporator Outlet	±0.57 psi
Compressor Suction Inlet	±0.58 psi
Condenser Inlet	±0.85 psi
Condenser Outlet	±0.84 psi
Capillary Tube Inlet	±0.85 psi

Sample calculation for capillary tube inlet:

$$P_{capinlet} = P_{condenser\ out} - \Delta P_{door\ heater}$$

$$\text{Uncertainty} = \sqrt{(\text{uncertainty in } P_{condenser})^2 + (\text{uncertainty in } \Delta P)^2}$$

$$\text{Uncertainty} = \sqrt{(0.84\ \text{psi})^2 + (0.11\ \text{psi})^2} = \pm 0.85\ \text{psi}$$

Watt Transducer Uncertainty

Watt Transducer	Transducer Uncertainty	Load Resistor	Voltage Ripple	Precision Error	Total Uncertainty
System	±7.5 W	±2.3 W	-	±2.2 W	±8.1 W
Compressor	±2.5 W	±0.8 W	-	±2.1 W	±3.4 W
Evaporator Fan	±0.5 W	-	-	±0.21 W	±0.5 W
Freezer Heater	±1.1 W	±0.6 W	±2.5 W	-	±2.8 W
Fresh Food Heater	±1.1 W	±0.6 W	±2.5 W	-	±2.8 W

Sample calculation, system power:

Transducer output: 4 - 20 mA through 25 Ω resistor to get 0.1 V to 0.5 V output

Transducer uncertainty = (transducer accuracy)(full scale)

$= (0.5\ \%)(1500\ \text{W}) = \pm 7.5\ \text{W}$

$$\text{Load resistor} = \frac{1500\ \text{W}}{0.4\ \text{V}}\ \text{[variation in voltage due to temperature flucuations]}$$

$$= \frac{1500\ \text{W}}{0.4\ \text{V}}\ [(30\ \text{ppm/°F})(40\ \text{°F})(25\ \Omega)(20\ \text{mA})(1/1000)] = \pm 2.3\ \text{W}$$

Precision error = $2(1.1\ \text{W}) = \pm 2.2\ \text{W}$

$$\text{Uncertainty} = \sqrt{(7.5\ \text{W})^2 + (2.3\ \text{W})^2 + (2.2\ \text{W})^2} = \pm 8.1\ \text{W}$$

Sample calculation, freezer heater power:

Transducer output - 0 to 1 ma through 10 kΩ resistor to get 0 to 10 V output

Transducer uncertainty = (transducer accuracy)(full scale)

$= (0.21\ \%)(500\ \text{W}) = \pm 1.05\ \text{W}$

Load resistor = $\frac{500\ W}{10\ V}$ [variation in voltage due to temperature flucuations]

$= \frac{500\ W}{10\ V}$ [(30 ppm/°F)(40 °F)(10 kΩ)(1 mA)] = ±0.6 W

Voltage ripple $= \frac{500\ W}{10\ V}$ [variation in voltage due to RC circuit]

Voltage ripple = $\frac{500\ W}{10\ V}$ (0.05 V) = ± 2.5 W

Uncertainty = $\sqrt{(1.05\ W)^2 + (0.6\ W)^2 + (2.5\ W)^2}$ = ±2.8 W

Uncertainty in Enthalpy Calculations

Location	$\frac{dh}{dT}$	Uncertainty in Temperature	$\frac{dh}{dP}$	Uncertainty in Pressure	Total Uncertainty
Evaporator Outlet - R12	0.14 Btu/lbm°F	±0.73 °F	-0.0552 Btu/lbm*psi	±0.57 psi	±0.11 Btu/lbm
Compressor Discharge - R12	0.17 Btu/lbm°F @ 140 psia, 160°F	±0.73 °F	-0.0335 Btu/lbm*psi	±0.85 psi	±0.13 Btu/lbm
Condenser Outlet - R12	0.24 Btu/lbm°F	±0.73 °F	0.131 Btu/lbm*psi	±0.84 psi	±0.21 Btu/lbm
Evaporator Outlet - R134a	0.19 Btu/lbm°F @ 10.4 psia, 20 °F	±0.73 °F	-0.089 Btu/lbm*psi	±0.0 psi	±0.14 Btu/lbm
Compressor Discharge - R134a	0.251 Btu/lbm°F @ 132 psia, 150 °F	±0.73 °F	-0.050 Btu/lbm*psi	±0.85 psi	±0.19 Btu/lbm
Condenser Outlet - R134a	0.35 Btu/lbm°F @ 132 psia, x=0.0	±0.73 °F	0.113 Btu/lbm*psi	±0.84 psi	±0.27 Btu/lbm

Sample calculation, evaporator outlet:

$\frac{\delta h}{\delta T} = \frac{\Delta h}{\Delta T} = \frac{80.767 - 79.345 Btu/lbm}{20\text{-}10°F}$ = 0.14 Btu/lbm°F @ P=20psia,T=10°F,20°F

$\frac{\delta h}{\delta P} = \frac{\Delta h}{\Delta P} = \frac{81.043 - 80.767 Btu/lbm}{15\text{-}20psia}$ = -0.0552 Btu/lbm*psi @T=20°F,P=15psia,20psia

Total uncertainty = $\sqrt{\left(\frac{\delta h}{\delta T} w(T)\right)^2 + \left(\frac{\delta h}{\delta T} w(P)\right)^2}$

$= \sqrt{(0.14*0.73)^2 + (-0.0552*0.57)^2}$ = ±0.11 Btu/lbm

Sample calculation, condenser outlet (assume saturated liquid)

$\frac{\delta h}{\delta T}$ = Cp(@100°F) = 0.24 Btu/lbm°F

$\frac{\delta h}{\delta P} = \frac{\Delta h}{\Delta P} = \frac{31.583 - 31.1 Btu/lbm}{135.56 - 131.86 psia}$ = 0.131 Btu/lbm*psia

Total uncertainty = $\sqrt{(0.24*0.73)^2 + (0.131*0.84)^2}$ = ±0.21 Btu/lbm

Refrigerant Mass Flow Rate Uncertainties

Source	Uncertainty
Compressor Map	±5.0 %
Turbine Flow Meter	± 2.9%

Turbine flow meter calculation:

Transducer accuracy = ±0.25%

Calbration error = ±1%

Mean deviation from curve fit = ±2.7%

Total uncertainty = $\sqrt{(0.0025)^2 + (0.01)^2 + (0.027)^2}$ = ±0.029

Condenser Volumetric Flow Rate Uncertainty

$$\dot{V}_c = \frac{1}{\rho C_p 60 \Delta T}\left[3.413\,(\dot{P}system - \dot{P}efan) + \dot{m}\,(h10 - h3)\right]$$

nominal values: ρ = 0.072 lbm/ft^3, C_p = 0.24 Btu/lbm°F, ΔT = 9.3 °F

Psystem = 160 W, Pefan = 12.5 W, $\dot{m}$ = 7.5 lbm/hr

h10 = 116 Btu/lbm, h3 = 35 Btu/lbm

$w(\rho) = \frac{\delta\rho}{\delta T}\ w(T) = (1.33e\text{-}4\ \text{lbm/ft}^3\text{°F})(\pm 0.73\ \text{°F}) = \pm 9.7e\text{-}5\ \text{lbm/ft}^3$

$w(\dot{V}_c(\rho)) = \frac{\delta\dot{V}_c}{\delta\rho}\ w(\rho) = (-1584.4)(\pm 9.7e\text{-}5) = \pm 0.154\ \text{ft}^3/\text{min}$

$w(C_p) = \frac{\delta C_p}{\delta T}\ w(T) = (2.24e\text{-}5\ \text{Btu/lbm°F}^2)(\pm 0.73\ \text{°F}) = \pm 1.64e\text{-}5\ \text{Btu/lbm°F}$

$w(\dot{V}_c(C_p)) = \frac{\delta\dot{V}_c}{\delta C_p}\ w(C_p) = (-475.3)(\pm 1.64e\text{-}5) = \pm 7.79e\text{-}3\ \text{ft}^3/\text{min}$

$w(\dot{V}_c(\Delta T)) = \frac{\delta\dot{V}_c}{\delta\Delta T}\ w(\Delta T) = (-12.3)(\pm 1.03\text{°F}) = \pm 12.7\ \text{ft}^3/\text{min}$

$w(\dot{V}_c(\dot{P}\,system)) = \frac{\delta\dot{V}_c}{\delta\dot{P}system})\ w(\dot{P}\,system)) = (0.354)(\pm 8.1\ \text{W}) = \pm 2.87\ \text{ft}^3/\text{min}$

$$w(\dot{V}_c(\dot{P}\,efan)) = \frac{\delta \dot{V}_C}{\delta \dot{P}efan}\ )\ w(\dot{P}\,efan)) = (-0.354)(\pm 0.5\ W) = \pm 0.177\ ft^3/min$$

$$w(\dot{V}_c(\dot{m})) = \frac{\delta \dot{V}_C}{\delta \dot{m}}\ w(\dot{m}) = (8.401)(2.9\%)(7.5\ lbm/hr) = \pm 1.8\ ft^3/min$$

$$w(\dot{V}_c(h10)) = \frac{\delta \dot{V}_C}{\delta h10}\ w(h10) = (0.778)(\pm 0.14\ Btu/lbm) = \pm 0.11\ ft^3/min$$

$$w(\dot{V}_c(h3)) = \frac{\delta \dot{V}_C}{\delta h3}\ w(h3) = (-0.778)(\pm 0.19\ Btu/lbm) = \pm 0.15\ ft^3/min$$

$$w(\dot{V}_c) = \sqrt{\sum_{i=1}^{8}\left[(w_i^2)\right]}\ = \pm 13.1\ ft^3/min$$

$$w(\rho C_p 60\Delta T) = (0.072\ lbm/ft^3)(0.24\ Btu/lbm°F)(60)(9.3\ °F)$$

$$\sqrt{\left(\frac{\pm 9.7e\text{-}5\ lbm/ft^3}{0.072\ lbm/ft^3}\right)^2 + \left(\frac{\pm 1.64e\text{-}5\ Btu/lbm°F}{0.24\ Btu/lbm°F}\right)^2 + \left(\frac{\pm 1.03\ °F}{9.3\ °F}\right)^2}$$

$$w(\rho C_p 60\Delta T) = \pm 1.07\ Btu*min/ft^3hr$$

$$w((3.413\,(\dot{P}\,system - \dot{P}\,efan)) = 3.413\sqrt{(\pm 8.1\ W)^2 + (\pm 0.5\ W)^2}\ = \pm 27.7\ Btu/hr$$

$$w(\dot{m}\,(h10 - h3)) = (7.5\ lbm/hr)(81\ Btu/lbm)\sqrt{\left(\frac{\pm 0.218\ lbm/hr}{7.5\ lbm/hr}\right)^2 + \left(\frac{\pm 0.24\ Btu/lbm}{81\ Btu/lbm}\right)^2}$$

$$w(\dot{m}\,(h10 - h3)) = \pm\ 17.8\ Btu/hr$$

$$w((3.413\,(\dot{P}\,system - \dot{P}\,efan) + \dot{m}\,(h10 - h3))$$

$$= \sqrt{(\pm 27.7\ W)^2 + (\pm 17.8\ W)^2}\ = \pm 32.9\ Btu/hr$$

Condenser Heat Transfer & Conductance Uncertainties

R134a case

nominal values: $\dot{Q}\,c = 705.2\ Btu/hr$, $\dot{Q}\,desup = 108.4\ Btu/hr$, $\dot{Q}\,2ph = 565.2\ Btu/hr$,

$\dot{Q}\,sub = 31.5\ Btu/hr$, h1 = 127.1 Btu/lbm, h1sat = 113 Btu/lbm

h2 = 39.5 Btu/lbm, h3 = 35.4 Btu/lbm, T1 = 143.9 °F

cmin = 1.925 Btu/hr°F, cminsub = 2.623 Btu/hr°F, T2 = 87.7 °F

cacond = 122.47 Btu/hr°F, Tconairin = 68.9°F, $\dot{m}$ = 7.69 lbm/hr

$U_{desup} = 4.79257, U_{2ph} = 29.6175, U_{sub} = 11.1398$ Btu/ft^{2}hr°F

adesup = 0.658 ft^2, a2ph = 1.185 ft^2, asub = 0.247 ft^2

Tconmid1 = 69.2°F, Tconmid2 = 73.8°F

$\dot{Q}c = \dot{m}(h1 - h3) = \dot{m}\ \Delta h$

$\dot{Q}desup = \dot{m}(h1 - h1sat) = \dot{m}\ \Delta h$

$\dot{Q}2ph = \dot{m}(h1sat - h2) = \dot{m}\ \Delta h$

$\dot{Q}sub = \dot{m}(h2 - h3) = \dot{m}\ \Delta h$

$$w(\dot{Q}c) = (7.69\text{ lbm/hr})(91.7\text{ Btu/lbm})\sqrt{\left(\frac{\pm 0.223\text{ lbm/hr}}{7.69\text{ lbm/hr}}\right)^2 + \left(\frac{\pm 0.33\text{ Btu/lbm}}{91.7\text{ Btu/lbm}}\right)^2}$$

$= \pm 20.6$ Btu/hr

$$w(\dot{Q}desup) = (7.69\text{ lbm/hr})(14.1\text{ Btu/lbm})\sqrt{\left(\frac{\pm 0.223\text{ lbm/hr}}{7.69\text{ lbm/hr}}\right)^2 + \left(\frac{\pm 0.27\text{ Btu/lbm}}{14.1\text{ Btu/lbm}}\right)^2}$$

$= \pm 3.8$ Btu/hr

$$w(\dot{Q}2ph) = (7.69\text{ lbm/hr})(73.5\text{ Btu/lbm})\sqrt{\left(\frac{\pm 0.223\text{ lbm/hr}}{7.69\text{ lbm/hr}}\right)^2 + \left(\frac{\pm 0.38\text{ Btu/lbm}}{73.5\text{ Btu/lbm}}\right)^2}$$

$= \pm 16.6$ Btu/hr

$$w(\dot{Q}sub) = (7.69\text{ lbm/hr})(4.1\text{ Btu/lbm})\sqrt{\left(\frac{\pm 0.223\text{ lbm/hr}}{7.69\text{ lbm/hr}}\right)^2 + \left(\frac{\pm 0.33\text{ Btu/lbm}}{4.1\text{ Btu/lbm}}\right)^2}$$

$= \pm 2.7$ Btu/hr

$$w(Tconmid1) = w\left(\frac{\dot{Q}sub}{cacond} + Tconairin\right)$$

$$w\left(\frac{\dot{Q}sub}{cacond}\right) = \frac{31.5\text{ Btu/hr}}{122.47\text{ Btu/hr°F}}\sqrt{\left(\frac{\pm 2.7\text{ Btu/hr}}{31.5\text{ Btu/hr}}\right)^2 + \left(\frac{\pm 13.6\text{ Btu/hr°F}}{122.47\text{ Btu/hr°F}}\right)^2} = \pm 0.036\text{ °F}$$

w(Tconairin) = ±0.73°F

w(Tconmid1) = ±0.73°F

$$w(Tconmid2) = w\left(\frac{\dot{Q}2ph}{cacond} + Tconmid1\right)$$

$$w\left(\frac{\dot{Q}2ph}{cacond}\right) = \frac{565.2\text{ Btu/hr}}{122.47\text{ Btu/hr°F}}\sqrt{\left(\frac{\pm 16.6\text{ Btu/hr}}{565.2\text{ Btu/hr}}\right)^2 + \left(\frac{\pm 13.6\text{ Btu/hr°F}}{122.47\text{ Btu/hr°F}}\right)^2} = \pm 0.53\text{ °F}$$

w(Tconmid2) = ±0.90°F

Desuperheating section

$$\dot{m}\,(h1\text{-}h1sat) = \dot{m}\,\Delta h =$$

$$\left(\frac{1 - e^{\left(\frac{-U_{desup}\ adesup}{cmin}\right)(1\text{-}cmin/cacond)}}{1 - (cmin/cacond)\ e^{\left(\frac{-U_{desup}\ adesup}{cmin}\right)(1\text{-}cmin/cacond)}} \right) cmin\ (T1 - Tconmid2)$$

$$w(U_{desup}(\dot{m})) = \frac{\delta U_{desup}}{\delta \dot{m}} \quad w(\dot{m}) = (1.61)(\pm 2.9\%)(7.69\ lbm/hr) = \pm 0.36\ Btu/hr°F*ft^2$$

$$w(U_{desup}(\Delta h)) = \frac{\delta U_{desup}}{\delta \Delta h} \quad w(\Delta h) = (0.876)(\pm 0.269\ Btu/lbm) = \pm 0.24\ Btu/hr°F*ft^2$$

$$w(U_{desup}(cmin)) = \frac{\delta U_{desup}}{\delta cmin} \quad w(cmin) \sim (-3.653)(\pm 2.9\%)(7.69\ lbm/hr)(0.25\ Bti/lbm°F)$$

$$= \pm 0.20\ Btu/hr°F*ft^2$$

$$w(U_{desup}(cacond)) = \frac{\delta U_{desup}}{\delta cacond} \quad w(cacond)$$

$$\sim (-3.12e\text{-}4)(0.072\ lbm/ft^3)(0.24\ Btu/lbm°F)(60)(\pm 13.1\ ft^3 min) = \pm 4.24e\text{-}3\ Btu/hr°F*ft^2$$

$$w(U_{desup}(T1)) = \frac{\delta U_{desup}}{\delta T1} \quad w(T1) = (-1.63e\text{-}1)(\pm 0.73°F) = \pm 0.12\ Btu/hr°F*ft^2$$

$$w(U_{desup}(Tconmid2)) = \frac{\delta U_{desup}}{\delta Tconmid2} \quad w(Tconmid2) = (1.78e\text{-}1)(\pm 0.9°F)$$

$$= \pm 0.16\ Btu/hr°F*ft^2$$

$$w(U_{desup}) = \sqrt{\sum_{i=1}^{6}\left[(w_i^2)\right]} \quad = \pm 0.52\ Btu/hr°F*ft^2$$

Two-phase section

$$\dot{m}\,(h1sat\text{-}h2) = \dot{m}\,\Delta h = \left(1 - e^{(-U_{2ph}\ a2ph/cacond)}\right) cacond\ (T2 - Tconmid1)$$

$$w(U_{2ph}(\dot{m})) = \frac{\delta U_{2ph}}{\delta \dot{m}} \quad w(\dot{m}) = (4.467)(\pm 2.9\%)(7.69\ lbm/hr) = \pm 1.0\ Btu/hr°F*ft^2$$

$$w(U_{2ph}(\Delta h)) = \frac{\delta U_{2ph}}{\delta \Delta h} \quad w(\Delta h) = (0.467)(\pm 0.38\ Btu/lbm) = \pm 0.18\ Btu/hr°F*ft^2$$

$$w(U_{2ph}(cacond)) = \frac{\delta U_{2ph}}{\delta cacond} \quad w(cacond)$$

$\tilde{}$ (-0.038)(0.072 lbm/ft^3)(0.24 Btu/lbm°F)(60)(±13.1 ft^{3}min) = ±0.52 Btu/hr°F*ft^2

$$w(U_{2ph}(T2)) = \frac{\delta U_{2ph}}{\delta T2}\ w(T2) = (-1.737)(\pm 0.73°F) = \pm 1.27 \text{ Btu/hr°F*ft}^2$$

$$w(U_{2ph}(Tconmid1)) = \frac{\delta U_{2ph}}{\delta Tconmid1}\ w(Tconmid1) = (1.935)(\pm 0.73°F)$$

$$= \pm 1.4 \text{ Btu/hr°F*ft}^2$$

$$w(U_{2ph}) = \sqrt{\sum_{i=1}^{5}\left[(w_i^2)\right]} = \pm 2.2 \text{ Btu/hr°F*ft}^2$$

Subcooled section

$$\dot{m}\,(h2-h3) = \dot{m}\ \Delta h =$$

$$\left(\frac{1 - e^{\left(\frac{-U_{sub}\ asub}{cminsub}\right)(1-cminsub/cacond)}}{1 - (cminsub/cacond)\ e^{\left(\frac{-U_{sub}\ asub}{cminsub}\right)(1-cminsub/cacond)}}\right) cminsub\ (T2 - Tconairin)$$

$$w(U_{sub}(\dot{m})) = \frac{\delta U_{sub}}{\delta \dot{m}}\ w(\dot{m}) = (2.584)(\pm 2.9\%)(7.69 \text{ lbm/hr}) = \pm 0.58 \text{ Btu/hr°F*ft}^2$$

$$w(U_{sub}(\Delta h)) = \frac{\delta U_{sub}}{\delta \Delta h}\ w(\Delta h) = (4.847)(\pm 0.33 \text{ Btu/lbm}) = \pm 1.6 \text{ Btu/hr°F*ft}^2$$

$$w(U_{sub}(cmin)) = \frac{\delta U_{sub}}{\delta cmin}\ w(cmin) \tilde{} (-3.158)(\pm 2.9\%)(7.69 \text{ lbm/hr})(0.341 \text{ Bti/lbm°F})$$

$$= \pm 0.24 \text{ Btu/hr°F*ft}^2$$

$$w(U_{sub}(cacond)) = \frac{\delta U_{sub}}{\delta cacond}\ w(cacond)$$

$\tilde{}$ (-7.38e-4)(0.072 lbm/ft^3)(0.24 Btu/lbm°F)(60)(±13.1 ft^{3}min) = ±0.01 Btu/hr°F*ft^2

$$w(U_{sub}(T2)) = \frac{\delta U_{sub}}{\delta T2}\ w(T2) = (-9.71e-1)(\pm 0.73°F) = \pm 0.71 \text{ Btu/hr°F*ft}^2$$

$$w(U_{sub}(Tconairin)) = \frac{\delta U_{sub}}{\delta Tconairin}\ w(Tconairin) = (1.14)(\pm 0.73°F)$$

$$= \pm 0.83 \text{ Btu/hr°F*ft}^2$$

$$w(U_{sub}) = \sqrt{\sum_{i=1}^{6}\left[(w_i^2)\right]} = \pm 2.0 \text{ Btu/hr°F*ft}^2$$

R12 case

nominal values: $\dot{Q}_c$ = 1103 Btu/hr, $\dot{Q}_{2ph}$ = 900 Btu/hr, $\dot{Q}_{desup}$ = 202.9 Btu/hr

$\dot{P}_{system}$ = 222.3 W, $\dot{P}_{efan}$ = 12.3 W, $\dot{m}$ = 15.41 lbm/hr, h1 = 101.7 Btu/lmb

h2 = 88.54 Btu/lbm, h10 = 91.93 Btu/lbm, T1 = 189.6 °F, T2 = 119.1°F

Tconairin = 89.1°F, Tconmid = 96.7 °F, Tconairout = 98.4°F

Tconfanout = 103.2°F, cmin = 2.86 Btu/hr°F, cacond = 118.1 Btu/hr°F

ρ = 0.071 lbm/ft^3, Cp = 0.24 Btu/lbm°F, $\dot{V}_c$ = 115.8 ft^3/min, a2ph = 0.916 ft^2

adesup = 1.174 ft^2, U_{desup} = 3.67 Btu/hr°F*ft^2, U_{2ph} = 38.28 Btu/hr°F*ft^2

$$\dot{Q}_c = \rho C_p 60 \dot{V}_c \Delta T - 3.413(\dot{P}_{system} - \dot{P}_{efan}) + \dot{m}(h1 - h10)$$

$$w(\dot{Q}_c(\dot{V}_c)) = \frac{\delta \dot{Q}_c}{\delta \dot{V}_c} \; w(\dot{V}_c) = (14.416)(\pm 13.1 \text{ ft}^3/\text{min}) = \pm 188.8 \text{ Btu/hr}$$

$$w(\dot{Q}_c(\Delta T)) = \frac{\delta \dot{Q}_c}{\delta \Delta T} \; w(\Delta T) = (118.394)(\pm 1.03°\text{F}) = \pm 121.9 \text{ Btu/hr}$$

$$w(\dot{Q}_c(\dot{P}_{system})) = \frac{\delta \dot{Q}_c}{\delta \dot{P}_{system}} \; w(\dot{P}_{system}) = (-3.413)(\pm 8.1\text{W}) = \pm 27.6 \text{ Btu/hr}$$

$$w(\dot{Q}_c(\dot{P}_{efan})) = \frac{\delta \dot{Q}_c}{\delta \dot{P}_{efan}} \; w(\dot{P}_{efan}) = (3.413)(\pm 0.5 \text{ W}) = \pm 1.7 \text{ Btu/hr}$$

$$w(\dot{Q}_c(\dot{m})) = \frac{\delta \dot{Q}_c}{\delta \dot{m}} \; w(\dot{m}) = (9.78)(\pm 5.0\%)(15.41 \text{ lbm/hr}) = \pm 7.5 \text{ Btu/hr}$$

$$w(\dot{Q}_c(\Delta h)) = \frac{\delta \dot{Q}_c}{\delta \Delta h} \; w(\Delta h) = (15.257)(\pm 0.17 \text{ Btu/lbm}) = \pm 2.6 \text{ Btu/hr}$$

$$w(\dot{Q}_c) = \sqrt{\sum_{i=1}^{6}\left[(w_i^2)\right]} = \pm 226.5 \text{ Btu/hr}$$

$$\dot{Q}_{desup} = \dot{m}(h1 - h2) = \dot{m}\,\Delta h$$

$$w(\dot{Q}_{desup}) = (15.41 \text{ lbm/hr})(13.17 \text{ Btu/lbm})\sqrt{\left(\frac{\pm 0.771 \text{ lbm/hr}}{15.41 \text{ lbm/hr}}\right)^2 + \left(\frac{\pm 0.18 \text{ Btu/lbm}}{13.17 \text{ Btu/lbm}}\right)^2}$$

$$= \pm 10.5 \text{ Btu/hr}$$

$$w(Tconairout) = w(\frac{\dot{Q}c}{cacond} + Tconairin)$$

$$w(cacond) \tilde{} (0.071\ lbm/ft^3)(0.24\ Btu/lbm°F)(60)(\pm 13.1\ ft^3/min) = \pm 13.4\ Btu/hr°F$$

$$w(\frac{\dot{Q}c}{cacond}) = \frac{1103\ Btu/hr}{118.1\ Btu/hr°F} \sqrt{\left(\frac{\pm 226.5\ Btu/hr}{1103\ Btu/hr}\right)^2 + \left(\frac{\pm 13.4\ Btu/hr°F}{118.1\ Btu/hr°F}\right)^2} = \pm 2.2\ °F$$

$$w(Tconairout) = \pm 2.3°F$$

$$w(Tconmid) = w(Tconairout - \frac{\dot{Q}desup}{cacond})$$

$$w(\frac{\dot{Q}desup}{cacond}) = \frac{202.9\ Btu/hr}{118.1\ Btu/hr°F} \sqrt{\left(\frac{\pm 10.5\ Btu/hr}{202.9\ Btu/hr}\right)^2 + \left(\frac{\pm 13.4\ Btu/hr°F}{118.1\ Btu/hr°F}\right)^2} = \pm 0.21\ °F$$

$$w(Tconmid) = \pm 2.3°F$$

$$w(\dot{Q}\ 2ph) = w(cacond*(Tconmid - Tconairin))$$

$$w(cacond\ \Delta T) = (118.1\ Btu/hr°F)(7.6°F) \sqrt{\left(\frac{\pm 2.41°F}{7.6°F}\right)^2 + \left(\frac{\pm 13.4\ Btu/hr°F}{118.1\ Btu/hr°F}\right)^2}$$

$$w(\dot{Q}\ 2ph) = \pm 302.2\ Btu/hr$$

Desuperheating Section

$$\dot{m}\,(h1\text{-}h2) = \dot{m}\ \Delta h =$$

$$\left(\frac{1 - e^{\left(\frac{-U_{desup}\ adesup}{cmin}\right)(1\text{-}cmin/cacond)}}{1 - (cmin/cacond)\, e^{\left(\frac{-U_{desup}\ adesup}{cmin}\right)(1\text{-}cmin/cacond)}} \right) cmin\ (T1 - Tconmid)$$

$$w(U_{desup}(\dot{m})) = \frac{\delta U_{desup}}{\delta \dot{m}}\ \ w(\dot{m}) = (0.563)(\pm 5.0\%)(15.41\ lbm/hr) = \pm 0.43\ Btu/hr°F*ft^2$$

$$w(U_{desup}(\Delta h)) = \frac{\delta U_{desup}}{\delta \Delta h}\ \ w(\Delta h) = (0.659)(\pm 0.18\ Btu/lbm) = \pm 0.12\ Btu/hr°F*ft^2$$

$$w(U_{desup}(cmin)) = \frac{\delta U_{desup}}{\delta cmin}\ \ w(cmin) \tilde{} (-1.632)(\pm 5.0\%)(15.41\ lbm/hr)(0.186\ Bti/lbm°F)$$

$$= \pm 0.23\ Btu/hr°F*ft^2$$

$$w(U_{desup}(cacond)) = \frac{\delta U_{desup}}{\delta cacond}\ \ w(cacond)$$

$$= (-3.64e\text{-}4)(\pm 13.4\ Btu/hr°F) = \pm 4.88e\text{-}3\ Btu/hr°F*ft^2$$

$$w(U_{desup}(T1)) = \frac{\delta U_{desup}}{\delta T1} \quad w(T1) = (-8.81e\text{-}2)(\pm 0.73°F) = \pm 0.064 \text{ Btu/hr°F*ft}^2$$

$$w(U_{desup}(Tconmid)) = \frac{\delta U_{desup}}{\delta Tconmid2} \quad w(Tconmid2) = (9.49e\text{-}2)(\pm 2.3°F)$$

$$= \pm 0.22 \text{ Btu/hr°F*ft}^2$$

$$w(U_{desup}) = \sqrt{\sum_{i=1}^{6}\left[(w_i^2)\right]} \quad = \pm 0.55 \text{ Btu/hr°F*ft}^2$$

Two-phase section

$$\dot{Q}_{2ph} = \left(1 - e^{(-U_{2ph}\, a2ph/cacond)}\right) cacond\ (T2 - Tconairin)$$

$$w(U_{2ph}(\dot{Q}_{2ph})) = \frac{\delta U_{2ph}}{\delta \dot{Q}_{2ph}} \quad w(\dot{Q}_{2ph}) = (4.91e\text{-}2)(\pm 302.2 \text{ Btu/hr}) = \pm 14.8 \text{ Btu/hr°F*ft}^2$$

$$w(U_{2ph}(cacond)) = \frac{\delta U_{2ph}}{\delta cacond} \quad w(cacond)$$

$$= (-5.26e\text{-}2)(\pm 13.4 \text{ Btu/hr°F}) = \pm 0.70 \text{ Btu/hr°F*ft}^2$$

$$w(U_{2ph}(T2)) = \frac{\delta U_{2ph}}{\delta T2} \quad w(T2) = (-1.42)(\pm 0.73°F) = \pm 1.04 \text{ Btu/hr°F*ft}^2$$

$$w(U_{2ph}(Tconairin)) = \frac{\delta U_{2ph}}{\delta Tconairin} \quad w(Tconairin) = (1.54)(\pm 0.73°F)$$

$$= \pm 1.12 \text{ Btu/hr°F*ft}^2$$

$$w(U_{2ph}) = \sqrt{\sum_{i=1}^{4}\left[(w_i^2)\right]} \quad = \pm 14.9 \text{ Btu/hr°F*ft}^2$$

Compressor Shell Heat Transfer Uncertainties

R12 nominal values: $\dot{Q}_{comp}$ = 459 Btu/hr, $\dot{P}_{comp}$ = 185.7 W, $\dot{m}$ = 18.4 lbm/hr

h1 = 98.3 Btu/lbm, h10 = 88.8 Btu/lbm, $\dot{P}_{evapfan}$ = 12.9 W

$\dot{P}_{system}$ = 213.2 W, $\dot{P}_{confan}$ = 14.6 W, Tcompair = 84.1°F

Tconfanout = 84.4°F, ρ = 0.072 lbm/ft^3, Cp = 0.24 Btu/lbm°F

T1 = 164.7°F

$$\dot{Q}_{comp} = (3.413\ \dot{P}_{comp}) - \dot{m}\,(h1 - h10)$$

$w(3.413\,\dot{P}\,comp) = \pm 11.6$ Btu/hr

$$w(\dot{m}\,\Delta h) = (18.4\text{ lbm/hr})(9.5\text{ Btu/lbm})\sqrt{\left(\frac{\pm 0.92\text{ lbm/hr}}{18.4\text{ lbm/hr}}\right)^2 + \left(\frac{\pm 0.17\text{ Btu/lbm}}{9.5\text{ Btu/lbm}}\right)^2}$$

$= \pm 9.3$ Btu/hr

$$w(\dot{Q}\,comp) = \sqrt{(11.6\text{ Btu/hr})^2 + (9.3\text{ Btu/hr})^2} \quad \pm 14.9\text{ Btu/hr}$$

$\dot{P}\,confan = \dot{P}\,system - \dot{P}\,comp - \dot{P}\,evapfan$

$$w(\dot{P}\,confan) = \sqrt{(8.1\text{W})^2 + (3.4\text{ W})^2 + (0.5\text{ W})^2} \quad = \pm 8.8\text{ W}$$

$$Tcompair = Tconfanout - \frac{3.413\,\dot{P}confan}{60\rho C_p \dot{V}}$$

$$w\left(\frac{3.413\,\dot{P}confan}{60\rho C_p \dot{V}}\right) = \frac{49.8\text{ Btu/hr}}{120.1\text{ Btu/hr°F}}\sqrt{\left(\frac{\pm 30.0\text{ Btu/hr}}{49.8\text{ Btu/hr}}\right)^2 + \left(\frac{\pm 13.6\text{ Btu/hr°F}}{120.1\text{ Btu/hr°F}}\right)^2}$$

$= \pm 0.25$ °F

$$w(Tcompair) = \sqrt{(0.73°\text{F})^2 + (0.25°\text{F})^2} \quad = \pm 0.77°\text{F}$$

$$w(T1 - Tcompair) = \sqrt{(0.73°\text{F})^2 + (0.77°\text{F})^2} \quad = \pm 1.06°\text{F}$$

$$\bar{h} = \frac{\dot{Q}comp}{\Delta T}$$

$$w\left(\frac{\dot{Q}comp}{\Delta T}\right) = \frac{459\text{ Btu/hr}}{80.6\text{ °F}}\sqrt{\left(\frac{\pm 14.9\text{ Btu/hr}}{459\text{ Btu/hr}}\right)^2 + \left(\frac{\pm 1.06\text{ °F}}{80.6\text{ °F}}\right)^2}$$

$w(\bar{h}) = \pm 0.2$ Btu/hr°F

R134a nominal values: $\dot{Q}comp = 376$ Btu/hr, $\dot{P}\,comp = 139$ W, $\dot{m} = 8.15$ lbm/hr

$h1 = 127.4$ Btu/lbm, $h10 = 115.3$ Btu/lbm, $\dot{P}\,evapfan = 12.9$ W

$\dot{P}\,system = 164.5$ W, $\dot{P}\,confan = 12.6$ W, $Tcompair = 77.8$°F

$Tconfanout = 78.1$°F, $\rho = 0.072$ lbm/ft^3, $Cp = 0.24$ Btu/lbm°F

$T1 = 144.8$°F

$$\dot{Q}\,comp = (3.413\,\dot{P}\,comp) - \dot{m}\,(h1 - h10)$$

$w(3.413\,\dot{P}\,\text{comp}) = \pm 11.6$ Btu/hr

$$w(\dot{m}\,\Delta h) = (8.15\text{ lbm/hr})(12.1\text{ Btu/lbm})\sqrt{\left(\frac{\pm 0.24\text{ lbm/hr}}{8.15\text{ lbm/hr}}\right)^2 + \left(\frac{\pm 0.24\text{ Btu/lbm}}{12.1\text{ Btu/lbm}}\right)^2}$$

$$= \pm 3.5\text{ Btu/hr}$$

$$w(\dot{Q}\,\text{comp}) = \sqrt{(11.6\text{ Btu/hr})^2 + (3.5\text{ Btu/hr})^2} \quad \pm 12.1\text{ Btu/hr}$$

$$\dot{P}\,\text{confan} = \dot{P}\,\text{system} - \dot{P}\,\text{comp} - \dot{P}\,\text{evapfan}$$

$$w(\dot{P}\,\text{confan}) = \sqrt{(8.1\text{W})^2 + (3.4\text{ W})^2 + (0.5\text{ W})^2} \quad = \pm 8.8\text{ W}$$

$$\text{Tcompair} = \text{Tconfanout} - \frac{3.413\,\dot{P}\text{confan}}{60\rho C_p \dot{V}}$$

$$w\left(\frac{3.413\,\dot{P}\text{confan}}{60\rho C_p \dot{V}}\right) = \frac{43\text{ Btu/hr}}{120.1\text{ Btu/hr°F}}\sqrt{\left(\frac{\pm 30.0\text{ Btu/hr}}{43\text{ Btu/hr}}\right)^2 + \left(\frac{\pm 13.6\text{ Btu/hr°F}}{120.1\text{ Btu/hr°F}}\right)^2}$$

$$= \pm 0.25\text{ °F}$$

$$w(\text{Tcompair}) = \sqrt{(0.73\text{°F})^2 + (0.25\text{°F})^2} \quad = \pm 0.77\text{°F}$$

$$w(\text{T1 - Tcompair}) = \sqrt{(0.73\text{°F})^2 + (0.77\text{°F})^2} \quad = \pm 1.06\text{°F}$$

$$\bar{h} = \frac{\dot{Q}\text{comp}}{\Delta T}$$

$$w\left(\frac{\dot{Q}\text{comp}}{\Delta T}\right) = \frac{376\text{ Btu/hr}}{67\text{ °F}}\sqrt{\left(\frac{\pm 12.1\text{ Btu/hr}}{376\text{ Btu/hr}}\right)^2 + \left(\frac{\pm 1.06\text{ °F}}{67\text{ °F}}\right)^2}$$

$w(\bar{h}) = \pm 0.2$ Btu/hr°F

$$\dot{Q}\,\text{comp} = \bar{h}\,\Delta T$$

R12

$$w(\dot{Q}\,\text{comp}) = (5.92\text{ Btu/hr°F})(80.6\text{°F})\sqrt{\left(\frac{\pm 0.2\text{ Btu/hr°F}}{5.92\text{ Btu/hr°F}}\right)^2 + \left(\frac{\pm 1.06\text{ °F}}{80.6\text{ °F}}\right)^2}$$

$w(\dot{Q}\,\text{comp}) = \pm 17.3$ Btu/hr

R134a

$$w(\dot{Q}\,\text{comp}) = (5.83\text{ Btu/hr°F})(67\text{°F})\sqrt{\left(\frac{\pm 0.2\text{ Btu/hr°F}}{5.83\text{ Btu/hr°F}}\right)^2 + \left(\frac{\pm 1.06\text{ °F}}{67\text{ °F}}\right)^2}$$

$w(\dot{Q}\,comp) = \pm 14.8$ Btu/hr

Interchanger Uncertainties

$$\varepsilon_{int} = \frac{\dot{m}\,(h10 - h9)}{cmin(T4 - T9)}$$

R12 case: nominal values - $\dot{m}$ = 16.0 lbm/hr, h10 = 88.94 Btu/lbm, h9 = 81.24 Btu/lbm

cmin = 2.33 Btu/hr°F, T4 = 91.6°F, T9 = 25.3 °F, ε = 0.80

cmax = 3.71 Btu/hr°F, UA_{int} = 6.14 Btu/hr°F

$$w(\dot{m}\,\Delta h) = (16.0\text{ lbm/hr})(7.7\text{ Btu/lbm})\sqrt{\left(\frac{\pm 0.8\text{ lbm/hr}}{16\text{ lbm/hr}}\right)^2 + \left(\frac{\pm 0.16\text{ Btu/lbm}}{7.7\text{ Btu/lbm}}\right)^2}$$

$w(\dot{m}\,\Delta h) = \pm 6.67$ Btu/hr

$w(cmin) = w(\dot{m})C_p = (16.0\text{ lbm/ hr})(\pm 5.0\%)(0.146\text{ Btu/lbm°F}) = \pm 0.117$ Btu/hr°F

$$w(cmin\Delta T) = (2.33\text{ Btu/hr°F})(66.3\text{°F})\sqrt{\left(\frac{\pm 0.117\text{ Btu/hr°F}}{2.33\text{ Btu/hr°F}}\right)^2 + \left(\frac{\pm 1.03\text{°F}}{66.3\text{°F}}\right)^2}$$

$w(cmin\Delta T) = \pm 8.1$ Btu/hr

$$w(\varepsilon_{int}) = \frac{123.2\text{ Btu/hr}}{154.5\text{ Btu/hr}}\sqrt{\left(\frac{\pm 6.67\text{ Btu/hr}}{123.2\text{ Btu/hr}}\right)^2 + \left(\frac{\pm 8.1\text{ Btu/hr}}{154.4\text{ Btu/hr}}\right)^2}$$

$w(\varepsilon_{int}) = \pm 0.06$

$\dot{Q}\,rate = \varepsilon_{int} cmin(T4 - T9)$

$w(\dot{Q}\,rate) = (0.80)(2.33\text{ Btu/lbm°F})(66.3\text{°F})$

$$\sqrt{\left(\frac{\pm 0.06}{0.80}\right)^2 + \left(\frac{\pm 0.117\text{ Btu/lbm°F}}{2.33\text{ Btu/hr°F}}\right)^2 + \left(\frac{\pm 1.03\text{°F}}{66.3\text{ °F}}\right)^2}$$

$w(\dot{Q}\,rate) = \pm 11.3$ Btu/hr

$\dot{m}\,(h10\text{-}h9) = \dot{m}\,\Delta h =$

$$\left(\frac{1 - e^{\left(\frac{-UA_{int}}{cmin}\right)(1\text{-}cmin/cmax)}}{1 - (cmin/cmax)\,e^{\left(\frac{-UA_{int}}{cmin}\right)(1\text{-}cmin/cmax)}}\right) cmin\,(T4 - T9)$$

$$w(UA_{int}(\dot{m})) = \frac{\delta UA_{int}}{\delta \dot{m}} \quad w(\dot{m}) = (1.378)(\pm 5.0\%)(16.0 \text{ lbm/hr}) = \pm 1.1 \text{ Btu/hr°F}$$

$$w(UA_{int}(\Delta h)) = \frac{\delta UA_{int}}{\delta \Delta h} \quad w(\Delta h) = (2.863)(\pm 0.16 \text{ Btu/lbm}) = \pm 0.46 \text{ Btu/hr°F}$$

$$w(UA_{int}(cmin)) = \frac{\delta UA_{int}}{\delta cmin} \quad w(cmin) \sim (-4.771)(\pm 5.0\%)(16.0 \text{ lbm/hr})(0.145 \text{ Bti/lbm°F})$$

$$= \pm 0.55 \text{ Btu/hr°F}$$

$$w(UA_{int}(cmax)) = \frac{\delta UA_{int}}{\delta cmax} \quad w(cmax) \sim (-0.996)(\pm 5.0\%)(16.0 \text{ lbm/hr})(0.232 \text{ Bti/lbm°F})$$

$$= = \pm 0.185 \text{ Btu/hr°F}$$

$$w(UA_{int}(T4)) = \frac{\delta UA_{int}}{\delta T4} \quad w(T4) = (-0.315)(\pm 0.73°F) = \pm 0.230 \text{ Btu/hr°F}$$

$$w(UA_{int}(T9)) = \frac{\delta UA_{int}}{\delta T9} \quad w(T9) = (0.337)(\pm 0.73°F) = \pm 0.246 \text{ Btu/hr°F}$$

$$w(UA_{int}) = \sqrt{\sum_{i=1}^{6} \left[(w_i^2) \right]} \quad = \pm 1.4 \text{ Btu/hr°F}$$

$$\dot{Q}\,\text{rate} = \left(\frac{1 - e^{\left(\frac{-UA_{int}}{cmin} \right)(1-cmin/cmax)}}{1 - (cmin/cmax)\, e^{\left(\frac{-UA_{int}}{cmin} \right)(1-cmin/cmax)}} \right) cmin\,(T4 - T9)$$

$$w(\dot{Q}\,\text{rate}(UA_{int})) = \frac{\delta \dot{Q}\text{rate}}{\delta UA_{int}} \quad w(UA_{int}) = (5.703)(\pm 1.4 \text{ Btu/hr°F}) = \pm 8.0 \text{ Btu/hr}$$

$$w(\dot{Q}\,\text{rate}(cmin)) = \frac{\delta \dot{Q}\text{rate}}{\delta cmin} \quad w(cmin) \sim (28.23)(\pm 5.0\%)(16.0 \text{ lbm/hr})(0.145 \text{ Bti/lbm°F})$$

$$= \pm 3.3 \text{ Btu/hr}$$

$$w(\dot{Q}\,\text{rate}(cmax)) = \frac{\delta \dot{Q}\text{rate}}{\delta cmax} \quad w(cmax) \sim (5.756)(\pm 5.0\%)(16.0 \text{ lbm/hr})(0.232 \text{ Bti/lbm°F})$$

$$= = \pm 1.07 \text{ Btu/hr}$$

$$w(\dot{Q}\,\text{rate}(T4)) = \frac{\delta \dot{Q}\text{rate}}{\delta T4} \quad w(T4) = (1.9045)(\pm 0.73°F) = \pm 1.39 \text{ Btu/hr}$$

$$w(\dot{Q}\,\text{rate}(T9)) = \frac{\delta \dot{Q}\text{rate}}{\delta T9} \quad w(T9) = (-1.9045)(\pm 0.73°F) = \pm 1.39 \text{ Btu/hr}$$

$$w(\dot{Q}\ \text{rate}) = \sqrt{\sum_{i=1}^{5}\left[(w_i^2)\right]} = \pm 8.94\ \text{Btu/hr}$$

$$\varepsilon_{int} = \frac{\dot{m}\,(h10 - h9)}{cmin(T4 - T9)}$$

R134a case: nominal values - $\dot{m}$ = 7.88 lbm/hr, h10 = 120.02 Btu/lbm, h9 = 107.31 Btu/lbm

cmin = 1.56 Btu/hr°F, T4 = 97.5°F,T9 = 24.0 °F,ε = 0.88

cmax = 2.677 Btu/hr°F, UA_{int} = 5.59 Btu/hr°F

$$w(\dot{m}\,\Delta h) = (7.88\ \text{lbm/hr})(12.71\ \text{Btu/lbm})\sqrt{\left(\frac{\pm 0.23\ \text{lbm/hr}}{7.88\ \text{lbm/hr}}\right)^2 + \left(\frac{\pm 0.20\ \text{Btu/lbm}}{12.71\ \text{Btu/lbm}}\right)^2}$$

$$w(\dot{m}\,\Delta h) = \pm 3.32\ \text{Btu/hr}$$

$$w(cmin) = w(\dot{m})C_p = (7.88\ \text{lbm/hr})(\pm 2.9\%)(0.198\ \text{Btu/lbm°F}) = \pm 0.045\ \text{Btu/hr°F}$$

$$w(cmin\,\Delta T) = (1.56\ \text{Btu/hr°F})(73.5\text{°F})\sqrt{\left(\frac{\pm 0.045\ \text{Btu/hr°F}}{1.56\ \text{Btu/hr°F}}\right)^2 + \left(\frac{\pm 1.03\text{°F}}{73.5\text{°F}}\right)^2}$$

$$w(cmin\,\Delta T) = \pm 3.7\ \text{Btu/hr}$$

$$w(\varepsilon_{int}) = \frac{100.1\ \text{Btu/hr}}{114.7\ \text{Btu/hr}}\sqrt{\left(\frac{\pm 3.32\ \text{Btu/hr}}{100.1\ \text{Btu/hr}}\right)^2 + \left(\frac{\pm 3.7\ \text{Btu/hr}}{114.7\ \text{Btu/hr}}\right)^2}$$

$$w(\varepsilon_{int}) = \pm 0.04$$

$$\dot{Q}\ \text{rate} = \varepsilon_{int} cmin(T4 - T9)$$

$$w(\dot{Q}\ \text{rate}) = (0.88)(1.56\ \text{Btu/lbm°F})(73.5\text{°F})$$
$$\sqrt{\left(\frac{\pm 0.04}{0.88}\right)^2 + \left(\frac{\pm 0.045\ \text{Btu/lbm°F}}{1.56\ \text{Btu/hr°F}}\right)^2 + \left(\frac{\pm 1.03\text{°F}}{73.5\ \text{°F}}\right)^2}$$

$$w(\dot{Q}\ \text{rate}) = \pm 5.6\ \text{Btu/hr}$$

$$\dot{m}\,(h10\text{-}h9) = \dot{m}\ \Delta h =$$

$$\left(\frac{1 - e^{\left(\frac{-UA_{int}}{cmin}\right)(1\text{-}cmin/cmax)}}{1 - (cmin/cmax)\,e^{\left(\frac{-UA_{int}}{cmin}\right)(1\text{-}cmin/cmax)}}\right) cmin\,(T4 - T9)$$

$$w(UA_{int}(\dot{m})) = \frac{\delta UA_{int}}{\delta \dot{m}}\quad w(\dot{m}) = (3.587)(\pm 2.9\%)(7.88\ \text{lbm/hr}) = \pm 0.82\ \text{Btu/hr°F}$$

$$w(UA_{int}(\Delta h)) = \frac{\delta UA_{int}}{\delta \Delta h} \quad w(\Delta h) = (2.224)(\pm 0.20 \text{ Btu/lbm}) = \pm 0.44 \text{ Btu/hr°F}$$

$$w(UA_{int}(cmin)) = \frac{\delta UA_{int}}{\delta cmin} \quad w(cmin) \tilde{} \ (-10.638)(\pm 2.9\%)(7.88 \text{ lbm/hr})(0.198 \text{ Bti/lbm°F})$$

$$= \pm 0.48 \text{ Btu/hr°F}$$

$$w(UA_{int}(cmax)) = \frac{\delta UA_{int}}{\delta cmax} \quad w(cmax) \tilde{} \ (-1.392)(\pm 2.9\%)(7.88 \text{ lbm/hr})(0.34 \text{ Bti/lbm°F})$$

$$= \ = \pm 0.11 \text{ Btu/hr°F}$$

$$w(UA_{int}(T4)) = \frac{\delta UA_{int}}{\delta T4} \quad w(T4) = (-0.348)(\pm 0.73°F) = \pm 0.25 \text{ Btu/hr°F}$$

$$w(UA_{int}(T9)) = \frac{\delta UA_{int}}{\delta T9} \quad w(T9) = (0.382)(\pm 0.73°F) = \pm 0.28 \text{ Btu/hr°F}$$

$$w(UA_{int}) = \sqrt{\sum_{i=1}^{6}\left[(w_i^2)\right]} \quad = \pm 1.1 \text{ Btu/hr°F}$$

$$\dot{Q}\,\text{rate} = \left(\frac{1 - e^{\left(\frac{-UA_{int}}{cmin}\right)(1-cmin/cmax)}}{1 - (cmin/cmax)\, e^{\left(\frac{-UA_{int}}{cmin}\right)(1-cmin/cmax)}} \right) cmin\ (T4 - T9)$$

$$w(\dot{Q}\,\text{rate}(UA_{int})) = \frac{\delta \dot{Q}\text{rate}}{\delta UA_{int}} \quad w(UA_{int}) = (3.68)(\pm 1.1 \text{ Btu/hr°F}) = \pm 4.05 \text{ Btu/hr}$$

$$w(\dot{Q}\,\text{rate}(cmin)) = \frac{\delta \dot{Q}\text{rate}}{\delta cmin} \quad w(cmin) \tilde{} \ (41.657)(\pm 2.9\%)(7.88 \text{ lbm/hr})(0.198 \text{ Bti/lbm°F})$$

$$= \pm 1.88 \text{ Btu/hr}$$

$$w(\dot{Q}\,\text{rate}(cmax)) = \frac{\delta \dot{Q}\text{rate}}{\delta cmax} \quad w(cmax) \tilde{} \ (5.1429)(\pm 2.9\%)(7.88 \text{ lbm/hr})(0.34 \text{ Bti/lbm°F})$$

$$= \ = \pm 0.40 \text{ Btu/hr}$$

$$w(\dot{Q}\,\text{rate}(T4)) = \frac{\delta \dot{Q}\text{rate}}{\delta T4} \quad w(T4) = (1.392)(\pm 0.73°F) = \pm 1.02 \text{ Btu/hr}$$

$$w(\dot{Q}\,\text{rate}(T9)) = \frac{\delta \dot{Q}\text{rate}}{\delta T9} \quad w(T9) = (-1.392)(\pm 0.73°F) = \pm 1.02 \text{ Btu/hr}$$

$$w(\dot{Q}\,\text{rate}) = \sqrt{\sum_{i=1}^{5}\left[(w_i^2)\right]} \quad = \pm 4.71 \text{ Btu/hr}$$

Evaporator Volumetric Air Flow Rate Uncertainty

$$\rho C_p 60 \dot{V}_e \Delta T = \dot{m}(h10 - h4) = \dot{Q}e$$

$$\dot{m}fz\, h(Tfz) + \dot{m}ff\, h(Tff) = \dot{m}a\, h(Tma)$$

$$3.413 \dot{P}fan = \dot{m}a\, C_p\, (Tfanout - Taevapout)$$

$$\dot{m}a = \dot{m}fz + \dot{m}ff$$

$$\dot{m}a = \rho 60 \dot{V}_e$$

$$a = \frac{\dot{m}fz}{\dot{m}a}$$

R12 nominal values: $\dot{m}$ = 18.12 lbm/hr, h10 = 88.95 Btu/lbm, h4 = 28.83 Btu/lbm

Tfz = 42.3°F, Tff = 59.4°F, $\dot{P}$ fan = 12.0 W, a = 0.871

Tfanout = 29.8°F, Tma = 44.41°F, Taevapout = 29.23°F

$\dot{V}_e$ = 62.6 ft^3/min, ρ = 0.079 lbm/ft^3, C_p = 0.24 Btu/lbm°F

$$w(\dot{V}_e(\dot{m})) = \frac{\delta \dot{V}_e}{\delta \dot{m}} \quad w(\dot{m}) = (3.59)(\pm 5.0\%)(18.12 \text{ lbm/hr}) = \pm 3.25 \text{ ft}^3\text{/min}$$

$$w(\dot{V}_e(\Delta h)) = \frac{\delta \dot{V}_e}{\delta \Delta h} \quad w(\Delta h) = (1.07)(\pm 0.16 \text{ Btu/lbm}) = \pm 0.17 \text{ ft}^3\text{/min}$$

$$w(\dot{V}_e(Tfz)) = \frac{\delta \dot{V}_e}{\delta Tfz} \quad w(Tfz) = (-3.62)(\pm 0.73°F) = \pm 2.64 \text{ ft}^3\text{/min}$$

$$w(\dot{V}_e(Tff)) = \frac{\delta \dot{V}_e}{\delta Tff} \quad w(Tff) = (-5.48e\text{-}1)(\pm 0.73°F) = \pm 0.40 \text{ ft}^3\text{/min}$$

$$w(\dot{V}_e(\dot{P}\text{ fan})) = \frac{\delta \dot{V}_e}{\delta \dot{P}fan} \quad w(\dot{P}\text{ fan}) = (-2.04e\text{-}1)(\pm 0.5W) = \pm 0.10 \text{ ft3/min}$$

$$w(\dot{V}_e(Tfanout)) = \frac{\delta \dot{V}_e}{\delta Tfanout} \quad w(Tfanout) = (4.35)(\pm 0.73°F) = \pm 3.18 \text{ ft3/min}$$

$$w(\dot{V}_e) = \sqrt{\sum_{i=1}^{6}[(w_i 2)]} = \pm 5.3 \text{ ft3/min}$$

$$w(a(\dot{m})) = \frac{\delta a}{\delta \dot{m}} \quad w(\dot{m}) = (-4.93e\text{-}2)(\pm 5.0\%)(18.12 \text{ lbm/hr}) = \pm 0.045$$

$$w(a(\Delta h)) = \frac{\delta a}{\delta \Delta h} \quad w(\Delta h) = (-1.47e\text{-}2)(\pm 0.16 \text{ Btu/lbm}) = \pm 0.0024$$

$$w(a(Tfz)) = \frac{\delta a}{\delta Tfz} \quad w(Tfz) = (5.22e\text{-}2)(\pm 0.73°F) = \pm 0.0038$$

$$w(a(Tff)) = \frac{\delta a}{\delta Tff} \quad w(Tff) = (7.3e\text{-}3)(\pm 0.73°F) = \pm 0.0053$$

$$w(a(\dot{P}\text{ fan})) = \frac{\delta a}{\delta \dot{P}fan} \quad w(\dot{P}\text{ fan}) = (2.8e\text{-}3)(\pm 0.5W) = \pm 0.0014$$

$$w(a(Tfanout)) = \frac{\delta a}{\delta Tfanout} \quad w(Tfanout) = (-5.84e\text{-}2)(\pm 0.73°F) = \pm 0.0426$$

$$w(a) = \sqrt{\sum_{i=1}^{6}\left[(w_i^2)\right]} = \pm 0.062$$

$$w(Tma(\dot{m})) = \frac{\delta Tma}{\delta \dot{m}} \quad w(\dot{m}) = (8.61e\text{-}11)(\pm 5.0\%)(18.12 \text{ lbm/hr}) \tilde{} \ 0.0°F$$

$$w(Tma(\Delta h)) = \frac{\delta Tma}{\delta \Delta h} \quad w(\Delta h) = (2.57e\text{-}11)(\pm 0.16 \text{ Btu/lbm}) \tilde{} \ 0.0°F$$

$$w(Tma(Tfz)) = \frac{\delta Tma}{\delta Tfz} \quad w(Tfz) = (8.71e\text{-}1)(\pm 0.73°F) = \pm 0.636°F$$

$$w(Tma(Tff)) = \frac{\delta Tma}{\delta Tff} \quad w(Tff) = (1.29e\text{-}1)(\pm 0.73°F) = \pm 0.0942°F$$

$$w(Tma(\dot{P}\text{ fan})) = \frac{\delta Tma}{\delta \dot{P}fan} \quad w(\dot{P}\text{ fan}) = (-4.95e\text{-}12)(\pm 0.5W) \tilde{} \ 0.0°F$$

$$w(Tma(Tfanout)) = \frac{\delta Tma}{\delta Tfanout} \quad w(Tfanout) = (1.05e\text{-}10)(\pm 0.73°F) \tilde{} \ 0.0°F$$

$$w(Tma) = \sqrt{\sum_{i=1}^{6}\left[(w_i^2)\right]} = \pm 0.64°F$$

$$w(\dot{Q}e) = (18.12 \text{ lbm/hr})(60.12 \text{ Btu/lbm})\sqrt{\left(\frac{\pm 0.91 \text{ lbm/hr}}{18.12 \text{ lbm/hr}}\right)^2 + \left(\frac{\pm 0.24 \text{ Btu.lbm}}{60.12 \text{ Btu/lbm}}\right)^2}$$

$$w(\dot{Q}e) = \pm 54.9 \text{ Btu/hr}$$

R134a nominal values: $\dot{m}$ = 7.69 lbm/hr, h10 = 115.59 Btu/lbm, h4 = 33.55 Btu/lbm

Tfz = 32.3°F, Tff = 55.0°F, $\dot{P}$ fan = 12.5 W, C_p = 0.24 Btu/lbm°F

ρ = 0.078 lbm/ft^3, Tfanout = 25.9°F, Tma = 34.6°F

Taevapout = 25.28°F, $\dot{V}_e$ = 60.2 ft^3/min, a = 0.899

$$w(\dot{V}_e(\dot{m})) = \frac{\delta \dot{V}_e}{\delta \dot{m}} \quad w(\dot{m}) = (8.40)(\pm 2.9\%)(7.69 \text{ lbm/hr}) = \pm 1.87 \text{ ft}^3\text{/min}$$

$$w(\dot{V}_e(\Delta h)) = \frac{\delta \dot{V}_e}{\delta \Delta h} \quad w(\Delta h) = (7.79\text{e-}1)(\pm 0.20 \text{ Btu/lbm}) = \pm 0.16 \text{ ft}^3\text{/min}$$

$$w(\dot{V}_e(Tfz)) = \frac{\delta \dot{V}_e}{\delta Tfz} \quad w(Tfz) = (-6.02)(\pm 0.73°F) = \pm 4.39 \text{ ft}^3\text{/min}$$

$$w(\dot{V}_e(Tff)) = \frac{\delta \dot{V}_e}{\delta Tff} \quad w(Tff) = (-6.97\text{e-}1)(\pm 0.73°F) = \pm 0.51 \text{ ft}^3\text{/min}$$

$$w(\dot{V}_e(\dot{P}\text{ fan})) = \frac{\delta \dot{V}_e}{\delta \dot{P}fan} \quad w(\dot{P}\text{ fan}) = (-3.49\text{e-}1)(\pm 0.5W) = \pm 0.175 \text{ ft}^3\text{/min}$$

$$w(\dot{V}_e(Tfanout)) = \frac{\delta \dot{V}_e}{\delta Tfanout} \quad w(Tfanout) = (7.14)(\pm 0.73°F) = \pm 5.2 \text{ ft}^3\text{/min}$$

$$w(\dot{V}_e) = \sqrt{\sum_{i=1}^{6}\left[(w_i^2)\right]} \quad = \pm 7.1 \text{ ft}^3\text{/min}$$

$$w(a(\dot{m})) = \frac{\delta a}{\delta \dot{m}} \quad w(\dot{m}) = (-5.34\text{e-}2)(\pm 2.9\%)(7.69 \text{ lbm/hr}) = \pm 0.012$$

$$w(a(\Delta h)) = \frac{\delta a}{\delta \Delta h} \quad w(\Delta h) = (-4.95\text{e-}3)(\pm 0.20 \text{ Btu/lbm}) = \pm 0.001$$

$$w(a(Tfz)) = \frac{\delta a}{\delta Tfz} \quad w(Tfz) = (4.01\text{e-}2)(\pm 0.73°F) = \pm 0.029$$

$$w(a(Tff)) = \frac{\delta a}{\delta Tff} \quad w(Tff) = (4.35\text{e-}3)(\pm 0.73°F) = \pm 0.0032$$

$$w(a(\dot{P}\text{ fan})) = \frac{\delta a}{\delta \dot{P}fan} \quad w(\dot{P}\text{ fan}) = (2.22\text{e-}3)(\pm 0.5W) = \pm 0.0011$$

$$w(a(Tfanout)) = \frac{\delta a}{\delta Tfanout} \quad w(Tfanout) = (-4.40\text{e-}2)(\pm 0.73°F) = \pm 0.032$$

$$w(a) = \sqrt{\sum_{i=1}^{6}\left[(w_i^2)\right]} = \pm 0.045$$

$$w(Tma(\dot{m})) = \frac{\delta Tma}{\delta \dot{m}} \quad w(\dot{m}) = (-9e\text{-}14)(\pm 2.9\%)(7.69\ \text{lbm/hr}) \tilde{} \ 0.0°F$$

$$w(Tma(\Delta h)) = \frac{\delta Tma}{\delta \Delta h} \quad w(\Delta h) = (-8.35e\text{-}15)(\pm 0.20\ \text{Btu/lbm}) \tilde{} \ 0.0°F$$

$$w(Tma(Tfz)) = \frac{\delta Tma}{\delta Tfz} \quad w(Tfz) = (8.99e\text{-}1)(\pm 0.73°F) = \pm 0.656°F$$

$$w(Tma(Tff)) = \frac{\delta Tma}{\delta Tff} \quad w(Tff) = (1.01e\text{-}1)(\pm 0.73°F) = \pm 0.074°F$$

$$w(Tma(\dot{P}\,fan)) = \frac{\delta Tma}{\delta \dot{P}fan} \quad w(\dot{P}\,fan) = (-3.33e\text{-}16)(\pm 0.5W) \tilde{} \ 0.0°F$$

$$w(Tma(Tfanout)) = \frac{\delta Tma}{\delta Tfanout} \quad w(Tfanout) = (-9.31e\text{-}14)(\pm 0.73°F) \tilde{} \ 0.0°F$$

$$w(Tma) = \sqrt{\sum_{i=1}^{6}\left[(w_i^2)\right]} = \pm 0.66°F$$

$$Taevapout = Tfanout - \frac{3.413\dot{P}fan}{\rho C_p 60 \dot{V}_e}$$

$$w\left(\frac{3.413\dot{P}fan}{\rho C_p 60\dot{V}_e}\right) = \frac{3.413(12.5W)}{67.62\,\text{Btu/hr}}\sqrt{\left(\frac{\pm 1.71\,\text{Btu/hr}}{42.66\,\text{Btu/hr}}\right)^2 + \left(\frac{\pm 9.88\,\text{Btu/hr°F}}{67.62\,\text{Btu/hr°F}}\right)^2}$$

$$w\left(\frac{3.413\dot{P}fan}{\rho C_p 60\dot{V}_e}\right) = \pm 0.1°F$$

$$w(Taevapout) = \sqrt{(0.1°F)^2 + (0.77°F)^2} = \pm 0.74°F$$

$$w(Tma - Taevapout) = \sqrt{(0.66°F)^2 + (0.77°F)^2} = \pm 1.01°F$$

$$w(\rho C_p 60\Delta T) = (0.078\ \text{lbm/ft}^3)(0.24\ \text{Btu/lbm°F})(60)(\pm 1.01°F) = \pm 1.13\ \text{Btu*min/ft}^3\text{hr})$$

$$w(\dot{Q}\,e) = (7.69\ \text{lbm/hr})(82.05\ \text{Btu/lbm})\sqrt{\left(\frac{\pm 0.223\ \text{lbm/hr}}{7.69\ \text{lbm/hr}}\right)^2 + \left(\frac{\pm 0.2\ \text{Btu.lbm}}{82.05\ \text{Btu/lbm}}\right)^2}$$

$$w(\dot{Q}\,e) = \pm 18.4\ \text{Btu/hr}$$

Evaporator Conductances and Heat Transfer Uncertainties

R12: nominal values : $\dot{Q}_e$ = 1089 Btu/hr, $\dot{Q}_{sup}$ = 85.0 Btu/hr, $\dot{Q}_{2ph}$ = 1004 Btu/hr

$\dot{m}$ = 18.12 lbm/hr, cmin = 2.62 Btu/hr°F, casup = 68.7 Btu/hr°F

Tma = 44.0 °F, T7 = -0.2°F, a2ph = 1.46 ft^2, asup = 2.34 ft^2

ca2ph = 52.7 Btu/hr°F,h4 = 28.8 Btu/lbm, h8 = 77.25 Btu/lbm

h9 = 81.96 Btu/lbm, h10 = 88.95 Btu/lbm, U_{sup} = 1.579 Btu/hr-ft^2°F

U_{2ph} = 20.51 Btu/hr-ft^2°F

Superheated section

$$\dot{m}\,(h9\text{-}h8) = \dot{m}\,\Delta h = \left(\frac{1 - e^{\left(\frac{-U_{sup}\ asup}{cmin}\right)(1+cmin/casup)}}{1 + (cmin/casup)}\right) cmin\ (Tma - T7)$$

$$w(U_{sup}(\dot{m})) = \frac{\delta U_{sup}}{\delta \dot{m}}\ \ w(\dot{m}) = (1.97e\text{-}1)(\pm 5.0\%)(18.12\ lbm/hr) = \pm 0.18\ Btu/hr°F*ft^2$$

$$w(U_{sup}(\Delta h)) = \frac{\delta U_{sup}}{\delta \Delta h}\ \ w(\Delta h) = (7.51e\text{-}1)(\pm 0.16\ Btu/lbm) = \pm 0.12\ Btu/hr°F*ft^2$$

$$w(U_{sup}(cmin)) = \frac{\delta U_{sup}}{\delta cmin}\ \ w(cmin) \sim (-6.98e\text{-}1)(\pm 5.0\%)(18.12\ lbm/hr)(0.14\ Bti/lbm°F)$$

$$= \pm 0.088\ Btu/hr°F*ft^2$$

$$w(U_{sup}(casup)) = \frac{\delta U_{sup}}{\delta casup}\ \ w(casup)$$

$$\sim (-1.03e\text{-}3)(0.079\ lbm/ft^3)(0.24\ Btu/lbm°F)(60)(\pm 7.1\ ft^3 min) = \pm 0.008\ Btu/hr°F*ft^2$$

$$w(U_{sup}(Tma)) = \frac{\delta U_{sup}}{\delta Tma}\ \ w(Tma) = (-7.75e\text{-}2)(\pm 0.64°F) = \pm 0.05\ Btu/hr°F*ft2$$

$$w(U_{sup}(T7)) = \frac{\delta U_{sup}}{\delta T7}\ \ w(T7) = (7.95e\text{-}2)(\pm 0.73°F) = \pm 0.058\ Btu/hr°F*ft2$$

$$w(U_{sup}) = \sqrt{\sum_{i=1}^{6}[(w_i 2)]}\ \ = \pm 0.25\ Btu/hr°F*ft2$$

Two-phase section

$$\dot{m}\,(h8\text{-}h7) = \left(1 - e^{(-U_{2ph}\ a2ph/ca2ph)}\right) ca2ph\ (Tma - T7)$$

$$w(U_{2ph}(\dot{m})) = \frac{\delta U_{2ph}}{\delta \dot{m}}\ \ w(\dot{m}) = (1.53)(\pm 5.0\%)(18.12\ lbm/hr) = \pm 1.39\ Btu/hr°F*ft^2$$

$$w(U_{2ph}(\Delta h)) = \frac{\delta U_{2ph}}{\delta \Delta h}\ w(\Delta h) = (4.95e\text{-}1)(\pm 0.16\ \text{Btu/lbm}) = \pm 0.079\ \text{Btu/hr°F*ft}^2$$

$$w(U_{2ph}(ca2ph)) = \frac{\delta U_{2ph}}{\delta ca2ph}\ w(ca2ph)$$

$$\sim (-1.33e\text{-}1)(0.079\ \text{lbm/ft}^3)(0.24\ \text{Btu/lbm°F})(60)(\pm 7.1\ \text{ft}^3\text{/min})(0.767)$$

$$= \pm 0.82\ \text{Btu/hr°F*ft}^2$$

$$w(U_{2ph}(Tma)) = \frac{\delta U_{2ph}}{\delta Tma}\ w(Tma) = (-6.19e\text{-}1)(\pm 0.64°F) = \pm 0.40\ \text{Btu/hr°F*ft}^2$$

$$w(U_{2ph}(T7)) = \frac{\delta U_{2ph}}{\delta T7}\ w(T7) = (6.27e\text{-}1)(\pm 0.73°F) = \pm 0.46\ \text{Btu/hr°F*ft}^2$$

$$w(U_{2ph}) = \sqrt{\sum_{i=1}^{5}\left[(w_i^2)\right]} = \pm 1.7\ \text{Btu/hr°F*ft}^2$$

$$w(\dot{Q}\ \text{rate}) = \sqrt{w(\dot{Q}_{sup})^2 + w(\dot{Q}_{2ph})^2}$$

$$w(\dot{Q}_{sup}(U_{sup})) = \frac{\delta \dot{Q}_{sup}}{\delta U_{sup}}\ w(U_{sup}) = (24.11)(\pm 0.25\ \text{Btu/hr°F*ft}^2) = \pm 6.03\ \text{Btu/hr}$$

$$w(\dot{Q}_{sup}(cmin)) = \frac{\delta \dot{Q}_{sup}}{\delta cmin}\ w(cmin) = (17.34)(\pm 5\%)(18.12\ \text{lbm/hr})(0.14\ \text{Btu/lbm°F})$$

$$= \pm 2.2\ \text{Btu/hr}$$

$$w(\dot{Q}_{sup}(casup)) = \frac{\delta \dot{Q}_{sup}}{\delta casup}\ w(casup)$$

$$\sim (2.51e\text{-}2)(0.079\ \text{lbm/ft}^3)(0.24\ \text{Btu/lbm°F})(60)(\pm 7.1\ \text{ft}^3\text{/min})$$

$$= \pm 0.20\ \text{Btu/hr}$$

$$w(\dot{Q}_{sup}(Tma)) = \frac{\delta \dot{Q}_{sup}}{\delta Tma}\ w(Tma) = (1.932)(\pm 0.64°F) = \pm 1.23\ \text{Btu/hr}$$

$$w(\dot{Q}_{sup}(T7)) = \frac{\delta \dot{Q}_{sup}}{\delta T7}\ w(T7) = (-1.932)(\pm 0.73°F) = \pm 1.41\ \text{Btu/hr}$$

$$w(\dot{Q}_{sup}) = \sqrt{\sum_{i=1}^{5}\left[(w_i^2)\right]} = \pm 6.7\ \text{Btu/hr}$$

$$w(\dot{Q}_{sup}(U_{2ph})) = \frac{\delta \dot{Q}_{2ph}}{\delta U_{2ph}}\ w(U_{2ph}) = (36.58)(\pm 1.7\ \text{Btu/hr°F*ft}^2) = \pm 62.2\ \text{Btu/hr}$$

$$w(\dot{Q}_{2ph}(ca2ph)) = \frac{\delta \dot{Q}_{2ph}}{\delta ca2ph} \; w(ca2ph)$$

$$\tilde{} \; (4.827)(0.079 \text{ lbm/ft}^3)(0.24 \text{ Btu/lbm°F})(60)(\pm 7.1 \text{ ft}^3\text{/min})(0.767)$$

$$= \pm 29.9 \text{ Btu/hr}$$

$$w(\dot{Q}_{2ph}(Tma)) = \frac{\delta \dot{Q}_{2ph}}{\delta Tma} \; w(Tma) = (22.715)(\pm 0.64°F) = \pm 14.5 \text{ Btu/hr}$$

$$w(\dot{Q}_{2ph}(T7)) = \frac{\delta \dot{Q}_{2ph}}{\delta T7} \; w(T7) = (22.715)(\pm 0.73°F) = \pm 16.6 \text{ Btu/hr}$$

$$w(\dot{Q}_{2ph}) = \tilde{} \sqrt{\sum_{i=1}^{4} \left[(w_i^2) \right]} = \pm 72.2 \text{ Btu/hr}$$

$$w(\dot{Q} \text{ rate}) = \sqrt{w(\dot{Q}_{sup})^2 + w(\dot{Q}_{2ph})^2} = \sqrt{(\pm 6.7 \text{ Btu/hr})^2 + (72.2 \text{ Btu/hr})^2}$$

$$= \pm 72.5 \text{ Btu/hr}$$

R134a: nonimal values: $\dot{Q}_e$ = 616.6 Btu/hr, $\dot{Q}_{sup}$ = 54.7 Btu/hr, $\dot{Q}_{2ph}$ = 561.9 Btu/hr

$\dot{m}$ = 7.32 lbm/hr, cmin = 1.35 Btu/hr°F, casup = 70.4 Btu/hr°F

Tma = 24.3 °F, T7 = -28.7°F, a2ph = 0.306 ft^2, asup = 3.49 ft^2

h4 = 28.8 Btu/lbm, h8 = 97.43 Btu/lbm, h9 = 104.9Btu/lbm

h10 = 113.0 Btu/lbm, U_{sup} = 0.5398Btu/hr-ft^2°F

$\dot{m}$ (h9-h8) = $\dot{m}$ Δh =

$$\left(\frac{1 - e^{\left(\frac{-U_{sup} \, asup}{cmin} \right)(1+cmin/casup)}}{1 + (cmin/casup)} \right) cmin \, (Tma - T7)$$

$$w(U_{sup}(\dot{m})) = \frac{\delta U_{sup}}{\delta \dot{m}} \; w(\dot{m}) = (1.86e\text{-}1)(\pm 2.9\%)(7.32 \text{ lbm/hr}) = \pm 0.039 \text{ Btu/hr°F*ft}^2$$

$$w(U_{sup}(\Delta h)) = \frac{\delta U_{sup}}{\delta \Delta h} \; w(\Delta h) = (1.81e\text{-}1)(\pm 0.20 \text{ Btu/lbm}) = \pm 0.036 \text{ Btu/hr°F*ft}^2$$

$$w(U_{sup}(cmin)) = \frac{\delta U_{sup}}{\delta cmin} \; w(cmin) \tilde{} \; (-5.41e\text{-}1)(\pm 2.9\%)(7.32 \text{ lbm/hr})(0.18 \text{ Bti/lbm°F})$$

$$= \pm 0.021 \text{ Btu/hr°F*ft}^2$$

$$w(U_{sup}(casup)) = \frac{\delta U_{sup}}{\delta casup} \; w(casup)$$

$$\tilde{} \; (-2.02e\text{-}4)(0.081 \text{ lbm/ft}^3)(0.24 \text{ Btu/lbm°F})(60)(\pm 7.1 \text{ ft}^3\text{min}) = \pm 0.002 \text{ Btu/hr°F*ft}^2$$

$$w(U_{sup}(Tma)) = \frac{\delta U_{sup}}{\delta Tma} \quad w(Tma) = (-2.49e\text{-}2)(\pm 0.66°F) = \pm 0.016 \text{ Btu/hr°F*ft}^2$$

$$w(U_{sup}(T7)) = \frac{\delta U_{sup}}{\delta T7} \quad w(T7) = (-2.487e\text{-}2)(\pm 0.73°F) = \pm 0.018 \text{ Btu/hr°F*ft}^2$$

$$w(U_{sup}) = \sqrt{\sum_{i=1}^{6}\left[(w_i^2)\right]} \quad = \pm 0.06 \text{ Btu/hr°F*ft}^2$$

Appendix E: Program Listings

{E.E.S. Worksheet - Model determines the convective heat transfer coefficient for the compressor by comparing the refrigerant side energy balance with the air side temperature difference. A non-linear least squares method is used to find the optimum. Dean M. Staley}

```
Vdotcond = 115.8

DUPLICATE i=1,33
Pfan[i] = lookup(i,13)
Pcomp[i] = lookup(i,12)
Psystem[i] = lookup(i,11)
Tconfanout[i] = lookup(i,8)
P1[i] = lookup(i,14)
T1[i] = lookup(i,15)
P10[i] = lookup(i,22)
T10[i] = lookup(i,23)
w[i] = lookup(i,27)

h1[i] = Enthalpy(R12,T=T1[i],P=P1[i]+14.4)
h10[i] = Enthalpy(R12,T=T10[i],P=P10[i]+14.4)
rho[i] = 1/Volume(Air,T=Tconfanout[i],P=14.4)
Cpair[i] = SpecHeat(Air,T=Tconfanout[i])
Pconfan[i] = Psystem[i]-Pcomp[i]-Pfan[i]
(Pconfan[i]*3.413) = rho[i]*Cpair[i]*Vdotcond*60*(Tconfanout[i]-Taircomp[i])
Qcomp[i] = (Pcomp[i]*3.413)-w[i]*(h1[i]-h10[i])

dPhbar[i] = (Qcomp[i]-hbar*(T1[i]-Taircomp[i]))*(-(T1[i]-Taircomp[i]))
error[i] = (Qcomp[i]-hbar*(T1[i]-Taircomp[i]))^2
percenterr[i] = sqrt(error[i])/Qcomp[i]

END

sum(dPhbar[i],i=1,33) = 0.0
totalerr = sum(error[i],i=1,33)
```

****

{ E.E.S. Worksheet - Model determines the best UA or effectiveness for the interchanger by the comparing refrigerant energy side balance with the rate equation for the interchanger. Data for cases with subcooling at the cap-tube inlet and superheat at the evaporator outlet are used. A nonlinear least squares approach is used.Dean M. Staley}

```
{DUPLICATE i=1,10
P9[i] = lookup(i,20)
T9[i] = lookup(i,21)
P10[i] = lookup(i,22)
T10[i] = lookup(i,23)
T4[i] = lookup(i,25)
w[i] = lookup(i,27)

h4[i] = Enthalpy(R12,T=T4[i],X=0.0)
h9[i] = Enthalpy(R12,T=T9[i],P=P9[i]+14.4)
h6[i] = h4 [i] - (h10[i]-h9[i])
```

```
T6[i] = Temperature(R12,H=h6[i],X=0.0)
h10[i] = Enthalpy(R12,P=P10[i]+14.4,T=T10[i])

Qint[i] = w[i]*(h10[i]-h9[i])
cmin[i]=w[i]*(h10[i]-h9[i])/(T10[i]-T9[i])
cmax[i]=w[i]*(h4[i]-h6[i])/(T4[i]-T6[i])
error[i] = (Qint[i]-Qrate[i])^2

{ Use the following equations to estimate the best effectiveness }
{Qrate[i] = eff*cmin[i]*(T4[i]-T9[i])
Qrateprime[i] = eff*1.01*cmin[i]*(T4[i]-T9[i])
dPeff[i] = (Qint[i]-Qrate[i])*(-((Qrateprime[i]-Qrate[i])/0.01))}

{ Use the following equations to estimate the best UA }
Qrate[i] = eff[i]*cmin[i]*(T4[i]-T9[i])
eff[i]=(1-exp(-(UAint/cmin[i])*(1-(cmin[i]/cmax[i]))))/(1-((cmin[i]/cmax[i])*exp(-(UAint/cmin[i])*(1-(cmin[i]/cmax[i])))))
effprime[i]=(1-exp(-(UAint*1.01/cmin[i])*(1-(cmin[i]/cmax[i]))))/(1-((cmin[i]/cmax[i])*exp(-(UAint*1.01/cmin[i])*(1-
(cmin[i]/cmax[i])))))
Qrateprime[i] = effprime[i]*cmin[i]*(T4[i]-T9[i])
dPua[i] = (Qint[i]-Qrate[i])*(-((Qrateprime[i]-Qrate[i])/0.01))

END

!*************************************************************************! Program finds
the optimum parameters that minimize the objective function. The objective
! function is defined in function subroutine OBJECT. The method of steepest-decent is used
! to search for the minimum. The search proceeds in the direction of the gradient calculated
! in subroutine grad. If the minimum lies within a narrow, curved valley, the steepest-decent
! routine will not converge in a reasonable time. To speed convergence in this case, a minimum
! at a point close to the current point is determined. The search then proceeds along the line
! formed by these two points. Note the line lies along the valley. After a new estimate of the
! minimum is found, the steepest-descent routine is continued. Dean M. Staley
! M&IE, University of Illinois, 4/92.
!
!*************************************************************************!
! Variables
! Parameter = array containing current parameters that are being sought
! Parmold = array containg last iteration parameter values
! Derv = array containing components of the gradient vector
! Temp = array containing temporary guesses of parameters
! cos() = array containing numbers proportional to direction cosines of line in a valley
! numparm = number of parameters
! totalerrold = last iteration value of the objective function
! totalerrnew = new iteration value of the objective function
! iter = number of search iterations performed
! toll = approximate tolerance on parameters
! minerr = minimum change in the objective function that causes the valley search routine to run
! deltaerror = change in the objective function from last iteration
! deltax = change in the parameter values from last iteration
! maxdeltax = maximum change in any parameter
! xlow = lower bound for a given parameter in the Fibonacci search routine
! xhigh = upper bound for a given parameter in the Fibonacci search routine
! LATTICE = array containing the value of the objective function around the minimum
! maxiter = maximum number of iterations
!
DECLARE DEF OBJECT
DIM Parameter(1),Parmold(1),Derv(1),Temp(1),cos(1),deltax(1),xlow(1),xhigh(1)
```

```
DIM LATTICE(-1 to 1,-1 to 1,-1 to 1,-1 to 1)
OPEN #1:NAME"UAR134condv3dat",CREATE NEWOLD,ORG TEXT
RESET #1:end
!
! Initial variables
!
CALL initial
LET numparm = 4
MAT REDIM Parameter(numparm),Parmold(numparm),Derv(numparm),Temp(numparm),cos(numparm)
MAT REDIM xlow(numparm),xhigh(numparm)
LET Parameter(1) = 0.0949275
LET xlow(1) = 0.05
LET xhigh(1) = 0.15
LET Parameter(2) = 5.6225
LET xlow(2) = 1.0
LET xhigh(2) = 15
LET Parameter(3) = 37.3385
LET xlow(3) = 20
LET xhigh(3) = 40
LET Parameter(4) = 13.0797
LET xlow(4) = 2
LET xhigh(4) = 25
MAT Parmold=zer(numparm)
MAT deltax=zer(numparm)
LET maxdeltax = 1
LET totalerrnew = 0
LET iter = 0
LET toll = 1e-4
LET minerr = 0.1
LET deltaerror = 2*minerr
LET maxiter = 40
!
! Output initial values
!
SET CURSOR 1,1
PRINT "Iteration =";iter;"          "
PRINT "K1 =";Parameter(1);"          "
PRINT "delta1 =";deltax(1);"          "
PRINT "C1 =";Parameter(2);"             "
PRINT "delta2 =";deltax(2);"            "
PRINT "U2ph =";Parameter(3);"             "
PRINT "delta3 =";deltax(3);"            "
PRINT "Usub =";Parameter(4);"             "
PRINT "delta4 =";deltax(4);"            "
PRINT "Total error =";totalerrnew;"          "
PRINT "Change in Error =";deltaerror;"          "
!
! Enter Minimization LOOP
!
FOR iter = 1 to maxiter
 !
 ! Calculate Gradient
 !
 SET CURSOR 20,1
 PRINT "Calculating gradient";"                "
 CALL grad(Parameter,Derv)
 SET CURSOR 12,1
```

```
PRINT "Derivative 1 =";Derv(1);"              "
PRINT "Derivative 2 =";Derv(2);"              "
PRINT "Derivative 3 =";Derv(3);"              "
PRINT "Derivative 4 =";Derv(4);"              "
!
! Output data to a file
!
PRINT #1:iter;",";Parameter(1);",";Parameter(2);",";Parameter(3);",";Parameter(4);",";totalerrnew;",";deltaerror
PRINT #1:"   ";Derv(1);",";Derv(2);",";Derv(3);",";Derv(4)
!
! Start search
!
IF ABS(deltaerror) < minerr AND maxdeltax < toll THEN
   ! In possible valley - Find another minimum point and search
   ! in direction of line formed by last minimum and new minimum
   SET CURSOR 20,1
   ! Find new minimum close to old point
   PRINT "Running valley search";"           "
   PRINT #1:"Running valley search"
   LET Temp(1) = Parameter(1)
   IF Derv(2) > 0.0 THEN
     LET Temp(2) = 0.99*Parameter(2)
   ELSE
     LET Temp(2) = 1.01*Parameter(2)
   END IF
   LET Temp(3) = Parameter(3)
   LET Temp(4) = Parameter(4)
   CALL fibonacci(Temp,xlow,xhigh,Derv,1,toll)
   CALL fibonacci(Temp,xlow,xhigh,Derv,3,toll)
   CALL fibonacci(Temp,xlow,xhigh,Derv,4,toll)
  !
  ! Calculate numbers proportional to the direction cosines of line
  !
  LET cos(1) = (Temp(1)-Parameter(1))/toll
  LET cos(2) = (Temp(2)-Parameter(2))/toll
  LET cos(3) = (Temp(3)-Parameter(3))/toll
  LET cos(4) = (Temp(4)-Parameter(4))/toll
  !
  ! Search in this direction
  !
  CALL fibonacci(Parameter,xlow,xhigh,cos,999,toll)
  SET CURSOR 20,1
  PRINT "                          "
ELSE !do steepest-decent
  !
  ! Calculate new parameters in direction of gradient
  !
  SET CURSOR 20,1
  PRINT "Running Parameter Search";"           "
  CALL fibonacci(Parameter,xlow,xhigh,Derv,999,toll)
  SET CURSOR 20,1
  PRINT "                              "
END IF
!
! Update Variables and Output New Results
!
LET totalerrold = totalerrnew
```

```
  LET totalerrnew = OBJECT(Parameter)
  LET deltaerror = totalerrnew-totalerrold
  FOR i = 1 to numparm
     LET deltax(i) = Parameter(i) - Parmold(i)
     LET Parmold(i) = Parameter(i)
  NEXT i
  LET maxdeltax = 0.0
  FOR i = 1 to numparm
     IF ABS(deltax(i)) > maxdeltax THEN LET maxdeltax = ABS(deltax(i))
  NEXT i
  SET CURSOR 1,1
  PRINT "Iteration =";iter;"           "
  PRINT "K1 =";Parameter(1);"          "
  PRINT "delta1 =";deltax(1);"         "
  PRINT "C1 =";Parameter(2);"              "
  PRINT "delta2 =";deltax(2);"            "
  PRINT "U2ph =";Parameter(3);"              "
  PRINT "delta3 =";deltax(3);"            "
  PRINT "Usub =";Parameter(4);"              "
  PRINT "delta4 =";deltax(4);"            "
  PRINT "Total error =";totalerrnew;"          "
  PRINT "Change in Error =";deltaerror;"          "
NEXT iter
!
! Output last iteration to file
!
PRINT #1:iter;",";Parameter(1);",";Parameter(2);",";Parameter(3);",";Parameter(4);",";totalerrnew;",";deltaerror
PRINT #1:Derv(1);",";Derv(2);",";Derv(3);",";Derv(4)
!
! Run short exhaustive search around minimum
!
FOR i = -1 to 1
   FOR j = -1 to 1
      FOR k = -1 to 1
         FOR l = -1 to 1
            LET Temp(1) = Parameter(1) + Parameter(1)*i*toll*100
            LET Temp(2) = Parameter(2) + Parameter(2)*j*toll*100
            LET Temp(3) = Parameter(3) + Parameter(3)*k*toll*100
            LET Temp(4) = Parameter(4) + Parameter(4)*l*toll*100
            LET LATTICE(i,j,k,l) = OBJECT(Temp)
         PRINT #1:LATTICE(i,j,k,l);
         NEXT l
      NEXT k
   NEXT j
NEXT i
!
CLOSE #1
!
END
!
!
!
MODULE Fibonacci
SUB fibonacci(Parameter(),lowbd(),highbd(),Derv(),optvar,toll)
!
! Subroutine performs a univariate Fibonacci search for the parameter eaual to optvar i.e.
! if optvar equals 2 then search for the second parameter. The subroutine was written to minimize
```

```
! the objective funtion defined by the function routine OBJECT. The routine could be easily extended
! to maximize a given objective function. If optvar equals 999 the routine performs a univariate
! search in the directions specified by the derivatives Derv(). In this way the search can proceed
! along directions that are not parallel to the parameter axes. Dean M. Staley 4/92
!
! Variables
!
! Parameter = array containging the parameters in the objective function
! lowbd = array containing lower bounds on the parameters
! highbd = array containing upper bounds on the parameters
! xlow = lower bound of specified search parameter for given iteration
! xhigh = upper bound of specified search parameter for given iteration
! Derv = array containing derivatives proportional to direction cosines
! optvar = number specifying which optimum parameter is to be determined
! toll = approximate tolerance of the final value of the specified parameter
! numparm = number of total parameters
! F = array containing Fibonacci numbers
! Temp = array containing temporary estimates of parameters
! OBJECT = objective function routine - specified outside module
! xleft = point nearest to xlow
! xright = point nearest to xhigh
! yleft = value of objective function at xleft
! yright = value of objective funtion at xright
! Int = interval within which to search for minimum
!
  DIM Temp(1),F(0 to 99)
  DECLARE DEF OBJECT
  LET numparm = SIZE(Parameter)
  MAT REDIM Temp(numparm)
  !
  IF optvar = 999 THEN
    LET pivot = 1
    LET xlow = lowbd(pivot)
    LET xhigh = highbd(pivot)
  ELSE
    LET xlow = lowbd(optvar)
    LET xhigh = highbd(optvar)
  END IF
  !
  ! Calculate approximate Fibonacci number
  !
  LET Fib = (xhigh-xlow)/toll
  !
  ! Search for actual Fibonacci number
  !
  LET F(0) = 1
  LET F(1) = 1
  LET n = 1
  DO WHILE Fib > F(n)
    LET F(n+1) = F(n-1) + F(n)
    LET n = n+1
  LOOP
  !
  ! Start minimization routine
  !
  LET Int = xhigh - xlow
  LET iter = 0.0
```

```
!
FOR i = 2 to n
   IF i = 2 THEN
     LET xright = xlow + Int*(F(n-1)/F(n))
     LET x = xright
     CALL reassign(x,Temp,Parameter,Derv,optvar,lowbd,highbd,pivot)
     LET yright = OBJECT(Temp)
     LET xleft = xlow + Int*(1-(F(n-1)/F(n)))
     LET x = xleft
     CALL reassign(x,Temp,Parameter,Derv,optvar,lowbd,highbd,pivot)
     LET yleft = OBJECT(Temp)
   ELSE IF i > 2 AND i < n THEN
     IF xhigh = xright THEN
       LET x = xlow + Int*(1-((xleft-xlow)/Int))
       CALL reassign(x,Temp,Parameter,Derv,optvar,lowbd,highbd,pivot)
       LET y = OBJECT(Temp)
       IF x < xleft THEN
         LET xright = xleft
         LET yright = yleft
         LET xleft = x
         LET yleft = y
       ELSE
         LET xleft = x
         LET yleft = y
       END IF
     ELSE
       LET x = xlow + Int*(1-((xright-xlow)/Int))
       CALL reassign(x,Temp,Parameter,Derv,optvar,lowbd,highbd,pivot)
       LET y = OBJECT(Temp)
       IF x > xright THEN
         LET xleft = xright
         LET yleft = yright
         LET xright = x
         LET yright = y
       ELSE
         LET xleft = x
         LET yleft = y
       END IF
     END IF
   ELSE
     IF xleft = xlow THEN
       LET xleft = xright - 0.01*toll
       LET x = xleft
       CALL reassign(x,Temp,Parameter,Derv,optvar,lowbd,highbd,pivot)
       LET yleft = OBJECT(Temp)
     ELSE
       LET xright = xleft + 0.01*toll
       LET x = xright
       CALL reassign(x,Temp,Parameter,Derv,optvar,lowbd,highbd,pivot)
       LET yright = OBJECT(Temp)
     END IF
   END IF
   IF yright > yleft THEN
    LET xhigh = xright
   ELSE
    LET xlow = xleft
   END IF
```

```
      LET Int = xhigh - xlow
      LET iter = iter +1
      SET CURSOR 21,1
      PRINT "Iteration =";iter;"                    "
   NEXT i
   SET CURSOR 21,1
   PRINT "                                      "
   !
   ! Update Parameters
   !
   IF optvar = 999 THEN
     LET minx = (xhigh+xlow)/2
     LET scale = (minx-Parameter(pivot))/Derv(pivot)
     FOR i = 1 to numparm
       IF i <> pivot THEN LET Parameter(i) = scale*Derv(i)+Parameter(i)
     NEXT i
     LET Parameter(pivot) = minx
   ELSE
     LET Parameter(optvar) = (xhigh+xlow)/2
   END IF
END SUB
!
SUB reassign(x,Temp(),Parameter(),Derv(),optvar,lowbd(),highbd(),pivot)
    LET numparm = SIZE(Parameter)
    IF optvar = 999 THEN
        LET Temp(pivot) = x
        LET scale = (Temp(pivot)-Parameter(pivot))/Derv(pivot)
        FOR i = 1 to numparm
          IF i <> pivot THEN LET Temp(i) = scale*Derv(i)+Parameter(i)
        NEXT i
    ELSE
        LET Temp(optvar) = x
        FOR i = 1 to numparm
           IF i<> optvar THEN LET Temp(i) = Parameter(i)
        NEXT i
    END IF
    !
    ! Check bounds
    !
    FOR i = 1 to numparm
       IF Temp(i) < lowbd(i) OR Temp(i) > highbd(i) THEN
          PRINT "Parameters out of bounds in subroutine Fibonacci - adjust bounds"
          PRINT "Pivot variable =";pivot
          PRINT "Scale =";scale
          PRINT "Variable out of bounds = #";i
          FOR j = 1 to numparm
             PRINT "Variable #";j;" =";Temp(j)
             PRINT "Derivative #";j;" =";Derv(j)
          NEXT j
          STOP
       END IF
    NEXT i
END SUB
!
END MODULE
!
!
```

```
SUB grad(Parameter(),Derv())
!
! Subroutine calculates the gradient at the point specified by Parameter().
!
! Variables
! Temp = array containing temporary values of parameters
! numparm = number of parameters
! deltak = increment in temporary parameters
! Parameter = array containg actual parameters
! Derv = array containg gradient components
!
  DECLARE DEF OBJECT
  DIM Temp(1)
  LET numparm = SIZE(Parameter)
  MAT REDIM Temp(numparm)
  LET deltak = 0.000001
  LET F = OBJECT(Parameter)
  FOR i = 1 to numparm
     LET Temp(i) = Parameter(i)
  NEXT i
  !
  FOR i = 1 to numparm
    LET Temp(i) = Parameter(i) + deltak
    LET Derv(i) = (OBJECT(Temp)-F)/deltak
    LET Temp(i) = Temp(i) - deltak
  NEXT i
END SUB
!
!
SUB initial
!
! Subroutine initializes variables for use in subroutine calcr - R134a condenser
!
! Variables
! w = refrigerant mass flow rate lbm/hr
! h1 = enthalpy of refrigerant at inlet of condenser Btu/lbm
! h1satvap = saturated vapor enthalpy at the condenser inlet pressure Btu/lbm
! h2 = saturated liquid enthalpy at the end of the two phase section Btu/lbm
! h3 = enthalpy of liquid refrigerant leaving condenser at the condenser outlet pressure Btu/lbm
! T1 = inlet tempeature to the condenser °F
! T2 = saturated condensing temperature °F
! cmin = mdot*Cp for desuperheating section Btu/hr°F
! cminsub = mdot Cp for subcooled section Btu/hr°F
! cacond = mdotair*Cpair for the condenser air flow rate Btu/hr°F
! Tconairin = condenser inlet air temperature °F
! numpt = number of data points
! hdesup = refrigerant side film coefficient for the despuerheating section Btu/ft^2-hr°R
! h2ph = refrigerant side film coefficient for the two-phase section Btu/ft^2-hr°R
! hsub = refrigerant side film coefficient for the subcooled section Btu/ft^2-hr°R
!
   PUBLIC w(1),h1(1),h1satvap(1),h2(1),h3(1),T1(1),T2(1)
   PUBLIC cmin(1),cminsub(1),cacond(1),Tconairin(1),numpt
   PUBLIC hdesup(1),h2ph(1),hsub(1),T3(1)
   !
   ! Input data set
   !
   READ numpt
```

```
  !
  MAT REDIM w(numpt),h1(numpt),h1satvap(numpt),h2(numpt),h3(numpt),T1(numpt)
  MAT REDIM T2(numpt),cmin(numpt),cminsub(numpt),cacond(numpt),Tconairin(numpt)
  MAT REDIM hdesup(numpt),h2ph(numpt),hsub(numpt),T3(numpt)
  !
  FOR k = 1 to numpt
    READ w(k),h1(k),h1satvap(k),h2(k),h3(k),T1(k),T2(k),cmin(k),cminsub(k),cacond(k),Tconairin(k)
    READ hdesup(k),h2ph(k),hsub(k),T3(k)
  NEXT k
  !
  ! R134a data subset - Form of w,h1,h1satvap,h2,h3,T1,T2,cmin,cminsub,cacond,Tconairin
  !                     hdesup,h2ph,hsub,T3
  !
DATA 30
DATA 7.575, 124.875, 111.069, 33.94, 32.509, 129.1, 71.378, 1.809, 2.532, 125.911, 53.5, 26.303, 141.69, 11.493, 67.1
DATA 7.554, 124.809, 111.081, 33.974, 32.576, 128.8, 71.479, 1.804, 2.525, 125.841, 53.8, 26.239, 141.31, 11.488, 67.3
DATA 7.321, 124.675, 111.033, 33.839, 31.81, 128.1, 71.076, 1.747, 2.442, 125.794, 54, 25.561, 138.10, 11.536, 65.0
DATA 7.188, 124.78, 110.938, 33.578, 31.412, 128.3, 70.297, 1.711, 2.394, 125.911, 53.5, 25.152, 136.62, 11.571, 63.8
DATA 6.976, 124.172, 110.859, 33.36, 31.246, 125.5, 69.647, 1.658, 2.321, 125.841, 53.8, 24.488, 133.82, 11.591, 63.3
DATA 6.689, 124.037, 110.775, 33.129, 30.585, 124.7, 68.958, 1.587, 2.221, 125.818, 53.9, 23.637, 129.86, 11.639, 61.3
DATA 8.145, 127.383, 112.845, 39.082, 37.64, 144.8, 86.507, 2.03, 2.791, 122.549, 68.3, 29.032, 139.26, 10.963, 82.3
DATA 8.031, 127.285, 112.851, 39.101, 38.633, 144.4, 86.562, 2.002, 2.759, 122.417, 68.9, 28.702, 137.67, 10.912, 85.2
DATA 7.924, 127.141, 112.97, 39.463, 35.938, 144.2, 87.614, 1.982, 2.706, 122.219, 69.8, 28.461, 135.49, 11.03, 77.3
DATA 7.816, 127.092, 112.97, 39.463, 35.599, 144, 87.614, 1.956, 2.667, 122.417, 68.9, 28.148, 134.02, 11.048, 76.3
DATA 7.776, 127.286, 112.759, 38.822, 38.358, 144.1, 85.751, 1.933, 2.667, 122.549, 68.3, 27.915, 134.70, 10.94, 84.4
DATA 7.689, 127.057, 112.982, 39.501, 35.362, 143.9, 87.723, 1.925, 2.623, 122.417, 68.9, 27.786, 132.19, 11.058, 75.6
DATA 7.453, 127.033, 112.945, 39.388, 34.654, 143.7, 87.393, 1.864, 2.537, 122.439, 68.8, 27.082, 129.15, 11.1, 73.5
DATA 7.418, 126.512, 112.765, 38.842, 35.16, 141, 85.808, 1.848, 2.525, 122.505, 68.5, 26.85, 129.68, 11.102, 75.0
DATA 7.247, 126.29, 112.681, 38.59, 35.498, 139.8, 85.074, 1.802, 2.467, 122.483, 68.6, 26.291, 127.74, 11.097, 76.0
DATA 6.389, 126.063, 112.72, 38.706, 34.553, 139, 85.413, 1.591, 2.171, 122.439, 68.8, 23.779, 115.30, 11.14, 73.2
DATA 8.703, 131.241, 115.181, 46.725, 44.909, 168.6, 108.301, 2.311, 3.094, 118.236, 88.6, 32.622, 131.95, 10.232, 103.2
DATA 8.233, 130.555, 114.928, 45.829, 45.69, 164.9, 105.79, 2.171, 2.301, 118.277, 88.4, 30.955, 127.77, 10.237, 105.4
DATA 8.208, 130.702, 114.806, 45.406, 45.299, 165, 104.599, 2.155, 2.282, 118.277, 88.4, 30.79, 128.21, 10.276, 104.3
DATA 7.494, 130.078, 115.04, 46.224, 42.866, 163.5, 106.9, 1.987, 2.647, 118.317, 88.2, 28.778, 117.88, 10.354, 97.4
DATA 7.876, 130.296, 114.78, 45.317, 45.158, 163.3, 104.35, 2.068, 2.188, 118.297, 88.3, 29.748, 124.20, 10.287, 103.9
DATA 8.238, 130.571, 115.231, 46.903, 42.026, 166.2, 108.799, 2.195, 2.908, 118.256, 88.5, 31.227, 125.97, 10.362, 95.0
DATA 8.103, 130.428, 115.196, 46.779, 41.852, 165.5, 108.453, 2.158, 2.859, 118.215, 88.7, 30.781, 124.53, 10.376, 94.5
DATA 7.954, 130.394, 115.058, 46.287, 45.228, 164.8, 107.076, 2.108, 2.827, 118.093, 89.3, 30.212, 123.52, 10.237, 104.1
DATA 9.154, 133.362, 116.02, 49.854, 49.534, 180.4, 116.98, 2.491, 3.322, 116.267, 98.4, 34.925, 131.71, 9.869, 116.1
DATA 8.789, 133.143, 116.05, 49.969, 49.57, 179.7, 117.296, 2.397, 3.191, 116.208, 98.7, 33.827, 127.30, 9.862, 116.2
DATA 8.633, 133.051, 116.04, 49.933, 49.534, 179.3, 117.198, 2.354, 3.134, 116.227, 98.6, 33.331, 125.55, 9.865, 116.1
DATA 8.527, 132.994, 116.044, 49.947, 49.461, 179.1, 117.237, 2.326, 3.095, 116.168, 98.9, 33.003, 124.29, 9.868, 115.9
DATA 8.375, 132.784, 116.018, 49.847, 49.353, 178.2, 116.96, 2.284, 3.038, 116.168, 98.9, 32.499, 122.68, 9.877, 115.6
DATA 8.167, 132.523, 115.978, 49.688, 49.135, 177, 116.524, 2.225, 2.959, 116.188, 98.8, 31.795, 120.48, 9.895, 115.0
!
END SUB
!
!
DEF OBJECT(Parameter())
!
! The function determines the value of the objective function at the specified parameters
! - Parameter (). For R134a GE condenser.
!
!  Variables
!
!  datapt = data point that is currently being evaluated
!  numpt = total number of data points
```

```
!  x() = array containing values of variables specified in subroutine calcr
!  r() = array containing residual values
!  niter = maximum number of iterations allowed to obtain convergence in Newton-Raphson
!  toll = specified convergence tolerance for variables x() in Newton-Raphson routines
!  delta = increment in x() required to calculate derivatives in Newton-Raphson rountines
!  nvar = number of variables
!  Parameter() = array containing parameters that are constant during objective function
!              evaluation
!  totalerr = accumulated error in objective function
!  xlow() = lower bounds on x() variables
!  xhigh() = upper bounds on x() variables
!
   PUBLIC datapt,K1,C1,u2ph,usub
   DECLARE PUBLIC numpt,cminsub(),T2(),T3()
   DIM x(12),r(12),xlow(12),xhigh(12)
   !
   ! Initialize constants
   !
   LET K1 = Parameter(1)
   LET C1 = Parameter(2)
   LET u2ph = Parameter(3)
   LET usub = Parameter(4)
   LET toll= 0.000001
   LET delta = 0.000001
   LET nvar = 12
   !
   ! Set initial guesses for Newton-Raphson subroutine
   !
   LET x(1) = 800   !Qrate
   LET x(2) = 600   !Qc2phrate
   LET x(3) = 180   !Qcdesuprate
   LET x(4) = 20    !Qcsubrate
   LET x(5) = 0.9   !adesup
   LET x(6) = 1.14  !a2ph
   LET x(7) = 0.05  !asub
   LET x(8) = 0.4   !esub
   LET x(9) = 0.8   !edesup
   LET x(10) = 2    !ntudesup
   LET x(11) = 0.8  !ntusub
   LET x(12) = 700  !Qc
   !
   ! Set variable bounds
   !
   FOR i = 1 to nvar
      LET xlow(i) = 1e-6
      LET xhigh(i) = 1e6
   NEXT i
   ! reset certain bounds
   LET xhigh(5) = 2.09
   LET xhigh(6) = 2.09
   LET xhigh(7) = 2.09
   LET xhigh(8) = 1
   LET xhigh(9) = 1
   !
   ! Calculate Total Squared Error - (T3calc-T3)^2
   !
   LET totalerr = 0.0
```

```
  FOR k = 1 to numpt
    LET niter=30
    LET datapt = k
    CALL nr(x,r,nvar,toll,niter,delta,xlow,xhigh)
    IF niter = 30 THEN
      PRINT "Newton-Raphson routine failed to converge"
      STOP
    END IF
    LET T3calc = T2(k) - (x(4)/cminsub(k))
    LET totalerr = totalerr + (T3calc-T3(k))^2
    SET CURSOR 1,50
    PRINT "Objective Function Evaluation"
    SET CURSOR 2,50
    PRINT "K1 =";Parameter(1);"        "
    SET CURSOR 3,50
    PRINT "C1 =";Parameter(2);"         "
    SET CURSOR 4,50
    PRINT "U2ph =";Parameter(3);"         "
    SET CURSOR 5,50
    PRINT "Usub =";Parameter(4);"         "
    SET CURSOR 6,50
    PRINT "Qrate = ";x(1);"        "
    SET CURSOR 7,50
    PRINT "Qc2ph = ";x(2);"        "
    SET CURSOR 8,50
    PRINT "Qcdesup = ";x(3);"       "
    SET CURSOR 9,50
    PRINT "Qcsub = ";x(4);"        "
    SET CURSOR 10,50
    PRINT "adesup = ";x(5);"       "
    SET CURSOR 11,50
    PRINT "a2ph = ";x(6);"        "
    SET CURSOR 12,50
    PRINT "asub = ";x(7);"        "
    SET CURSOR 13,50
    PRINT "esub = ";x(8);"        "
    SET CURSOR 14,50
    PRINT "edesup = ";x(9);"       "
    SET CURSOR 15,50
    PRINT "ntudesup = ";x(10);"      "
    SET CURSOR 16,50
    PRINT "ntusub = ";x(11);"       "
    SET CURSOR 17,50
    PRINT "Qc = ";x(12);"     "
    SET CURSOR 18,50
    PRINT "Total error = ";totalerr;"       "
    SET CURSOR 19,50
    PRINT "Iteration = ";k;"      "
  NEXT k
  LET OBJECT=totalerr
END DEF
!
! Newton-Raphson subroutines
!
SUB nr(x(),r(),nvar,toll,niter,delta,xlow(),xhigh())
   !    Generalized newton-raphson subroutine
   !    Numerical partial derivative version
```

```
!    c o pedersen,  m&ie dept, u of illinois
!    Replacement of matrix inversion function with XGAUSS was implemented by Kevin J. Porter
!         M&IE  University of Illinois, 1991.
!    Checking for variables being out of specified bounds was added by Dean M. Staley
!         M&IE  University of Illinois, 1992.
!
! Inputs:
!    x = variable array, should contain initial values on entry
!    xlow = lower bounds for variables in x array
!    xhigh = upper bounds for variables in x array
!    nvar = number of variables
!    toll = convergence criterion (toll*dot(x,x), suggest.001)
!    niter = max number of iterations allowed
!    delta = increment of x in partial deriv calc (suggest .001)
! Outputs:
!    r = residual equation values
!    x = final x values
!    niter = actual number of iterations
!  Required Subroutines:
!       rcalc(r(),x())  !  subroutine to evaluate residual
!          equations (supplied by user).
!  Subroutines used:
!       calcfp(r(),ro(),x(),fprime(,),delta)1  evaluates
!            numerical partial derivatives
!       XGAUSS Sparse matrix equation solver adapted to invert fprime matrix
!
DIM dx(1),ro(1),fprime(1,1),invfprime(1,1)
PUBLIC MAX,MT,IROW(1),JCOL(1,1),A(1) !Used by XGauss
!  initialize, resize and zero arrays
LET maxiter=niter    ! pass in max number of iterations, return actual number
MAT r=zer(nvar)
MAT dx=zer(nvar)
MAT ro=zer(nvar)
MAT fprime=zer(nvar,nvar)
MAT invfprime=zer(nvar,nvar)
LET Max = nvar*nvar ! the following variables are used in XGAUSS
MAT IROW = zer(nvar)
MAT JCOL = zer(2,MAX)
MAT A = zer(MAX)
!
FOR niter = 1 to maxiter
   CALL calcfp(r,ro,x,fprime,delta)
   CALL calcr(r,x)
   ! **
   ! **    solve for corrections
   ! **    note +r is used on rhs
   ! **    corrections will be subtracted from base value
   ! **
   ! Can replace the next two lines with the code below - use one or the other
!    MAT invfprime = inv(fprime)
!    MAT dx = invfprime*r

   !The following equations can be used to find dx. The use of XGAUSS considerably
   !improves convergence time. However, XGAUSS is susceptible to round-off errors.
   !If problems are encountered use the True Basic inversion code above. - Staley

   !Set up variables to use XGauss
```

```
      LET JA = 0
      FOR i = 1 to nvar
         FOR j =1 to nvar
            IF fprime(i,j) <> 0 THEN
              CALL NZero(i,j,fprime(i,j),JA,nvar)
            END IF
         NEXT j
      NEXT i
      CALL XGauss(IROW,JCOL,A,ro,dx,nvar,MAX,MT)
      !
      !
      MAT x=x-dx
      LET err=dot(dx,dx)
      LET xnorm = dot(x,x)
      IF  err  < toll*xnorm  then    ! termination condition
        CALL calcr(r,x)       !reevaluate r
        EXIT SUB
      END IF
      ! Check variables against bounds
      FOR k = 1 to nvar
         IF x(k) < xlow(k) THEN LET x(k) = xlow(k)
         IF x(k) > xhigh(k) THEN LET x(k) = xhigh(k)
      NEXT K
   NEXT niter
END SUB
!
!
SUB calcfp(r(),ro(),x(),fprime(,),delta)
   ! **
   !  subroutine to fill partial derivative matrix
   ! **
   LET nvar=size(x)
   CALL calcr(ro,x)
   FOR i=1 to nvar
      LET  deltax=delta*x(i)
      LET x(i)=x(i)+deltax
      CALL calcr(r,x)
      FOR  j=1 to nvar
         LET fprime(j,i)=(r(j)-ro(j))/(deltax)
      NEXT j
      LET x(i)=x(i)-deltax
   NEXT i
END SUB
!
!
SUB  calcr(r(),x())
!
! The following equations calculate the residuals for the GE R134a condenser
!
! Variables
! Qc = measured heat transfer rate from condenser Btu/hr
! Qcdesup = measured heat transfer rate from the desuperheating section of condenser Btu/hr
! Qc2ph = measured heat transfer rate from the two phase section of the condenser Btu/hr
! Qcsub = measured heat transfer rate from the subcooled section of the condenser Btu/hr
! Qrate = calculated heat transfer rate from the condenser Btu/lbm*hr
! Qcdesuprate = calculated heat transfer rate from the desuperheating section of condenser Btu/hr
! Qc2phrate = calculated heat transfer rate from the two phase section of condenser Btu/hr
```

```
! Qcsubrate = calculated heat transfer rate from the subcooled section of condenser Btu/hr
! acond = total area of condenser ft^2
! adesup = area of desuperheating section ft^2
! a2ph = area of two phase section ft^2
! asub = area of subcooled section ft^2
! edesup = effectiveness of the desuperating section
! esub = effectiveness of the subcooled section
! ntudesup = number of transfer units for the desuperheating section
! ntusub = number of transfer units for the subcooled section
! var/varsub = dummy variables
! Tconmid1 = air temperature after subcooled section °F
! Tconmid2 = air temperature after two phase section °F
! PUBLIC variables - see subroutine initial
!
DIM Qcdesup(1),var(1),varsub(1),Qc(1),Qrate(1),Qc2ph(1),Qc2phrate(1),Qcdesuprate(1),Qcsubrate(1)
DIM Qcsub(1),a2ph(1),adesup(1),asub(1),esub(1),edesup(1),ntudesup(1),ntusub(1)
DIM Tconmid1(1),Tconmid2(1),udesup(1)
DECLARE PUBLIC w(),h1(),h1satvap(),h2(),h3()
DECLARE PUBLIC T1(),T2(),cmin(),cminsub(),cacond(),Tconairin(),hdesup(),h2ph(),hsub()
DECLARE PUBLIC datapt,numpt,K1,C1,usub,u2ph
MAT REDIM Qcdesup(numpt),var(numpt),varsub(numpt),Qc(numpt),Qrate(numpt),Qc2ph(numpt)
MAT REDIM Qc2phrate(numpt),Qcdesuprate(numpt),Qcsubrate(numpt),a2ph(numpt),adesup(numpt)
MAT REDIM Qcsub(numpt),asub(numpt),esub(numpt),edesup(numpt),ntudesup(numpt),ntusub(numpt)
MAT REDIM Tconmid1(numpt),Tconmid2(numpt),udesup(numpt)
   !
   ! Set up variables
   !
   LET i = datapt
   LET acond = 2.09
   LET Qcdesup(i) = w(i)*(h1(i)-h1satvap(i))
   LET Qc2ph(i) = w(i)*(h1satvap(i)-h2(i))
   LET Qcsub(i) = w(i)*(h2(i)-h3(i))
   LET Tconmid1(i) = (Qcsub(i)/cacond(i)) + Tconairin(i)
   LET Tconmid2(i) = (Qc2ph(i)/cacond(i)) + Tconmid1(i)
   LET var(i) = 1-(cmin(i)/cacond(i))
   LET varsub(i) = 1-(cminsub(i)/cacond(i))
   LET udesup(i) = 1/(K1 + (C1/hdesup(i)))
   !
   LET Qrate(i) = x(1)
   LET Qc2phrate(i) = x(2)
   LET Qcdesuprate(i) = x(3)
   LET Qcsubrate(i) = x(4)
   LET adesup(i) = x(5)
   LET a2ph(i) = x(6)
   LET asub(i) = x(7)
   LET esub(i) = x(8)
   LET edesup(i) = x(9)
   LET ntudesup(i) = x(10)
   LET ntusub(i) = x(11)
   LET Qc(i) = x(12)
   !
   ! **  residual equations
   !
   LET r(1) = acond - adesup(i) - a2ph(i) - asub(i)
   LET r(2) = Qrate(i) - Qc2phrate(i) - Qcdesuprate(i) - Qcsubrate(i)
   LET r(3) = (Qc2ph(i)/Qc(i))-(Qc2phrate(i)/Qrate(i))
   LET r(4) = (Qcdesup(i)/Qc(i))-(Qcdesuprate(i)/Qrate(i))
```

```
   LET r(5) = Qcdesuprate(i) - (edesup(i)*cmin(i)*(T1(i)-Tconmid2(i)))
   LET r(6) = edesup(i) - (1-exp(-ntudesup(i)*var(i)))/(1-(cmin(i)/cacond(i))*exp(-ntudesup(i)*var(i)))
   LET r(7) = ntudesup(i) - ((udesup(i)*adesup(i))/cmin(i))
   LET r(8) = Qc2phrate(i) - ((1-exp(-u2ph*a2ph(i)/cacond(i)))*cacond(i)*(T2(i)-Tconmid1(i)))
   LET r(9) = Qcsubrate(i) - (esub(i)*cminsub(i)*(T2(i)-Tconairin(i)))
   LET r(10) = esub(i) - (1-exp(-ntusub(i)*varsub(i)))/(1-(cminsub(i)/cacond(i))*exp(-ntusub(i)*varsub(i)))
   LET r(11) = ntusub(i) - ((usub*asub(i))/cminsub(i))
   LET r(12) = Qc(i) - (w(i)*(h1(i)-h3(i)))
END SUB
!
!
!
SUB NZero(I,J,R,JA,Nvar)

   !   From Design of Thermal Systems 3rd Ed.
   !       W. F. Stoecker p. 556 - 557
   !   Translated by Kevin J. Porter from FORTRAN to TRUE BASIC

   !   PURPOSE - This subroutine stores the nonzero elements in the proper order
   !           to be used with the subroutine XGauss
   !   INPUTS
   !       I    - row number of new nonzero element
   !       J    - column number of new nonzero element
   !       R    - coefficient of new nonzero element
   !       JA   - test variable, set equal to zero at start of calling subroutine
   !       Nvar - Number of variables

   !*********************************************************************

   !   PUBLIC and LOCAL Variables
   DECLARE PUBLIC Max, MT, IROW(), JCOL(,), A()
   !   Max       - maximum number of nonzero elements at any time
   !   MT        - number of the first empty location
   !   IROW()    - location of first nonzero element of each row
   !   JCOL(1, ) - column number of nonzero element or 0 if location empty
   !   JCOL(2, ) - location of next nonzero element or no of next empty location
   !   A()       - value of coefficient
   !   L         - counter
   !   LCT, LCTOLD -

   !*********************************************************************

   ! First Time NZero is called matrices are initialized

   IF JA = 0 then
     LET JA = JA + 1
     LET MT = 1
     MAT IROW = ZER(Nvar)
     FOR L = 1 to MAX
        LET JCOL(1,L) = 0
        LET JCOL(2,L) = L + 1
        LET A(L) = 0
     NEXT L
   END IF

   IF (IROW(I) = 0) then
     ! New element is the first nonzero element found in row I
```

```
    LET IROW(I) = MT
    LET JCOL(1,MT) = J
    LET A(MT) = R
    LET MT = JCOL(2,MT)
    LET JCOL(2,IROW(I)) = 0
    EXIT SUB
  END IF

  ! Search to find proper location of new element in ROW I

  LET LCT = IROW(I)
  LET LCTOLD = 0
  DO
    IF (J < JCOL(1,LCT)) then
      IF (LCTOLD = 0) then
        LET JCOL(1,MT) = J
        LET A(MT) = R
        LET IROW(I) = MT
        LET MT = JCOL(2,MT)
        LET JCOL(2,IROW(I)) = LCT
        EXIT SUB
      ELSE
        LET JCOL(1,MT) = J
        LET A(MT) = R
        LET JCOL(2,LCTOLD) = MT
        LET MT = JCOL(2,MT)
        LET JCOL(2,JCOL(2,LCTOLD)) = LCT
        EXIT SUB
      END IF
    ELSE IF (JCOL(2,LCT) = 0) then
      LET JCOL(2,LCT) = MT
      LET JCOL(1,MT) = J
      LET A(MT) = R
      LET MT = JCOL(2,MT)
      LET JCOL(2,JCOL(2,LCT)) = 0
      EXIT SUB
    ELSE
      LET LCTOLD = LCT
      LET LCT = JCOL(2,LCT)
    END IF
  LOOP WHILE (1 = 1)
END SUB
!
!@@@@@@@@@@@@@@@@@@@@@@@@@@@@@@@@@@@@@@@@@@@@@@@@@@@
@@@@@@@@@@@@@@@@@@@@
!
SUB XGauss(IROW(),JCOL(,),A(),B(),X(),N,MAX,MT)

  !   From Design of Thermal Systems 3rd Ed.
  !      W. F. Stoecker p. 558 - 560
  !   Translated by Kevin J. Porter from FORTRAN to TRUE BASIC

  !   PURPOSE - Solution of simulataneous linear equations by Gauss Elimination of
  !            the form [A]{X} = {B}

  !   USAGE  -  This subroutine stores only nonzero elements using linked storage
  !            to be used on sparse matrices in conjunction with subroutine NZero.
```

```
!           Causes Error 100 to occur if equations are not independent.

!   INPUTS
!      IROW()    - location of first nonzero element of each row
!      JCOL(1, ) - column number of nonzero element or 0 if location empty
!      JCOL(2, ) - location of next nonzero element or no of next empty location
!      A()       - value of coefficient
!      B()       - RHS of equation
!      X()       - dependent variable array
!      N         - number of variables
!      Max       - max number of nonzero elements at any time
!      MT        - Number of first empty location

LET MTMAX = 0

FOR K = 1 to N

   ! Moving largest coefficient into diagonal position

   LET AMAX = 0

   FOR I = K to N
      IF (JCOL(1,IROW(I)) <> K) then
      ELSE IF (ABS(AMAX) >= ABS(A(IROW(I)))) then
      ELSE
        LET AMAX = A(IROW(I))
        LET IMAX = I
      END IF
   NEXT I

   ! Testing for the independence of the equations

   !Test for independence of equations
   IF ABS(AMAX) < 1e-15 THEN
     CAUSE ERROR 100, "Equations are not independent in XGauss"
   END IF

   ! Exchanging ROW IMAX and ROW K

   LET BTEMP = B(K)
   LET B(K) = B(IMAX)
   LET B(IMAX) = BTEMP
   LET ITEMP = IROW(K)
   LET IROW(K) = IROW(IMAX)
   LET IROW(IMAX) = ITEMP

   ! Subtraction A(I,K)/A(K,K) times term in first Eq from others

   LET KPLUS = K + 1
   IF (K = N) then
     EXIT FOR
   END IF
   FOR I = KPLUS to N
      LET TEST = 0
      IF (JCOL(1,IROW(I)) <> K) then
      ELSE
        LET LI = JCOL(2,IROW(I))
```

```
        LET LK = JCOL(2,IROW(K))
        LET LIOLD = IROW(I)
        LET B(I) = B(I) - (A(IROW(I))/A(IROW(K)))*B(K)
        DO
          IF (LK = 0) and (TEST = 0) then
            ! Element I,K is now zero, add location to list of empty spaces
            LET LCT = IROW(I)
            LET JCOL(1,LCT) = 0
            LET A(LCT) = 0
            LET IROW(I) = JCOL(2,LCT)
            LET JCOL(2,LCT) = MT
            LET MT = LCT
            EXIT DO
          END IF
          LET TEST = 0
          IF (LI = 0) or (JCOL(1,LI) > JCOL(1,LK)) then
            ! No corresponding element in row I as in row K create new nonzero element
            LET LCT = MT
            LET MT = JCOL(2,MT)
            IF (MTMAX < MT) then
              LET MTMAX = MT
            END IF
            IF (MT < MAX) then
              LET JCOL(1,LCT) = JCOL(1,LK)
              LET A(LCT) = -(A(IROW(I))/A(IROW(K)))*A(LK)
              LET JCOL(2,LIOLD) = LCT
              LET JCOL(2,LCT) = LI
              LET LIOLD = LCT
              LET LK = JCOL(2,LK)
            ELSE
              CAUSE ERROR 102, "Allocation storage exceeded, MAX = " & str$(Max)
            END IF
          ELSE IF (JCOL(1,LI) = JCOL(1,LK)) then
            ! Corresponding element in row I and in Row K
            LET A(LI) = A(LI) - (A(IROW(I))/A(IROW(K)))*A(LK)
            LET LIOLD = LI
            LET LK = JCOL(2,LK)
            LET LI = JCOL(2,LI)
          ELSE
            LET LIOLD = LI
            LET LI = JCOL(2,LI)
            LET TEST = 1
          END IF
        LOOP WHILE (1 = 1)
      END IF
    NEXT I
  NEXT K

  ! BACK SUBSTITUTION

  FOR I = 1 to N
    LET PART = B(N + 1 - I)/A(IROW(N + 1 - I))
    LET LCT = JCOL(2, IROW(N + 1 - I))
    DO WHILE (LCT <> 0)
      LET PART = PART - A(LCT)*X(JCOL(1,LCT))/A(IROW(N + 1 - I))
      LET LCT = JCOL(2,LCT)
    LOOP
```

```
      LET X(N + 1 - I) = PART
   NEXT I

END SUB
```

Appendix F: Experimental Data

R12 – Data

Date	Tfreshfood	Tfreshfdret	Tfreezer	Tfreezret	Tevapfanout	Tchamber
	°F	°F	°F	°F	°F	°F
6/1/91	50.4	49.5	9.5	10.8	3.7	70.9
6/2/91	60.6	59.9	29.2	30.6	21.8	70.7
6/28/91	60.2	59.9	30.1	31.2	21.4	70.4
6/3/91	59.5	58.5	-0.35	0.48	-3.5	70.2
7/22/91	58.8	58.2	-1.3	-0.54	-4.6	71.3
6/19/91	34.3	33.5	-6.23	-5.4	-9.4	70.4
6/4/91	49	48.3	29.9	31.7	20.5	70
6/20/91	47.6	47.2	29.5	32.4	20.3	70.7
6/9/91	41.4	40.8	3.2	4.3	-1.4	70.3
7/29/91	41.3	40.6	3.2	4.2	-2	69.1
6/11/91	42.8	42	3.5	4.4	-0.33	90.5
6/13/91	42.1	41.2	3.2	4	-0.48	90.3
6/12/91	49.9	49.1	11.4	12.7	6.1	90.3
6/14/91	58.4	57.6	5.2	5.9	2	90.3
6/15/91	57.3	56.7	29.9	32.3	22.2	90.4
6/17/91	40.9	40.1	1.5	2.3	-1.7	90.2
6/18/91	60.4	59.8	29.7	31.8	22.5	89.9
6/28/91	63.3	62.7	30.1	31.6	24.8	100.4
7/1/91	59.9	59.1	14.5	15.2	11	100.5
7/2/91	53.5	52.7	14.1	14.9	10.7	100.4
7/3/91	65.2	64.6	29.6	31.3	23.6	100.5
7/23/91	59.4	58.9	-5.3	-4.6	-8.4	55.6
7/24/91	44	43.5	29.4	30.7	20.1	55.6
7/25/91	60.8	60.4	29.8	31.1	21.4	55.8
7/26/91	50.3	49.6	10.3	11.4	3.4	55.8
7/27/91	41.5	40.8	3.5	4.5	-2.2	55.7
Overcharged data - 7.5 oz. charge						
9/1/91	50	48.9	25.5	27.6	16.4	70.8
9/3/91	60.3	59.4	39.9	42.3	29.8	70.7
9/5/91	62.5	61.3	39.1	41.8	27.5	90.3
9/6/91	57.5	56.3	30	32.2	20.6	90.5
9/7/91	54.3	53.6	39.8	42.2	30.4	56.6
9/7/91	46.1	45.4	29.3	31.5	20.6	56.4
9/8/91	50	49.8	49.1	51.9	38	56.8

Date	Tconairin	Tconfanout	Qfreezer	Qfreshfood	P-system	P-compressor
	°F	°F	W	W	W	W
6/1/91	69.5	81.3	89.3	57.5	187.2	163.8
6/2/91	69.3	81.8	132.5	55.7	194.4	168.3
6/28/91	68.7	84.4	175.6	60.4	213.2	185.7
6/3/91	68.8	79.3	20.1	92.6	167.5	143.8
7/22/91	69.4	81.6	24.2	101.2	181	153.8
6/19/91	68.5	78.5	22.7	41.5	160.7	135.3
6/4/91	68.6	81.9	181	23.5	201.8	176.7
6/20/91	68.9	82.6	180.4	23.2	198.7	173.9
6/9/91	68.7	78.9	70	47.8	182.4	155.7
7/29/91	67.9	78.4	79.5	46.6	185	158.3
6/11/91	88.6	99.9	34	24.2	184.2	159.6
6/13/91	88.8	99.9	32.4	24.6	185.3	159.3
6/12/91	88.9	101.3	74	33.3	201.5	176.3
6/14/91	88.9	100.2	21.1	65	184.8	161.3
6/15/91	89.1	103.2	138.3	24.8	222.3	196.6
6/17/91	88.7	99.4	22.7	24.9	179.8	154.9
6/18/91	88.7	101.8	120.9	30.7	204.3	180.7
6/28/91	99.2	111.4	73.2	26.5	205.6	179.9
7/1/91	99.1	110.5	22.8	44.7	190.8	166
7/2/91	99.1	110	24.5	26.4	189.7	164
7/3/91	99.2	112.9	82.1	24.8	201.3	176.4
7/23/91	53	65	23.4	127.8	169.1	142.3
7/24/91	53.2	67.5	190.4	25.4	185.7	160.7
7/25/91	53.6	67.7	159.5	68.8	184.5	157.8
7/26/91	53.4	67.5	128.5	77.2	187	160.3
7/27/91	53.4	66.5	98.5	64.2	183.9	155.7
Overcharged data - 7.5 oz. charge						
9/1/91	69.2	84.3	173.8	37.6	211.7	184.3
9/3/91	69.1	84.2	199.1	36.7	207	181
9/5/91	89.3	107.7	223.8	25.1	263.2	237
9/6/91	89.1	105.9	173.8	25.5	238	212.3
9/7/91	54.4	68	188.2	26.2	181.6	154.6
9/7/91	54.3	68	175.3	27.2	185.2	157.4
9/8/91	54.2	68.3	225.8	0	185.7	158.7

Date	P-evap.fan	Pc-inlet	Tc-inlet	Pc-outlet	Tc-outlet	Pe-inlet	Te-inlet	Pe-outlet
		P1	T1	P3	T3	P7	T7	P9
	W	Psig	°F	Psig	°F	Psig	°F	Psig
6/1/91	12	111.8	153.9	110.3	97.4	5.68	-8.2	3.15
6/2/91	11.9	116.2	158.1	114.8	99.9	6.96	-4.9	4.28
6/28/91	12.9	124.7	164.7	123.1	104.3	9.63	0.49	6.71
6/3/91	11.2	102.3	144.7	101	91.8	3.03	-14.5	0.8
7/22/91	13	106.6	147.9	105.2	94.2	4.2	-11.5	1.6
6/19/91	12.4	97.8	140.7	96.5	89	1.47	-18.2	-0.52
6/4/91	11.6	119	161.7	117.5	101.6	8.43	-1.9	5.68
6/20/91	11.4	119.9	162	118.4	102.1	8.74	-1.38	5.81
6/9/91	12.8	105.9	148.5	104.6	94	4.36	-11	2.04
7/29/91	12.9	106.7	149	105.3	94.4	4.96	-9.7	2.45
6/11/91	12.1	137.6	170.2	136.1	111.6	3.39	-10.9	1.17
6/13/91	12.4	135.8	170.5	134.3	111.4	3.19	-11.2	1.05
6/12/91	12.2	146.7	178.3	145.4	116.2	5.34	-4.7	2.91
6/14/91	11.6	139.2	172	137.8	112.4	3.52	-10.1	1.34
6/15/91	12.3	156.1	189.6	155.8	121.1	7.9	2	5.07
6/17/91	12.5	134.8	168.1	133.4	110.2	2.76	-12.8	0.67
6/18/91	11.4	150.1	182.7	149.2	118	6.46	-1.7	3.74
6/28/91	12.8	163	190.3	163	124.5	5.21	-4.3	2.77
7/1/91	12.3	157	183.8	157	121.7	3.73	-8.7	1.53
7/2/91	13	154.6	182	154.4	120.5	3.38	-10	1.22
7/3/91	12.2	162.9	190	162.9	124.4	5.1	-4.6	2.6
7/23/91	12.7	81.5	128.3	80.2	77.8	2.85	-14.7	0.26
7/24/91	12.3	93.8	138.9	92.4	85.6	5.79	-7.3	3.06
7/25/91	12.4	93.3	138.4	91.9	84.7	5.51	-8.1	2.74
7/26/91	12.5	91.8	138.8	90.4	84.9	5.9	-7.1	3.3
7/27/91	13.4	87	133.5	85.6	81.7	4.59	-10	2.07
Overcharged data - 7.5 oz. charge								
9/1/91	12.8	122.8	163.8	121.1	103.6	9.54	0.2	6.61
9/3/91	12	123.6	162.6	121.9	103.9	9.34	-0.18	6.22
9/5/91	12.2	176.3	202.5	174.8	129.6	14.1	13.1	10.7
9/6/91	12.3	163.6	192.7	163.6	124.7	10.1	6.9	7.03
9/7/91	12.4	92.2	136.6	90.8	82.6	4.96	-9.2	2.14
9/7/91	12.9	92.6	137.5	91.1	85.1	5.25	-8.6	2.47
9/8/91	12.4	94.2	138.3	92.7	81.7	5.62	-7.8	2.67

Date	Te-outlet	Psuc.	Tsuc.	Pcap.-inlet	Tcap-inlet	Tma	Mdot
	T9	P10	T10	P4	T4		
	°F	Psig	°F	Psig	°F	°F	lbm/hr
6/1/91	-11.1	2.87	71.1	109.3	96.6	14.715	15.17
6/2/91	25.3	3.94	78	114.3	91.6	33.563	15.999
6/28/91	24	6.38	77.8	123.1	89.9	34.102	18.433
6/3/91	-18.6	0.6	67.1	100.2	91.1	6.354	13.049
7/22/91	-16.7	1.41	60.9	104.8	93.5	5.407	14.004
6/19/91	-12.1	-0.71	68.2	96	88.3	-1.465	11.708
6/4/91	15.5	5.31	80	116.2	99.3	33.378	17.34
6/20/91	23	5.44	82.3	117.3	101.1	33.896	17.376
6/9/91	-14.7	1.79	68.3	105.6	93.3	7.992	14.227
7/29/91	-14.4	2.25	59.8	104.7	93.5	7.882	14.975
6/11/91	-14.2	1.17	86.1	135.4	110.8	8.203	12.254
6/13/91	-3.4	1.05	87.2	135.2	110.6	7.763	12.147
6/12/91	-7.2	2.88	88.3	144.6	115.4	16.382	13.767
6/14/91	3	1.34	88.5	137.3	111.6	11.133	12.333
6/15/91	25.7	4.95	98.3	154.8	120.2	34.767	15.408
6/17/91	-1.7	0.67	86.8	132.9	109.4	6.124	11.782
6/18/91	25.3	3.65	96.5	148.6	117.2	34.631	14.261
6/28/91	28.2	2.73	101.8	162.4	123.7	34.745	12.849
7/1/91	13.9	1.53	98.1	156.6	120.8	19.642	11.854
7/2/91	13.4	1.22	97.2	153.9	119.7	18.724	11.615
7/3/91	25.2	2.58	101.5	162.6	123.6	34.668	12.705
7/23/91	-20.4	-0.12	46.7	79.5	77	1.83	13.376
7/24/91	21.5	2.58	58.7	91.6	66.6	31.993	15.733
7/25/91	23.2	2.28	58.9	91.1	66.5	34.063	15.402
7/26/91	-5.9	2.84	58.7	89.9	77	15.264	16.08
7/27/91	-15	1.66	48	84.5	80.8	8.172	15.228
Overcharged data - 7.5 oz. Charge							
9/1/91	19.6	6.47	80.9	120.8	97.3	29.753	18.464
9/3/91	31.1	6.1	78.7	121.9	90.5	44.028	18.123
9/5/91	10.9	10.6	100.8	173.6	128.6	43.771	20.7
9/6/91	9.2	6.98	94.9	162.9	122.5	34.637	17.447
9/7/91	30	1.81	59.2	90.4	65.8	43.352	14.895
9/7/91	22	2.14	58.7	90.7	67	32.905	15.27
9/8/91	34.2	2.34	60	92.3	66.1	51.688	15.409

Subcooling	Subcooling	Superheat
Condenser	Cap. Inlet	Evaporator
°F	°F	°F
-1.388	-1.159	2.856
-1.357	6.665	36.493
-1.256	13.144	29.663
-1.239	-1.023	1.577
-1.139	-0.674	1.28
-1.195	-0.806	11.908
-1.57	0.017	23.443
-1.579	-1.18	30.651
-1.292	-0.004	2.108
-1.28	-0.733	1.338
-1.892	-1.44	4.95
-2.589	-1.339	16.081
-1.98	-1.561	7.36
-1.852	-1.298	21.684
-2.059	-1.613	35.037
-1.84	-1.292	18.842
-1.993	-1.473	37.796
-2.246	-1.71	43.116
-2.117	-1.397	32.069
-2.095	-1.523	32.413
-2.19	-1.522	40.551
-0.726	-0.417	1.311
-0.378	18.11	35.682
0.202	17.888	38.193
-0.965	6.611	7.681
-0.929	-0.77	1.729
Overcharged Data - 7.5 oz. charge		
-1.622	4.517	25.48
-1.494	11.906	37.837
-2.283	-1.787	8.466
-2.183	-0.29	14.172
1.594	18.135	46.545
-0.712	17.13	37.686
3.714	19.058	49.371

R134a - Data

Date	Tfreshfood	Tfreshsupply	Tfreshfdret	Tfreezer	Tfreezret	Tevapfanout
	°F	°F	°F	°F	°F	°F
3/11/92	27.4	7.6	27.4	0.71	2.4	-2.7
3/16/92	35.7	18.9	35.6	9.8	11.7	6
3/17/92	43.1	28.6	43.1	20.4	22.2	16.3
3/18/92	50.2	37.9	50.2	30.6	32.7	26.1
3/19/92	45.9	42.2	45.8	39.1	40.8	33.7
3/20/92	53.3	52.1	53.1	50.3	52.2	45.4
2/27/92	31.1	7.5	31.1	0.5	1.9	-2.5
3/2/92	39.9	18.9	39.9	10.1	11.7	6.7
3/4/92	40.3	19.7	40.3	10.1	11.8	6.6
3/4/92	47.5	29.9	47.6	20.6	22.4	16.6
3/21/92	48.8	30.5	48.9	20.4	22.1	16.4
3/5/92	54.9	38.9	55	30.3	32.3	25.9
3/6/92	57.9	42.9	57.9	34.3	36.4	30
2/25/92	64.8	52.5	64.9	45.3	47.6	40.6
2/28/92	60.9	56.9	60.9	54.3	56.8	49.1
3/9/92	67.5	67	67.4	65.8	68.1	60.5
2/21/92	41.9	14.1	41.9	5.6	6.8	2.7
2/5/92	48.9	21.3	47.6	9.1	10.6	5.9
2/6/92	52.7	26.1	51.6	14.7	16.3	11.4
2/12/92	58.4	36.8	58.4	25.4	26.6	21.6
2/13/92	65.4	45.6	65.4	35.5	37.4	31.6
2/19/92	72.9	56	73	46.5	48.8	41.7
2/20/92	78.6	63.9	78.7	55.3	57.8	50.2
3/3/92	78.3	63.1	78.4	54.9	56.8	50.2
3/22/92	48.7	19.3	48.8	10.8	12.1	7.7
3/23/92	60.2	34.1	60.2	21.2	22.6	17.3
3/23/92	66.6	43.2	66.7	30.9	32.5	26.5
3/24/92	73.4	52.4	73.4	40.6	42.4	36.1
3/24/92	79.2	60.4	79.3	49.5	51.4	44.8
3/25/92	86.6	70.9	86.8	61	63	56.1

Date	Tchamber	Tconairin	Tconfanout	Qfreezer	Qfreshfood	P-system	P-compressor
	°F	°F	°F	W	W	W	W
3/11/92	54.4	53.5	62.9	48.2	24.8	158.8	132.5
3/16/92	54.6	53.8	63	58.9	24.8	157.6	130.6
3/17/92	54.8	54	63	65.2	24.5	155.5	128.9
3/18/92	54.1	53.5	62.5	74.1	24.8	153.7	127.7
3/19/92	54.5	53.8	62.4	94	0	150.8	124.8
3/20/92	54.6	53.9	62.3	98.8	0	148	121.6
2/27/92	69.4	68.3	78.1	34.4	24.2	164.5	139
3/2/92	69.7	68.9	78.2	44.3	24.7	164.1	137.7
3/4/92	69.5	69.8	78.2	44.9	25.3	163.4	137
3/4/92	69.5	68.9	78.2	59.1	24.8	162.5	135.4
3/21/92	69	68.3	77.5	58.1	24.9	161.2	135.6
3/5/92	69.5	68.9	78.7	68.6	24.8	161.2	135
3/6/92	69.5	68.8	78.2	71.6	24.7	160.2	134.1
2/25/92	69.3	68.5	77.8	78.7	24.7	156	130.9
2/28/92	69.4	68.6	77.6	97.2	0	154.1	129.2
3/9/92	69.4	68.8	77.5	109	0	151.6	127
2/21/92	89.6	88.6	99.1	24.9	24.8	176.9	152.9
2/5/92	89.5	88.4	98.1	24.4	24.6	170.2	146.3
2/6/92	89.5	88.4	97.9	26.2	24.1	168.1	144.4
2/12/92	89	88.2	97.7	45.9	24.6	167.9	144.6
2/13/92	89.1	88.3	97.4	50.6	24.5	165.9	142.7
2/19/92	89.2	88.5	97.4	74.1	24.3	171.2	147.8
2/20/92	89.4	88.7	98.8	81.6	24.2	169	145.6
3/3/92	89.9	89.3	98.8	74.6	24.1	167.9	142.9
3/22/92	99.3	98.4	108.7	25.2	24.9	181.2	158.4
3/23/92	99.7	98.7	108.2	36.4	24.6	180.1	156.7
3/23/92	99.5	98.6	108.7	48.4	24.4	177.7	155.1
3/24/92	99.7	98.9	108.8	58.1	24.3	177	153.6
3/24/92	99.6	98.9	108.7	65.7	24.2	174.8	151.7
3/25/92	99.5	98.8	108.5	76.1	24	172.5	149.4

Date	P-evap.fan	Pc-inlet	Tc-inlet	Pc-outlet	Tc-outlet	Pe-inlet	Te-inlet
		P1	T1	P3	T3	P7	T7
	W	Psig	°F	Psig	°F	Psig	°F
3/11/92	12.9	73.8	129.1	73.3	67.1	-3.841	-27.7
3/16/92	12.8	73.7	128.8	73.7	67.3	-3.812	-27.6
3/17/92	12.6	73.1	128.1	73.1	65	-4.123	-28.7
3/18/92	12.5	72	128.3	71.9	63.8	-4.481	-30
3/19/92	12.4	71	125.5	71	63.3	-4.802	-31.2
3/20/92	12.3	70	124.7	70	61.3	-5.217	-32.8
2/27/92	12.9	98.9	144.8	97.8	82.3	-2.773	-24.1
3/2/92	12.8	98.9	144.4	98	85.2	-2.773	-24.1
3/4/92	12.8	100.8	144.2	99.9	77.3	-2.742	-24
3/4/92	12.6	100.8	144	99.9	76.3	-2.773	-24.1
3/21/92	12.6	97.4	144.1	96.6	84.4	-2.926	-24.6
3/5/92	12.5	101	143.9	100.1	75.6	-2.926	-24.6
3/6/92	12.5	100.5	143.7	99.4	73.5	-4.481	-30
2/25/92	12.4	97.7	141	96.5	75	-3.726	-27.3
2/28/92	12.3	96.3	139.8	95.3	76	-4.011	-28.3
3/9/92	12.1	96.9	139	95.9	73.2	-4.123	-28.7
2/21/92	12.9	143.4	168.6	142.3	103.2	-0.906	-18.4
2/5/92	12.8	137.7	164.9	136.6	105.4	-1.452	-20
2/6/92	12.7	135.1	165	133.9	104.3	-1.62	-20.5
2/12/92	12.5	140.2	163.5	139.1	97.4	-1.686	-20.7
2/13/92	12.4	134.5	163.3	133.4	103.9	-2.014	-21.7
2/19/92	12.3	144.5	166.2	143.5	95	-1.25	-19.4
2/20/92	12.3	143.7	165.5	142.7	94.5	-1.419	-19.9
3/3/92	12.2	140.6	164.8	139.5	104.1	-1.752	-20.9
3/22/92	12.8	164.4	180.4	163.2	116.1	-0.124	-16.2
3/23/92	12.6	165.2	179.7	164	116.2	-0.088	-16.1
3/23/92	12.5	164.9	179.3	163.8	116.1	-0.269	-16.6
3/24/92	12.4	165	179.1	163.9	115.9	-0.412	-17
3/24/92	12.3	164.4	178.2	163.1	115.6	-0.59	-17.5
3/25/92	12.2	163.2	177	162.1	115	-0.836	-18.2

Date	Pe-outlet	Te-outlet	Psuc.	Tsuc.	Pcap.-inlet	Tcap-inlet	Tma
	P9	T9	P10	T10	P4	T4	
	Psig	°F	Psig	°F	Psig	°F	°F
3/11/92	-6.201	-2.5	-6.651	50.3	71	55.7	4.928
3/16/92	-6.252	2.2	-6.652	51.4	71.2	56.1	14.116
3/17/92	-6.463	10.2	-7.033	52.3	70.2	55.9	24.313
3/18/92	-6.681	16	-7.081	52.5	69.1	55.5	34.469
3/19/92	-6.902	17.1	-7.282	53	68.4	55.6	41.305
3/20/92	-7.147	25.1	-7.507	53.9	67.1	55.6	52.291
2/27/92	-5.133	-1.6	-5.453	64.2	96.4	73.4	4.853
3/2/92	-5.333	4.2	-5.493	65.8	96.4	73	14.551
3/4/92	-5.152	6.7	-5.372	63.8	98	69.8	14.682
3/4/92	-5.123	14	-5.333	64.7	97.9	69.9	24.948
3/21/92	-5.306	10.8	-5.656	66.4	95.5	73.1	24.81
3/5/92	-5.146	20.9	-5.356	65.8	98.2	70.2	34.595
3/6/92	-6.691	19.5	-6.871	65.8	97.5	70	38.573
2/25/92	-5.776	30.3	-6.056	67.5	94.5	70.5	49.349
2/28/92	-5.951	34.6	-6.181	68.1	93.3	70.9	57.214
3/9/92	-6.113	43.5	-6.413	68.3	94.3	70.1	68.029
2/21/92	-3.206	4.1	-3.346	83.1	140.2	92.4	10.35
2/5/92	-3.912	5.2	-4.122	85.2	135.5	96	14.343
2/6/92	-4.02	10.4	-4.15	89.1	130.7	102.5	19.87
2/12/92	-3.946	15.5	-4.046	82.4	125.7	89.2	29.816
2/13/92	-4.184	24	-4.244	88	132	97.5	40.231
2/19/92	-3.5	33.5	-3.64	85.1	141.3	90.2	51.247
2/20/92	-3.529	38.5	-3.649	86.1	140.6	90.6	59.913
3/3/92	-3.792	35	-3.832	87.1	137.8	92.9	58.984
3/22/92	-2.284	8	-2.304	96.6	161.3	111.4	15.812
3/23/92	-2.298	15.8	-2.448	95.7	162.6	108.2	26.403
3/23/92	-2.439	22	-2.589	95.8	162.4	107	35.959
3/24/92	-2.482	28.9	-2.482	96.8	162.5	107	45.535
3/24/92	-2.6	34.7	-2.6	97.2	161.8	106.4	54.221
3/25/92	-2.756	42.4	-2.756	97.9	160.9	105.9	65.406

Flow Volt	Mdot	Subcooling	Subcooling	Superheat
		Condenser	Cap. Inlet	Evaporator
V	lbm/hr	°F	°F	°F
2.7396	7.574749167	4.11	13.947	34.338
2.73558	7.553656662	4.179	13.684	39.26
2.66872	7.321241241	6.076	13.196	48.18
2.62904	7.187969161	6.463	12.832	54.953
2.56951	6.976199144	6.347	12.242	57.064
2.48825	6.689417783	7.658	11.323	66.213
2.9937429	8.144909481	3.9	12.013	30.87
2.958604	8.03108987	1.112	12.413	37.456
2.910817	7.924096445	10.066	16.512	39.245
2.880265	7.81647368	11.066	16.356	46.431
2.88525	7.77628128	1.126	11.804	43.95
2.844979	7.688931096	11.876	16.223	53.422
2.775904	7.453278817	13.59	16.032	58.498
2.7683269	7.41833037	10.47	13.834	65.349
2.720745	7.246784015	8.79	12.745	70.376
2.46903	6.388971507	11.931	14.12	79.962
3.264222	8.703099093	4.861	14.742	29.626
3.1447963	8.23288978	0.145	9.051	33.152
3.1748774	8.208101817	0.027	0.363	38.731
2.887366	7.494338083	9.257	11.327	43.57
3.046514	7.8762388	0.2	5.961	52.918
3.113294	8.237783691	13.583	17.425	60.019
3.07561	8.103250821	13.735	16.718	65.119
3.044135	7.954255861	2.734	13.18	62.53
3.51624	9.153628627	0.643	4.586	30.541
3.38506	8.789124222	0.859	8.304	38.384
3.33031	8.633139747	0.88	9.425	45.029
3.29809	8.527041559	1.12	9.465	52.068
3.24834	8.374992975	1.103	9.786	58.244
3.18216	8.166544511	1.305	9.926	66.446

Data Acquisition Channel Numbers

Channel #	T.C. Location
1	Frig. Cabinet Air - Front Center
2	Frig. Cabinet Air - Back Center
3	Frig. Cabinet Air - Top
4	Frig. Cabinet Air - Bottom
5	Frig. Cabinet Air - Return
6	Frig. Cabinet Air - Supply
7	Freezer Air - Top
8	Freezer Air Return
9	Evap. Air In
10	Evap. Fan Outlet Air
11	Evap. Inlet R12 - immersion
12	Evap. R12,1/2 way - surface
13	Evap. R12,3/4 way - surface
14	Evap. R12,7/8 way - surface
15	Evap. Outlet R12 - immersion
16	Suction Line HX - Inlet R12 - immersion
17	Condenser Fan Air Outlet
18	Compressor Can - Top
19	Compressor Can - Side
20	Chamber Temperature
21	Suction Line HX - 1' from outlet - surface
22	Suction Line HX Exit - surface
23	Condenser Inlet - R12 - immersion
24	Condenser - 1/2 way - surface
25	Condenser - 3/4 way - surface
26	Condenser Outlet R12 - immersion
27	Cap. Tube Inlet - R12 - immersion
28	Condenser Air Inlet Temperature
29	Compressor Suction Inlet - R12 - immers.
30	Outside Air

Appendix G: Film Coefficients

G.1 Condenser Film Coefficients

The air side film coefficient for the condenser was estimated from Equation G.1 which is the correlation by Hilpert [1] for a cylinder in crossflow. Evaluating this expression for the nominal conditions listed results in an air side convective film coefficient of 14.0 Btu/hr-ft^2°F

$$\overline{Nu}_D = 0.683\, Re_D^{0.466}\, Pr^{0.33} \qquad \text{(G.1)}$$

where $Re_D = 838$ (based on condenser inlet area of 40 in^2)

$D = 0.25$ in

$Pr = 0.713$

$Tair = 80$°F

The internal film coefficients must be determined from convective heat transfer correlations. For the desuperheating section, the Dittus-Boelter equation given by Equation G.2 was used [2]. For the R134a subcooled section, the maximum calculated Reynolds number is 1500, well below the transition Reynolds number to turbulent flow. The theoretical expression for laminar flow with constant heat flux given by Equation G.3 was used for the subcooled section [3].

$$h_{desup} = 0.023 Re^{0.8} Pr^{0.3} \left(\frac{k_{desup}}{D} \right) \qquad \text{(G.2)}$$

$$h_{sub} = 4.36 \left(\frac{k_{sub}}{D} \right) \qquad \text{(G.3)}$$

The film coefficient for the two phase section is more complicated. The correlation by Cavallini-Zecchin [4] was chosen and is given by Equation G.4. The two phase film coefficient in this correlation is a function of quality. Since the quality in the two phase section of the condenser varies from one to zero, the film coefficient must also vary. To simplify the model an average value was determined by integrating. For reference Figure G-1 shows the variation in the film coefficient for typical data points for both the R12 and R134a cases. Note that the film coefficient for the R12 case is higher than the R134a case because the Reynolds number for the R12 data point is higher.

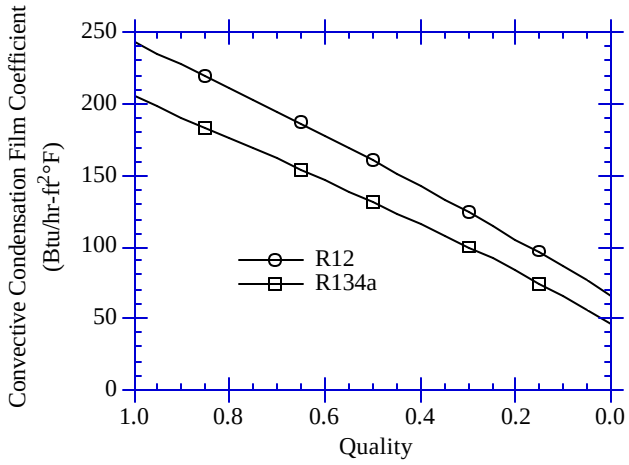

Figure G-1. Variation in Convective Condensation Film Coefficient for R12 and R134a

$$h_{2ph} = 0.05 Re_{eq}^{0.8} \, Pr_l^{0.33} \left(\frac{k_1}{D} \right) \qquad \text{(G.4)}$$

where $Re_{eq} = Re_l + \left(\frac{\mu_g}{\mu_l} \right) \left(\frac{\rho_l}{\rho_g} \right)^{0.5} Re_g$

$$Re_l = \frac{GD(1-x)}{\mu_l}$$

$$Re_g = \frac{GDx}{\mu_g}$$

with Re_{eq} = equivalent Reynolds number

Re_g = Reynolds number of gas

Re_l = Reynolds number of liquid

Pr_l = Prandtl number of liquid

G = mass flux

D = tube diameter

x = quality

ρ_l = density of liquid

ρ_g = density of gas

μ_l = viscosity of liquid

μ_g = viscosity of gas

k_l = thermal conductivity of liquid

The air side film coefficient and the film coefficients on the refrigerant side can be used to calculate a theoretical estimate of the overall conductance in each zone of the condenser by using Equation G.5. In this equation

the wall resistance has been neglected. However, because the condenser does have wire fins, the fin effectiveness is accounted for.

$$\frac{1}{U_x} = \frac{A_x / A_o}{\eta_o h_o} + \frac{A_x / A_i}{h_i} \qquad \text{(G.5)}$$

where η_o = fin effectiveness

A_x = outside surface area of the condenser tubing in either section

A_o = total outside surface area - includes wire fins

A_i = inside surface area of the condenser tubing

h_o = air side convective film coefficient

h_i = refrigerant side convective film coefficient for either section

The fin effectiveness is determined from Equation G.6 where the fin efficiency is given by Equation G.7. Note that the fin effectiveness is for a pin fin and it is assumed that this closely approximates the wire fins in the condenser. A summary of the fin effectiveness calculations is given in Table G.1

$$\eta_o = 1 - \frac{A_f}{A_o}(1 - \eta_f) \qquad \text{(G.6)}$$

where A_f = fin surface area (ft^2)

A_o = total outside surface area (ft^2)

$$\eta_f = \frac{\tanh(mL)}{mL} \qquad \text{(G.7)}$$

where $m^2 = \frac{4h_{spine}}{kd}$

h_{spine} = film coefficient for spine fin (Btu/hr-ft^2°F)

k = thermal conductivity of fin material (Btu/hr-ft°F)

d = spine diameter (ft)

L = spine length

Table G.1. Condenser Fin Effectiveness Calculation Results

dwire	0.0625 in.
L/tube	0.625 in
hspine	10.2 Btu/hr-ft^2°F
m	15.0/ft
ηf	0.836
Wire spacing	3.5 wires/in.
Af	0.01193 ft^2/in
Atube	0.00545 ft^2/in
Af/Ao	0.686
ηo	0.888

The results of solving Equation G.5 for all the data points in both the R12 and R134a data sets are summarized in Table G.2. The last row shows the ranges of the theoretical conductances for the variation in the internal film coefficients.

Table G.2. Theoretical Condenser Conductances

	R12		R134a		
Condenser Section	**Desuperheating Section**	**Two Phase Section**	**Desuperheating Section**	**Two Phase Section**	**Subcooled Section**
h_o (Btu/hr-ft^2°F)	10.2	10.2	10.2	10.2	10.2
Minimum h_i (Btu/hr-ft^2°F)	25.8	119.8	23.6	115.3	9.9
Maximum h_i (Btu/hr-ft^2°F)	44.2	190.2	34.9	141.7	11.6
Average h_i (Btu/hr-ft^2°F)	32.0	160.9	29.0	129.8	10.7
A_x/A_o	0.31	0.31	0.31	0.31	0.31
A_x/A_i	1.14	1.14	1.14	1.14	1.14
η_o	0.89	0.89	0.89	0.89	0.89
Conductances (Btu/hr-ft^2°F)	12.8 - 16.7	22.9 - 24.9	12.1 - 15.0	22.7 - 23.7	6.7 - 7.6

G.2 Evaporator Film Coefficients

The calculation of the evaporator film coefficients is very similar to the condenser except for the two phase film coefficient. As for the condenser the correlation by Hilpert [1] was used to calculate the air side film coefficient. Equation G.1 is repeated here as Equation G.8 with the conditions used in the equation listed. The outside film coefficient was found to be 7.1 Btu/hr-ft^2°F. Further for the superheated section film coefficient, the Dittus-Boelter correlation given by Equation G.2 was used except the Prandtl number is raised to the 0.4 power.

$$\overline{\overline{Nu}}_D = 0.683\, Re_D^{0.466}\, Pr^{0.33} \qquad \text{(G.8)}$$

where $Re_D = 795$ (based on evaporator inlet area of 36 in^2)

$D = 0.3125$ in.

$Pr = 0.72$

Tair = 8°F

The two phase film coefficient was determined from the correlation by Kandlikar given by Equation G.9. This correlation was chosen to calculate the two phase film coefficients because it is based on a large data set for 10 fluids [4].

$$\frac{h_{tp}}{h_l} = c_1 Co^{c_2} (25 Fr_l)^{c_5} + c_3 Bo^{c_4} F_{fl} \qquad \text{(G.9)}$$

$$h_l = 0.023 Re_l^{0.8} Pr_l^{0.4} \left(\frac{k_l}{D}\right)$$

$$Re_l = \frac{GD(1-x)}{\mu}$$

Where h_{tp} = two phase film coefficient

h_l = film coefficient for liquid

Re_l = Reynolds for liquid

Pr_l = Prandtl for liquid

k_l = thermal conductivity for liquid

Co = convection number

Fr_l = Froude number for liquid

Bo = boiling number

F_{fl} = fluid specific parameter

c_1,c_2, etc. = constants - see reference

G = mass flux

x = refrigerant quality

Since the Reynolds number is a function of quality, the film coefficient varies not only as a function of fluid properties but also with quality. An average film coefficient was determined by integrating over the typical quality range for the evaporator. For reference, Figure G-2 shows the variation in two phase film coefficient with quality for typical R12 and R134a data points.

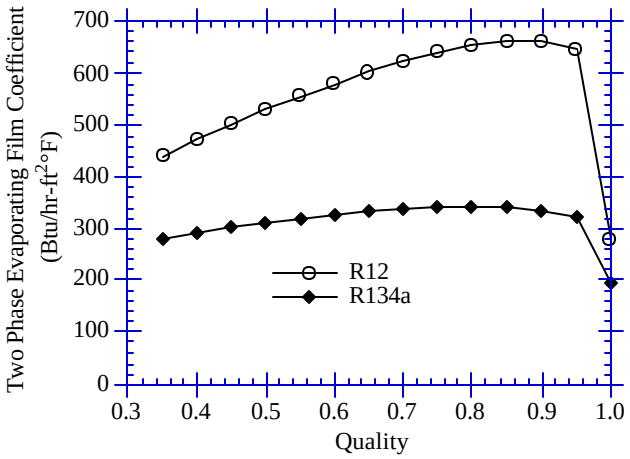

Figure G-2. Variation in Two Phase Film Coefficients with Quality

Using the estimates of the air side and refrigerant side film coefficients it is also possible to use Equation G.5 to estimate theoretical conductances for the evaporator. The evaporator instead of wire fins has spine fins. As a result, the fin effectiveness of the spines is considered. The same equations given by Equations G.6 and G.7 were also used for the evaporator. The fin effectiveness calculations for the evaporator are summarized in Table G.3. The results of solving Equation G.5 for each zone in the evaporator is given in Table G.4.

Table G.3. Evaporator Fin Effectiveness Calculation Results

dspine	0.0625 in.
L	1.0 in
hspine	15.5 Btu/hr-ft^2°F
m	9.3/ft
ηf	0.838
Spine spacing	18 spines/in.
Af	0.0249 ft^2/in
Atube	0.0818 ft^2/in
Af/Ao	0.233
ηo	0.962

Table G.4. Theoretical Evaporator Conductances

	R12-T9		R134a	
Evaporator Section	**Superheat Section**	**Two Phase Section**	**Superheat Section**	**Two Phase Section**
h_o (Btu/hr-ft^2°F)	7.1	7.1	7.1	7.1
Minimum h_i (Btu/hr-ft^2°F)	32.9	474	25.6	292
Maximum h_i (Btu/hr-ft^2°F)	39.4	582	33.0	373
Average h_i (Btu/hr-ft^2°F)	35.7	521	29.4	337
A_x/A_o	0.214	0.214	0.214	0.214
A_x/A_i	1.667	1.667	1.667	1.667
η_o	0.864	0.864	0.864	0.864
Conductances (Btu/hr-ft^2°F)	11.7 - 13.0	26.0 - 26.5	10.0 - 11.7	24.6 - 25.4

References

[1] Incropera, F.P. and D.P. DeWitt., Fundamentals of Heat and Mass Transfer, Second Edition, John Wiley & Sons, Inc., New York, 1985, p. 334.

[2] Incropera & DeWitt. p. 394.

[3] Incropera & DeWitt. p. 389.

[4] Eckels, S.J. and M.B. Pate. 1990. "A Comparison of R-134a and R-12 In-Tube Heat Transfer Coefficients Based on Existing Correlations.", ASHRAE Transactions, Vol. 96, Part 1, pp. 256 to 265.